The Dissertation Committee for John Hundley Slater
Certifies that this is the approved version of the following dissertation:

Engineering Endothelial Cell Behavior via Cell-Surface Interactions with Chemically-Defined Nanoscale Adhesion Sites

Committee:

Wolfgang Frey, Supervisor

Martin Poenie

Krishnendu Roy

Christine Schmidt

Muhammad Zaman

Engineering Endothelial Cell Behavior via Cell-Surface Interactions with Chemically-Defined Nanoscale Adhesion Sites

by

John Hundley Slater, B.S.M.E

Dissertation

Presented to the Faculty of the Graduate School of

The University of Texas at Austin

in Partial Fulfillment

of the Requirements

for the Degree of

Doctor of Philosophy

The University of Texas at Austin

May 2008

Dedication

This work is dedicated to my loving fiancée Kathryn who has always been there for me and to my supportive family who have never turned me away in a time of need.

Much thanks to all of you.

Acknowledgements

I would first and foremost like to acknowledge my advisor Dr. Wolfgang Frey. Without his help and experience this project would not be to the level of completion that it is today. I want to thank my lab mates, Ruben Morones, Bongsu Jung, and Ted Gaubert for insightful discussions and "good times" in the lab. I would also like to extend thanks to three excellent undergraduate students Matt Jancaitis, Alex Chang, and particularly Patrick Boyce for his dedication to this project. I also acknowledge the Center for Nano and Molecular Science for providing excellent facilities that were essential in completing this work and finally, I would like to acknowledge the National Science Foundation for providing a Graduate Research Fellowship.

Engineering Endothelial Cell Behavior via Cell-Surface Interactions with Chemically-Defined Nanoscale Adhesion Sites

Publication No._____

John Hundley Slater, Ph.D.

The University of Texas at Austin, 2008

Supervisor: Wolfgang Frey

Current biomaterials are designed to be passive in nature to prevent the initiation of adverse immune responses upon contact with biological substances. While this approach of inertness is still a crucial design component for some applications, the possibility of engineering desired cell responses in the local environment of the material exists and is of particular interest in implantable devices and tissue engineered constructs. Fundamental knowledge of the relationships between cell adhesion and gross cell behavior will provide key design criteria for the creation of advanced biomaterials that induced locally controlled cellular responses. This work investigates the possibility of engineering cell behavior by limiting adhesion site maturation. Chemically-defined nanoislands of fibronectin were created using a combination of nanosphere lithography and an orthogonal surface functionalization strategy.

Investigation of the adhesive and cytoskeletal components of cells cultured on these surfaces demonstrates that chemically-defined nanopatterns provide an upper size limit to adhesion site growth which in turn influences the degree of cytoskeletal formation. The imposed restriction on adhesion site growth results in the formation of a relatively higher number of more evenly distributed, small adhesions throughout the cell body. The adhesive behavior can be tuned by changing the nanopattern properties with respect to their size, spacing, and density. Furthermore, it is demonstrated that the observed differences in cell adhesion as imposed by the nanopatterned surfaces induces changes in gross cell behavior with respect to spreading, proliferation, and motility. The results presented here parallel observations documented in cells cultured on elastic surfaces and indicate that intracellular signaling cascades initiated and governed by cellular adhesion sites are sensitive to adhesion size/maturation and possibly the amount of force generated locally at these adhesion sites. The conclusions drawn from these studies give insight into the possibility of implementing nanostructured biomaterials for cell engineering purposes and provide design criteria for the next generation of tissue engineered constructs.

Table of Contents

List of Tables

List of Figures

Chapter 1

Introduction

1.1 Introduction and Motivation

Biomaterial design has shifted from creating materials that are biologically inert to materials that display chemical and biological cues mimicking that of natural tissues.[1] While inertness may be desirable for some material applications, the ability to control cellular response in the local environment of the implanted material would be advantageous. For implantable sensors, drug releasing devices, and BioMEMS applications, the surface is the main component that interacts with the surrounding tissue and the ability to tune the properties of these surfaces to elicit desired cellular responses is of great interest. Toward this goal, implantable materials that release soluble factors have been created and include drug-eluting stents that slowly release anti-restenosis drugs such as sirolimus and paclitaxel. While the release of soluble factors from these stents can give some control over the behavior of cells in the local environment, it does not govern direct cell interactions with the surface. It is crucial that implanted stents induce the formation of an endothelial cell (EC) monolayer for the prevention of thrombosis. Currently, there is no design consideration for inducing the formation of this EC lining. The work presented here gives some insight into how nanostructured biomaterials can be implemented to gain control over EC phenotype expression and may provide some design parameters for the next generation of advanced biomaterials.

While control over cellular behavior via adhesive interactions with biomaterials is evident for some implanted materials, it is even more evident in the creation of tissue engineered devices in which cells interact with both the surface and eventually the entire volume of the synthetic construct. For these constructs to be viable they must allow for directed growth of tissue, precise placement of desired cell types, avoid creating adverse immune responses, be highly vascularized, and have the ability to link to the existing vascular network. Much attention in recent years has focused on designing methods to induce blood vessel growth in desired areas of these constructs. [2-5] In order for cells within these constructs to survive, a vascular network must be in place to deliver necessary oxygen, chemicals, and nutrients. A number of methods have been implemented to induce endothelial cell migration into these artificial materials for blood vessel formation and growth. Most current techniques rely on the controlled release or tethering of growth hormones, VEGF and bFGF, to produce gradients that direct endothelial cell movement and proliferation into the artificial tissue construct. [4] Another approach currently being investigated involves incorporating matrix metalloproteinase (MMP) sensitive linkers, RGD binding sequences, and VEGF into one matrix scaffold. [4] This bioactive scaffold allows ECs to "drill" their own pathways through the matrix, guided by VEGF concentration gradients. This technique has shown to work quite well in animal models yet still has limitations in linking into the existing vascular network. All of the mentioned studies rely on growth factor signaling to transform ECs from a quiescent state to an angiogenic phenotype.

The work presented here gives an alternative to soluble factor release and provides insight into how biomaterial surface structure on the nanometer scale can also be implemented to initiate angiogenic characteristics in ECs. Rather than solely relying

on the release of growth factors to guide EC penetration and growth, the results indicate that presenting nanoscale domains of ECM proteins can simultaneously induce increased EC motility and proliferation, even at extremely low protein concentrations. It is known that ECM concentration influences cell behavior and those findings are validated here, but further insight into the underlying mechanisms that provide this modulation are explored. The studies show that local ligand density on the nanoscale and the ability for cells to quickly cluster integrins into discrete adhesions is more important for initial cell attachment and long term proliferation than the overall ECM surface concentration. The ability to tune cellular response by varying the underlying nanoscale surface structure of the material is demonstrated. This work provides insight into the complex relationships between ECM concentration, adhesion maturation, intracellular force generation, and gross cell behavior and lays a foundation for further studies on mechano-regulation of EC phenotype expression.

1.2 Objectives

The purpose of this work was to investigate how limiting adhesion site maturation to early stages of adhesion can be harnessed to gain control over cell behavior. This was accomplished by creating chemically-defined nanoscale islands of ECM protein that provided direct control over the number of integrins allowed to cluster in a given adhesion site. Through modulation of the ECM nanoisland size, the number of integrins per adhesion site and subsequently the maturation of adhesion sites were controlled. Endothelial cells cultured on these surfaces displayed significant differences in mechanotransductive abilities and gross behavior in an adhesion site size dependent manner.

While previous studies have focused on the relationships between ECM presentation at the macro and micro scale and cell behavior, this work focused on gaining insight into how nanoscale presentation of ECM can be implemented to guide cell response. To explore this relationship a nanofabrication technique that met a few requirements had to be developed. First, the technique had to allow for the creation of large surface areas of chemically-defined nanoislands of ECM to be created for statistically sound quantification of cell behavior. Second, the technique had to provide for direct control over cell adhesion by displaying ECM components, full proteins or adhesive peptide sequences, in well-defined nanoscale islands with controlled size, spacing, density, and topography surrounded by an inert background. Furthermore, the fabrication process needed to allow for the use of glass substrates for easy implementation of fluorescent studies. To meet these demands, nanosphere lithography and an orthogonal surface functionalization scheme were implemented to create surfaces displaying FN nanoislands against a non-adhesive or passive background. [6] Much effort was taken to verify that the chemically-defined nanoislands were indeed imposing limitations on adhesion site growth. After verification of the chemical modification, the nanoscale FN islands were varied with respect to their size, spacing, and overall density. Changes in cell adhesive properties with respect to their size and location where analyzed and correlated to changes in cytoskeletal formation, spreading, proliferation, and mechanotransductive processes such as FN fibril formation and cell motility. The results indicate that limiting adhesion site size leads to significant changes in adhesion site and cytoskeletal properties. Furthermore, observations were made that indicated that these induced changes in adhesive and cytoskeletal properties may influence the amount of intracellular and traction force generated by cells on these

surfaces as reflected by reduced cell spreading and increased motility of cells cultured on very small nanopatterns. It is proposed that the differences in force generation may in turn influence adhesion composition and signaling cascades and lead to the observed changes in gross cell behavior.

1.3 Overview

The following document discusses how the studies were carried out and why. The necessary background is covered in Chapter 2. The process of cell adhesion, signaling from adhesion sites, previously reported relationships between engineered surfaces and cell behavior, and a brief introduction to ECs is covered. Chapter 3 details the nanofabrication process and lists the properties of the various surfaces implemented in this study. Chapter 4 discusses the chemical modification protocol and how the surfaces were characterized with XPS and AFM to verify the creation of fibronectin nanoislands on a passive/non-adhesive background. Chapters 5 and 6 discuss observed differences in adhesion site and cytoskeletal properties induced by the nanopatterned surfaces. Chapter 7 discusses FN fibril formation on these surfaces and gives insight into the mechanotransductive properties of cells on nanopatterned surfaces. Chapters 8 though 10 demonstrate how nanopattern properties influence cell spreading, motility, and proliferation, respectively. Finally, Chapter 11 discusses the results in detail and relates the observed changes in adhesive and cytoskeletal components to changes in cell behavior followed by speculation on how intracellular force generation may play a role in regulating signaling cascades and how this may be related to some of the observed cellular responses to these surfaces.

Chapter 2

Background

2.1 Introduction

Cell adhesion to ECM components is a complex process that is still not fully understood. Much attention has been given to classifying adhesions based upon their location in the cell, their size, lifetime, molecular composition, and the amount of force they generate and apply to the underlying surface. The idea that signaling cascades initiated and governed by cellular adhesion plaques can be controlled by engineering how cells adhere to surfaces is relatively new and much attention has recently been focused on gaining a better understanding of the relationships between adhesive properties, intracellular force, the generation of traction force, and downstream cell behavior. While many of these findings come from studies utilizing rigid 2D surfaces such as glass and polystyrene, an increasing number of scientists believe that the formation of large adhesion sites and associated stress fibers is an artifact of the culturing process on rigid surfaces and not representative of cells *in vivo*. Detailed studies of cellular components in engineered 3-D or natural matrices are underway but are more difficult to gain insight from due to difficulties in imaging cells in these environments. A fundamental understanding of the cell adhesion process, intracellular force generation, and how these processes can be manipulated to control cell behavior using engineered surfaces is necessary to understand the scope of this project. The current state of these relationships will be discussed in detail in the following sections.

2.2 Cells and Their Environment

Cells in native tissues receive signals from their environment via four primary sources, (1) soluble factors, (2) neighboring cells through cell-cell contacts, (3) cellular interactions with the extracellular matrix, and (4) outside environmental changes such as the application of shear stress induced by fluid flow. Although much is known about the effects of soluble factor signaling and some about cell-cell mediated signaling, the effects of surface topography and attachment site size on the nanometer length scale are relatively unexplored. Cell-ECM interactions mediated by integrin binding and clustering to form focal complexes and adhesions are known to play a key role in many cellular processes including adhesion strength, differentiation, cancer metastasis, cytoskeletal morphology, proliferation, motility, and phenotype control, but the underlying mechanisms and complex interplay between adhesion components and force generation is relatively unknown.[7-16] Ultimately, a combination of all of these influences will have to be harnessed to gain control over the cells microenvironment and to truly engineer a functioning artificial material based tissue. A short review concerning ECs, cell adhesion, adhesion site signaling, and engineered surfaces is discussed in this chapter. The other three signaling sources and their influence on cell behavior are not discussed in order to keep the background as concise and relevant as possible.

2.3 Endothelial Cells

Since endothelial cells were used for these experiments it is important to know a little about their primary function and the role they play *in vivo*. ECs, fibroblasts, and smooth muscle cells are responsible for the formation and maintenance of blood vessels

in all tissue types. ECs form the inner lining of all blood vessels and release a number of factors; endothelin-1, prostacyclin, and nitric oxide, that control vessel dilation, blood coagulation, and new vessel formation, whereas fibroblasts and smooth muscle cells provide structure and mechanical strength. ECs take on two basic quiescent phenotypes while lining blood vessels. In straight sections ECs are highly elongated with well-defined actin cytoskeletal networks induced by applied shear stress caused by the passing flow of the blood and its constituents. At branch points or curves in vessels, ECs display a cobblestone morphology yet are still inactive and stationary. Both types of quiescent cells can be disrupted by a number of factors that induce a wound healing or angiogenic phenotype including inflammatory cytokines, growth factors, hormones, and bacterial products.[7] The role of ECs and their reactions to wound healing responses are currently being explored and the molecular basis that drives them is relatively unknown. In response to a wound healing signal, ECs disassemble the dense peripheral band of actin and disassociate contacts with neighboring cells, then extend lamellapodia and/or filopodia to spread into the wound, followed by increased proliferation to fill in the wound area. The growth of new blood vessels follows a similar trend in cellular response and is a multistep process that involves remodeling of the extracellular matrix, migration, proliferation, and maturation of the newly assembled vessels. A number of EC markers have been characterized and used to determine when ECs have entered an angiogenic or wound healing phenotype including changes in cytoskeletal arrangement, the formation of lamellapodia and/or filopodia, the release of growth factors, increases in cell proliferation and migration, changes in gene expression, the production and release of MMPs, the expression of $\alpha_V\beta_3$ and $\alpha_V\beta_5$ integrins, and the display of chemical markers, such as monocyte chemotactic protein-1, on EC surfaces.[17-26] This study

utilizes some of these key events to indicate a change in EC phenotype from a quiescent to an active cell.

2.4 The Complex Relationships between Cell Adhesion, Intracellular Force Generation, Signaling Cascades, and Cell Behavior

2.4.1 The Cell Adhesion Process

Integrins

Integrins are the primary anchoring mechanism utilized for cell adhesion and they mediate cellular interactions with the underlying extracellular matrix to form adhesion sites that are key regulators of intracellular signaling cascades that govern many aspects of cellular behavior.[8-12] These heterodimeric transmembrane glycoproteins consist of an α and β subunit and to date, 18 α and 8 β subunits have been discovered that combine to form 24 documented adhesion receptors. ECs display and utilize 11 of the existing 24 forms.[11] Once activated, integrins undergo a conformational change allowing the extracellular component of these receptors to form a binding pocket that recognizes and interacts with specific peptide sequences displayed on ECM proteins, such as RGD, REDV, and YIGSR. Activated and clustered integrins therefore act synergistically and recruit a large variety of scaffold and signaling molecules with spatial and temporal dependence, leading to the formation of focal complexes that mature into focal adhesions.[13-16] Three key integrin receptors, $\alpha_5\beta_1$, $\alpha_V\beta_3$, and $\alpha_V\beta_5$ are predominately incorporated in adhesions of ECs with angiogenic phenotypes.[11] These integrins specifically bind to fibronectin, vitronectin, and a number of other ECM proteins found in high abundance at sites of angiogenesis and tissue injuries.

Integrin clustering is a crucial step in adhesion site formation and sites of clustered integrins act as a docking platform for intracellular protein aggregation during adhesion site formation. While still not fully understood, much effort has focused on determining what mechanisms induce the formation of integrin clusters. Mechanical force applied to the adhesions from both outside and inside the cell,[17-19] integrin activation,[20] immobilized ligand,[20] talin,[20-24] PIP_2 activation,[20] transmembrane domain-mediated homo-oligomerization,[25,26] and interactions with glycosphingolipids,[27] have all been implicated in the induction of integrin clusters. Putting all of the pieces together shows that integrin clustering is a multistep process. Unligated, non-activated integrins form small clusters in the cell membrane via lateral associations with each other through both their β integrin cytoplasmic and transmembrane domains.[25,26] Interactions with glycosphigolipids in the cell membrane can increase the extent of clustering to form microdomains of clustered but non-activated integrins.[27] Mathematical simulations have shown that preclustering of integrins into small domains is energetically beneficial in the formation of ligand-integrin interactions needed for adhesion site formation.[28,29] These small clustered integrin domains can become activated in the presence of immobilized ligand through integrin binding which induces conformational changes in the bound integrin.[20] These integrin conformational changes lead to PIP_2-mediated integrin interactions with talin.[20-24] Talin further acts with F-actin to allow for actomyosin-mediated force application to the ligand bound integrins.[20-24] While not fully supported by literature, it may be that local changes in the viscoelastic properties of the cell membrane near the site of the ligated integrin cluster and force application induce the flow of more integrins to the sight thereby increasing the amount of clustering and allowing for adhesion site growth.[17-19] This complex process of

preclustering, ligand binding, integrin activation, talin recruitment, force application, and increased integrin clustering is crucial for the formation of a platform for the docking of intracellular proteins and signaling molecules during adhesion site formation as discussed in the following section.

Maturation and Classification of Cell-ECM Adhesions

Cellular adhesions have demonstrated the ability to regulate cell motility, [30-33] proliferation, [9,34-36] differentiation, [34,36] and apoptosis. [37,38] While often biochemical in nature, these regulatory processes are also governed by the endogenous force generated by the cell via actomyosin contraction that is transferred to the underlying substrate via adhesions. [39-41] Identifying and classifying different stages of adhesion is important for understanding the relationships between intracellular force generation, adhesion maturation, and adhesion site mediated regulation of intracellular signaling cascades. To address this issue, a few classes of adhesions have been identified and include hyaluronan-mediated adhesions, focal complexes, focal adhesions, fibrillar adhesions, and 3-D matrix adhesions (Figure 2.1). [11,16,42,43]

The first few seconds of cell attachment to surfaces for some cell types is regulated by the glycosaminoglycan hyaluronan. When displayed on the cell surface, this linear polymer forms weak interactions with ECM components to start the adhesion process by bringing the cell in close proximity to the ECM. [16,44] Once the cell has made contact with the surface, integrin mediated adhesions begin to form. These early adhesions, known as focal complexes, are relatively small adhesion sites usually located at the leading edge of motile cells (Figure 2.1). The complexes are often observed associating with filopodia and lamellapodia protrusions used for probing of the local

environment during cell migration.[45] These highly dynamic complexes are found in abundance in motile cells and their formation is regulated by Rac1 and Cdc42 activation.[16,42] Focal complexes can be further classified as either early or late, depending on their lifetime and molecular composition. Early focal complexes are designated by the presence of $\alpha_v\beta_3$ integrins, talin, paxillin, and phosphotyrosine. Shortly after their formation, these adhesions mature to become late focal complexes that are identified by the addition of vinculin, FAK, VASP, α-actinin, and Arp 2/3 to the adhesion complex. Both of these adhesive plaques display a typical surface contact size of 0.25 μm^2, a size indicative of the limitations of light microscopy, with a short lifetime of only a few minutes. Many of these complexes disappear shortly after their formation, particularly when lamellapodia advancement is stopped, but some of them grow in size and recruit more cytoplasmic proteins that promote linkage to actin stress fibers thereby further maturing into focal adhesions. The maturation process from small complexes to larger adhesions is induced by intracellular force generation produced by actomyosin-driven contractility and due to this force-dependent maturation, classical focal adhesions are found almost exclusively at the ends of actin stress fibers (Figure 2.1).[11,16,42] To promote this maturation of adhesive states, Rho also stimulates PIP_2 synthesis that mediates cytoskeletal interactions with the focal adhesion adapter and linking proteins vinculin and α-actinin thereby forming the crucial link between stress fibers and cellular adhesion sites.[42] Focal adhesions are much larger in size compared to focal complexes and the increase in adhesive area and unfolding of force-mediated adaptor proteins allows for the incorporation of $\alpha_5\beta_1$ integrins, tensin, and zyxin into the existing complex.

If cells are cultured on FN, a final stage of adhesion formation known as fibrillar adhesions is achieved. These adhesions are typically found near the center of the cell and can be seen as a series of small dots or as highly elongated fibril type structures (Figure 2.1). [16] Their molecular composition is similar to that of focal adhesions and is characterized by the presence of increased levels of tensin and $\alpha_5\beta_1$ integrins, while there are relatively little to no $\alpha_v\beta_3$ integrins in these adhesions. [16] Fibrillar adhesions, attached to the underlying FN, are pulled to the cell center via their association with the actin cytoskeleton (Figure 2.1). During this process the bound FN is stretched and unraveled exposing cryptic adhesion sites and binding domains for FN and other ECM proteins. [43]

Even though the molecular composition of these diverse adhesion types is different they contain many of the same adaptor and regulatory proteins. Adaptor proteins containing multiple protein binding sites are responsible for recruiting both structural and signaling molecules and include paxillin, p130Cas, SH2/SH3 adapters (Grb2), and calcium-dependent calpain. Some of the cytoskeletal associated proteins responsible for cytoskeletal linkage to the adhesions include vinculin, talin, α-actinin, and filamin. These proteins provide distinct binding and nucleation domains for both actin and tubulin via association with a number of cytoskeletal linking proteins that control actin dynamics such as gelsolin, tensin, radixin, VASP, and zyxin. Regulatory proteins associated in focal adhesions, mainly p125FAK (focal adhesion kinase), p60Src, Csk, PKC, PI3K (phosphatidylinositol 3-kinase), p59ILK, and various phosphotases (Shp-2, PTP-PEST, PTEN, and PTP1B phosphatase), are responsible for integrin-mediated signaling cascades. These signaling molecules have been implicated in basic cellular events including adhesion, cell spreading, cell motility, and cellular proliferation. [11,42]

The previously discussed events concerning the formation of large focal adhesions and fibrillar adhesions may not be entirely representative of what happens *in vivo*. As the possibility of creating tissue engineered constructs becomes more realizable, differences in properties between cells cultured in 2-D and 3-D environments are being explored. Differences in cell morphology and increased motility and proliferation have all been observed in 3-D culture systems. [43,46-48] Cells cultured on 2-D surfaces spread out flat and display a polarity with respect to where cell-matrix adhesions are formed that is not observed in cells in 3-D matrices. [49] Furthermore, it has been shown that epithelial cells grow to form a monolayer on 2-D surfaces but form aggregates, make cell-cell contacts, become polarized, and form spherical acini in 3-D matrices. [49] Amoeboid migration is seen in some cells in 3-D where the cells use non-adhesive means to adapt their cell shape to the surrounding matrix and match their shape to the path of least resistance to use propulsive squeezing for motility. [49] Some of these observed cellular changes may be induced by changes in adhesion composition and levels of FAK phosphorylation. [48] 3-D matrix adhesions are composed primarily of $\alpha_5\beta_1$ integrins, paxillin, vinculin, and FAK. [48] Furthermore, these 3-D matrix adhesions display lower levels of FAK phosphorylation and Rac activation compared to cell on 2-D surfaces. [48,49] This low level of FAK activity may be responsible for the increased proliferation response observed in cells cultured in 3-D systems. [50] Matrix elasticity also influences adhesion properties of cells cultured in 3-D matrices. Cells cultured in cross-linked cell-derived 3-D matrices revert back to using adhesions similar to those seen in 2-D culture systems. [48] These findings demonstrate that adhesion composition and signaling cascades regulated by adhesions can be influenced by the spatial arrangement of ECM binding sequences and the overall matrix stiffness or elasticity. Based on these

results, the occurrence of very large focal adhesions may be a consequence of culture in 2-D rigid systems and not indicative of *in vivo* adhesions.

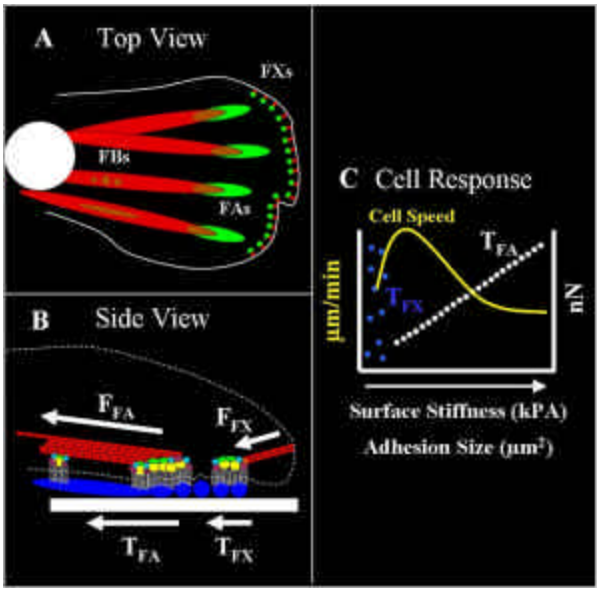

Figure 2.1: Cell Adhesion Types, Location, and Force Generation: Cells create three primary types of integrin mediated adhesions, focal complexes (FXs), focal adhesions (FAs), and fibrillar adhesions (FBs). FXs are typically located at leading edge of cells (A) and act as docking points for F-actin polymerization (A,B). The traction force measured at FXs can vary greatly (blue dots in C) and is reflective of membrane resistivity as the F-actin pushes against the membrane (B). FXs mature into FAs with a typical size > 1 µm2 that are terminating points for actin stress fibers (A,B). The traction force created by FAs is linearly dependent on adhesion site size (C) and created through Rho-mediated actomyosin contraction of actin stress fibers (B). FBs link to the underlying FN fibrils and through association with actin stress fibers pull the FN apart, a term known as fibrillogenesis (A,B). Cell speed is known to have a biphasic relationship to adhesion site size, the amount of traction force created, and to surface elasticity.

2.4.2 Intracellular Force Generation and Adhesion Site Signaling

Cells display the ability to create highly localized points of intracellular force that result in propulsive and contractile forces necessary for cell spreading and motility. The relationship between intracellular force generation and signaling cascades initiated and governed by adhesion sites will be discussed in the following section. It is known that many cell types are adhesion dependent, meaning that their attachment and prolonged adhesion to surfaces is crucial for survival. The adhesion process governed by protein plaque interactions with cytoskeletal components inherently produces highly localized points or foci of force generated by the actomyosin contractility of actin fibers. Naturally, the question that arises is, ow do these highly focused points of force result in signaling cascades? Currently, many force-mediated mechanisms that control signaling are thought to exist. To address this issue, the amount of force that cells apply at adhesions and possible force-sensitive signaling mechanisms are discussed in this section.

How Much Force do Cells Produce?

Many studies have come to the same conclusion that the amount of force applied to the substrate by individual focal adhesions, adhesions with a typical size ranging from 1 to 15 μm^2, directly corresponds to the contact area of the adhesion (Figure 2.1 C).[51-54] This relationship shows that cells apply a constant stress of 5.5 $nN/\mu m^2$ to the underlying surface through adhesion sites regardless of the adhesion site size.[51] Actomyosin mediated contraction plays an important role in this process and if interrupted by inhibitors, both the force and concentration of adhesive components drop simultaneously, supporting the idea that force applied to cellular adhesion sites

induces conformational changes of adhesion components to reveal binding sites for other molecules.[51] Some candidates for force sensitive adhesion components include vinculin, talin, pp60src, and zyxin.[55-59] While the force to size relationship holds true for focal adhesions it does not apply to smaller focal complexes with a typical size of 0.25 μm^2. These small, highly dynamic adhesions often apply extremely high forces for their size and can create forces equal to focal adhesions 12 times larger (Figure 2.1 C).[53,60] Furthermore, while inhibition of actomyosin contractility abolishes focal adhesions it has no effect on focal complexes, hinting to a different and to date not fully understood mechanism of force generation for these very small adhesions.[15,61] This indicates that focal complexes and focal adhesions associate with different subsets of actin cytoskeletal organization. Focal adhesions clearly interact with large actin stress fibers and focal complexes associate with small F-actin fibers in lamellapodia. Focal complexes, but not focal adhesions, contain Arp 2/3, a molecule responsible for actin polymerization and branching in lamellapodia.[55,62] These complexes also contain talin, a proposed molecular clutch that in combination with myosin V, zyxin, and perhaps Ena/VASP facilitate filipodia extension of the cell membrane during cell spreading and motility.[63,64] The association of focal complexes with F-actin near the leading edge explains why the inhibition of actomyosin contraction does not induce the dissolution of these complexes as it does for focal adhesions. Furthermore, the generation of large traction forces at these small complexes may give insight into their role during lamellapodia and filipodial formation. Since Arp 2/3 nucleates actin branching and new sites of polymerization, and since talin acts as a molecular clutch to allow for actin slippage, the association of these molecules with focal complexes indicates that the complexes act as docking points for F-actin polymerization thereby allowing actin driven

membrane protrusion during lamellapodial driven cell migration. [45,63-67] The resistance provided by the cell membrane as the polymerizing actin pushes against it may be translated to the complexes and reflected in the traction studies as local points of high force (Figure 2.1). Furthermore, the adhesion components that compose these small adhesive complexes create shells around F-actin rich cores that make up podosomes for enzymatic release during cell migration through tissue, further implicating their importance in motility and early adhesion site formation. [68,69]

Adhesion- and Force-mediated Intracellular Signaling Cascades

Integrins alone, without forming adhesions, play an important role in signaling. The accumulation of proteins and signaling molecules to clustered integrins is a hierarchical process including phosphorylation, ligation with ECM components, and linkage to the cytoskeleton. [70] The clustering of integrins alone without ligand ligation or phosphorylation induces the accumulation of both FAK and tensin. [70] If the same site is ligated with ECM components, but not allowed to be activated through phosphorylation, a number of cytoskeletal linkage proteins including talin, a-actinin, vinculin, and tensin and one kinase, FAK, aggregate to form an intracellular protein plaque. [70] If removal of integrin ligation to ECM components is induced and the plaque allowed to phosphorylate, then the clustered integrins induce the accumulation of 20 signal transduction molecules while only one cytoskeletal associated molecule, tensin, is present. [70] Furthermore, this non-ligated phosphorylated complex displays the ability to initiate both ERK and SAPK/JNK signaling cascades. [70] Finally, if this activated cluster of integrins and signaling molecules is allowed to ligate to ECM, there is a massive influx of cytoskeletal associated proteins that allow for integrin linkage to the cytoskeleton. [70]

This demonstrates the hierarchical process of adhesion formation from the initial clustering of integrins and shows that the creation of fully formed adhesions includes integrin aggregation, integrin occupancy, tyrosine kinase activity, and association with actin cytoskeleton. [70]

Once an adhesion is fully formed, the application of force through actomyosin contraction can be applied to the ligated integrin cluster or focal adhesion site. The force exerted by a single focal adhesion site can range from 10 to 60 nN depending on the location, size, and type of adhesion. [51,53,71,72] Back calculation of the forces exerted at focal adhesions shows that the force applied by a single integrin is similar to that produced by a single myosin molecule. [51] It has been shown that integrin signaling is dependent on cellular contractility, [73-75] but the underlying mechanism or exact force sensitive molecules involved in this process are still unknown. Applied force may induce unfolding of integrin domains [76] or adhesion associated molecules. [77] Some hypothesize that the amount of force that a cell applies to adhesion molecules can mediate molecular interactions at that site acting as a "feedback response". [51] Support for this idea comes from the discovery of a few force-sensitive adhesion components that include vinculin, talin, pp60src, and zyxin. [55-59] Vinculin, talin, and pp60src exist in both active (open) and inactive (closed) forms. [55,56,58] These conformational changes regulating activity may be mediated by mechanical force but it is known that PIP_2 also promotes the activation of both vinculin and talin. [56,57] The idea of a force sensitive protein or protein aggregate has been hypothesized for a long time and while some adhesion associated proteins display force dependence, the golden goose per se, has yet to be discovered. The discovery of cryptic binding sites in FN that are revealed

during FN unfolding via association with $\alpha_5\beta_1$ integrin movement through actomyosin contraction have further fueled the search. [77,78]

FAK Mediated Signaling

FAK is the only kinase that localizes to non-ligated, unphosphorylated integrin clusters and has shown to play a key role in both adhesion and actin dynamics and cellular proliferation. [32,50,70] As FAK clusters into adhesions, the molecules cross-phosphorylate themselves creating distinct binding sites for members of the Src family of tyrosine kinases. [79] The bound Srcs in turn phosphorylate FAK at specific residues creating docking platforms for additional signaling molecules that allow for FAK mediated control over Ras and MAPK pathways that in turn modulate changes in gene expression and protein activity to induce changes in cell behavior. [79] Furthermore, the Src kinases have also been shown to regulate force generation by inhibiting cytoskeletal interactions with adhesion components and Src knockout cells do not spread well. [74] This direct link with FAK may provide FAK the ability to disassociate adhesions by interacting with Src to disassemble cytoskeleton linkage to adhesion sites, as FAK null cells display highly increased levels of adhesion formation and impaired motility. [32] The reintroduction of FAK leads to the dynamic assembly of actin and adhesion sites thereby reinstating normal spreading and motility. [32] Surprisingly, the distributions of vinculin, paxillin, and talin remain unaffected during the knockout and reinstatement of FAK, hinting that integrin ligation is unaffected. [32] This implies that Src family kinases provide the necessary linkage between cytoskeletal components and adhesion sites and that the dynamic relationship of these components is regulated by FAK signaling. More evidence of FAK's role in cytoskeletal linkage has been demonstrated with cells lacking Shp2. [80]

These cells display a higher density of small focal complexes deficient in α-actinin.[80] Force-dependent strengthening of these adhesion sites correlated with α-actinin assembly and decreased adhesion site dynamics and it was demonstrated that FAK played an important role in regulating this process.[80]

FAK is a rather complicated molecule and displays sensitivity to both the extent and location of phosphorylation. Phosphorylation of specific residues induces interactions with specific signaling molecules thereby giving FAK the ability to control cell behavior depending on its state or local of phosphorylation. While it has been shown that FAK null cells can not move,[32] many cancers overexpress FAK leading to overly increased motility states.[79] A link between cell proliferation and FAK has also been established.[50] The overexpression of FAK leads to growth arrested or uncontrolled cell proliferation,[50] again indicating its possible role in cancer. Surprisingly, FAK null cells also display unregulated proliferation, but if non-phosphorylatable forms of FAK are inserted, proliferation control is re-established.[50] These findings demonstrate that FAK plays multiple roles in proliferation, if it is not there or over-expressed, proliferation is greatly increased; if it is present but inactive then proliferation is regulated.[50]

Other Possible Force-Mediated Signaling Mechanisms

It was discovered that the unbinding kinetics of zyxin are increased when force is dissipated at adhesion sites[59] thereby allowing it to move to the nucleus and alter gene transcription of endothelin-B receptors.[81] The combined increased expression of endothelin-B receptors on smooth muscle cells (SMCs) and release of endothelin-B from endothelial cells in response to tissue injury results in vascular remodeling.[81] This coordinated response between SMCs and ECs demonstrates how changes in applied

force at adhesion sites can lead to changes in gross cell behavior and to physiological changes in tissue. Another possible mode of force-mediated signaling is from the application of local stresses on the cell membrane at adhesion sites that could possibly open stress sensitive ion channels thereby increasing the influx of Ca^{2+} at cellular adhesion sites.[82-84] Whether this increased influx is due to cytoskeletal tension applied on the membrane, direct association of ion channels with integrins, or other possible mechanisms remains unresolved.

Summary

In summary, there appear to be many possible force-mediated signaling mechanisms that can influence signaling both locally, at the sites of adhesion, and globally throughout the cell. In reality, the combination or "synergistic" interplay between these multiple mechanisms and between other signaling mechanisms like soluble factor binding is what ultimately controls cell behavior. Despite the fact that all of the relationships between intracellular force generation and adhesion site maturation are still not fully understood, their importance in governing intracellular signaling cascades and their implications on gross cell behavior are obvious. As new cell engineering techniques are needed to meet the demands of biomedical applications, scientists have started probing the possibility of regulating adhesion formation as a tool for cell engineering purposes.[1] So the question becomes, How can you engineer surfaces to induce desired cell behavior? Insight into answering this question is discussed in the following section.

2.5 Engineering Cell Behavior via Cell-Surface Interactions

Much research in recent years has focused on cellular interactions with biomaterials structured on the macro and micrometer length scales. Although subcellular in size, these material structures that confine cell adhesion to desired regions of controlled size have shown profound influences on cellular proliferation, motility, and stem cell differentiation.[85-92] Recent studies employing biomaterial surfaces that control cellular adhesion on the molecular and supramolecular scales have also demonstrated interesting influences on cellular behavior. Surfaces presenting adhesion peptides in varying densities, with different peptide to peptide spacing, surfaces that present clustered adhesion peptides, and surfaces with varying topography on the nanometer scale have all been used to gain insight into adhesion formation and subsequent downstream cellular effects induced by manipulating adhesion properties.[93-99] This section discusses some of the findings linking adhesion and cell behavior using engineered surfaces with controlled properties.

2.5.1 Protein Influence on Cell Behavior: Concentration, Orientation, Spatial Arrangement, and Adhesive Area

Protein Influence

Since integrin expression is regulated by which peptide binding sequences are available for cell attachment, and integrin expression, adhesion composition, and signaling are linked, the most straight forward way to engineer cell behavior is to change the protein that cells adhere to. This approach has been used to induce capillary morphogenesis of ECs.[100] ECs seeded on collagen form capillary-like structures through increased activation of Src kinase and Rho GTPase pathways via association with β_1

integrins.[100] Culturing of ECs on laminin induces increased Rac activation and the cells do not undergo any morphological transformations.[100] These differences in cell behavior can be directly linked to differences in signaling cascades initiated by changes in adhesion composition. A detailed explanation of each ECM component's influence on signaling and cell behavior with respect to angiogenesis is reviewed in detail in Ref 100.[101]

Protein/Ligand Concentration Influence

While different proteins have an influence on adhesion composition and associated signaling cascades, cells also display dose-dependent responses to concentrations of single proteins. Rather than probing chemical influences on cell behavior, these studies explore how varying surface protein concentrations influence cell adhesion and give insight into how cells respond to these surfaces with respect to adhesion formation, cell spreading, proliferation, and motility. It has been shown that varying levels of adhesion peptide density, GRGDY and GRGDSP, as well as varying concentrations of full proteins have an influence on cell adhesion, spreading and proliferation.[98,102] Both fibroblasts and ECs display a relationship between ligand surface concentration and cell spreading.[98,102] Fibroblasts achieve maximum spreading when the peptide density is at least 6 ligands/μm^2 (12,000 ligands/cell) with a corresponding peptide to peptide spacing of 440 nm.[98] While these low peptide densities supported cell spreading they did not induce the formation of well-defined focal adhesions or stress fibers, yet cells were still able to make focal contacts, an early form of cell adhesion. Cells seeded on surfaces with higher concentrations of ligand did not spread more yet they did form large focal adhesions and assembled a well organized

actin fiber network.[98] The results imply that focal contact formation into well-defined adhesion sites requires a peptide to peptide spacing of at least 140 nm.[98] Further investigations into the relationships between protein concentration, cell spreading, and proliferation have shown that cell spreading and proliferation are directly linked.[102] Both spreading and proliferation are greatly impaired in cells seeded on surfaces displaying low surface concentrations of FN, less than 550 FN/μm^2.[102] The idea that protein surface concentration is important in regulating proliferation is somewhat true but misleading. In fact, it seems that the ability of a cell to quickly cluster integrins to form well-defined adhesions is more important for initiating cell attachment[6,99] and maintaining long term proliferation, regardless of the protein surface density.[74] Studies older than 10 years or so concerning the relationship between protein surface density and cell behavior are not entirely accurate due to the lack of micro- and nanofabrication techniques to precisely place proteins in desired locations, although attempts to produce well-defined areas of ECM were undertaken.[102]

The idea that the local density of ligands is more important than the overall density has been suggested. To date, Spatz *et al.* have performed studies with the highest precision over RGD placement on a surface to probe cell adhesion and spreading.[99] Using micelle nanolithography, cyclic RGDfk peptides were spaced either, 28, 58, 73, or 85 nm apart. It was demonstrated with a number of cell types (MC3T3 osteoblasts, REF52 fibroblasts, 3T3 fibroblasts, and B16 melanocytes) that an integrin binding spacing greater than 58 nm resulted in highly decreased cellular attachment and spreading, and led to a reduction of well-defined focal adhesions and stress fiber networks.[99] To separate integrin spacing from ligand density influences, "micro-nanostructured surfaces" presenting the same ligand spacing but varying overall

densities were created with additional e-beam lithography steps.[99] Fibroblast adhesion to these surfaces demonstrated that integrin clustering is much more important than overall ligand density to induce focal adhesion formation, cytoskeletal organization, and subsequent cellular attachment.[99] Since all of the cell types utilized in this study exhibited the same phenomenon, it seems that a universal trend exists for adherent dependent cells and that integrins can not be linked or provide the necessary docking platform for the recruitment of adhesion components when spaced further than 60 to 70 nm apart. Interestingly, this integrin spacing corresponds to the typical range of sizes and repeats found in key adhesion molecules such as fibronectin, collagen, and talin.[79] The results discussed in the work presented here verify that local ligand density and the ability to quickly cluster integrins to form adhesions is more important for initial cell attachment and long term proliferation than the overall surface density of ECM.[6]

Cellular Corals to Control Cellular Adhesion Area

Since the type, spacing, and density of adhesive ligands has an influence on adhesion formation, it makes sense that the total adhesive area presented to cells for attachment may also have an influence by limiting the number of adhesions formed. Elaborate studies using soft lithography[103-106] to direct the placement of thiols,[107-109] full proteins,[110,111] or cells[112] have allowed for the exploration of the relationship between total adhesive area and the underlying geometry of adhesive proteins on the micrometer scale and the influence of these parameters on cell behavior. Microcontact printing studies have shed light on the relationship between total adhesive area and downstream cell behavior and indicate that for cells to maintain their function in culture they should feel as though they are in physiological relevant tissue.[113] As the total

available area of adhesion increases, so does proliferation, while cell function simultaneously decreases.[113] Furthermore, long term cell function can be maintained by confining cells to small adhesive areas during which proliferation is suppressed.[113] This implies that proliferation and de-differentiation of cells is tightly linked and is supported by other studies with similar conclusions,[85,113-118] although it should be noted that increased cell proliferation may be indicative of a specific phenotype for certain cell types. Studies with ECs have shown that these cells respond to the geometry of the available adhesive area.[85] Cells can be coerced into switching between growth, apoptosis, and differentiation by simply changing the geometry of the presented adhesive area.[85] If ECs are seeded on small ECM islands, less than 500 μm^2, then the cells undergo apoptosis, if greater than 1,500 μm^2 proliferation is induced, and if intermediate values of area are displayed for attachment created by using 10 μm wide lines, then ECs shut off apoptosis and proliferation and form capillary tube-like structures with a central lumen.[85] Furthermore, if line widths are increased to 30 μm, then no capillary formation is induced and the cells behave as if on large islands and display increased proliferation.[85] Further studies into these relationships have confirmed that the underlying adhesive area and geometry allows for geometric control of cytoskeletal formation, FN deposition, and ultimately cell life and death.[90,119]

Surface Chemistry Control over Fibronectin Confirmation

The influence of changing whole proteins or the concentration of a single type of protein on cell behavior and how cells sense and respond to spatial arrangement of proteins or adhesive peptides have been discussed. The following section describes how surfaces can be tuned to induce alterations in the functional presentation of major

integrin binding domains of adsorbed FN and how these changes can be harnessed to induce changes in cell proliferation and differentiation.

The shape of absorbed FN is influenced by the surface properties of the underlying material. Adsorption of FN to hydrophobic surfaces induces a compact confirmation, while an elongated strand-like confirmation is observed on hydrophilic surfaces.[120] This phenomenon is the underlying principle in modulating integrin binding activity to FN adsorbed to materials with varying levels of surface energy. In general, the more compact form should hide various integrin engagement sites while the elongated form should leave most of these sites accessible for integrin binding. Conformational changes of FN as induced by the surface energy properties of the underlying chemistry influence the quantity of bound $\alpha_5\beta_1$ integrins but have little influence on $\alpha_v\beta_3$ integrins.[114,118] Using alkanethiol SAMs on gold with varying functional groups it was shown that the elongated FN shape on hydrophilic surfaces allows for increased binding of $\alpha_5\beta_1$ integrins compared to the compact form on hydrophobic surfaces.[121] The induced changes in integrin binding led to changes in focal adhesion composition and site specific levels of FAK phosphorylation.[117] Higher concentrations of talin, alpha-actinin, paxillin, and tyrosine-phosphorylated proteins coincided with increased $\alpha_5\beta_1$ integrin binding.[117] Furthermore, adhesions formed on hydrophilic surfaces rich in $\alpha_5\beta_1$ integrins with high levels of FAK phosphorylation resulted in increased proliferation and adhesion strength.[114,117,118] Interestingly, proliferation and differentiation show opposite trends with respect to integrin expression, similar to the trends observed on micropatterned surfaces. Using myoblasts and osteoblasts it was demonstrated that proliferation decreases with decreasing levels of $\alpha_5\beta_1$ integrins while differentiation increases as $\alpha_v\beta_3$ integrins become the dominant mechanism of attachment.[114,117,118]

These studies indicate integrin-type dependent signaling pathways that can have influence over proliferation, differentiation, and adhesion strength. It is interesting that increased adhesion strength coincides with increased FAK phosphorylation and higher levels of structural and adaptor proteins and points to the relationship between intracellular force generation and the initiation of specific signaling cascades.

Summary

Through the studies described in this section, it is clearly evident that many aspects of protein presentation can influence integrin usage and adhesion composition, and that these changes can induce profound changes in cell behavior. Incorporating these findings to engineer biomaterial surface properties with respect to the surface energy and geometric display of adhesive ligands could be harnessed to engineer cell behavior on the material itself. Further insight into the mechanical properties of biomaterials and how varying levels of elasticity can be sensed by cells and used to control their behavior is discussed in the following section.

2.5.2 Elastic Surfaces

Various approaches to control cell behavior via cell-surface interactions with surfaces that manipulate protein properties have been discussed. Another aspect of surfaces, in particular elasticity, is reviewed in the following section. This section discusses how surfaces with varying elasticity influence cell behavior and how they may produce more *in vivo* like cell responses. Most studies regarding cell adhesion and its influence on cell behavior have been conducted on 2-D rigid surfaces but these studies, while 2-D in nature, mimic the elasticity of natural ECM.

Cells display the ability to sense elasticity to a depth of approximately 0.5 to 1 μm as indicated by cell spreading studies on thin, soft films. [122] Since the generation of intracellular force results in the production of traction forces, then very soft surfaces should not be able to resist applied cellular forces at adhesion sites and should therefore impose the opening or activation of force-sensitive adhesion components such as vinculin, talin, and pp60src as discussed earlier. If these components can not be activated on soft surfaces or are partially activated on surfaces with medium levels of elasticity then there should be some influences on adhesion and cytoskeletal formation and the associated signaling cascades that regulate cell behavior, and indeed there are.

Cells cultured on soft substrates display diffuse and highly dynamic adhesions as opposed to cells on rigid surfaces that form larger, more static adhesions. [39,40,123] While traction forces increase linearly with increasing substrate stiffness and focal adhesion size, cell motility displays a biphasic relationship with substrate stiffness. [71,124,125 122,123] Studies with elastic surfaces have shown that faster cells with smaller adhesions apply lower levels of traction force than well-spread static cells with large adhesions. [124] Other studies have shown that nascent adhesions at the leading edge can apply very high forces that are not proportional to their size indicating that the location of small adhesions may be an important parameter to include in traction studies. [53,60] The increases in applied force and adhesion size on more stiff surfaces coincide with increased tyrosine phosphorylation of adhesion proteins. [126] Studies show that dynamic, diffuse adhesions in ECs cultured on soft substrates correspond to more diffuse actin networks and these cell shows suppressed formation of actin stress fibers. The formation of larger static adhesions on hard surfaces corresponds to the formation of dense, thicker actin stress fibers. These differences in adhesive and cytoskeletal

properties as induced by surfaces with varying elasticity must be force dependent since there were observed differences in the amount of traction force produced. [39,40,123] More proof that cytoskeletal organization depends on substrate stiffness comes from the finding that there is a range of stiffness that results in an optimal setting for the striation of actomyosin in muscle cells and not surprisingly, the optimal elasticity value found experimentally matches that of natural muscle tissues. [127,128]

Since cells recognize and respond to the underlying matrix elasticity, can creating surfaces with varying elasticity be used to harness cell behavior? Experiments involving differentiation of naive mesenchymal stem cells revealed that stem cell differentiation can be directed by varying levels of matrix elasticity. [122] The seeded cells took on phenotypes relating to elasticity measures similar to *in vivo* tissues; cells on soft matrices became neurogenic, whereas cells on hard matrices became osteogenic, and cells cultured on surfaces with intermediate elasticity became myogenic. [122] In the first week of culture, this elasticity guided differentiation could be reversed using soluble factors but after several weeks the cells had committed to specific lineages and could not be reverted with soluble factors. [122] The blocking of myosin activity inhibited the matrix elastic driven differentiation thereby implicating the importance of intracellular force generation in this process. [122] The stiff substrates promoted adhesion site growth and increased expression of α-actinin, filamin, talin, and FAK. [122] Actin formation followed the same trend as adhesion formation, less actin on soft surfaces and less concentrated adhesions. [122]

These studies show the importance of intracellular force generation on signaling and provide further evidence of force-mediated signaling within cellular adhesion sites and hint towards the existence of a force sensitive molecular component in adhesion

sites that controls cellular signaling cascades in a force dependent manner as discussed earlier.

2.5.3 Nanostructured Surfaces

While many interesting results have come from using surfaces structured on the micrometer scale, the explosive interest in nanotechnology and its applications to biotechnology have led to the fabrication of nanostructured surfaces for exploring cell interactions with nanoscale features. Although many nanopatterning techniques exist, relatively few have been implemented for detailed cell studies and most studies have been performed only on surfaces displaying nanoscale topography, not surfaces that provide direct control over adhesion site growth as presented here.

Nanotopographical Surfaces

Nanotopographic surfaces for studying cell behavior have been fabricated using polymer demixing,[129] embossing,[129] photolithography,[129,130] reactive ion etching,[131] colloidal lithography,[132-134] cast molding,[135] and electropolishing, anodizing, and acid etching of metallic surfaces.[136] It has been shown that numerous cell types recognize and react to nanotopography, including alignment to grooves,[130] and compared to flat surfaces, cells exhibit decreased adhesion site formation, decreased adhesion strength, and reduced spreading on nanopit arrays[137-139] as well as increased cell adhesion, spreading area, and cytoskeletal formation on raised nanopatterns.[93,140] Increased filopodia formation,[141,142] Rac localization to the cell periphery,[93] and an upregulation of genes associated with cell signaling, proliferation, cytoskeletal components, and the production of ECM[140] have all been documented on nanotopographical surfaces. While

ECs and fibroblasts show increased cellular responses, as indicated in the previous sentence, to decreasing nanotopography,[93] osteoblasts behave oppositely, displaying increased adhesion, proliferation, and function with increasing topography.[135,136,143-145] There is some discrepancy in these observations and others have reported that a combination of nano- and microtopography is necessary for increased proliferation in human bone-derived cells (MG63 cells).[136] Furthermore, the observed increases in osteoblast proliferation on nanotopographic surfaces may be a consequence of enhanced vitronectin adsorption rather than a consequence of topography.[145]

Although surfaces with varying levels of nanotopography have given insight into the effects of nanoscale features on cellular behavior, without the use of chemical modifications they do not provide a basis for understanding how surface chemistry and the confinement of ligands to small nanoscale islands influences cellular behavior. Furthermore, there are indications that changes in nanotopography induce the adsorption of specific proteins, implying that the observed changes in cell behavior on nanotopographical surfaces may be reflective of the type or density of protein present and not a consequence of changes in topography.

Chemically-Defined Nanopatterned Surfaces

Micropatterning of proteins to form adhesive islands of varying size, spacing, and geometry have been implemented to demonstrate the influence of adhesive area and underlying spatial geometry on cell behavior. The extension of protein patterning techniques to the nanoscale has been much more difficult and while many nanofabrication techniques exist relatively few have been implemented for systematic cell studies.

Over the past few years there has been intense interest in creating surfaces that display nanometer-sized features of isolated biological molecules, namely DNA and proteins, for a broad range of applications. While many existing fabrication techniques can produce arrays of biological material with high precision and accuracy, only a limited number fit the necessary criteria for detailed cell-adhesion studies. To investigate cell-surface interactions, more specifically integrin engagement and focal adhesion formation, it is crucial that the surface fabrication process provide the ability to place the desired adhesion ligand in clusters with a range of sizes, since adhesion sites can be as small as three integrins binding to three RGD sequences or as large as clusters of thousands of integrins spanning lengths of 10 μm or more. Micelle nanolithography and variations of electron beam and AFM based lithography techniques provide the highest precision in creating very small areas of patterned SAMs or proteins.[99,146-148] While micelle nanolithography has proven to be a powerful technique for exploring individual interactions of immobilized RGD sequences with integrins, it does not allow for the formation of larger adhesion sites that incorporate the interactions of many integrins with the surface unless further e-beam lithography steps are applied. Even then, it neglects cell interactions with full FN proteins, a dynamic interaction that may influence cell behavior upon the exposure of cryptic binding sites through cell-induced stretching.[43]

Other techniques promise to be useful for cell analysis, but so far have not been implemented. These include capillary or imprint lithography with PEG,[149] molecular assembly patterning by lift-off (MAPL),[150,151] and variations of NSL.[152,153] Protein and cell adhesion have been observed on PEG pillars, but due to the repulsive properties of PEG, the level of cell adhesion was significantly lower than adhesion to similarly treated

glass surfaces.[149] It is still a challenge, however, to produce nanopatterned dual-functional surfaces that are large enough for statistical cell studies. Serial lithography techniques such as dip-pen nanolithography,[154-158] other scanning probe lithography techniques,[159-162] and electron beam lithography[146-148] are too time consuming in their fabrication to allow for systematic cell studies, although parallel versions of dip-pen nanolithography are being developed.[158]

Parallel patterning techniques such as imprint lithography,[163,164] micelle nanolithography,[165,166] particle lithography,[167] and capillary lithography[149] are better suited for quickly fabricating nanostructured surfaces over large areas. For controlled chemical functionality at the nanometer scale, these fabrication processes have to create surface nanopatterns of ECM components, either full proteins or peptide sequences, which are adsorbed or covalently linked to the surface in nanometer-sized patches surrounded by a passive background, a background that does not support protein adsorption or cellular attachment.

To date, only three of these nanopatterning strategies have been used for cell adhesion experiments.[99,149,156,168] It has been demonstrated that surfaces presenting nanopatterned proteins support cell adhesion.[149,156] Furthermore, adhesion strength is increased and cells show higher motility on small clusters of RGD peptides compared to equivalent densities of homogeneous distribution, although only statistical averages of cluster distances could be controlled.[97,169,170] To date, only micelle nanolithographic patterned surfaces are able to control the placement of individual integrins. With these surfaces it was revealed, for several cell types, that an integrin spacing grater than 58 nm significantly decreased cellular attachment and spreading and led to a reduction of well-defined focal adhesions and stress fiber networks.[99] It was also shown that

integrin clustering is more influential than ligand surface density for cellular adhesion, focal adhesion formation, and cell survival.[99] Recently these surfaces were implemented to study the influence of integrin spacing on focal adhesion dynamics, cell spreading, and cell motility.[168] Cells cultured on surfaces with RGD peptides spaced 108 nm apart exhibited delayed spreading, erratic, non-persistent, and higher levels of migration, and reduced levels of zyxin incorporation into adhesion sites compared to surfaces with 58 nm RGD spacing or homogenously RGD coated surfaces.[168] Furthermore, increased spacing between integrins induced the formation of highly dynamic adhesion sites and at early time points, reduced levels of cytoskeletal formation.[168] The simultaneous discovery of low levels of adhesion associated zyxin and reduced cytoskeletal formation[168] confirms earlier studies relating increased zyxin dissociation from adhesion sites to reductions in applied force.[59]

Summary

The topics covered in this section shows that nanopatterning of RGD peptides to control integrin spacing and clustering events can have a profound influence on adhesion composition, cytoskeletal formation, adhesion strength, and cell motility. While these studies give some insight into adhesion formation, the ability to cluster integrins into larger sites with well-controlled size and spacing may be useful in discovering the influence of limiting adhesion site size or maturation on downstream cell behavior.

2.6 Discussion

The cell adhesion process including the maturation of adhesions, generation of intracellular forces, application of traction force, and force-mediated signaling are all related and together form a complex feedback mechanism based on force-mediated unfolding of adhesion proteins and their interplay with signaling molecules. Harnessing control of intracellular signaling cascades by implementing surfaces that manipulate cell adhesion on both the micro and nanometer length scales have shown to have profound influences on cell behavior. While much knowledge about the influence of integrin spacing and clustering has been attained with surfaces presenting very small nanoscale features, there have not been any experimental investigations to analyze the range of cluster sizes from 40 to 300 nm, corresponding to about 4 to 250 FN per adhesion cluster. This size range could be key to understanding the importance of the immediate aggregation seen with ligand trimers, [171] the different levels of integrin activation found at early adhesions, [172] and the early processes in the maturation of focal complexes into adhesions during motility [173] and spreading. [174] One would therefore also expect adhesions restricted to the size range of 40 to 300 nm to allow for an important range of forces per adhesion cluster and the impact on cell adhesion, cytoskeletal development, and cell motility to be investigated.

This work introduces a nanopatterning technique based on nanosphere lithography (NSL), [175,176] which has been used as a template for the fabrication of protein [167] or chemical arrays, but here is expanded to use orthogonal functionalization to tightly control the growth of cellular adhesion sites with respect to their size. The technique allows for the production of large surface areas (cm^2) of nanoislands whose size and spacing is controlled by the sphere diameter and by the use of monolayer or

bilayer mask configurations.[167,176,177] Thiolated gold nanoislands surrounded by poly(ethylene glycol) (PEG) passivated areas were adsorbed with FN. Full-length FN proteins instead of RGD-containing peptides were used for these studies so that the synergistic and cryptic integrin binding domains could be included in the adhesion studies, as these domains are necessary for the formation of fully mature fibrillar adhesions. Since the goal of this project is to present well-defined nanoscale FN adhesion sites for cell attachment, the surfaces were characterized using X-ray photoelectron spectroscopy (XPS), atomic force microscopy (AFM), and cell-seeding studies to show that FN adsorbs specifically to the nanopatterned islands but not to the PEG-treated background. Surfaces with varying adhesion site properties with respect to size, spacing, and overall density were implemented to characterize the influence of limiting adhesion site size on focal adhesion formation, cytoskeletal formation, spreading, proliferation, and motility. This combination of nanopatterning and dual surface functionalization provides an experimental platform that can be used for future studies relating adhesion site maturation and intracellular force generation to changes in adhesion site regulated signaling cascades.

2.7 Conclusion

Combining all of these factors together, one can see that focal adhesions and their associated protein complexes are major regulators of cellular attachment, cytoskeletal arrangement, and overall cell behavior controlled via adhesion-mediated signaling cascades leading to different cellular phenotypes. By manipulating cellular adhesion sites through cell-surface interactions with engineered surfaces, one can design biomaterials that induce a desired phenotype in adherent dependent cells.

Unfortunately, a number of existing studies disagree as to which ligand spacing, density, and clustering parameters are important in eliciting varied cellular responses.[98,99] This may be due to the lack of precise control over ligand placement and the use of statistical analysis to determine the surface chemical properties. Fabrication techniques that allow for the production of surfaces with direct control over both nanotopography and chemical functionalization allow for the independent investigation of surface properties on cellular behavior. The focus here was to study changes in gross cellular morphology, cellular proliferation, motility, cytoskeletal organization, and intracellular signaling induced by changes in binding and aggregation events to determine how varying focal adhesion nanogeometry can be harnessed to induce changes in cell behavior and EC phenotype expression.

Chapter 3

Nanopattern Fabrication

3.1 Introduction

The goal of the work presented here is to gain an understanding of how limiting adhesion site size via cell-surface interactions with chemically-defined FN nanoislands can limit adhesion maturation and to explore how this adhesion control can be implemented to modulate changes in cell behavior. To achieve this goal a fabrication scheme to produce nanometer sized protein or peptide islands against a non-adhesive background that provides direct control over adhesion site size had to be determined. While the fabrication of micrometer sized ECM islands is relatively easy using soft lithography techniques such as microcontact printing, [103-112] translating this idea to the nanometer length scale has proven to be quite difficult. Even though many nanopatterning techniques exist, [92,139-161] most are serial in nature and if implemented for these studies, would take too much time to create enough samples to perform all of the proposed experiments. A nanopattern fabrication technique to perform the proposed experiments must meet several requirements. The fabrication process should allow for precise control over the nanopatterns with respect to their size, spacing, topography, and overall surface density, as all three parameters influence cell adhesion and behavior. The technique should also allow for the formation of chemical contrast between the adhesive areas and background, thereby providing the ability to isolate proteins or specific peptide sequences into well-defined nanoislands. The chemically-defined nanoislands should be the only biologically active part of the surface; the cells should not be able to interact with the supporting background. The technique should

also allow for the fabrication of large surface areas of nanopatterns to be produced so that many cells can be analyzed in one experiment to gain enough data for statistical analysis and finally, the technique should allow for quick production time at low costs so that many variables can be changed for systematic studies.

To meet these demands nanosphere lithography was implemented. NSL is a parallel, self-assembly nanofabrication method that allows for the creation of well-defined metallic nanopatterns of controlled topography, size, and spacing on a glass support. The fabrication technique was invented by Dunsmuir in 1982 and at the time coined, "natural lithography".[175] In 1995 van Duyne started implementing the technique to create surface plasmon based sensors and changed the name to nanosphere lithography.[177] Due to its versatility, low cost, and relative ease of implementation, the technique and variations of it have been used to create chemical and protein patterns, several types of biosensors, and to create surfaces for guided nanotube growth.[145,160,169,171-178] This chapter details the ins and outs of NSL and the characteristics of the nano-composite surfaces that were created using this fabrication process.

3.2 Materials and Methods

3.2.1 Nanopattern Fabrication

Plain microscope glass slides (Erie Scientific Company, Portsmouth, NH) were cleaned in piranha solution (H_2SO_4:H_2O_2 3:1) (Fisher Scientific, Pittsburgh, PA) for at least 20 minutes at 85 °C. The slides were thoroughly rinsed with distilled de-ionized (DI) water (Barnstead International, Dubuque, IA) to remove residual acid. NSL was used to create the nanopatterns. Briefly, polystyrene spheres (Duke Scientific, Fremont, CA) of a

chosen diameter were dialyzed for 48 hours, using a 10,000 MW cutoff membrane, (Pierce Biotechnology Inc., Rockford, IL) following the sphere manufacturer's instructions, to remove unwanted surfactants and then deposited in either a monolayer or bilayer configuration onto a clean glass surface using a custom-built capillary deposition machine similar to References 178 and 179. [178,179] Two nanometers of chromium (Cr) (R.D. Mathis, Long Beach, CA) and 8 nm of gold (Au) (Alfa Aesar, Ward Hill, MA) were thermally evaporated onto the surfaces (Denton Vacuum, Moorestown, NJ). After metal deposition, the spheres were removed by sonication in methanol and the resulting nanopatterned surfaces were imaged with AFM and SEM to determine the individual island sizes, areas, spacing between islands, and percent surface coverage. Refer to Figure 3.1 for a schematic of the NSL fabrication process and representative images of M- and B-type surfaces.

3.2.2 Optical Microscopy of NSL Surfaces

After nanosphere deposition, the surfaces were examined in both phase-contrast and dark-field modes using a Leica DM IRB inverted microscope (Leica Microsystems, Wetzlar, Germany) to visually determine areas of acceptable mask formation. After inspection, the desirable surface areas were outlined with a scalpel to produce Au lines around the useable nanopatterned areas, thereby making it easy to locate cells on "good" nanopatterned areas during experiments.

3.2.3 Nanopattern Imaging and Characterization

Atomic force microscope images were acquired using a MFP-3D AFM (Asylum Research, Santa Barbara, CA). Standard silicon cantilevers, AC240TS (72 kHz, Olympus Optical, Japan) were used for alternating current mode imaging, and non-conducting

silicon nitride sharpened cantilevers (Veeco Metrology, Santa Barbara, CA) were used for contact mode imaging. Image processing, analysis, and 3-D enhancement were performed using MFP-3D software in Igor Pro 5 (WaveMetrics Inc., Lake Oswego, OR) and with ImageJ (NIH, Bethesda, MD). The individual island size/characteristic length, island area, island-to-island spacing, topography, and percent surface coverage were measured using the AFM images without performing tip deconvolution.

Scanning electron microscopy (SEM) images were acquired using a Leo 1530 scanning electron microscope (Carl Zeiss MicroImaging, Inc., Thornwood, NY). Two nanometers of Cr (R.D. Mathis, Long Beach, CA) and 15 nm of Au (Alfa Aesar, Ward Hill, MA) were thermally evaporated onto the nanopatterned surfaces (Denton Vacuum, Moorestown, NJ) after the initial metal deposition and sphere removal. Since the SEM allows for larger surface areas to be imaged than AFM, the SEM images were used to quantify and verify the AFM measurements for the percent surface coverage of the nanopatterns. Refer to Table 3.1 for a list of the nanopattern properties created using NSL for the studies presented here.

Name	Sphere Diameter (nm)	Characteristic Length (nm)	Center-to-Center Spacing {Rim-to-Rim Spacing} (nm)	Island Area (nm^2)
1500M	1,500	405 ± 41	883 ± 51 {478}	85,653 ± 17,044
1500B	1,500	222 ± 25	1,534 ± 19 {1,312}	46,550 ± 7,548
1000M	1,000	305 ± 39	589 ± 27 {284}	55,923 ± 7,273
0820M	820	255 ± 24	470 ± 22 {215}	37,049 ± 4,974
0820B	820	201 ± 48	830 ± 22 {629}	12,395 ± 6,502
0500M	500	157 ± 19	285 ± 16 {128}	14,947 ± 2,778
0400M/0420M	400/420	97 ± 9	253 ± 13 {156}	6,485 ± 686
0400B/0420B	400/420	102 ± 16	414 ± 12 {312}	4,675 ± 2,481
0300M	300	94 ± 11	177 ± 13 {83}	5,191 ± 1,298
0300B	300	92 ± 33	308 ± 11 {216}	3,629 ± 1,013
0100M	100	28 ± 4	58 ± 7 {30}	499 ± 151
0100B	100	42 ± 14	106 ± 11 {64}	1,045 ± 601

Table 3.1: Nanopattern Properties: The pattern names are reflective of the sphere diameter used to create the mask and the number of layers of spheres in the mask. M corresponds to surfaces created using a monolayer mask and B to a bilayer mask of spheres. The table lists the characteristic lengths of the nanopatterns, the center-to-center spacing, rim-to-rim spacing, and island area as measured using AFM images. The nanopatterns cover 7.2 ± 0.4 % and 2.3 ± 0.4 % of the surface for M- and B-type layers respectively as determined using both AFM and SEM images. The topography of the patterns for all of the surfaces is 10 to 13 nm as measured using AFM images.

3.3 Nanopattern Fabrication Procedure: Nanosphere Lithography

The NSL process allows for the fabrication of nanopatterns with a wide range of sizes displaying homogenous topography of a chosen value over cm^2 areas.[152,167,175-177,180,181] Figure 3.1 schematically outlines the process used to create the surfaces and depicts representative images of the surface after each step. First, a monolayer or bilayer of densely-packed nanospheres is deposited onto the surface with a custom-built deposition machine designed and built by Dr. Bongsu Jung (Figure 3.1 A,B). Second, the nanospheres are removed and a 2 nm adhesion layer of chromium and an 8 nm layer of gold were thermally evaporated onto the surfaces (Figure 3.1 A). This process results in an array of truncated triangular pyramids or hexagonal shaped islands of gold in a hexagonal or orthorhombic lattice surrounded by glass (Figure 3.1 A,C,D). Third, the glass support and gold nanoislands were functionalized to create PEG-terminated silane and hexadecane thiol self-assembled monolayers of the glass and gold areas respectively, discussed in detail in Chapter 4 (Figure 3.1 A). Finally, the dual surface chemistry directs the adsorption of FN to the thiolated Au nanoislands when the surface is exposed to a solution of FN, discussed in detail in Chapter 4 (Figure 3.1 A,E).

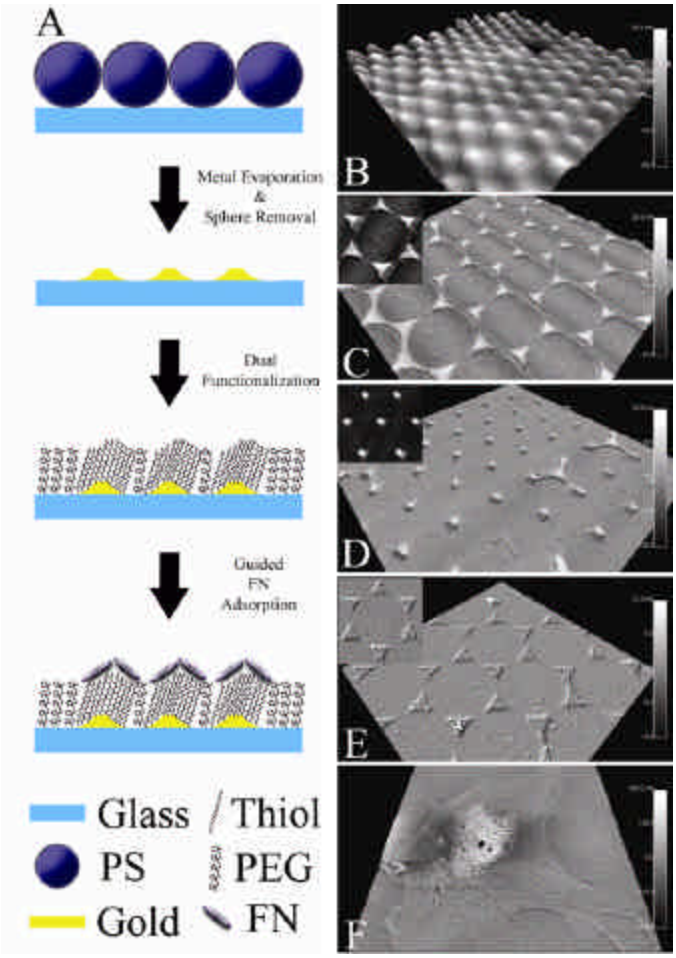

Figure 3.1: Nanopattern Fabrication and Functionalization Procedure: (A) Schematic depicting the nanopattern fabrication process, chemical functionalization, and directed fibronectin adsorption to the chemically modified nanopatterns. 3-D AFM images with zoomed in inserts of (B) monolayer mask of 500 nm diameter spheres {5 X 5 µm scan} (C) 0420M surface {2 X 2µm scan} (D) 1500B surface {10 X 10 µm scan} (E) 1500M surface after dual chemical functionalization and fibronectin adsorption {5 X 5 µm scan} and (F) HUVEC seeded on a 0300M surface after the full surface treatment {90 X 90 µm scan}.

To test whether limiting adhesion site size has an influence on cell adhesion and behavior, the ability to fabricate varying sizes of nanoislands with similar overall surface densities is needed. With NSL, the geometry and dimensions of the nanopatterns can be controlled by choosing spheres of a certain diameter and performing deposition in either monolayer or bilayer spherical mask configurations.[177] When a monolayer mask is chosen, the resulting triangle size or characteristic length (actual bisector length of formed triangle) can be determined by simple geometry as follows:

$$h_T = \frac{3}{2}\left(\sqrt{3} - 1 - \frac{1}{\sqrt{3}}\right)D = 0.233D \tag{3.1}$$

where D is the diameter of the sphere. The center to center spacing between the nanotriangles is:

$$s_T = \frac{1}{\sqrt{3}}D = 0.577D \tag{3.2}$$

The resulting nanopattern utilizing spherical monolayer masks covers 7.2 % of the substrate regardless of sphere diameter used. Hexagonal patterns can also be formed using a spherical bilayer mask and their characteristic length is determined by:

$$h_H = \left(\sqrt{3} - 1 - \frac{1}{\sqrt{3}}\right)D = 0.155D \tag{3.3}$$

and the corresponding center to center spacing is characterized by:

$$s_H = D \tag{3.4}$$

The resulting nanopattern covers approximately 2.2 % of the substrate area, again independent of the sphere size. Refer to Figure 3.2 for plots of the theoretical nanopattern sizes, spacing, and individual pattern area as a function of sphere diameter and mask configuration.

3.4 Nanopattern Fabrication Results

After fabrication, the nanopattern properties were analyzed using both AFM and SEM. NSL allowed for the fabrication of Au nanoislands with characteristic lengths ranging from 28 to 405 nm displaying topographical features from 10 to 13 nm. (Table 3.1).[6,181] The measured nanoislands were larger than the theoretical estimates predicted yet their spacing closely matched theory. The measured characteristic lengths (Figure 3.2 A: triangles for M-type layers and dots for B-type layers) ranged between 12 to 25 % larger than the theoretical values calculated from Equations 3.1 and 3.3 (Figure 3.2 A: black line at top for M-type layers and black line at bottom for B-type layers). Although the characteristic lengths and nanoisland areas were larger than expected, the center-to-center spacing was within 2 % of the theoretical values calculated from equations 3.2 and 3.4 (Figure 3.2 B: triangles for M-type layers, dots for B-type layers, theoretical values shows as black lines on top for B-type and bottom for M-type layers).[176,177] The differences in size between theory and actual measured values could be attributed to inhomogeneities in the sphere size, non-perpendicular metal evaporation, or to convolution effects from the AFM tips. The most likely source is from non-perpendicular metal evaporation as the equations do not take metal evaporation from angles into account. The measured percent surface coverage of the

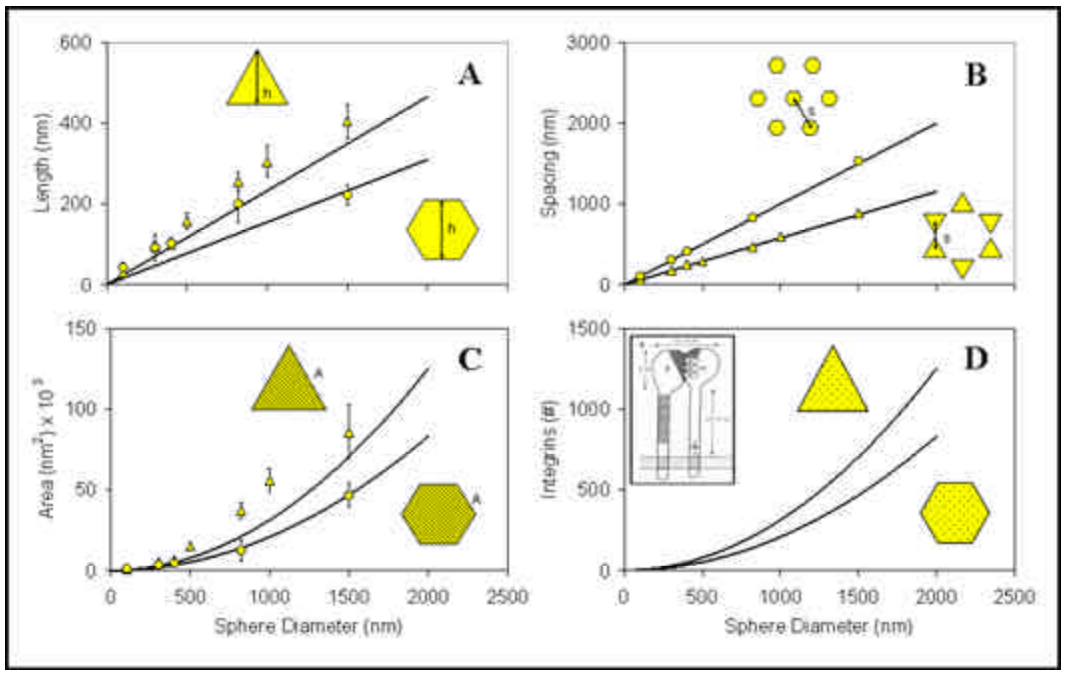

Figure 3.2: Measured versus Theoretical Nanopattern Properties: Measured (yellow triangle = M-type layers, yellow dot = B-type layers) and theoretical (black lines) values for nanopattern properties as a function of the mask sphere diameter. (A) Characteristic lengths of the nanoislands. (B) Center-to-center spacing between the nanoislands. (C) Surface area of individual nanoislands. (D) Theoretical maximum number of integrins that can bind to one nanoisland, assuming integrin binding area of 100 nm2. Inset in (D) reproduced from Reference 8**.** [8]

nanoislands was 7.2 ± 0.4 % and 2.3 ± 0.4 %, for mono- and bilayers, respectively, and closely matched the calculated theoretical values of 7.2 % and 2.2 %. Approximating a single integrin binding area of 100 nm^2 and tight integrin packing, [95] the nanopatterns can theoretically provide cellular adhesion sites that limit the number of associated integrins in each adhesion from 5 to 857 integrin bonds (Figure 3.2 D).

The NSL process is highly versatile and micrometer sized cellular corals of nanopatterned areas can be created using additional traditional photolithography steps. Figure 3.3 displays 20 by 20 µm sized squares of 1500M nanopatterns separated by 20 µm of silane treated glass between each coral. Individual cells or multiple cells can be seeded into these corals. The formation of these cellular corals could be useful for performing single cell studies for drug screening applications.

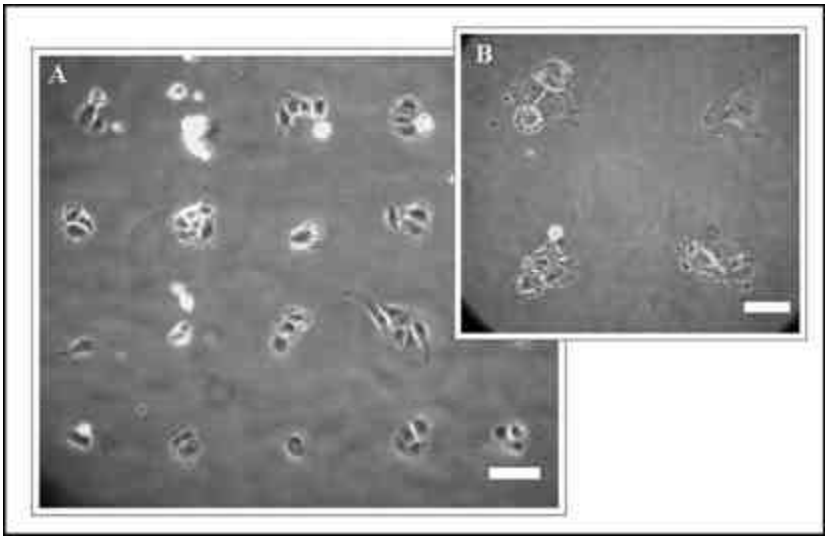

Figure 3.3: Cellular Corals of Nanopatterns: Additional traditional photolithography steps were applied to the nanopatterned surfaces to create 20 by 20 µm cellular corals. Phase-contrast images of HUVECs in nanopatterned corals in (B) shows a zoomed in region of (A). Scale bar = 20 µm.

3.5 Discussion

While the fabrication of surfaces displaying micron-scale features is relatively easy to achieve using traditional lithography or contact printing methods, the extension into nanometer-scale fabrication of surfaces for investigating cell adhesion has been

much more difficult. Serial lithography techniques such as dip-pen nanolithography, [154-158] other scanning probe lithography techniques, [159-162] and electron beam lithography, [146-148] are too time consuming in their fabrication to allow for systematic cell studies. Parallel patterning techniques such as imprint lithography, [163,164] micelle nanolithography, [166,182] particle lithography, [167] and capillary lithography [149] are better suited for quickly fabricating nanostructured surfaces over large areas but have yet to be implemented for systematic cell studies.

Experimental tools for systematic investigations of adhesion site sizes ranging from about 40 to 300 nm, a size range in which a number of critical molecular and mechanical processes in cell adhesion may occur, have been missing so far. Here it is shown that NSL, a highly parallel self-assembly process, can be used to create large, cm^2-sized areas of nanopatterns of exactly this adhesion site size range, with defined size, spacing, and topography. These nanopatterned surfaces are a composite of two materials and can therefore be chemically modified with two distinct chemical functionalities to create surfaces displaying nanoislands of ECM components for cell adhesion, see Chapter 4 for chemical modification.

While NSL meets many of the desired requirements to perform detailed systematic studies on cell adhesion maturation, it clearly has some limitations. Only two pattern size to spacing ratios can be achieved, resulting in a constant average FN surface density of 7.2 or 2.2 % for M- and B-type samples, respectively. Pattern size and spacing are coupled, but pattern pairs from M- and B-type surfaces can be created that display similar adhesion site areas with varying interadhesion site spacing and vice versa. Since spheres are used as the mask, the choice of shapes is strongly limited and mostly consists of truncated pyramids and circular disks, a limitation that, however, is unlikely

to be important for the goal of adhesion size limitation. Also, as a self-assembly method, NSL has defects that could possibly present additional adhesion sites. However, as discussed in Chapter 5, there have been minimal effects on cell behavior attributed to the inherent defects in the patterns fabricated by NSL. Although the limitations of NSL do not have a significant influence on cell behavior in the experiments presented here, a second generation of large-scale nanopatterned surfaces created using nanoscale orthogonal biofunctionalization imprint lithography (NOBIL), a variation of step-and-flash nanoimprint lithography (SFIL), has been developed to create defect-free surfaces with a wider range of pattern properties. [164]

3.6 Conclusions

It was demonstrated that NSL can be used to consistently create Au nanopatterns with controlled size, spacing, and topography against a glass background. Due to the parallel nature of the self-assembly process, surface areas large enough for statistically sound cell studies can easily be created in short time periods. Since the nanocomposite surface is composed of two materials, a dual chemical functionalization, silanes and thiols in this case, can be applied to create surface energy contrast between the nanopatterns and supporting background. As discussed in Chapter 4, this energy difference can be exploited to direct ECM protein, FN in this case, adsorption to the nanopatterns while leaving the background free of protein.

Chapter 4

Orthogonal Functionalization

4.1 Introduction

To create nanoscale cell adhesion sites, the experimental surfaces must be able to display ECM proteins or adhesive peptide sequences against a passive or non-biologically active background. This chapter details how nanoislands of FN were created against a passive glass background. Since the surfaces created using NSL are a composite of Au and glass; thiols [1,107-109] and silanes, [1,183,184] two relatively well-documented surface functionalization molecules were implemented to create surface energy contrast between the Au nanopatterns and underlying glass. In this case, the Au nanopatterns were functionalized with methyl-terminated thiols and the glass background with PEG-terminated silanes. Since the thiols are hydrophobic in nature and the PEG a protein repulsive layer, [1] protein exposed to these composite surfaces will preferentially adsorb to the thiolated Au nanoislands leaving the glass background free of protein. This functionalization method is the crucial step in creating surfaces that limit adhesion site growth and maturation and without it protein would adsorb to the entire surface and limitations on adhesion site growth would not be imposed.

The following chapter details the functionalization procedure and explains how the creation of FN nanoislands was verified. A combination of fluorescent microscopy, X-ray photoelectron spectroscopy, atomic force microscopy, combined AFM-fluorescent microscopy, and cell seeding studies were implemented to show that cells recognize, adhere to, and proliferate on the functionalized nanopatterned surfaces and to show

that the PEG functionalized background is indeed a protein repulsive layer that inhibits cell attachment.

4.2 Materials and Methods

4.2.1 Nanopattern Fabrication

Refer to Sections 3.2.1 and 3.3.

4.2.2 Dual Chemical Functionalization of Nanopatterned and Control Surfaces

Nanopatterned surfaces, glass and gold control surfaces, and ½Au - ½glass surfaces were exposed to an air plasma at 300 µTorr at approximately 50 W for 10 minutes (March Instruments Inc., Concord, CA). The slides were then immersed in a 26.5 mM hydrochloric acid (Fisher Scientific, Pittsburgh, PA), 1mM hexadecane thiol (Aldrich, St. Louis, MO) and 41 mM 2-methoxy(polyethyleneoxy)–propyltrimethoxysilane (PEG-silane) (Gelest, Morrisville, PA) solution in toluene (Fisher Scientific, Pittsburgh, PA) in a self-standing centrifuge tube (Corning, Corning, NY) for 48 hours with continuous stirring, adapted and extended from Reference 183. [183] The samples were vigorously rinsed once in toluene and twice in ethanol, dried with nitrogen, and baked at 105 °C for 1 hour. The chemically functionalized nanopatterned surfaces were exposed to 3 ml of human plasma fibronectin (Sigma, Saint Louis, MO) solution at a concentration of 10 µg/ml in 50 mM HEPES for 20 minutes. Control surfaces with varying surface FN densities were created by exposing clean glass and functionalized Au surfaces to FN solution at concentrations of 2, 5, 10, 25, and 50 µg/ml in 50 mM HEPES for 20 minutes. The protein adsorbed surfaces were thoroughly rinsed twice in HEPES solution to remove any excess fibronectin. The functionalized and

protein adsorbed surfaces were rinsed three times with DI H_2O to remove salts deposited from the HEPES solution followed by gentle drying with nitrogen.

4.2.3 XPS Analysis of Surface Modifications

A PHI 5700 X-ray photoelectron spectroscopy system (Physical Electronics, Chanhassen, MN) equipped with a dual Mg and monochromatic Al X-ray source was used at a fixed angle of 45° for elemental analysis of the chemically modified surfaces. The surfaces were survey scanned to determine the elemental composition percentages for Si_{2p}, C_{1s}, N_{1s}, Au_{4f}, and O_{1s} on each surface and S_{2p} on some. High resolution scans with a dwell time of 500 ms and a pass energy of 58.7 eV were used to acquire the Au_{4f}, N_{1s}, S_{2p}, and Si_{2p} spectra and a pass energy of 11.75 eV was used for the C_{1s} spectra with charge correction set to 285 eV for non-conducting samples. Three distinct areas were measured and averaged for each sample. PeakFit software (Systat Software, Inc., Point Richmond, CA) and a multipeak fitting package in Igor Pro 5 (WaveMetrics Inc., Lake Oswego, OR) were used to fit the high resolution C_{1s} scans with multiple Gaussian curves and linear baseline correction to analyze the bond types present within each peak. Nine different surface types were examined: (1) dual functionalized gold surfaces, (2) dual functionalized gold surfaces with FN adsorbed at concentrations of 2, 5, 10, 25 and 50 μg/ml, (3) dual functionalized glass surfaces, (4) dual functionalized glass surfaces with adsorbed FN at a concentration of 10 μg/ml, (5) plain glass surfaces with adsorbed FN at concentrations of 2, 5, 10, 25 and 50 μg/ml, and (6) 0400M, (7) 0400B, (8) 0300B and (9) 0300M nanopatterned surfaces that were functionalized and exposed to FN at a concentration of 10 μg/ml (see Table 3.1 for nanopattern descriptions). It should be noted that even pure gold or glass surfaces were treated with the full

chemistry, thiol and silane, to insure that no non-specific interactions took place during the functionalization procedure.

4.2.4 AFM Imaging of Adsorbed FN on Nanopatterned Surfaces

Nanopatterned samples functionalized with fibronectin were analyzed before and after cell seeding. After fibronectin adsorption, following a procedure modified from Reference 185,[185] the nanopatterned surfaces were incubated in 1 mM bis(sulfosuccinimidyl)suberate (BS^3) (Pierce, Rockland, IL), a water-soluble, non-cleavable, and membrane impermeable crosslinker, at 20 °C for 10 minutes. Un-reacted cross-linker was quenched with 20 mM glycine in PBS. Samples that had been seeded with cells were treated similarly, with the addition of a cell removal step using 0.2 % SDS (sodiumdodecylsulfate) in PBS for 10 minutes after cross-linking. Each surface was finally washed three times with PBS and imaged with AFM as described in Section 3.2.3.

4.2.5 Cell and Reagents

Pooled and non-pooled human umbilical vein endothelial cells (HUVECs), passages 2-4, were cultured in endothelial growth media (EGM) supplemented with 2 ml of bovine brain extract, 0.5 ml of human endothelial growth factor, 0.5 ml of hydrocortisone, 0.5 ml of gentamicin/amphotericin-B, and 10 ml of fetal bovine serum according to manufacturer's instructions (all reagents and cells: Cambrex Bio Science Walkersville, Inc., Walkersville, MD). The cells were grown to 90 % confluence in T-25 tissue culture flasks that were coated with 30 µg of bovine or human plasma fibronectin (Sigma, Saint Louis, MO) at 37 °C and 5 % CO_2. Before seeding onto sample slides, the cells were trypsinized with 3.0 ml of 0.25 % trypsin and 1 mM ethylenediaminotetraacetic acid in PBS at 37 °C for 5 minutes. The cells were collected

and centrifuged at 240 g for 10 minutes. The cell pellet was then re-suspended in full EGM media and seeded onto the desired substrate at a density of approximately 40 cells/mm^2.

4.2.6 Fluorescent Immunolabeling and Imaging of Adsorbed FN and Vinculin-Containing Adhesions

After 72 hours of incubation, the samples were rinsed with 25 ml of warm PBS-T (phosphate buffered saline with 0.02 % Tween 20) and immediately immersed into ice-cold cytoskeleton stabilizing buffer (CSK) (10 mM HEPES, 0.5 % Triton X-100, 300 mM sucrose, 3 mM $MgCl_2$, and 50 mM NaCl, pH 6.8 in DI H_2O) for 1 minute. CSK is effective in preventing staining of cytoplasmic proteins during fluorescent labeling. The solution induces the removal of cytoplasmic proteins from the cell via osmotic pressure differences while leaving the cytoskeleton and its components intact [186] and is sometimes used for the preparation of cells for fluorescent imaging to prevent staining of soluble adhesion components in the cytoplasm. [125,187,188] The samples were removed from the CSK and immediately submersed into ice-cold 5 % formaldehyde in PBS-T and set in a 37 °C water bath for 10 minutes. The samples were rinsed with 25 ml of warm PBS-T followed by a blocking solution of 1 % BSA in PBS for 20 minutes. The cells were then labeled with a tri-stain solution {1:50 dilution of FITC-conjugated monoclonal anti-vinculin (Sigma Chemicals, Saint Louis, MO), 1:1100 dlution of Rhodamine-phalloidin (Sigma Chemicals, Saint Louis, MO), and 1:550 dilution of rabbit anti-fibronectin (Abcam, Cambridge, MA) in PBS supplemented with 0.002 % Tween 20 and 1 % BSA} overnight at 4 °C. The samples were rinsed with room temperature PBS-T and washed in 0.1 % Tween 20 in PBS for 20 minutes on a rocker. The samples were exposed to a 1:500

dilution of marina blue conjugated goat anti-rabbit (Invitrogen, Eugene, OR) solution in PBS supplemented with 0.1 % Tween 20 and 1 % BSA for 1 hour. The surfaces were thoroughly rinsed with room temperature PBS-T and washed in 0.1 % Tween 20 in PBS for 20 minutes on a rocker followed by a final rinse in DI H_2O with 0.02 % Tween 20 and dried with nitrogen. A drop of ProLong Gold antifade reagent (Molecular Probes, Inc., Eugene, OR) was added and the sample covered with a 24 by 60 mm coverslip (Erie Scientific Company, Portsmouth, NH) and secured at the edges with clear fingernail polish (Noxell Corporation, Hunt Valley, MD).

Fluorescent images were acquired using a Zeiss Axiovert 200 ApoTome (Carl Zeiss MicroImaging, Inc., Thornwood, NY) inverted microscope equipped with a Zeiss Axiocam MRm charge-coupled device (CCD) camera (Carl Zeiss MicroImaging, Inc., Thornwood, NY).

4.2.7 Dual Fluorescent-AFM Imaging of Vinculin-Containing Adhesions

After 72 hours of incubation, the samples were rinsed twice with PBS followed by fixation in 5 % formaldehyde in PBS for 20 minutes at 37 °C. The samples were rinsed with PBS and blocked with 1.0 % BSA solution in PBS for 20 minutes and rinsed twice with PBS. Samples were then incubated in a vinculin stain solution (1 % by volume of FITC-conjugated mouse anti-vinculin in 1.0 % BSA and 0.01 % Tween 20 in PBS) (all Sigma, Saint Louis, MO) overnight at 4°C. The samples were rinsed twice with PBS supplemented with 0.01 % Tween 20 and rocked in PBS with 0.1 % Tween 20 for 20 minutes followed by a DI H_2O rinse and nitrogen drying. Fluorescent images were acquired with an Olympus IX70 inverted microscope equipped with an X-100 CCD camera with InstaGater on-chip integration (Dage-MTI, Michigan City, IN) connected to

an MFP-3D AFM (Asylum Research, Santa Barbara, CA). AFM images were collected over the fluorescently imaged areas as described in Section 3.2.3. The vinculin-containing adhesions in the AFM images were identified by matching the location to that observed in the simultaneous fluorescent images and by their increased height above the background. Height traces were drawn and the adhesion heights measured using MFP-3D software in Igor Pro 5 (WaveMetrics Inc., Lake Oswego, OR). For the two cells shown in Figure 4.6, each adhesion site's length (dash adhesions) or diameter (dot adhesions) and area were determined from the AFM scans using ImageJ (NIH, Bethesda, MD).

4.3 Functionalization Procedure

The nanopatterned surfaces are composed of two materials that allow for two separate functionalization chemistries to be applied, thiols for the gold and silanes for the glass areas (Figure 3.1). After sphere removal, the surfaces were exposed to an O_2 plasma to produce hydroxyl groups on the glass surface. The hydroxyls are necessary to create a high density of coupling sites for the silane self-assembled monolayer. Low-density PEG-SAMs are not effective in preventing protein adsorption and subsequent cellular attachment. For dual SAM functionalization, the freshly oxidized surface was immediately immersed in a solution containing the hexadecane thiol and PEG-silane for 48 hours. Since the oxygen plasma treatment would destroy the thiol molecules, and with the tendency of the silane to non-specifically adsorb to the gold if no thiol is present, the thiol and silane surface functionalizations were performed simultaneously. The combination of solvents does not mix completely and thus must be stirred vigorously. Shorter incubation times and different concentrations of PEG-silane in the mixture led to increased cell adhesion to the PEG-surfaces, refer to Section 4.4.5. The

SAM-functionalized composite surfaces were then exposed to a FN solution, where FN is only able to adsorb to the gold nanopatterns, producing FN nanoislands of controlled size and pitch surrounded by a non-adhesive background (see the changed texture of the pattern in Figure 3.1 E compared to Figure 3.1 C). Finally, cells are seeded onto the surface (Figure 3.1 F).

4.4 Functionalization Characterization

The ability to create nanoislands of FN against a non-adhesive background is the foundation of the cell studies proposed here and much effort was focused on characterizing the functionalization procedure. Multiple characterization strategies were implemented to verify the creation of protein nanoislands. XPS was used to confirm that the dual functionalization technique is surface material dependent on both the macro and nano length scales, to show that PEG-silane functionalized glass surfaces act as a protein repulsive layer, to determine the surface concentration of FN on both nanopatterned and control surfaces, and to prove that the nanopatterned surfaces adsorb protein exclusively to the nanoislands. The XPS studies were confirmed with AFM imaging of adsorbed FN on the nanopatterned surfaces. Fluorescent immunolabeling experiments of FN and vinculin and combined fluorescent immunolabeling-AFM experiments were performed on adherent cells to confirm that the vinculin-containing adhesion sites were localized to the underlying functionalized nanopatterns, that the protein nanoislands provide direct control over adhesion site size, and that the defects in the nanopatterning process have relatively little influence on adhesion formation. Combining the results of these characterization techniques validates the claim that the surface functionalization procedure retains its desired properties at the nanoscale and

that cells recognize and adhere to these surfaces with imposed restrictions on adhesion site growth. In some cases the cells can overcome the chemically-defined boundaries and form fibrillar adhesions that span multiple patterns discussed in Chapter 8. This occurrence is mostly limited to early time points and the formation of large classical focal adhesions on nanopatterned surfaces is suppressed. These issues concerning the types of adhesions formed and their properties are discussed in detail in Chapter 5 and only covered in this chapter to validate the functionalization procedure.

4.4.1 Orthogonal Functionalization of Homogeneous Surfaces

To verify the material dependent selectivity of thiol and silane SAM coupling, homogenous glass and gold coated glass slides underwent the dual chemical modification process. The samples were analyzed with XPS before protein adsorption to characterize which molecules were present on the surfaces after the functionalization procedure. PEG-silane SAMs can be easily identified by the presence of a 286.5 eV peak indicative of poly(ethylene oxide) and a 285.0 eV peak due to the C-C spacer. Thiol SAMs can be identified by both a 285.0 eV peak from the C-C backbone and by the presence of sulfur, the main indicator used here to distinguish thiol from silane SAMs.

After chemical modification, thiol binding to the gold surfaces was confirmed by the appearance of a sulfur S_{2p} peak and by shadowing of the Au_{4f} signal (Table 4.1). Shadowing or the decrease in signal intensity is due to a phenomenon that occurs as material is coupled or adsorbed to a surface thereby inhibiting the release of electrons from the underlying surface during XPS. No S_{2p} signal was observed on the functionalized glass surface, indicating no or minimal non-specific interaction of the thiol with the silane or glass (Table 4.1). A comparison of the C_{1s} spectra for the

Surface	Au_{4f}	Si_{2p}	S_{2p}	O_{1s}	N_{1s}	C_{1s}
Glass-PEG&Thiol	0.01	20.84	0.00	60.39	0.14	18.63
Glass-PEG&Thiol-10 µg/mL FN	0.01	17.68	ND	57.97	0.27	24.06
Au-PEG&Thiol	15.43	0.00	3.13	46.85	0.51	34.08
Au-PEG&Thiol-1,882 FN/µm^2	11.06	2.34	ND	31.69	4.32	50.59
0400B-PEG&Thiol-41 FN/ µm^2	0.20	19.72	ND	49.08	0.75	30.25
0400M-PEG&Thiol-217 FN/ µm^2	0.77	20.28	ND	49.87	0.81	28.26

Table 4.1: Elemental Composition of Functionalized Surfaces: Measured XPS elemental composition for each test sample as a percent of the total signal from survey scans, extracted from Gauss-fits to the peaks. ND = Not determined.

functionalized glass and gold surfaces also indicates selectivity of the surface modification (Figure 4.1). The modified gold surface C_{1s} spectrum displays a distinct peak at 285.0 eV corresponding to the thiol backbone and a small peak at 286.5 eV attributed to a small amount of PEG-silane contamination (Figure 4.1 B), whereas the PEGylated glass surface shows a characteristic PEO peak at 286.5 eV and a smaller peak at 285.0 eV attributed to the C-C linker in the silane molecule and possibly a small amount of thiol orother contaminants (Figure 4.1 A). Thiol adsorption to the glass surface, however, should be minimal since no sulfur was detected (Table 4.1). Since each surface was treated with the full chemical functionalization, the data indicate that the two chemistries are selective for gold and glass surfaces, respectively.

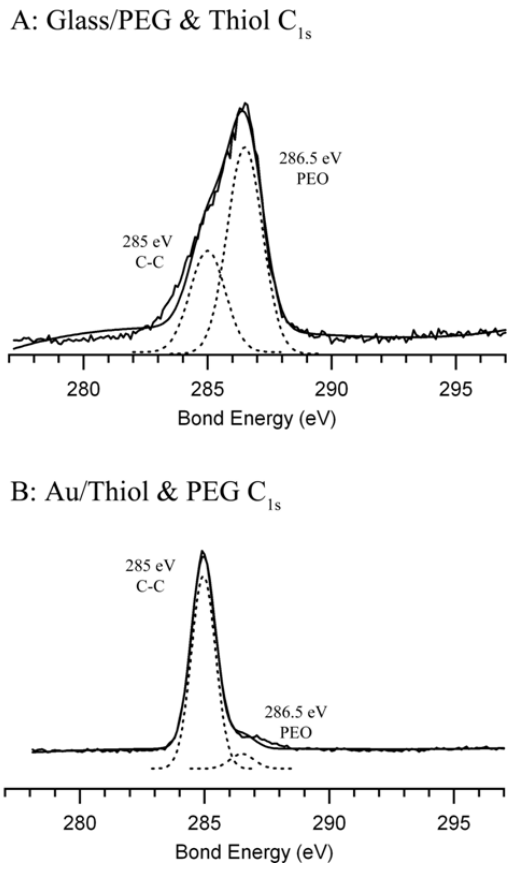

Figure 4.1: C_{1s} XPS Spectra for Glass and Gold Surfaces after Orthogonal Functionalization: The C_{1s} spectra for the PEG and thiol treated (A) glass and (B) gold surfaces before FN adsorption. The data indicates chemical specificity of the PEG-silane towards the glass and thiol towards the gold. A characteristic PEO peak at 286.5 eV is seen on the PEGylated glass comprising 67 % of the total C_{1s} signal as well as a smaller 285.0 eV peak (33 %) from the C-C linker and possibly a small amount of thiol or other contamination, although no sulfur was detected. A characteristic C-C peak (93 %) is observed on the thiolated gold along with a small PEO (7 %) signal attributed to a small amount of silane contamination.

4.4.2 FN Adsorption to Functionalized Homogeneous Surfaces

The results from Section 4.4.1 confirm that the SAM formation is indeed material dependent. After chemical modification, the surfaces were exposed to FN solution promoting FN adsorption to the surfaces. Several indicators have been used to confirm protein adsorption by XPS analysis:[189-191] the appearance of a distinct N_{1s} peak indicating the presence of nitrogen in protein, an increase in the C-N, C-C, C-O, and N-C=O bond contributions to the C_{1s} spectra from FN, and a decrease in the background signal, Au_{4f} and Si_{2p} in this case, as the protein shadows the substrate signal.

To verify FN adsorption to these surfaces the most direct and specific indicator for the presence of protein, the appearance of a nitrogen N_{1s} peak, which is absent in all samples before FN absorption was used to verify the presence of FN. While a clear N_{1s} peak was observed after protein adsorption on the modified gold (Figure 4.2 F) and plain glass surfaces (Figure 4.2 E), no distinct N_{1s} peak was seen on PEGylated glass samples either before or after FN adsorption, indicating that no FN adsorbed to the PEG silane SAM (Figure 4.2 D).

In order to quantify the amount of adsorbed FN, a calibration relation of the Gaussian-fit area under the N_{1s} peak at different concentrations of FN in solution was established. The typical sigmoidal behavior that has been observed with ^{125}I-labeled FN [185] is reproduced with the N_{1s} area measurements (Figure 4.2 A). A quantification of the amount of FN can be achieved by fitting the data to a sigmoidal curve and comparing the saturation value of the XPS signal of FN on thiolated gold surfaces to published data of ^{125}I-labeled FN adsorbed to CH_3-terminated silane SAMs, [185] which is very similar to adsorption curves found for tissue culture polystyrene and glass. [118] The

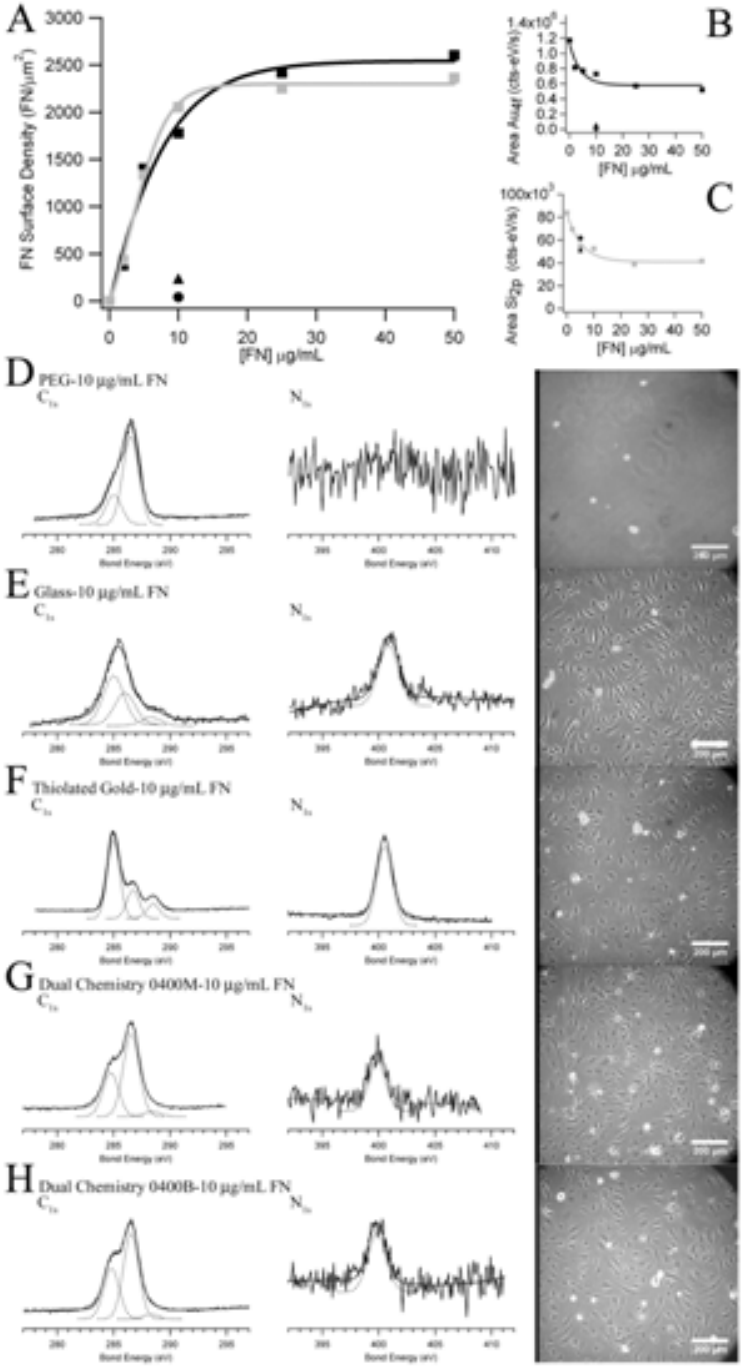
A
FN Surface Density (FN)/μm²
[FN] μg/mL
B
Area Au4f (cts-eV/s)
[FN] μg/mL
C
Area Si2p (cts-eV/s)
[FN] μg/mL
D PEG-10 μg/mL FN
E Glass-10 μg/mL FN
F Thiolated Gold-10 μg/mL FN
G Dual Chemistry 0400M-10 μg/mL FN
H Dual Chemistry 0400B-10 μg/mL FN
Bond Energy (eV)

Figure 4.2 C_{1s} and N_{1s} Spectra of Gold, Glass, and Nanopatterned Surfaces after FN Adsorption and FN Surface Concentration Calibration: (A) Calibration curves depicting the surface density of FN (FN/μm^2) on (grey squares) clean glass and (black squares) functionalized gold surfaces as a function of the solution concentration. The surface density of FN is also shown for both (black triangle) M and (block dot) B nanopatterned surfaces. Calibration curves showing the exponential decay of the background signal (Au_{4f} for gold and Si_{2p} for glass) as protein is adsorbed at higher concentrations for functionalized (B) gold and (C) clean glass surfaces, (black triangle) M and (block dot) B show values for the nanopatterned surfaces. (D-H) XPS data comparing C_{1s} and N_{1s} spectra for non-patterned and nanopatterned surfaces after dual functionalization and FN adsorption (10 µg/mL) and phase contrast images of seeded cells on the respective surface. (D) PEGylated glass surface, (E) unmodified glass, (F) thiolated gold, (G) 0400M, and (H) 0400B surfaces. The FN contribution to the C_{1s} spectra (C-C, C-N, N-C=O) is shown for the (E) glass, (F) gold, (G) 0400M, and (H) 0400B surfaces and the N-C=O is not seen on the (D) PEGylated glass. The characteristic N_{1s} peak corresponding to adsorbed FN is detected on the (E) untreated glass sample, (F) gold, (G) 0400M, and (H) 0400B surfaces and not on the (D) PEGylated glass. Cells adhered to, spread, and proliferated on the (E) unmodified glass (F) gold, (G) 0400M, and (H) 0400B surfaces over 3 days whereas almost no cells attached to the (D) PEGylated glass surface.

background signal was also examined to quantify the extent of shadowing as FN is adsorbed to the surfaces. The background signals, Au_{4f} for gold and Si_{2p} for glass, exponentially decreased as the FN surface density increased (Figure 4.2 B,C).

A FN saturation value of 190 ng/cm^2 (2,543 FN/μm^2) occurred on CH_3-terminated silane SAMs when exposed to a 20 µg/ml solution of FN.[185] The calibration curves

indicate that a monolayer of FN is formed on clean glass at a surface concentration of 2,300 FN/μm^2 (Figure 4.2 A). The saturation value for a thiolated gold surface is slightly higher at 2,605 FN/μm^2 (Figure 4.2 A). The higher saturation value is attributed to the fact that FN has a more compact form when adsorbed to hydrophobic surfaces thereby inducing a higher packing density for a monolayer of protein on thiolated gold than would be expected on a glass surface. [120]

The C_{1s} signals were deconvolved to determine contributions from chemical bond energies that are expected in the PEG, thiol, and FN chemical structures. The C_{1s} spectra for the functionalized and protein-treated homogenous gold and plain glass samples were fit with three Gaussian curves corresponding to the expected bond energies of the C-C (285.0 eV), C-N (286.0 eV), C-O and PEO (286.5 eV), and N-C=O (288.3 eV) bonds. [192] Previous XPS studies on proteins, including FN, have shown that it is difficult to differentiate the C-O and C-N peaks from one another and that they can be fit as a single peak centered in the range of 285.7 to 286.5 eV. [193] In this study, the peak position occurred in this same range, usually centered at 286.5 eV. The relative contribution of each bond to the total C_{1s} energy for the gold and nanopatterned surfaces is displayed in Table 4.2; glass data are not shown due to their similarity to the gold surfaces.

After protein adsorption, the appearance of a nitrogen N_{1s} peak on the gold sample is accompanied by the appearance of two additional peaks in the C_{1s} spectra at 286.5 and 288.3 eV, which indicate the presence of amine, ether, and amide bonds (Figure 4.2 F), similar to previous results. [193,194] The characteristic protein peak contributions to the C_{1s} spectra consisted of 64.5 % C-C bonds from the thiol and the FN backbone, 23.4 % C-N and C-O bonds, and 12.0 % N-C=O bonds for the gold surface with

a FN density of 1,882 FN/μm^2 (Table 4.2). The C-C contribution to the C_{1s} spectra decreases and the C-N, C-O, and N-C=O contributions increase as more protein was added to the thiolated gold surfaces (Table 4.2). The PEG-silane functionalized glass samples show the expected C-C and PEG peaks, but no amide bond peak (Figure 4.2 D) after FN adsorption, indicating that no protein was present. A ratio of C-C to PEG components of about 1:4 would be expected, but the contribution of the C-C peak is larger (Figure 4.2 D). This occurrence could be contributed to a small amount of hydrocarbon contamination or possibly to some thiols entrapped in the PEG layer, although no sulfur was detected (Table 4.1). Still, the absence of a 288.3 eV amide bond peak and a nitrogen N_{1s} peak on the PEGylated surface exposed to FN solution at a concentration of 10 µg/mL for 20 minutes confirms that the silane SAM acts as a protein-repulsive surface.

The results confirm that FN adsorbs to thiol SAM surfaces in a more compact form than to plain glass surfaces and does not adsorb to PEG silane SAMs. Furthermore, the data shows that Au surfaces with varying FN surface densities can easily be created by changing the FN solution concentration that the surface is exposed to. This technique was used to create Au control surfaces for cell experiments as described in the following chapters.

Surface	C-C	C-N, C-O, PEO	N-C=O
	285.0 eV	285.7 – 286.5 eV	288.3 eV
Glass-PEG&Thiol	32.93	67.07	---
Glass-PEG-Thiol&10 μg/mL FN	25.16	74.84	---
Au-Thiol&PEG	92.88	7.12	---
Au-Thiol&PEG-537 FN/μm^2	81.79	13.53	4.68
Au-Thiol&PEG-1,199 FN/μm^2	64.35	24.58	11.06
Au-Thiol&PEG-1,882 FN/μm^2	64.54	23.42	12.04
Au-Thiol&PEG-2,474 FN/μm^2	56.87	26.29	16.84
Au-Thiol&PEG-2,605 FN/μm^2	55.55	27.39	17.70
0400B-Thoil&PEG- 41 FN/μm^2	35.88	60.69	3.43
0400M-Thiol&PEG- 217 FN/μm^2	33.35	63.01	3.65

Table 4.2: Deconvolved C_{1s} XPS Spectra of Functionalized and FN Adsorbed Glass, Gold, and Nanopatterned Surfaces: Deconvolution of the XPS C_{1s} peak into the chemical bond energies for each test sample. The appearance of C-N and N-C=O bonds was observed after the addition of FN to the modified gold surfaces. A small N-C=O peak was also detected on both nanopatterned surfaces and was not observed after FN adsorption to the PEG-functionalized glass surfaces.

4.4.3 Orthogonal Functionalization and FN Adsorption to Nanopatterned Surfaces

The previously discussed XPS analysis proves the selectivity of SAM formation and FN adsorption to homogenous surfaces. The same XPS analysis was implemented to prove this occurrence on the functionalized nanopatterned surfaces although the analysis is slightly more complicated due the presence of both thiol and silane SAMs on the nanocomposite surface. To cope with this complication, the nanopatterned surfaces were analyzed only after the full chemical treatment; thiol/silane and FN adsorption.

On the four nanopatterned surfaces used in the experiments, small N_{1s} peaks appeared after functionalization with thiol/silane and FN (Figure 4.2 G,H). Data for 0300M and 0300B are very similar to the 0400M and 0400B surfaces respectively and are not shown. An evaluation of the C_{1s} spectra shows that both nanopatterned surfaces have a noticeable N-C=O signature that is not present on the PEG-functionalized glass, which, together with the appearance of an N_{1s} peak, indicates FN adsorption as seen on the functionalized non-patterned gold surfaces (Figure 4.2 G,H). A comparison of the area under the N_{1s} curves of the nanopatterned surfaces to the non-patterned gold surfaces after FN adsorption shows that the amount of protein surface coverage (8.3 % for M- and 1.6 % for B-type surfaces) on the nanopatterns is close to the measured nanopattern surface coverage (7.2 % for the M- and 2.3 % for the B-type samples) indicating that the FN adsorbs almost exclusively to the thiolated gold nanopatterns and avoids the passive PEG background. Using the calibration curve from Figure 4.2 A indicates that the nanopatterned surfaces display 217 FN/μm^2 and 41 FN/μm^2 for the M- and B-layer surfaces respectively. Furthermore, the area under the amide bond peak at 288.3 eV for the monolayer nanopatterned surfaces is 7 % of the area for the same

portion of the C_{1s} spectra of the protein-adsorbed gold sample. The gold background on the monolayer nanopatterned surfaces displayed 8.9 % the amount of gold compared to the non-patterned controls, in good agreement with the measured 8.3 % surface coverage of FN (Figure 4.2 B). As expected, the nanopatterned surfaces had higher signals from the Si_{2p} spectra, indicating that no protein was adsorbed to the functionalized glass background (Figure 4.2 C).

The results from the analysis indicate that the dual surface chemistry is selective on the nanometer scale and that the nanocomposite surfaces direct FN adsorption almost exclusively to the functionalized gold nanopatterns. AFM imaging of nanopatterned surfaces was performed to further validate these claims and is presented in the following section.

4.4.4 Imaging FN Adsorption

To control the clustering of integrins it is important to know the number of adhesion ligands displayed on each nanoisland. To measure this density, nanopatterned surfaces underwent the full functionalization and the FN was crosslinked with cell-impermeable amine-reactive BS^3 before and after cell seeding. AFM images of the surfaces before cell seeding show distinct ordered arrays of protein on the gold nanopatterns (Figure 4.3 A,C). The protein clusters have an approximate size and height of 36 and 7 nm respectively, which is in agreement with lateral dimensions of globular FN determined using electron microscopy. 195,196 The protein clusters also have a rounded or compact shape typical of FN adsorbed to hydrophobic surfaces, [120] and practically no protein was observed on the PEG-modified glass between the

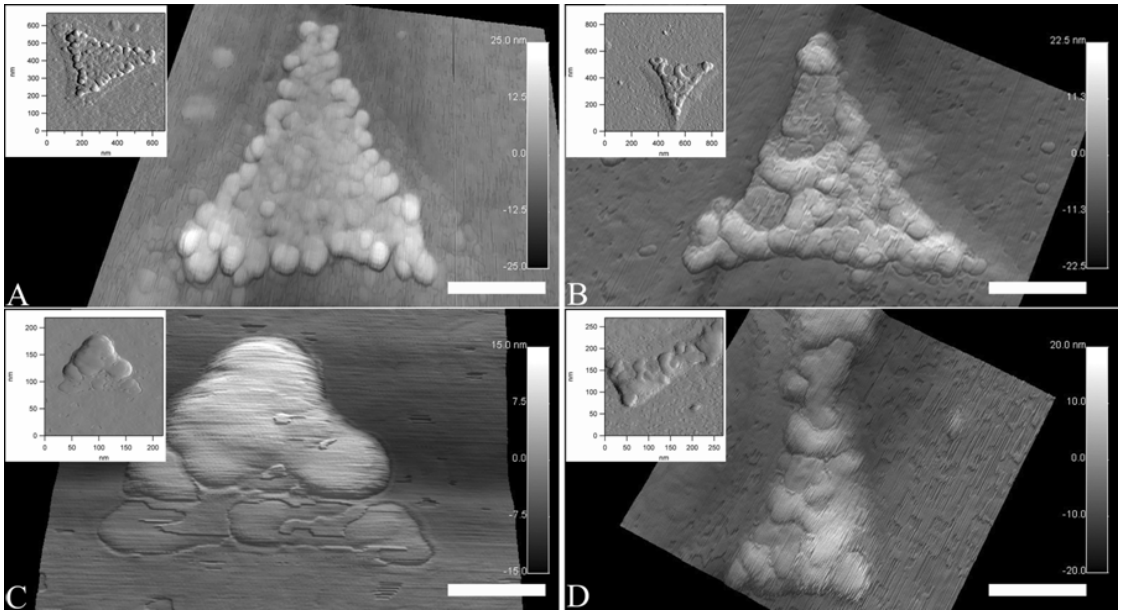

Figure 4.3: AFM Images Adsorbed FN on Functionalized Nanopatterned Surfaces: 3-D images from AFM scans (inserts) displaying cross-linked FN on one nanoisland. FN on 1500M before (A) {Scale bar = 143 nm} and after (B) cell attachment {Scale bar = 158 nm}, and FN on 0420M before (C) {Scale bar = 47 nm} and after (D) cell attachment {Scale bar = 57 nm}. In both cases the FN is clearly seen in a compact shape before cell seeding and is rearranged into a more elongated shape after cell seeding and attachment. Cells have been removed in (B) and (D) (see text).

nanoislands, which is in agreement with the XPS results. Taking each spherical entity as a single FN, there are approximately 60 to 70 FN proteins on each nanopattern for the 1500M surface (Figure 4.3 A) and 2 to 5 on the 0420M pattern (Figure 4.3 C), resulting in an approximate density of 714 FN/μm^2 on the pattern or an average of 55 FN/μm^2 for the composite surface, which includes the surrounding glass-PEG background. However, the XPS data indicate that a composite average of 217 FN/μm^2 should be measured for the monolayer surfaces, which is in agreement with the estimated total volume of

0.72 ml/g of FN. [197] This discrepancy may be induced by the BS^3 crosslinker used to secure the protein before AFM analysis by artificially enlarging the imaged proteins during the crosslinking process, or by making it difficult to distinguish between two separate proteins and thereby inducing a lower-than-actual protein count. Even though the measured FN dimensions appear in agreement with AFM measurements by others, [120] the higher surface concentration of FN derived from the XPS-radiolabeling was used for comparison during the following cell studies. Still, the density of FN, averaged over the patterned and non-patterned areas of the nanocomposite surfaces is very low. For comparison, endothelial cell adhesion has been shown on homogenous surfaces displaying as low as 250 FN/μm^2, but these surfaces led to reduced proliferation or cell death over time. [102]

To gain an understanding of cell interactions with the adsorbed FN, the FN morphology before cell seeding was compared to its morphology after HUVECs adhered to and spread on the nanopatterned surfaces. After 1 day, all surface proteins were crosslinked and rinsed with SDS to remove the majority of each cell, leaving behind only cell sections that are crosslinked to the surface, or bare ECM in areas where no cells were attached at the time of crosslinking. In some areas, instead of displaying ordered arrays of clustered FN, the FN was rearranged or removed (Figure 4.3 B,D). A reorganization of FN could be expected as the cells remodel and stretch FN as stress is applied during cell movement, the process of FN fibril formation or fibrillogenesis in cells cultured on nanopatterned surfaces is discussed in detail in Chapter 7. [43]

These images validate the XPS experimental results of FN adsorption exclusively to the thiolated gold nanoislands. Furthermore, it demonstrates that the cells recognize, interact with, and remodel the displayed FN. The following sections further validate the

XPS and AFM studies by implementing cell seeding studies on ½Au – ½glass surfaces and by examining differences in cell adhesion formation by cells seeded on control and nanopatterned surfaces.

4.4.5 Cell Seeding Experiments

Time-dependent functional controls to show that the surfaces selectively support cell adhesion and repulsion on the functionalized gold and glass areas respectively were performed on ½Au – ½glass slides. Slides underwent full chemical functionalization as described above, but with varying concentrations of PEG-silane (1, 2, 3 and 5 % by volume). Cells adhered to and proliferated on all of the surfaces (Figure 4.4 B,E) except for the PEG-silane functionalized glass surfaces, (Figure 4.4 A,C), again reaffirming that the PEG layer prevents protein adsorption to the glass areas and consequently inhibits cell attachment. Figure 4.4 D shows a phase-contrast image of the intersection of the gold and glass halves after 3 days of culture. The HUVECs have grown to near confluence on the gold half and align to the boundary. A small strip of cells can be seen protruding into the lighter glass side, most likely caused by imperfect shadowing of the deposition mask allowing a small amount of gold to deposit in the transition zone. The density of adhered cells increased on the gold-coated side over 3 days for all four silane concentrations, while very few cells adhered to the PEG-treated glass side (Figure 4.4). However, the density of cells was the lowest on the PEG surfaces for 2 % silane, which was therefore used as the standard concentration for all subsequent experiments.

In addition to the initial ability of the PEG surfaces to reject cell adhesion, it was tested whether ECM adsorption from the serum-containing media could support cell

attachment. After 3 days of culture in serum-containing media the ½Au - ½glass surfaces (3 % PEG) were re-seeded with four times the number of cells used for the original seeding. On the fourth day, 24 hours after the samples had been seeded again, a large spike in cell density was observed on the gold half, while almost no cells were seen on the PEG-functionalized glass half (Figure 4.4 A,B). This indicates that the PEG-functionalized glass retained its passivating properties against protein adsorption and subsequent cellular attachment for at least 4 days in serum-containing media.

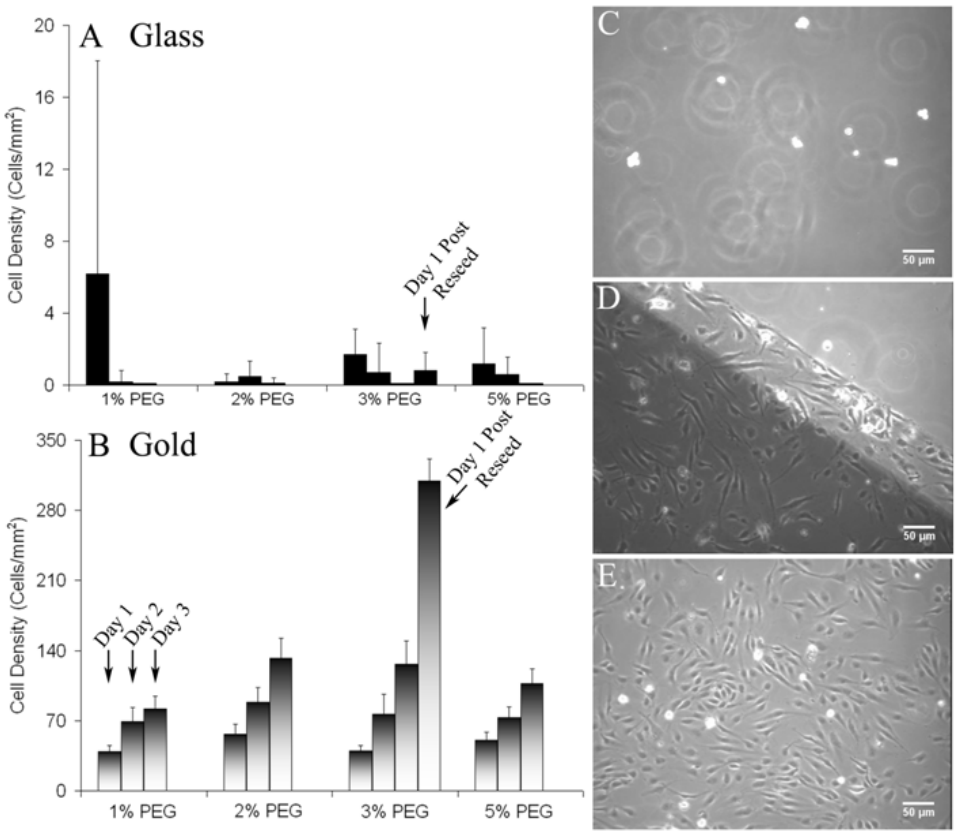

Figure 4.4: Cell Seeding on ½Au – ½Glass Surfaces with Varying PEG-Silane Concentrations: Number of cells per surface area for HUVECs seeded on ½Au – ½glass slides after chemical functionalization and FN adsorption. (A) Density of adherent cells on the PEG treated glass half, and (B) on the functionalized gold half measured at 24 hour intervals. The fourth bar on the 3 % PEG sample shows the cell density 24 hours after reseeding cells at day 3 to test the stability of the chemical pattern contrast. Phase-contrast images of HUVECs on the ½Au – ½glass slides after 3 days in culture. (D) HUVECs grow to and align with the gold-glass intersection. Representative images of cell density on Au half (E) and glass half (C) after 3 days. (C-E) Scale bar = 50 µm.

4.4.6 Functionalized Nanopatterned Surfaces Provide an Upper Limit to Adhesion Site Growth

For proof of principle and to validate that surfaces displaying nanoislands of FN surrounded by a passive background limit adhesion site size and growth; fluorescent immunolabeling of adsorbed FN and vinculin and dual fluorescent-AFM imaging of vinculin-containing adhesion sites on control and nanopatterned surfaces was performed. Fluorescent imaging of FN and vinculin-containing adhesions of cells on control and nanopatterned surfaces with large patterns, greater than 300 nm, is relatively simple, but becomes challenging when imaging components on smaller nanopatterned surfaces. Figure 4.5 A2 and B2 shows that the FN adsorbs exclusively to the functionalized nanopatterns while leaving the passive background free of protein, further proving that the orthogonal surface modifications work on the nanometer scale. Furthermore, cells seeded on these surfaces recognize and adhere exclusively to the FN nanoislands and the island size provides an upper limit on adhesion site growth as hypothesized (Figure 4.5 A1). The size limitation holds true for cellular adhesion formation on smaller nanopatterned surfaces, Figure 4.5 B1, but is more difficult to visualize with light microscopy techniques due to diffraction limitations.

To gain a better understanding of adhesive interactions with the underlying smaller nanopatterned surfaces and to avoid resolution limitations of light microscopy techniques, dual fluorescent-AFM studies were implemented. Figure 4.6 shows an example of cells fixed and immunostained for vinculin after 72 hours culture time on a 0400M nanopatterned and glass control surface. While the vinculin-containing adhesions on the glass control surface could be easily correlated between fluorescence and AFM images (Figure 4.6 A-C), on the nanopattern this matching was more difficult

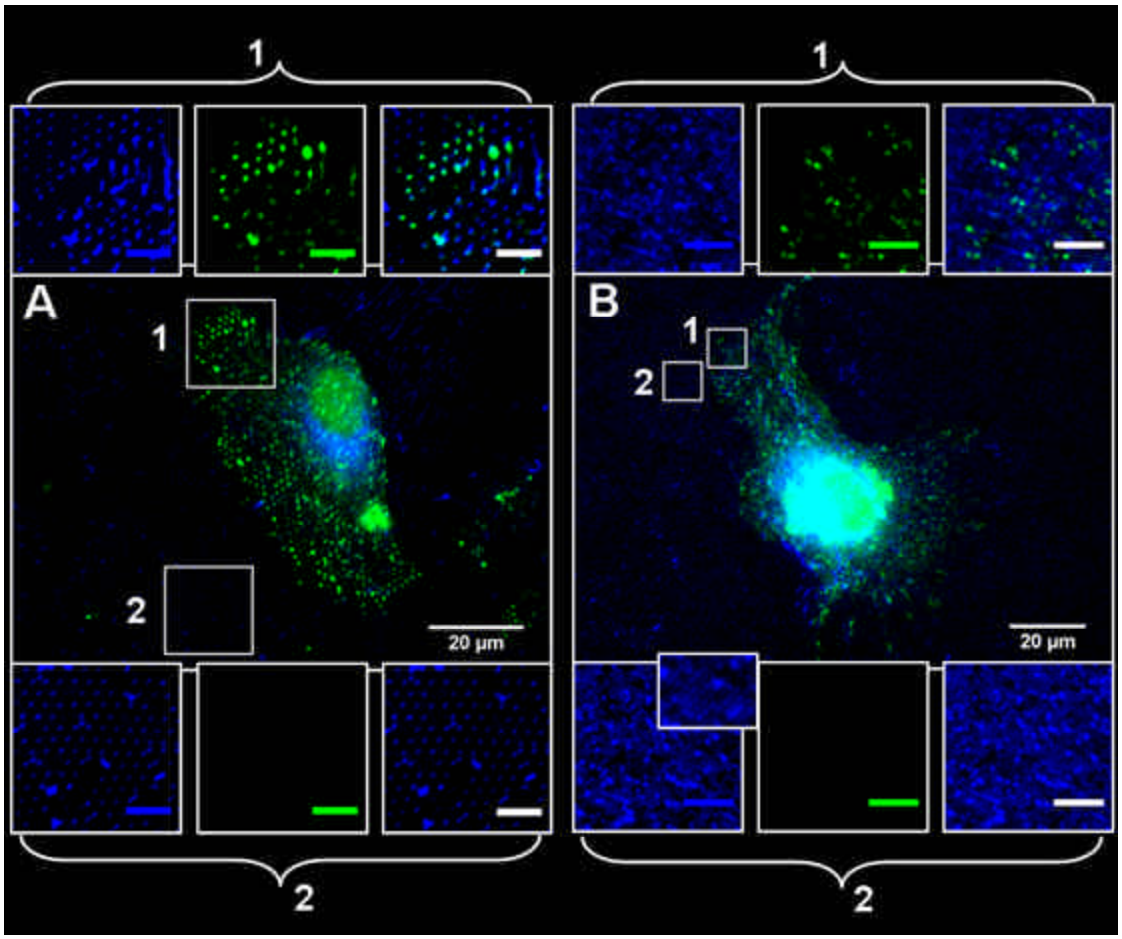
1
1
A
1
2
20 µm
B
1
2
20 µm
2
2

Figure 4.5: FN Nanopatterns Provide an Upper Limit on Adhesion Site Size: Fluorescent images of FN (blue) and vinculin-containing cell adhesions (green) on (A) 1500B and (B) 0300B nanopatterned surfaces. Inserts labeled 1 show zoomed in areas of cell adhesion and inserts labeled 2 show zoomed in areas without cell adhesion. (A1) FN isolated to the chemically-defined nanopatterns (blue) on the left, the vinculin-containing adhesions (green) in the middle, and the merge of the two on the right. Scale bar = 5 µm. (B1) Shows same as A1 but for a cell on the 0300B nanopatterned surface. Scale bar = 3 µm. (A2) FN nanopatterns (blue) on left, no adhesions in middle, and merge on right. Scale bar = 5µm. (B2) Same as A2 but for a cell on the 0300B nanopatterned surface. Scale bar = 3 µm. It can be seen from inserts 1 in A and B that the FN adsorbs almost exclusively to the functionalized nanopatterns leaving the background free of protein, that vinculin-containing cellular adhesions are isolated on the FN nanopatterns, and that the nanopatterns provide an upper limit and direct control over adhesion site growth.

due to the small size of the adhesions. To positively confirm the location of vinculin-containing adhesions in the AFM images, the fluorescent image was slightly scaled and overlaid on the AFM image using multiple points on the cell rim as alignment markers (Figure 4.6 F). Fluorescently labeled adhesions closely matched increased height features in the AFM image across the entire cell (Figure 4.6 G). The matched features were terminations of up to 20 µm long, thin non-fluorescent raised lines that could be traced across the cell, presumably actin microfilaments. High-resolution AFM scans (Figure 4.6 J, white box in F) were then correlated using zoomed portions of Figure 4.6 F and G as a reference (Figure 4.6 H,I). Although the adhesions incorporate a defect line in some instances, they most often do not align with the direction of defect lines and the

overwhelming majority of the vinculin-stained areas are not on defects. The large, optically resolution-limited fluorescence areas decompose into single or double thin elongated features in the AFM images, as seen to the left and center in Figure 4.6 I and J, respectively. The optical resolution limitation does not allow for positive determination of whether the vinculin is localized exclusively over the nanopatterns, or whether it bridges between patterns, but co-localization between the FN nanopatterns and vinculin-containing adhesions is easily seen in fluorescent images of cellular adhesions on larger nanopatterns (Figure 4.5 A1).

Detailed AFM height measurements can give further insight into how the adhesions are structured. The dash adhesion on the control glass surface (long arrow in Figure 4.6 A–D) had a measured height of approximately 25 nm above the glass background, including an 8 - 10 nm contribution from the cell membrane (Figure 4.6 E). The adhesion on the 0400M surface (arrow in Figure 4.6 H–J) had a measured height of about 32 nm (Figure 4.6 K). This included approximately 19 nm due to the height of the nanopattern, FN, and the cell membrane as measured separately. The adhesion sites formed on both the glass and 0400M surfaces have a measured height of about 13 to 17 nm. For a comparison, the thin fibers, presumably thin actin fibers seen in the cells on the 0400M surfaces had a measured height of 7 to 9nm, which is close to the thickness of an actin microfilament of 7 nm in diameter.

To gain more insight into the structure of the adhesions, height traces were made across the adhesion sites. Following the profile along the line in Figure 4.6 J from top to bottom (right to left in Figure 4.6 K), starts with an adhesion-free area (~ 7 – 8 nm thick) then passes over a hole in the membrane and two nanopatterns, rises to the adhesion on a nanopattern at 2.2 µm and continues at a height of 20 to 22 nm to the

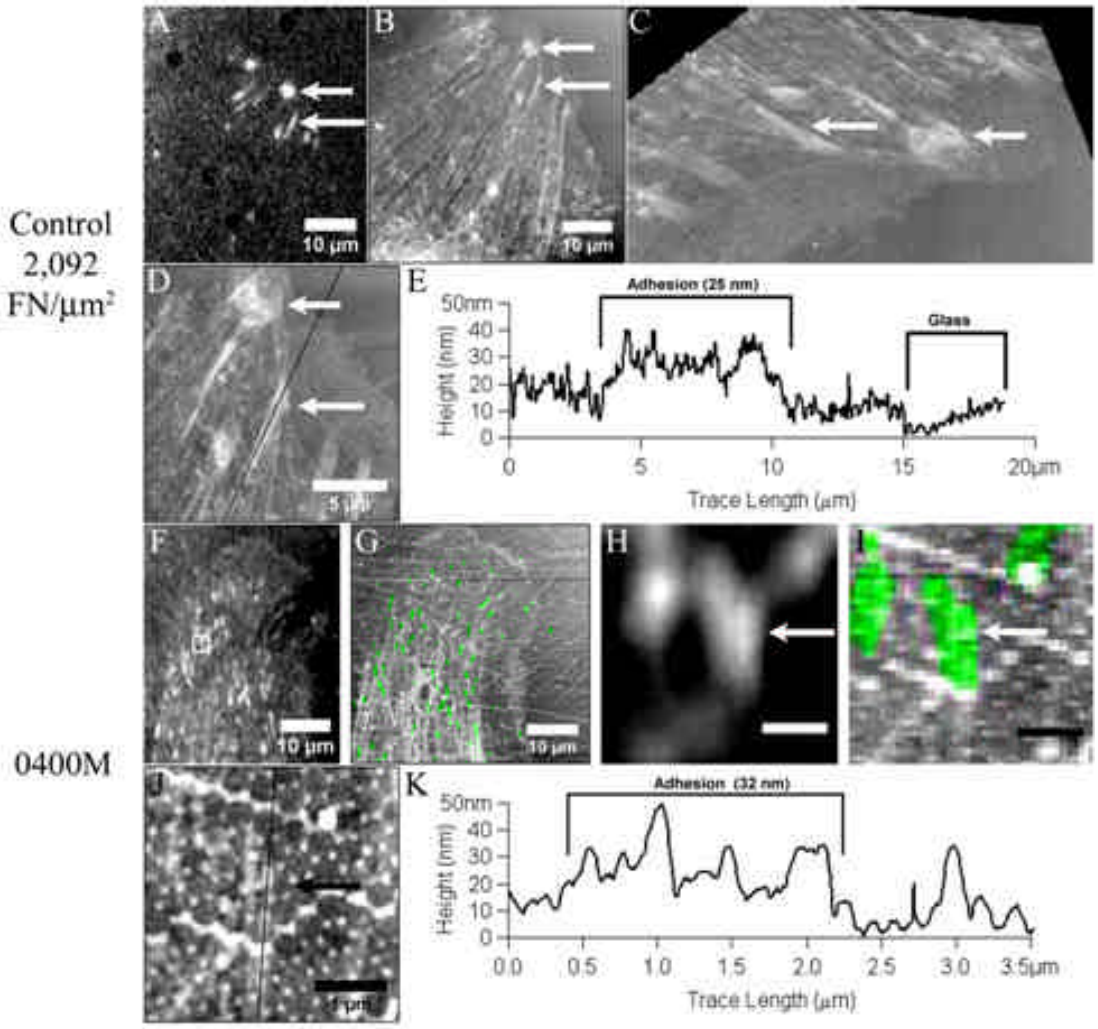
Control
2,092
FN/μm²
0400M
A
B
C
D
E
F
G
H
I
J
K
10 μm
Adhesion (25 nm)
Glass
50nm
40
30
20
10
0
Height (nm)
0
5
10
15
20μm
Trace Length (μm)
Adhesion (32 nm)
0.0
0.5
1.0
1.5
2.0
2.5
3.0
3.5μm

Figure 4.6: Dual Fluorescence-AFM Images of Vinculin-Containing Adhesions on Control and Nanopatterned Surfaces: After 3 days in culture, HUVECS were fixed and their vinculin-containing adhesions fluorescently labeled. The adhesions were imaged by fluorescent and atomic force microscopy for glass control (A: fluorescence; B,C,D: AFM) and 0400M (F,H: fluorescence; G,I,J: AFM) surfaces. A dot and dash adhesion are labeled with arrows on the glass control in (A: fluorescence), (B: AFM), (C: 3-D AFM), and (D: high resolution AFM). A single adhesion is indicated with an arrow on the 0400M in (H: fluorescence), (AFM w/ overlaid fluorescence), and (J: high resolution AFM). Height traces were measured over the adhesion sites; the black line indicates the trace path that begins at the top of the image, for the control (D) and 0400M surface (J). The corresponding height data is shown for the control (E) and 0400M (K). The dash adhesion on the control surface had a measured height of 25 nm above the glass background whereas the adhesion on the 0400M had a measured height of 32 nm. The 11 nm difference is due to the height of the nanopattern. The adhesions in the cell on the glass control were much larger ($Area_{DOT}$ = 6.80 μm^2 and $Area_{DASH}$ = 7.29 μm^2) and located mainly at the cell periphery (A), whereas adhesions formed on the 0400M surface were smaller ($Area_{0400M}$ = 0.036 μm^2) and more homogenously distributed throughout the cell (F). Large amounts of actin fibers can be seen terminating in the adhesions formed on the glass control (B), while only one actin fiber terminates in the adhesion on the 0400M (J) surface. This data indicates that the HUVECs recognize and adhere to the functionalized nanopatterns and that the nanopattern size limits the adhesion size and the amount of actin able to tie into the adhesion, thereby potentially influencing mechanotransduction processes and signaling.

next pattern at 1.5 µm. The line then crosses a defect line at 1.0 µm, and one more nanopattern at 0.6 µm, before continuing at a reduced height of about 15 nm as actin fibers. These measured heights agree with the 13 to 17 nm measured height for the adhesions and the actin height of 7 nm. The height between each of the nanopatterns is close to the thickness of the adhesions. This may be a result of firmly cross-linked bridges of cytoplasmic adhesion components spanning between the raised adhesions or indicate FN stretching between the patterns. The length of the adhesion structure is about 1.7 µm, but it is only about 120 nm wide, which leads to a total area of 0.2 μm^2. The two adhesions in Figure 4.6 J that together compose the vinculin fluorescence area are completely separated, as the height between them reaches background levels (not shown).

Striking differences in the size and distribution of adhesions between control and nanopatterned surfaces was also discovered and is discussed in detail in Chapter 5. HUVECs on non-patterned glass surfaces have large adhesions mostly at the cell periphery (Figure 4.6 A,B) ranging in size, for the cell analyzed here, from about 1 to 6 µm and from 6.8 to 7.3 μm^2 in area for a dot adhesion (short arrow Figure 4.6 A,D) and a dash adhesion (long arrow Figure 4.6 A,D), respectively, as determined from the AFM images. These adhesions act as terminating sites for multiple actin fibers as seen in the AFM images (Figure 4.6 B,C). In contrast, HUVECs on the 0400M surface displayed a more homogenous distribution of small adhesions (Figure 4.6 F). The adhesion site area for the adhesion indicated in Figure 4.6 H is 0.036 μm^2 or 0.2 μm^2, depending on whether only the pattern or the full area indicated by vinculin staining is counted. In any case, this is far smaller than adhesions formed on the control surface. The smaller adhesions on the nanopatterned surfaces were not coupled to large stress fibers but

seem to interact with single actin filaments or F-actin (Figure 4.6 I,J), as opposed to multiple stress fibers seen in cells seeded on the glass surfaces. Although this provides just a snapshot of adhesive states, more detailed investigations of differences in adhesive states are discussed in Chapter 5. Most importantly, this detailed examination of adhesive properties shows that the adhesions terminate on the functionalized nanopatterns and that the nanopatterns can indeed limit adhesion site growth. However, it appears that is some cases the cytoplasmic components of adhesions can bridge between individual patterns, at least if the distance is not too great. In other cases both FN and adhesion components can bridge multiple patterns in the direction of the actin stress fibers, indicating the formation of fibrillar adhesions which is further discussed in Chapter 7.

4.5 Discussion

Integrin binding to ECM ligands and integrin clustering are synergistic events necessary for the induction of signaling cascades and engagement of the cytoskeleton with cellular adhesion sites. Cluster size is an indicator of the maturation of adhesions, which is driven by the applied force of the actomyosin machinery of the cell. The size of each cluster can range from about 30 nm for a trimer, to submicron-sized for motile cells, to many microns for fully matured adhesions. Due to this wide range of adhesion sizes, restrictions in the growth process induced by chemical patterns are expected to influence both the adhesion of adhesion-dependent cells and the molecular signaling events initiated and controlled by adhesion sites.

Chemically defined patterns of cell adhesion ligands provide direct molecular control over the processes of cell adhesion as well as over the mechanics of force

transduction. This control has been successfully implemented to investigate cell adhesion, spreading, and differentiation on the micron scale with tools such as microcontact printing of thiols on gold. Cell adhesion size control down to 0.1 μm^2 using thiol stamping has shown that cells can adhere and spread well using such areas for integrin binding, unless the distance between the adhesion sites exceeds 2 μm.[198] The extension into nanometer-scale adhesion size control has been much more difficult, as serial lithography techniques, such as dip-pen nanolithography,[154-158] other scanning probe lithography techniques,[159-162] and electron beam lithography,[146-148] are too time consuming in their fabrication to allow for systematic cell studies. Parallel patterning techniques such as imprint lithography,[163,164] micelle nanolithography,[166,182] particle lithography,[167] and capillary lithography[149] are better suited for quickly fabricating nanostructured surfaces over large areas.

Several nanopatterning techniques have been used to demonstrate cell adhesion,[199-201] but have so far not been used for systematic adhesion studies. Protein and cell adhesion have been observed on PEG pillars, but due to the repulsive properties of PEG, the level of cell adhesion was significantly lower than adhesion to similarly treated protein-coated glass surfaces.[149] Other techniques such as micelle lithography or star polymers have provided significant insights into the importance of integrin proximity in the clustering process, but they do not allow for the formation of larger adhesion sites except when used in conjunction with a serial technique such as e-beam lithography. Additionally, most techniques rely on RGD sequences for cell adhesion, and investigations of cell interactions with the full FN protein have not yet been possible on nanopatterns. Furthermore, these studies have yet to prove imposed restrictions on adhesion site growth in the detail described here.

The results presented and conclusions drawn here through the implementation of multiple surface characterization methods consistently show that modification of the glass background with PEG and thiolization of the gold nanostructures directs FN adsorption exclusively to the gold nanostructures. By performing the functionalization for both materials simultaneously, PEG adsorption to the gold areas was minimized, and the lack of sulfur on the glass areas indicates no or little thiol on the PEG surface. The ability to immobilize the full FN protein as opposed to RGD peptides alone on the gold areas enables the use of the synergistic sites in FN. Moreover, the terminal functionality used here presents FN in a compact form similar to that found on non-patterned hydrophobic surfaces,[120] but changing the thiol functionality to a hydrophilic end group would induce FN to appear in an extended form.[120] This flexibility allows for studies testing the preferential engagement of different integrins based on the presentation of FN on different thiol terminal functionalities to be undertaken.[117,121] Although non-covalent immobilization of FN on the nanopatterns was implemented in these studies, the use of other functional thiols would allow for specific and covalent anchoring by bioconjugation procedures. Of course, the presentation of small peptides tethered to thiols could also be easily achieved.

As confirmed by XPS, M- and B-type nanopatterned surfaces contain 7 – 8 % and 2 %, respectively, of the saturation amount of FN on a homogenous gold surface; in agreement with the average surface coverage of the pattern. The immunolabeling studies confirm the AFM and XPS results and indicate that the orthogonal surface chemistry does indeed work on the nanometer scale. Vinculin and AFM imaging indicate that cells recognize and adhere exclusively to the functionalized nanopatterns with imposed restrictions and adhesion site growth. The analysis of individual adhesions

shows that cellular adhesions are located on the nanopatterns, although in some instances the adhesion complex may bridge between patterns in the direction of associated actin fibers. The complexes can therefore sometimes reach lengths in the micron range, but their width is only around 120 nm, leading to adhesion areas well below 1 μm^2. This corresponds to the nanoisland size discussed in this section and more detailed analysis of adhesive properties is discussed in detail in Chapter 5. The AFM results of HUVEC adhesion properties on glass agree qualitatively with earlier studies, except that the adhesion height is lower than found for large adhesions of rat embryo fibroblasts after 72 hours on glass surfaces that had been de-roofed to allow for AFM analysis of the adhesions in cytosolic buffer. [202] This discrepancy could be attributed to much more rigid cross-linking and imaging in air that could lead to a more collapsed structure.

4.6 Conclusions

Taken together, these results indicate selective binding of the silane and thiol functionalities to the glass and gold areas respectively, and selective FN adsorption to the thiolated gold areas. The presence of signatures for the thiol and PEG and distinct N_{1s} peaks on the protein-adsorbed gold, unmodified glass surface, and on nanopatterned surfaces that are absent on the PEGylated glass sample indicate that the chemical functionality can be translated to the nanometer scale and FN can be adsorbed to very small thiolated gold nanoislands. This precise placement of chemical functionality and subsequent protein adsorption is the basis for the proposed studies. The restriction on adhesion site size was confirmed using fluorescent labeling and AFM measurements and the influences of nanopattern size, spacing, and percent surface

coverage on adhesion formation, actin cytoskeleton formation, and cell spreading, proliferation, and motility are discussed in the following chapters.

Chapter 5

Vinculin-Containing Adhesion Site Analysis

5.1 Introduction

A common design goal for the next generation of advanced biomaterials is to move from passive materials that avoid the initialization of adverse immune responses to biologically active materials that allow for direct control of the surrounding cells and tissue via cellular interactions with the material surface. For most applications the interface between the implanted device and the surrounding tissue lies at the material-tissue interface or biomaterial surface, except for tissue engineered constructs that try to induce cell growth into the volume of the material. Toward achieving the goal of producing advanced material surfaces that control cell function, scientists have determined material surface properties that can be used to gain direct control over cell behavior through the manipulation of cell adhesive properties with respect to integrin usage, adhesion composition, corralling cells into small ECM patches, or by limiting adhesions site growth.[84-91,96-107,110,111] Most of these findings come from studies performed using surfaces presenting features on the micrometer length scale and relatively few have explored the use of nanostructured materials to guide cell behavior. To date, no study has presented absolute proof of direct control over adhesion site size in the 30 to 400 nm size range and the work presented here is the first to show direct control over cell adhesion growth on this length scale. Through the use of meticulous image processing techniques and multiple quantification parameters, it is demonstrated that limiting adhesion site growth to the formation of small focal complexes via cell interactions with chemically-defined nanoscale FN islands can have a profound influence

on cell adhesive properties and consequently on downstream cell behavior. This chapter details changes in adhesion site properties as induced by differences in surface chemistry, FN surface density, and by limiting adhesion site growth using nanopatterned surfaces. The image processing technique that was developed and the quantification parameters that were designed to compare adhesive states of cells on control and nanopatterned surfaces is introduced and discussed. Significant differences in cell adhesive states as induced by cell interactions with surfaces presenting varied parameters with respect to surface energy, protein concentration, and FN nanoisland properties are all discussed. The results indicate that limiting cellular adhesion site growth to the nanometer regime using chemically defined nanopatterned surfaces can be implemented as a design strategy to manipulate cell adhesive states, modulate changes in actin cytoskeletal formation, and ultimately lead to control over cellular phenotype expression.

5.2 Materials and Methods

5.2.1 Cell and Reagents

Refer to Section 4.2.5, only non-pooled human umbilical vein endothelial cells were used for the experiments presented in this chapter.

5.2.2 Nanopattern Fabrication and Functionalization

Refer to Chapters 3 and 4 for fabrication and functionalization respectively.

5.2.3 Fluorescent Labeling and Imaging

Refer to Section 4.2.6, cells were also labeled and imaged after 1 day in culture.

5.2.4 Image Processing of Vinculin-Containing Adhesions

A semi-automated method was developed to quantify the size, number, density, and distribution of vinculin-containing adhesions from the acquired fluorescent images. The raw fluorescent images were low-pass filtered with a Fast Fourier Transformation (FFT) using ImageJ (NIH, Bethesda, MD) to remove any background signal present and to increase the contrast between the fluorescently labeled adhesions and background. [203] The FFT filter embeds the original image in a larger square image with a side length N that is a power of 2. To prevent artifacts, mirrored replicas of the original image are used to fill the edges and corners of the larger square image. The composite image is Fourier transformed and multiplied by a Difference of Gaussian (DoG) transfer function as a low-pass filter:

$$DoG(k) = \exp\left[-\left(\frac{2s_{small}}{N}k\right)^2\right]\left\{1-\exp\left[-\left(\frac{2s_{large}}{N}k\right)^2\right]\right\} \qquad (5.1)$$

Here s_{small} and s_{large} are user defined inputs, in terms of pixels, corresponding to the lower and upper size limits of the filter. The lower limit was set to 2 pixels to avoid the incorporation of single pixel noise from the imaging system and the upper limit was set to a pixel size corresponding to 20 μm^2, as typical adhesions do not grow this large. In Equation 5.1, the wave vector, k, is defined as the distance to the current pixel from the center of the Fourier image.

$$k = \sqrt{k_x^2 + k_y^2} = \frac{2p}{d} \qquad (5.2)$$

The final filtered image is created by applying an inverse Fourier transform and cropping back to its original size.

After filtration, the images were further processed with an iterative threshold algorithm using Igor Pro 5 (WaveMetrics, Lake Oswego, OR) to create binary images for automated adhesion site analysis. The iterative algorithm chooses an arbitrary threshold level and determines the average intensity value for all pixels that are less than the chosen value and for all pixels that are greater than the chosen threshold level. It calculates a mean of the two values and selects the optimal threshold level as determined by a calculated, modified version of the Pearson's correlation coefficient between the thresholded and FFT processed images through an iterative process. The filter was implemented to remove human error from traditional threshold techniques in which the threshold value is chosen by the user or automatically selected by a simple grey scale average algorithm.

After processing, the binary threshold images of the fluorescently-labeled vinculin-containing adhesion sites were used to quantify the cell adhesive properties using an in-house developed adhesion analysis algorithm created in ImageJ by an undergraduate student Matt Janciatis. The unprocessed, original fluorescent images were used to locate the cell outline with the magic wand tool in ImageJ and the processed images to locate and quantify the adhesion site properties. The algorithm locates each pixel in the cell outline from the cell outline image, measures the cell spreading area, and calculates the coordinates for the centroid of the cell. The centroid of each adhesion site in x, y coordinates and the surface contact area or size of each adhesion is measured from the processed images. After the algorithm analyzes the size of each adhesion, it creates two images based on a size threshold. The first image

created contains all of the adhesions less than 1 μm^2 in area (focal complexes) and the second only contains adhesions larger than 1 μm^2 in area (focal adhesions). Each of the three adhesion site images, one containing all of the adhesions, one with only small adhesions, and one with only large adhesions, is analyzed independently. The total number of adhesions per cell, the density of adhesions as described by Equation 5.3, and the distribution of adhesions with respect to their position in the cell is quantified.

$$D_A = \frac{N_A}{SA} * 5{,}000 mm^2 \tag{5.3}$$

where D_A is the calculated adhesion site density, N_A is the number of adhesions detected, and SA is the measured cell spread area. The calculated density in adhesions per μm^2 is scaled by 5,000 μm^2, the typical spread area of an EC. The analysis routine thereby reports the average size, density, and location of all the adhesions, the small adhesions, and the large adhesions independently. The distribution of the adhesion sites with respect to their ratiometric distance from the cell center to the cell periphery was also measured (R_A/R_{CP}). The radial distance to each adhesion site centroid at a given angle was measured from the centroid of the cell. This distance, R_A, was divided by the distance from the cell center to the cell periphery at the same angle to provide R_{CP}. A normalized value (R_A/R_{CP}) of zero indicates that the adhesion is located at the cell center, which often corresponds to the location of the nucleus, while a value of one indicates that the adhesion site is located at the cell periphery. Each analyzed cell was broken into ten separate regions, converted to a unit circle, and the number and density of adhesions was measured in each region. Plotting the data provides a location map of adhesion sites based on their size and normalized distance between the cell center and

cell periphery. Further analysis of the measured adhesive properties allowed for the quantification of the total adhesion area (sum of the surface contact area of all of the adhesions), percent adhesion (total adhesion area divided by the cell spread area), and allowed for investigation of the relationships of these adhesion properties with respect to cell spreading.

5.2.5 Statistical Analysis

Statistical analysis was performed using SPSS 12.0 (SPSS, Chicago, IL). Data sets were randomly chosen and their distributions tested for normality by evaluating the standard error of skewness and kurtosis. The calculated standard errors for all tested data sets were between -2 and 2, thereby indicating normally distributed data. ANOVA with either a post hoc Tukey or Dunnett's T3 test was implemented with a significance level of 0.05 to determine any significant differences in the adhesion site properties of the analyzed cells. Levene's test for the equality of variances was performed on the data sets to determine if equal variances could be assumed. If the significance of the Levene's test was greater than 0.1, equal variances were assumed and a post hoc Tukey procedure was used; if less than 0.1, unequal variances were assumed and a post hoc Dunnett's T3 test was implemented.

5.3 Results

The following sections discuss the results of the image processing protocol and observed changes in cell adhesive behavior as influenced by varying multiple surface parameters. Choosing a single control to compare to cells cultured on nanopatterned surfaces is not possible and many controls were implemented to separate the influences of varying FN surface density and surface energy on cellular adhesion formation. The

nanopatterned surfaces are a composite of 93 to 98 % glass and 7 to 2 % gold, but the FN is adsorbed only to the thiolated gold areas. Since it is known that FN adsorbs to hydrophobic and hydrophilic surfaces in different confirmations [120] and that these conformational differences influence adhesion composition and cell behavior, [114,115,117,118,121] thiolated Au surfaces were used as controls to accurately represent the confirmation of FN on the nanopatterns. However, since the nanopatterned surfaces are composed mostly of glass, although it is PEGylated and should not be recognized by the cells, adhesion site studies were also performed on FN adsorbed to glass surfaces. Furthermore, most conclusions in available literature concerning cell adhesion were drawn from studies using glass surfaces and the use of glass as a control surface here allows for ease of comparison to previous findings. The nanopatterned surfaces display very low global concentrations of FN composed of two components, very high local FN densities on the nanopatterns, surrounded by very little to no protein on the PEGylated glass support. For this reason, surfaces with varying levels of FN were included in the control group to separate FN density influence from the influence of limiting adhesion site growth using nanopatterned surfaces. Thiolated Au surfaces saturated with adsorbed FN accurately represent FN densities on the nanopatterns but have much higher global FN densities than the composite nanopatterned surfaces. Conversely, surfaces presenting low densities of homogenously adsorbed FN more accurately reproduce the global densities measured on the nanopatterned surfaces but do not accurately reproduce the FN saturation levels on the nanoislands. To elucidate the separate influences from each other, four different control surfaces were implemented. Cell adhesion studies were performed on thiolated Au and plain glass surfaces, both adsorbed with FN at a concentration of 10 µg/mL for

20 minutes, named 10Au and 10G respectively, to determine the influence of varying surface chemistry on adhesion site formation. Adhesion site studies were also performed in cells on thiolated Au surfaces with varying densities of adsorbed FN at concentrations of 2, 10, and 25 µg/mL to determine the influence of global FN surface concentration on adhesion site formation. Finally, the nanopatterned surfaces were compared to all of the controls to separate local FN density, global FN density, and varying surface chemistry influences on adhesion site properties. Table 5.1 displays the surface properties and introduces the nomenclature for all of the surfaces implemented in the adhesion analysis studies.

Name	FN Density ($FN/\mu m^2$)	Characteristic Length (nm)	Nanoisland Area (nm^2)	Spacing (nm)
0300B	41	92 ± 33	3,629 ± 1,013	308 ± 11 {216}
0300M	217	94 ± 11	5,191 ± 1,298	177 ± 13 {83}
1500B	41	222 ± 25	46,550 ± 7,548	1,534 ± 19 {1,312}
1500M	217	405 ± 41	85,653 ± 17,044	883 ± 51 {478}
02Au	537	ND	ND	ND
10Au	1,882	ND	ND	ND
25Au	2,474	ND	ND	ND
10G	2,052	ND	ND	ND

Table 5.1: Measured Surface Properties for Control and Nanopatterned Surfaces Used in Cell Adhesion Studies: The FN surface density ($FN/\mu m^2$) was determined from the XPS calibration. The characteristic length, corresponding to the length of the longest bisector of individual nanopatterns, the pattern area for individual patterns, and the spacing between the nanopatterns were all measured from high-resolution AFM images. Both the center-to-center spacing and {rim-to-rim} spacing are listed for the nanopatterned surfaces. ND = Not Determined.

5.3.1 Image Processing and Adhesion Site Quantification

Cells adhere to 2-D surfaces with three primary types of integrin-mediated adhesions; focal complexes, focal adhesions, and fibrillar adhesions. Focal complexes are small, immature adhesions with short lifetimes and a typical size of 0.25 μm^2. [16] These immature complexes often disappear shortly after their formation but sometimes mature into focal adhesions. The adhesion maturation process requires adaptor protein mediated linkage to actin stress fibers and the application of force to the adhesion plaques as induced by Rho-mediated actomyosin contraction. [11,42] Once formed, mature focal adhesions are typically larger than 1μm^2 in size and can grow up to 12 to 15 μm^2. [16] Fibrillar adhesions, a late stage of maturation only formed in the presence of FN, can range from the size of focal complexes to that of focal adhesions making it difficult to identify their presence based on size alone. [16] While these three adhesion types have different molecular compositions they all contain vinculin. [16] Therefore, vinculin labeling with fluorescently tagged monoclonal antibodies was implemented in this study to identify and locate cellular adhesion sites.

To date, most studies concerning the quantification of cellular adhesion sites have used a minimum size cutoff of ~ 0.25 μm^2 due to resolution limitations of light microscopy. [50,204] Others have implemented segmentation algorithms to locate and patch together pixels from single adhesion sites but still used a large minimum size limit of 0.56 μm^2. [205] While this minimum size cutoff prevents the incorporation of noise and background signal into adhesion site analysis, it also biases analysis towards focal adhesions and neglects smaller focal complexes. Since these smaller complexes and their maturation to larger adhesions is an important regulator of intracellular signaling and cell motility, a more complete picture relating adhesive properties to downstream

cell behavior can be formed if they are incorporated into adhesion site analysis. Previous reports have shown that adhesions as small as 0.1 μm^2 can be detected if much effort is taken in the processing of the fluorescent images.[198] As demonstrated in Section 4.4.6, the combination of atomic force with fluorescent microscopy allows for a detailed analysis of the small adhesions formed to the nanopatterned surfaces but the technique is to time consuming to be implemented on the large population of cells needed for statistically valid studies. To better cope with the resolution limitations of light microscopy, an image processing technique was developed that allowed for the detection and quantification of very small adhesions such as focal complexes and those formed by cells cultured on nanopatterned surfaces.

The first and one of the most crucial steps in being able to identify and analyze very small adhesions in fluorescent images is the sample preparation process. The use of CSK buffer to remove soluble proteins from the cytoplasm was essential for the elimination of unwanted background signal. Imaged cells exposed to this buffer displayed enhanced contrast between the labeled adhesion sites and background compared to cells not treated with the buffer. The CSK treatment of cells proved to be highly effective in preventing labeling of soluble vinculin and by preventing non-specific adsorption of the fluorescently labeled antibody to other cytoplasmic proteins. After preparation, the cells were imaged and the images processed for quantification of cell adhesion sites.

A semi-automated method was created to accurately identify and quantify the properties of vinculin-containing adhesions in the acquired fluorescent images. The raw images were Fourier transformed and multiplied by a Difference of Gaussians transfer function that allowed for user defined control of lower and upper feature size limits. The

DoG function is especially useful for removing high-frequency spatial noise while preserving the spatial information that lie in the range of the chosen frequencies, in this case, the range of adhesion site sizes. After filtering, an iterative threshold algorithm was applied to the images. Traditional thresholding techniques are useful for creating binary images from fluorescent images that contain features of a similar size but can artificially enlarge small features or artificially shrink large features when a wide range of sizes are present in the image (Figure 5.1 A,D,E, and I). To bypass this problem, an iterative threshold algorithm that more accurately thresholds images containing features of interest with a wide range of sizes was implemented. The combined application of the FFT filtering and iterative thresholding techniques resulted in processed images with well-defined fluorescently labeled cellular adhesions against an almost non-existent background (Figure 5.1 C,G,H, and K).

A comparison of the effectiveness in accurately reproducing fluorescently imaged cellular adhesion sites was made between images processed with traditional techniques and those processed with the method developed here. In this case, traditionally processed images were defined as those that were exposed to a rolling ball background subtraction algorithm followed by automated thresholding in which the threshold level is chosen through grey scale averaging.

Figure 5.1 B shows the original unprocessed fluorescent image used for the image processing technique comparison. The original image was artificially colored green and the final processed images from both techniques were artificially colored red. The final image created using the traditional image processing technique is shown in Figure 5.1 A and the final image created using the method developed here in Figure 5.1 C. A comparison between the accuracy of adhesion site recognition and

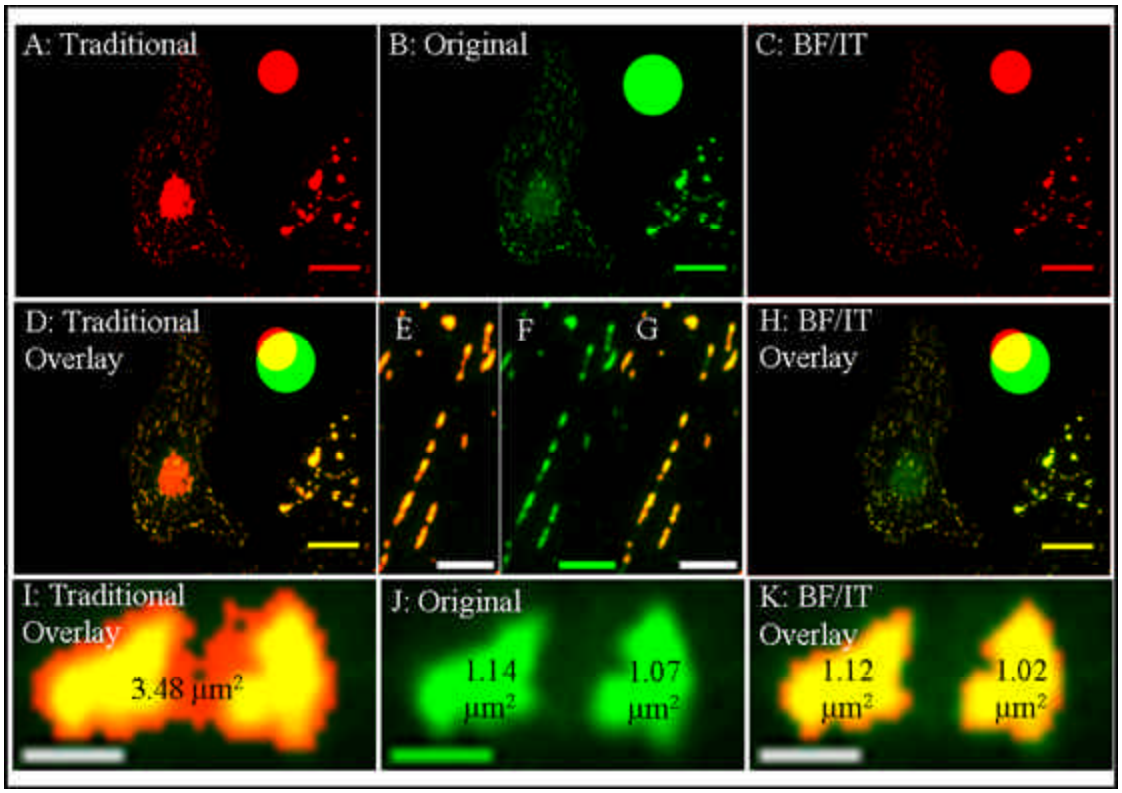

Figure 5.1: Image Processing of Adhesion Site Fluorescent Images: Comparison between traditional thresholding and the semi-automated technique developed to quantify cellular adhesion properties. Depicts artificially colored (B) original, (A) traditional threshold, and (C) semi-automated threshold images. (D,H,I,K) The threshold images were merged with the original to show correlation, yellow = match, red/green = no match. (E-G, I-K) Zoomed in regions showing better correlation using the semi-automated process compared to the traditional threshold process. (I-K) The adhesion site areas were measured and compared between the original image and the two thresholding techniques. A-C, D, H: Scale bar = 20 µm. E-G: Scale bar = 3 µm. I-K: Scale bar = 1 µm.

adhesion site size reproduction between the two processing techniques can be made by simply overlaying the red processed and green original images. Yellow areas indicate correlation between the original and processed images, green areas indicate adhesion size underestimation, red areas indicate adhesion size overestimation, and orange areas indicate edge detection. Comparing the image in Figure 5.1 D with H shows that the image processing method developed here more accurately reproduces the adhesion sites as indicated by the dominate presence of yellow, whereas the traditional method shows gross overestimation of adhesion site size as indicated by the dominate red color, particularly near the cell nucleus. Further investigation of single adhesion sites as shown in Figure 5.1 I-K demonstrates the more accurate size reproduction of adhesion site dimensions produced using the newly developed image processing method. Two adhesions, 1.14 and 1.07 μm^2 in area were isolated in the original image (Figure 5.1 J), the traditional method overestimated the size of the adhesions and merged them into one adhesion site with a size of 3.48 μm^2 (Figure 5.1 I), while the enhanced image processing method reported two adhesions with sizes very similar to those measured from the original image, 1.12 and 1.02 μm^2 respectively (Figure 5.1 K).

To test the limitations of the image processing method, it was applied to images of fluorescently labeled FN adsorbed to the smallest nanopatterns used in the cell studies, the 0300B surfaces (Figure 5.2 A). From AFM analysis of these surfaces it is known that the nanopatterns have a characteristic spacing of 308 ± 11 nm and an area of 3,629 ± 1,013 nm^2 (Figure 3, Table 1, and Table 4). Measurements made from the processed images showed enough resolution to accurately reproduce the spacing, 300 ± 41 nm, but drastically overestimated the area of the nanoislands, 36,882 nm^2. Figure 5.2 graphically represents the processing method and displays the processed images after

each step. Figure 5.2 A shows the original image of fluorescently labeled FN adsorbed to a 0300B nanopatterned surface and subsequent zoomed in regions are shown in Figure 5.2 B, E. The corresponding FFT filtered images are shown in Figure 5.2 C, F and the final FFT filtered and iterative thresholded (FFT/IT) images in Figure 5.2 D,G. Comparing Figure 5.2 E to G shows that the FFT/IT processing method can detect very small fluorescent features, 92 nm sized FN nanoislands in this case, if the features of interest are spaced far enough apart. While the FFT/IT image processing technique has limitations on size and area measurements for very small features below 300 nm in size, the method can be implemented to accurately identify small adhesions and allows for their quantification with respect to the number present in the image, their density, and their location. Area measurements made from the processed fluorescent images of vinculin-containing adhesions smaller than 300 nm in size will be resolution limited and reported as larger than their actual size. Due to this limitation the total adhesion area and percent adhesion analysis were not performed on cells cultured on nanopatterned surfaces, as adhesions formed on these surfaces are well below 300 nm in size for all of the surfaces except the 1500M surface.

This combined image processing and adhesion analysis protocol resulted in a powerful tool for relating observed changes in gross cell behavior to quantified changes in adhesive states. The use of this combined protocol allowed for the incorporation of previously unanalyzed focal complexes into a thorough adhesion site analysis that provided new insight into control over cell adhesion behavior via cell-surface interactions with engineered surfaces.

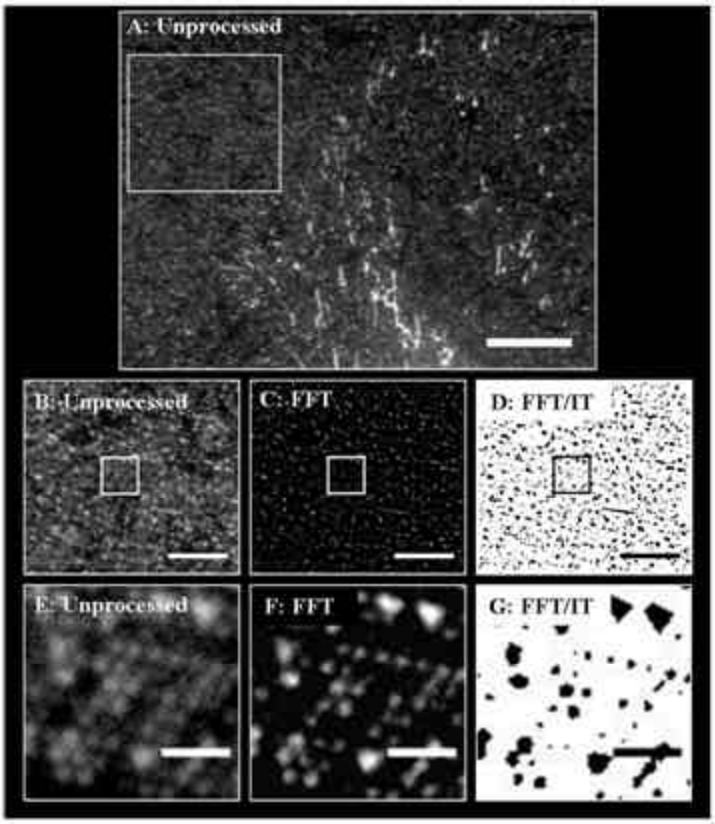

Figure 5.2: Resolution Limitations in FFT/IT Processing of Fluorescent Images: While the Fast Fourier Transform and Iterative Thresholding (FFT/IT) processing method can accurately detect small fluorescent features, 92 nm fluorescently labeled FN nanoislands in this case, their size is grossly overestimated, see text. (A) A raw fluorescent image of FN adsorbed to a 0300B nanopatterned surface. The white box in (A) indicates the location of (B-D). The white boxes in (B-E) represent the zoomed in regions shown in (E-G). (B, E) Zoomed in regions of the unprocessed image. (C, F) The same images as B and E after the application of the FFT filter. (D,G) The same images as B and E after FFT filtering and iterative thresholding. (A) Scale bar = 10 µm. (B-D) Scale bar = 5 µm. (E-G) Scale bar = 1 µm.

5.3.2 Surface Chemistry Influence on Adhesion Site Properties

It is known that changes in surface energy induce conformational changes in adsorbed FN [120] and that these FN conformational differences influence integrin binding, adhesion composition, and FAK phosphorylation in a surface energy dependent manner. [115,117,121] Furthermore, the changes in adhesion composition can induce changes in cellular phenotype expression. Tuning the free energy of the surface that FN is adsorbed too provides the ability to modulate cell behavior between proliferation or differentiation. [114,115] Hydrophilic surfaces, glass in this case, presenting more extended confirmations of adsorbed FN, induce the formation of focal and fibrillar adhesions rich in $\alpha_5\beta_1$ integrins that lead to increased levels of cell proliferation [114,115] while hydrophobic surfaces, thiolated Au in this case, presenting more compact confirmations of FN lead to the formation of adhesion sites dominated by $\alpha_v\beta_3$ integrins that results in cell differentiation. [114,115] These two independent pathways in cell behavior hint to either integrin-mediated influence of signaling strength or the existence of different integrin mediated signaling cascades.

The influence of varying surface chemistry on adhesion site formation was determined by comparing the quantified adhesion properties of cells cultured on thiolated Au and plain glass surfaces with similar FN surface densities. Since the nanopatterned surfaces used in these studies are more than 90 % glass, although it is PEGylated and therefore passive, glass surfaces were used as controls. Since the FN is presented on thiolated Au nanoislands, cells were cultured on homogenously FN coated gold surfaces to accurately reproduce the conformational state of FN as presented for cell attachment. Au and glass surfaces with similar FN densities were used to insure that any observed differences in cell adhesive properties in cells cultured on these surfaces

were solely a function of differences in surface chemistry and not of FN concentration. Furthermore, the comparison of adhesion properties between cells cultured on 10Au and 10G surfaces, see Table 5.1 for surface properties, can be implemented to show that changes in adhesive behavior induced in cells grown on nanopatterned surfaces are not an artifact of differences in surface chemistry but are consequences of limitations imposed on adhesion site growth.

Number, Sizes, and Types of Adhesions

The results indicate that surface chemistry has almost no influence on adhesion formation in cells after 1 day in culture but induces significant changes in adhesive states after 3 days. While cells on both hydrophilic and hydrophobic surfaces display very similar adhesion properties after 1 day, cells cultured on hydrophilic glass surfaces display statistically fewer small adhesions and statistically larger focal adhesions after 3 days compared to cells on hydrophobic gold surfaces. The data indicates that cells on Au surfaces do not undergo adhesive changes with time while cells cultured on glass surfaces display an adhesive state transformation or maturation process.

After 24 hours in culture, cells adhere to both 10Au and 10G surfaces with almost identical numbers, densities, and sizes of adhesions (Figure 5.3 A-C and Figure 5.5 A-C). Approximately 1,000 vinculin-containing adhesions are formed with an average density of 750 adhesions/5,000 μm^2 in cells on both surfaces (Figure 5.3 A-C and Figure 5.5 A-C). Cells on these surfaces also display very similar trends of adhesion site formation as a function of cell spreading, showing linear increases in the number of all, small, and large adhesions with increased cell spreading. (Figure 5.3 D-F).

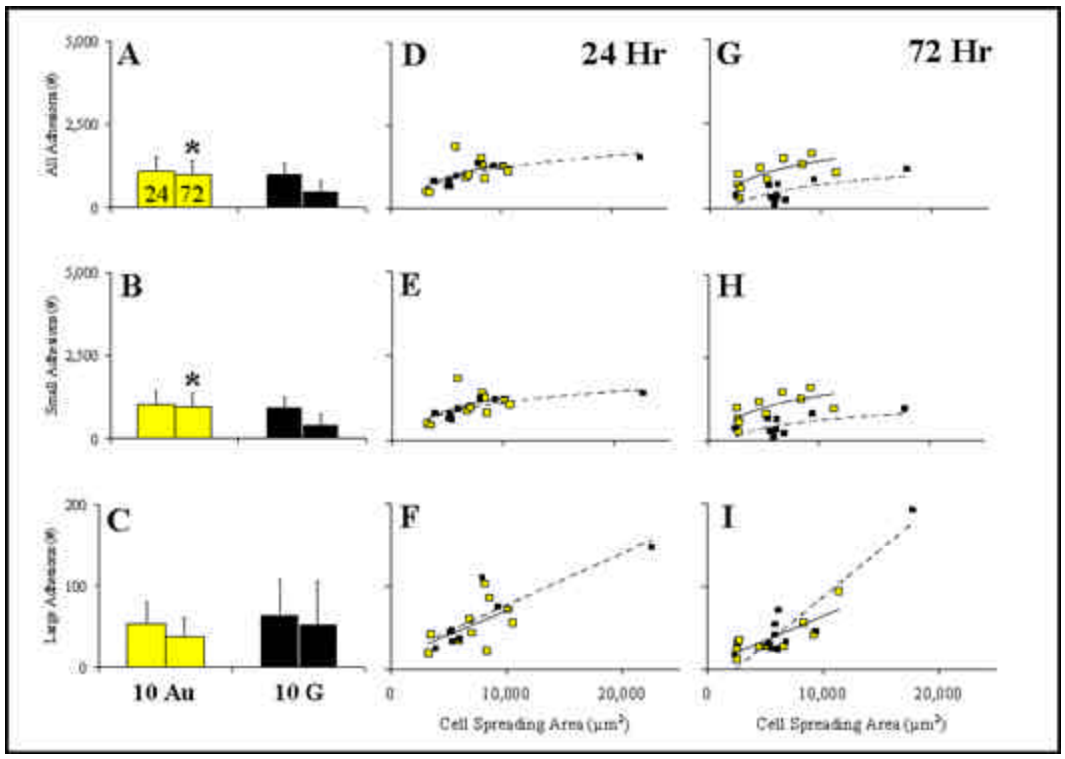

Figure 5.3 Average Number of Adhesions and Number of Adhesions versus Cell Spreading for Cells on 10Au and 10G Surfaces: After 1 and 3 days in culture, cells on 10Au (yellow) and 10G (black) surfaces were fixed and their vinculin-containing adhesions fluorescently labeled and the number of adhesions per cell quantified. The average number of adhesions per cell (A-C) and their relationship to cell spreading (D-G) was analyzed. The average number of adhesions formed per cell for (A) all adhesions, (B) the small adhesions (< 1 μm^2), and (C) the large adhesions (> 1 μm^2). (D-F) Adhesion number as a function of increased cell spreading after 1 day in culture for (D) all of the adhesions, (E) the small adhesions, and (F) the large adhesions. (G-I) Same as D-F but after 3 days. * = Significantly more adhesions than cells on 10G surfaces ($p = 0.007$).

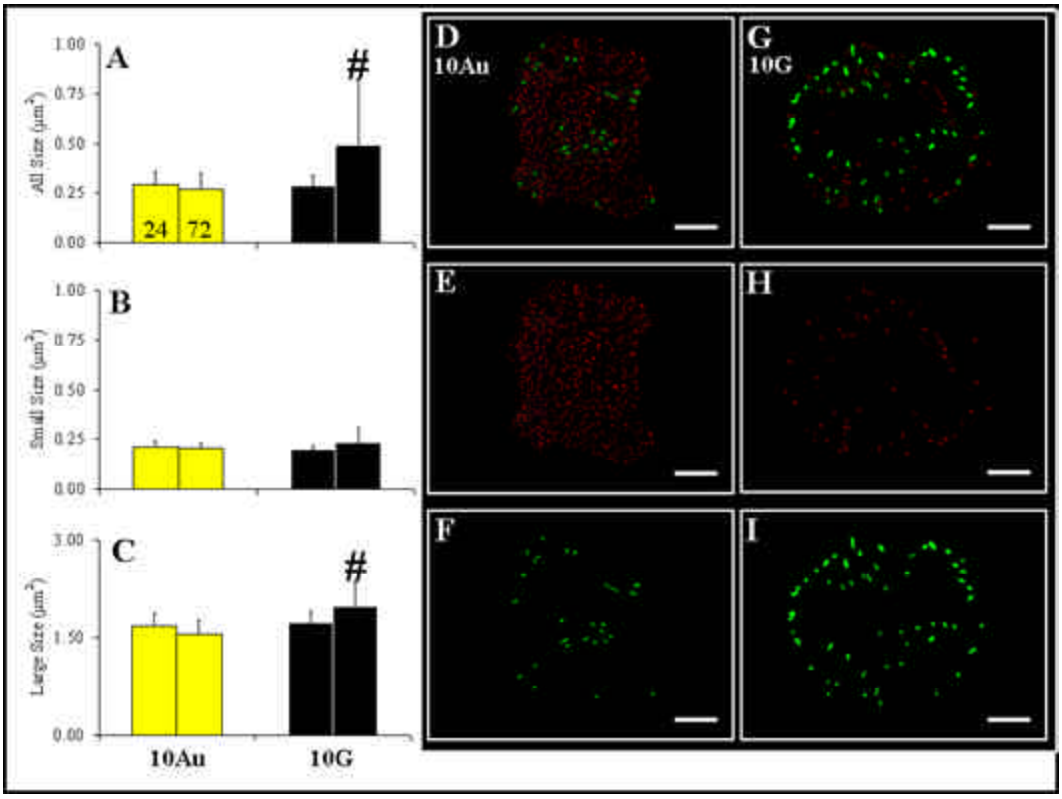

Figure 5.4: Adhesion Site Sizes for Cells on 10Au and 10G Surfaces: After 1 and 3 days in culture, cells on 10Au (yellow) and 10G (black) surfaces were fixed and their vinculin-containing adhesions fluorescently labeled and sizes measured. The average adhesion site sizes were measured for (A) all of the adhesions (B) the small adhesions (< 1 μm^2), and (C) the large adhesions (> 1 μm^2). After 3 days in culture the cells were fixed and their vinculin-containing adhesions fluorescently labeled, imaged, and processed with the FFT/IT method and analyzed. (D-F) A FFT/IT processed image of a cell on a 10Au surface showing (D) all of the adhesions, (E) the small adhesions (red), and (F) the large adhesions (green). (G-I) Same as (D-F) but for a cell on a 10G surface. (D-I) Scale bar = 20 μm. # indicates significantly larger adhesions than cells on 10Au surfaces ($p = 0.008$).

After 3 days in culture the differences in surface chemistry induce significant changes in cellular adhesive states, compare Figure 5.4 D-F to G-I. While cells cultured on 10Au surfaces remain in the same adhesive state as they were after 1 day displaying almost identical numbers, densities, and sizes of adhesions, cells cultured on hydrophilic glass surfaces reduce the number and density of small adhesions used to attach to the surface (Figure 5.3 B and Figure 5.5 B) while simultaneously increasing the average size of the large adhesions (Figure 5.4 C). Cells grown on 10Au surfaces maintain a fairly high number and density of vinculin-containing adhesions with time (Figure 5.3 A-C and Figure 5.5 A-C). The adhesion sites formed are composed of small adhesions with an average size of 0.21 ± 0.03 μm^2, presumably focal complexes as cells on these surfaces form very few FN fibrils as discussed in Chapter 7, and focal adhesions with an average size of 1.56 ± 0.21 μm^2 (Figure 5.4 A-F). Cells on 10G surfaces behave differently and show a decrease in the number of small adhesions from 1,019 ± 334 after 24 hours to 498 ± 338 and density from 732 ± 216 to 381 ± 235 small adhesions/5,000 μm^2 after 3 days in culture (Figure 5.3 B and Figure 5.5 B). While changes are observed in the maintenance of small adhesions over a 3 day period for cells cultured on 10G surfaces there are almost no changes in the number or density of large focal adhesions (Figure 5.3 C and Figure 5.5 C), although the large adhesions do show a slight increase in size from 1.72 ± 0.18 μm^2 to 1.97 ± 0.39 μm^2 over a 3 day period thereby making them significantly larger than the adhesions in cells on Au surfaces (Figure 5.4 C, I).

These changes in adhesive states are also reflected in the relationship between adhesion site formation and cell spreading. While cells on 10Au surfaces show the same trend of linear increases of both small and large adhesions with increased cell spreading (Figure 5.3 E,F,H, and I), cells on 10G surfaces more quickly reach saturation of small

adhesion formation at approximately 800 small adhesions regardless of the extent of cell spreading (Figure 5.3 H). While significant differences in the maintenance of small adhesions were observed there is relatively little difference in the maintenance of large adhesions between cells on 10Au and 10G surfaces (Figure 5.3 I).

Combining these results implies that cells cultured on glass surfaces have the ability to enlarge existing focal adhesions while decreasing the density of small adhesions with time and show maturation of adhesive states that can not be achieved by cells on 10Au surfaces. These differences in adhesive states are most likely due to differences in integrin expression and adhesion composition as dictated by conformational differences in adsorbed FN to surfaces with varying energy. [114,115,117,121]

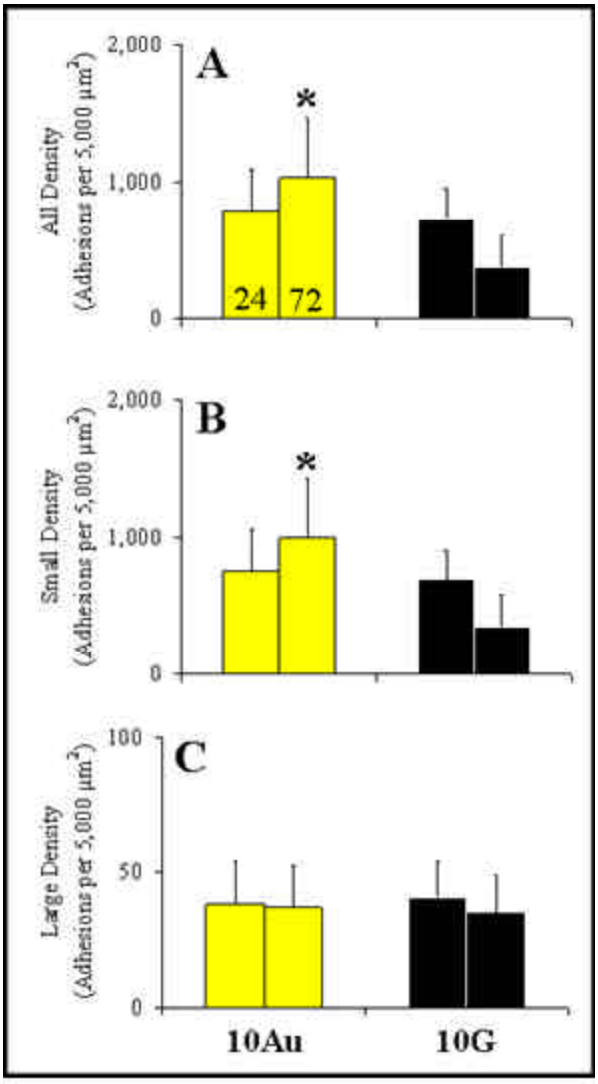

Figure 5.5: Average Adhesion Site Densities for Cells on 10Au and 10G Surfaces: After 1 and 3 days in culture, cells on 10Au (yellow) and 10G (black) surfaces were fixed, their vinculin-containing adhesions fluorescently labeled, and adhesion site densities quantified. The average adhesion site density for (A) all of the adhesions, (B) the small adhesions (< 1 μm^2), and (C) the large adhesions (> 1 μm^2) was measured. * Indicates higher density than cells on 10G surfaces ($p = 0.001$)

Adhesion Area and Percent Adhesion

Further insight into the different adhesive states of cells grown on 10Au and 10G surfaces can be gained from analyzing the cellular adhesion area (sum of the areas of all adhesions) and the percent adhesion (sum of the areas of all adhesions divided by the cell spread area). The differences in these quantified parameters between cells cultured on 10Au and 10G surfaces are reflective of the observed differences in the number and density of small adhesions maintained with time as discussed in the previous section. It was demonstrated in the previous section that the cells on 10G surfaces decrease the number and density of small adhesions used to attach to the surface over a 3 day period while simultaneously enlarging the size of existing adhesions. This transition in adhesion states in cells on 10G surfaces that is not observed in cells on 10Au surfaces is also reflected in the adhesion area and percent adhesion data.

After 24 hours in culture, cells on both 10Au and 10G surfaces have almost identical values of adhesion area and percent adhesion, ~ 300 μm^2 and 4.25 % respectively (Figure 5.6 A and Figure 5.7 A). As time persists the total adhesion area for cells on 10Au surfaces remains the same while the attachment area of cells on 10G surfaces display a slight decrease to ~200 μm^2 (Figure 5.6 A). The measured decrease in total adhesion area of cells grown on 10G surfaces stems from a drastic decrease in the contribution of adhesive area from small vinculin-containing adhesions from a value of 192 ± 77 to 95 ± 74 μm^2 confirming the observed decrease in the number of small adhesions as discussed in the previous section. The drop in the number of small adhesions in cells on 10G surfaces results in a statistically lower average of adhesion area due to small adhesions compared to cells on 10Au controls. However, there is no statistical difference between

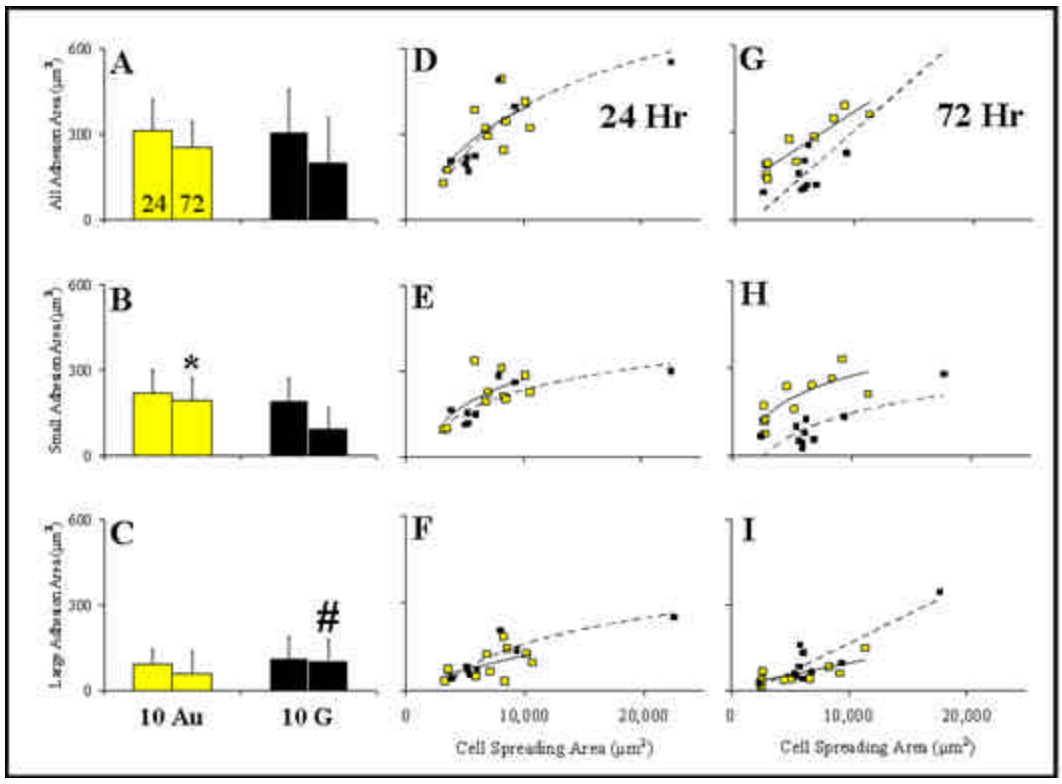

Figure 5.6: Adhesion Area for Cells on 10Au and 10G Surfaces: After 1 and 3 days in culture, cells on 10Au (yellow) and 10G (black) surfaces were fixed, their vinculin-containing adhesions fluorescently labeled, and the adhesion area per cell quantified. The average adhesion area for (A) all of the adhesions, (B) the small adhesions (< 1 μm^2), and (C) the large adhesions (> 1 μm^2)was measured. The relationship between adhesion area and cell spreading is shown in (D,G) for all adhesions, (E, H) for the small adhesions, and (F, I) for the large adhesions. * Indicates significantly more adhesion area than cells on 10G surfaces ($p = 0.009$). # Indicates significantly more adhesion area than cells on 10Au surfaces ($p = 0.013$).

the total adhesive areas achieved by cells on these two different types of surfaces. This implies that the cells on 10G surfaces make up for this decrease in small adhesions through the large adhesion sites.

The contact area of large focal adhesions remains unchanged at ~ 100 μm^2 (Figure 5.6 B,C) for cells on 10G surfaces while cells on 10Au surfaces behave oppositely and show no change in area attributed to small adhesions but display a slight decrease in contact area from large adhesions from 92 ± 51 to 59 ± 37 μm^2 over a 3 day period (Figure 5.6 B,C). The data indicates that cells strive to achieve the same contact area regardless of the surface properties but attain this desired contact area through different modes of attachment. Cells on 10Au surfaces maintain their adhesive area by increasing the number of small adhesions while cells on 10G surfaces attain the same overall area but do so by slightly enlarging existing focal adhesions while decreasing the number of small adhesions.

The differences in adhesive areas are also reflected in the percent adhesion data. After 24 hours, cells on both 10Au and 10G surfaces maintain a fairly constant portion of their spread area in contact with the surface regardless of the amount of spreading, ~ 4.5 % (Figure 5.7 D). After 72 hours this value drops to ~ 3 % for cells on 10G surfaces but stays at ~4.5 % for cells on 10Au surfaces and there is a significant difference between the two values (Figure 5.7 G). The drop in percent adhesion in cells on 10G surfaces stems from a decrease in the percent adhesion due to small adhesions and closely matches the observed decreases in the number, density, and contact area of small adhesions.

The quantified changes in adhesion area and percent adhesion parallel the observed differences in the number and density of small and large adhesions

maintained with time between cells on the two surfaces. As the number of small adhesions decrease in cells on 10G surfaces so does their contribution to adhesive area and percent adhesion. Since the cells cultured on 10Au surfaces do not undergo as drastic of changes with respect to the number and density of adhesions their total adhesion area and percent adhesion stay fairly constant with time. These results concerning differences in adhesion area and percent adhesion as induced by the surface chemistry parallel the observed differences in adhesion site maintenance and provide validation of surface chemistry induced changes in adhesive states.

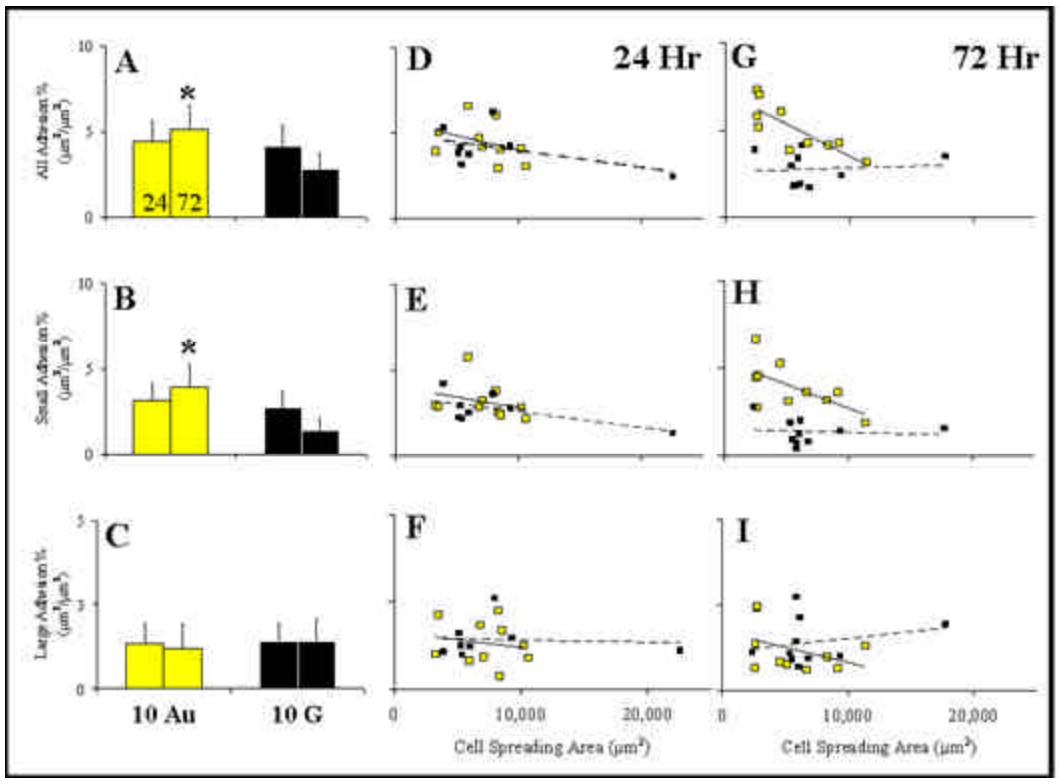

Figure 5.7: Percent Adhesion for Cells on 10Au and 10G Surfaces: After 1 and 3 days in culture, cells on 10Au (yellow) and 10G (black) surfaces were fixed, their vinculin-containing adhesions fluorescently labeled, and the percent adhesion per cell quantified. The average percent adhesion for (A) all of the adhesions, (B) the small adhesions (< 1 μm^2), and (C) the large adhesions (> 1 μm^2) was measured. The relationship between percent adhesion and cell spreading is shown in (D,G) for all adhesions, (E, H) for the small adhesions, and in (F, I) for the large adhesions. * Indicates significantly more adhesion area than cells on 10G surfaces ($p < 0.001$).

Adhesion Site Distributions

Insight into differences of adhesion site formation can be developed by analyzing the location of different sized vinculin-containing adhesions. To do this, each individual adhesion site was normalized by its ratiometric distance between the cell œnter and periphery. After normalization, the number and density of adhesions per cell region were plotted to provide a location map of all of the adhesion sites. The results of the analysis indicate that while there were observed differences in the number, adhesive area, and percent adhesion of small adhesions between cells on 10Au and 10G surfaces their distributions or location within the cell are very similar.

After 24 hours, cells on both 10Au and 10G surfaces display almost identical distributions of adhesions (Figure 5.8 A-C), while after 3 days in culture some slight differences arise in the absolute number and density of adhesions but the trends remain very similar (Figure 5.8 D-F). Cells cultured on both 10Au and 10G surfaces show an increase in the total number of adhesions as you move from the cell center, 0 on the x-axis, toward the cell periphery, 1 on the x-axis (Figure 5.8 A,D). Normalizing this trend to cell spreading area shows that the cells quickly reach saturation in the density of adhesions formed and consequently maintain this density throughout the cell (Figure 5.9 A). The only difference observed after 24 hours in culture is that cells seeded on 10Au surfaces show a slightly higher density of large focal adhesions a short distance from the cell center that then levels off to a constant value almost identical to that of cells on 10G surfaces (Figure 5.9 C).

After 72 hours, the trends of adhesion site distribution remain similar for the adhesions but cells cultured on 10Au and 10G surfaces show different absolute values

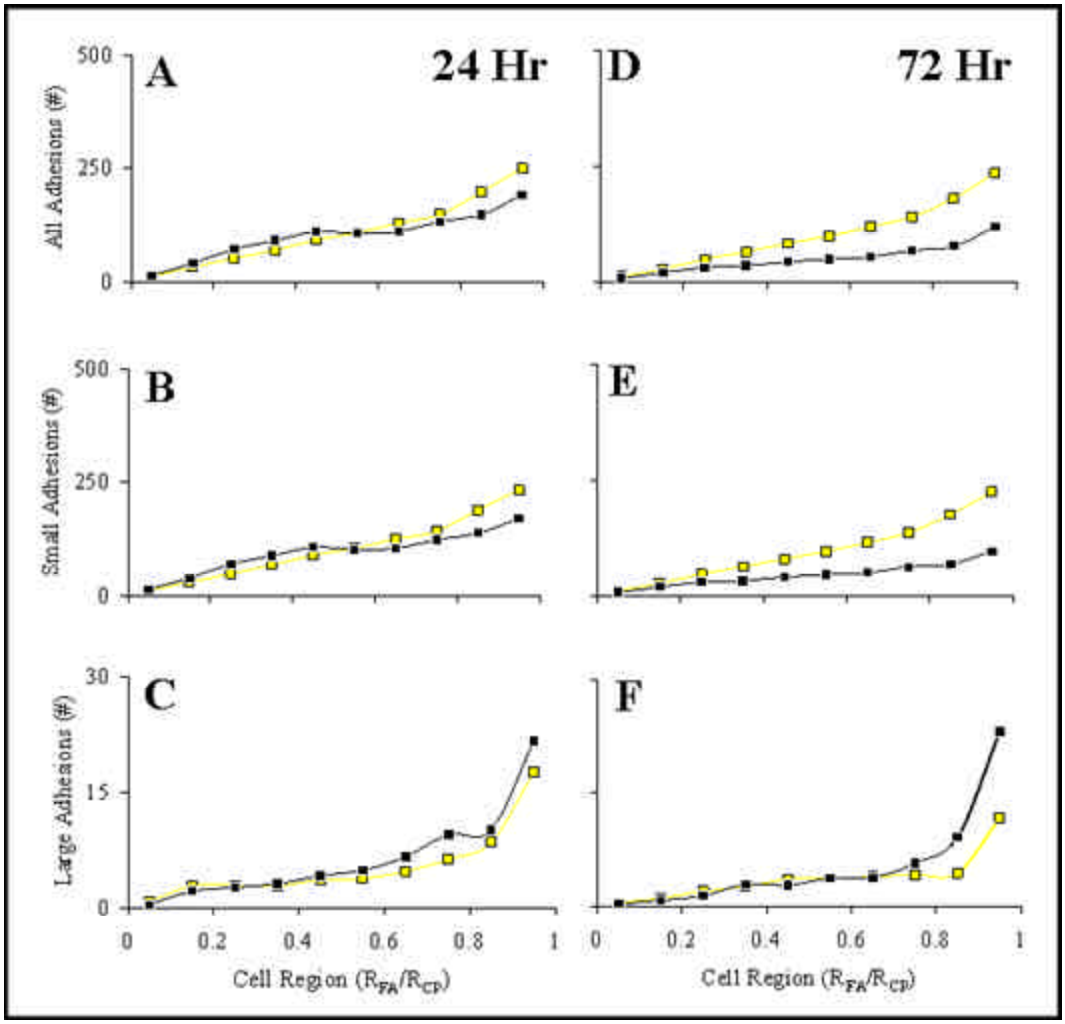

Figure 5.8: Number Distributions of Cells on 10Au and 10G Surfaces: After 1 and 3 days in culture, cells on 10Au (yellow) and 10G (black) surfaces were fixed, their vinculin-containing adhesions fluorescently labeled, and the number of adhesion sites in each cellular region as a function of their normalized distance from the cell center quantified. The adhesion site number distributions for (A, D) all of the adhesions, (B, E) the small adhesions (< 1 μm^2), and (C, F) the large adhesions (> 1 μm^2) are shown.

(Figure 5.9 E). Cells on 10G surfaces display a lower number and density in small adhesion distribution after 3days while cells on 10Au surfaces show relatively little change (Figure 5.8 B,E and Figure 5.9 B,E). Furthermore, cells on 10G surfaces show a more pronounced formation of large adhesions at the cell periphery after 3days compared to cells on 10Au surfaces (Figure 5.8 F), although the density values that take cell spreading into account show that they follow very similar trends (Figure 5.9 F). These differences in adhesion site distribution properties confirm the observed drop in small adhesion formation of cells on 10G surfaces and show that the decrease in small adhesions is not isolated to one area of the cells but instead is a homogenous decrease in the maintenance of small adhesions throughout the cell body.

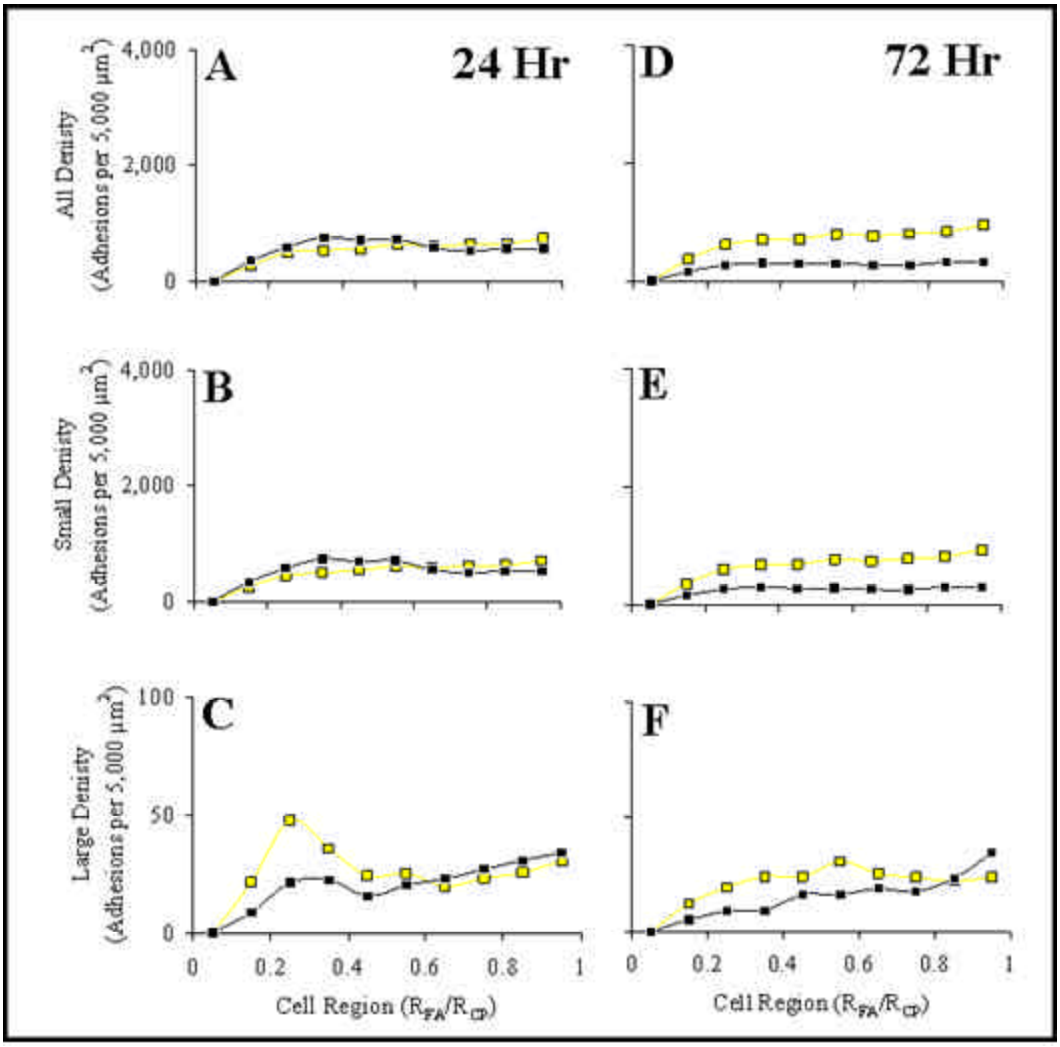

Figure 5.9 Density Distribution of Cells on 10Au and 10G Surfaces: After 1 and 3 days in culture, cells on 10Au (yellow) and 10G (black) surfaces were fixed, their vinculin-containing adhesions fluorescently labeled, and the density of adhesion sites in each cellular region as a function of their normalized distance from the cell center quantified. The adhesion site density distributions for (A, D) all of the adhesions, (B, E) the small adhesions (< 1 μm^2), and (C, F) the large adhesions (> 1 μm^2) are shown.

Summary

Correlating all of the results of the quantified adhesive properties gives some insight into differences in adhesion site maturation as induced by surface energy influence over different conformational states of adsorbed FN. First off, the finding that cells on both 10G and 10Au surfaces show almost identical trends with respect to adhesion site formation after 1 day but significant differences after 3 days indicates that it takes at least 3 days for cells to fully react to changes in surface properties. This 3 day lag time indicates slight differences in signaling pathways, as larger differences in signaling would produce quantifiable changes at early time points. The dominance of $\alpha_5\beta_1$ integrin-mediated adhesion formation in cells cultured on hydrophilic surfaces, the 10G surfaces in this case, promotes the formation of mature focal and fibrillar adhesions, as indicated by adhesion site size and the formation of dense-interconnected FN fibrillar networks as discussed in Chapter 7. While cells cultured on 10G surfaces undergo a maturation of adhesion states indicated by the abolishment of small focal complexes and dominance and growth of larger focal and fibrillar adhesions, cells on 10Au surfaces do not follow this trend. ECs cultured on 10Au surfaces do show the ability to form large focal adhesions and maintain these large adhesions with time but also show a slight increase in the number of small focal complexes used for cell attachment after 3 days in culture. Cells on these surfaces also form very few fibrillar adhesions as indicated by the studies in Chapter 7. Since it is known that cells cultured on hydrophobic surfaces form adhesion sites dominated by $\alpha_v\beta_3$ integrins, the transition to $\alpha_5\beta_1$ integrin-mediated fibrillar and focal adhesions is probably impaired by the underlying surface chemistry. This impairment on integrin transition is most likely responsible for limiting adhesion state maturation and the cells compensate for this

restriction by maintaining the same adhesive state with time. These results parallel previous studies demonstrating the influence of surface chemistry on adhesion formation, but rather than probing molecular compositional differences, gross changes in adhesive properties were observed and quantified. The observed changes in adhesive states are related to changes in gross cell behavior as discussed in following chapters.

5.3.3 Fibronectin Surface Density Influence on Adhesion Site Properties

Since the nanopatterned surfaces display low global densities of FN, 41 and 217 FN/μm^2 for the B- and M-type surfaces respectively (Table 5.1), and it is known that low surface concentrations of FN, less than ~ 550 FN/μm^2 inhibit initial cell attachment, spreading, and proliferation, [6,102] the adhesive properties of cells cultured on thiolated Au surfaces displaying varying FN surface densities were quantified and analyzed as controls for comparison to the nanopatterned surfaces. The FN surface concentrations for the 2Au, 10Au, and 25Au surfaces are 537, 1,882, and 2,474 FN/μm^2 respectively (Table 5.1) as determined from the XPS calibration discussed in Section 4.4.2.

Number, Density, and Sizes of Adhesions

Surprisingly, the results of the analysis indicate that FN surface density has very little influence on adhesion site formation. Cells cultured on the 2Au, 10Au, and 25Au surfaces displayed no significant differences in the size, number, or density of adhesions formed and the only significant differences were between cells on 2Au and 25Au surfaces. Cells on 25Au surfaces displayed an increased ability to form large adhesions compared to cells on low FN surface density controls.

Cells cultured on 2Au and 10Au surfaces formed approximately 1,000 vinculin-containing adhesions (Figure 5.11 A) composed of ~ 950 small adhesions (Figure 5.11 B) with an average size of 0.29 μm^2 (Figure 5.10 B) and ~ 50 large adhesions (Figure 5.11 C) with an average size of 1.65 μm^2 (Figure 5.10 C). Cells cultured on 25 Au surfaces created a similar number and size of small adhesions but displayed the ability to form twice as many large focal adhesions, 96, (Figure 5.11 C) with a similar average size as those created by cells on 2Au and 10Au surfaces (Figure 5.10 C). Furthermore, cells cultured on all three surfaces shows similar trends of linear increases in the number of both small and large adhesions with increased cell spreading (Figure 5.11 D-F).

After 3 days, cells on all three surfaces show a significant reduction in the number of large adhesions (Figure 5.11 C), but only cells on 2Au surfaces show a drastic decrease in the density of large adhesions (Figure 5.12 C), meaning that the observed decrease in large adhesions in cells on 10Au and 25Au surfaces was an artifact of reduced cell spreading. A simultaneous increase in the number and density of small adhesions is observed on all three surfaces (Figure 5.11 B and Figure 5.12 B) but is slightly more pronounced in cells cultured on low density FN, 2Au surfaces. Investigations of the relationships between adhesion site formation and cell spreading indicate that after 3 days cells on all three gold control surfaces achieve similar adhesive states as indicated by linear increases in the number of both small and large adhesions with increased cell spreading (Figure 5.11 H,I), although the slope of the linear increase for large adhesion formation is slightly decreased compared to the 24 hour time point (Figure 5.11 I). The only difference between the surfaces is that cells seeded on low density FN, 2Au surfaces, display an impaired ability to maintain large adhesions over time and display quick saturation of large adhesion formation with increased cell

spreading at approximately 30 large adhesions regardless of the amount of spreading (Figure 5.11 I).

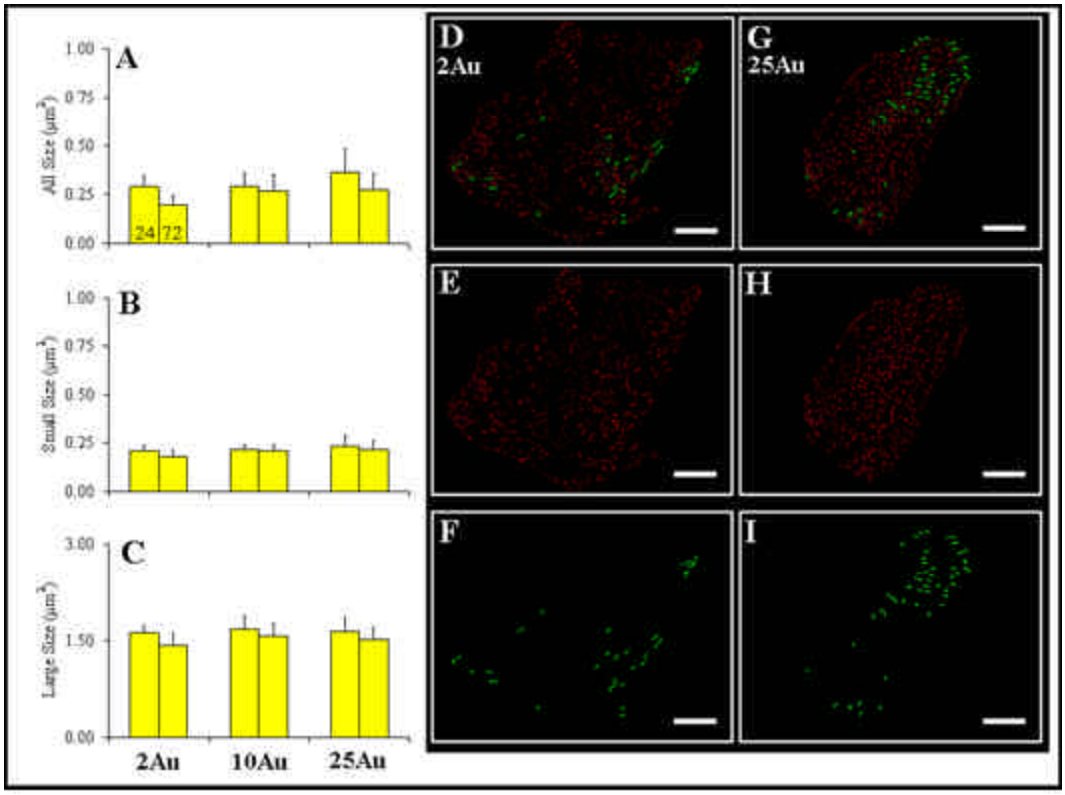

Figure 5.10: Average Adhesion Site Sizes for Cells on 2Au, 10Au and 25Au Surfaces: After 1 and 3 days in culture, cells on 2Au, 10Au, and 25Au surfaces were fixed, their vinculin-containing adhesions fluorescently labeled, and the average size of adhesions measured. The average adhesion site sizes were measured for (A) all of the adhesions (B) the small adhesions (< 1 μm^2), and (C) the large adhesions (> 1 μm^2). FFT/IT processed images of (D-F) a cell on a 2Au surface showing (D) all of the adhesions, (E) the small adhesions (red), and (F) the large adhesions (green). (G-I) Same as (D-F) but for a cell on a 25Au surface. (D-I) Scale bar = 20 μm.

The results indicate that FN surface density has relatively little influence on adhesion site formation and that higher FN surface concentrations induce the formation of more large adhesions while low FN density surfaces impair large adhesion formation. While true, the previous statement is slightly flawed. It should be noted that most of the cells seeded on 2Au surfaces do not even attach to the surface and those that do most likely find denser packed areas of FN to attach to that are probably more similar to the amount of FN on the higher FN density surfaces.

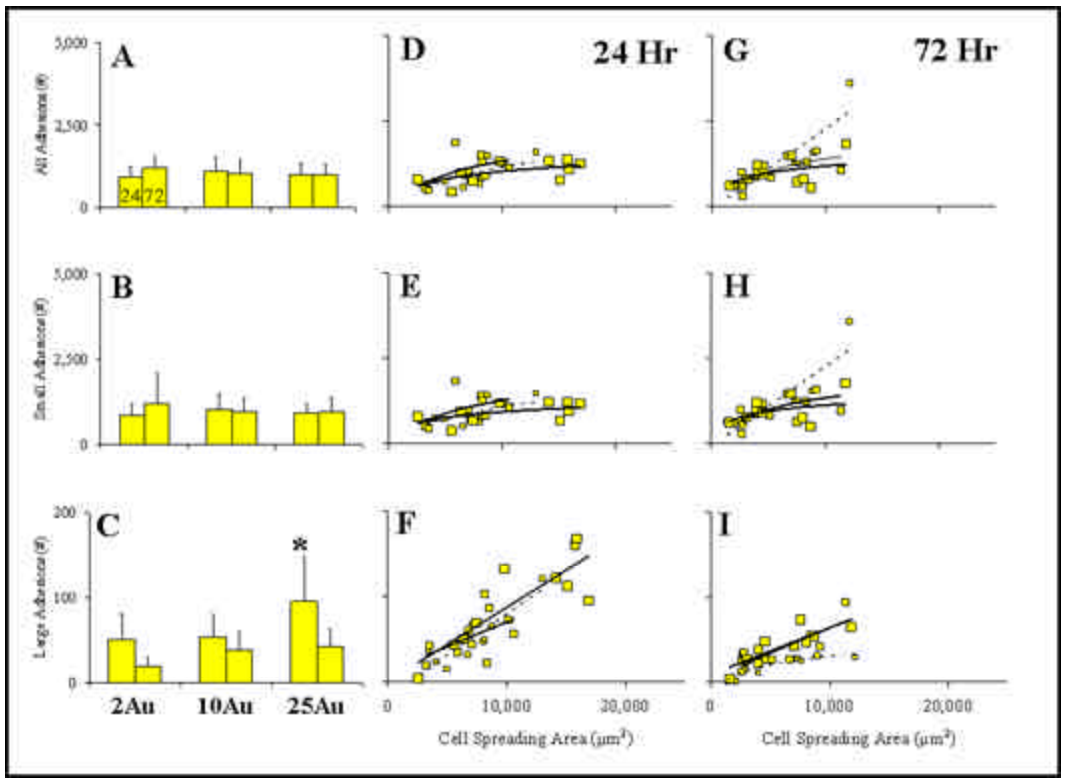

Figure 5.11: Number of Adhesions for Cells on 2Au, 10Au, and 25Au Surfaces: After 1 and 3 days in culture, cells on 2Au, 10Au, and 25Au surfaces were fixed, their vinculin-containing adhesions fluorescently labeled, and the average number of adhesions per cell measured. The average number of adhesions for (A) all of the adhesions, (B) the small adhesions (< 1 μm^2), and (C) the large adhesions (> 1 μm^2) was measured. The relationship between percent adhesion and cell spreading is shown in (D,G) for all adhesions, (E, H) for the small adhesions, and in (F, I) for the large adhesions for cells on 2Au (smallest yellow square), 10Au (medium sized yellow square), and 25Au (largest yellow square) surfaces. * Indicates significantly more adhesions than cells on 2Au surfaces ($p = 0.027$).

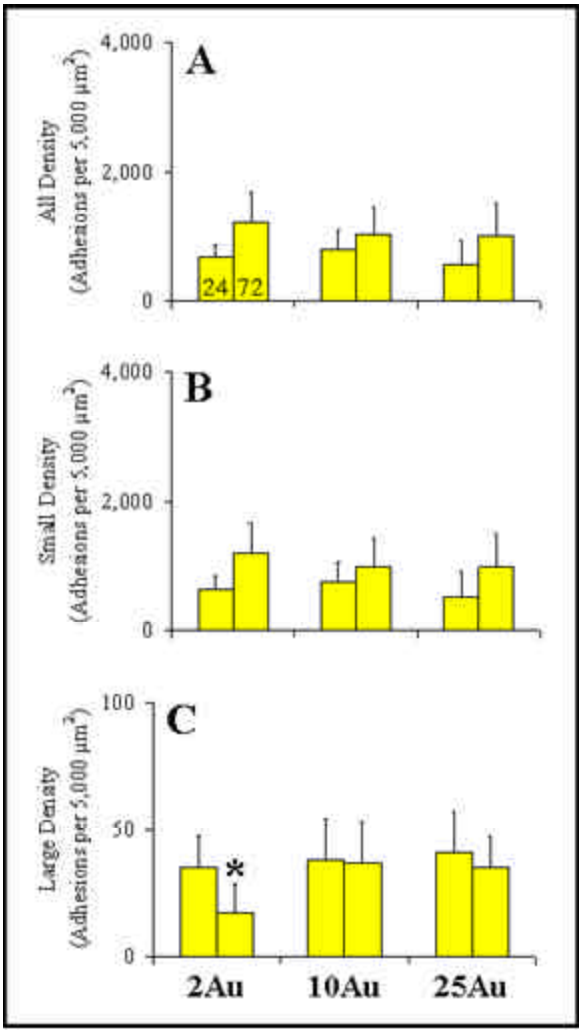

Figure 5.12: Average Adhesion Site Density for Cells on 2Au, 10Au, and 25Au Surfaces: After 1 and 3 days in culture, cells on 2Au, 10Au, and 25Au surfaces were fixed, their vinculin-containing adhesions fluorescently labeled, and their adhesion site densities quantified. The average adhesion site density for (A) all of the adhesions, (B) the small adhesions (< 1 μm^2), and (C) the large adhesions (> 1 μm^2) was measured. * Indicates lower density value than in cells on 10Au and 25Au surfaces ($p = 0.007$).

Adhesion Area and Percent Adhesion

As with the adhesion number, density, and size analysis, the only differences in adhesion area and percent adhesion induced by thiolated Au surfaces displaying varying surface concentrations of FN concern the increased formation of large adhesions in cells cultured on high density FN surfaces compared to cells on lower density surfaces.

These observed differences in large adhesion formation are also reflected in the adhesion area (Figure 5.13) and percent adhesion analysis (Figure 5.14). After 24 hours of culture, cells on all three surfaces have similar values of total adhesive area (Figure 5.13 A) and display similar trends of linear increases in the adhesion area from both small and large adhesions with increased cell spreading (Figure 5.13 D-F). These trends tightly parallel the trends discovered in the adhesion number analysis. Cells cultured on all three surfaces also show very similar values and trends with respect to percent adhesion and maintain a fairly constant portion of their spread area in contact with the underlying surfaces via vinculin-containing adhesions regardless of the extent of cell spreading after 1 day in culture (Figure 5.14 A-F).

After 3 days in culture, the trends of increased adhesion area with increased cell spreading still hold (Figure 5.13 G-I), although the slope of the linear increase in adhesion area due to large adhesions is slightly reduced (Figure 5.13 I). Furthermore cells on the 2Au surfaces reach saturation in the adhesion area due to large adhesions that is reflective of the observed saturation in the number of large adhesions formed as discussed in the previous section (Figure 5.13 I). This quick saturation of adhesive area attributed to large adhesion sites on 2Au surfaces is also observed in the low level of percent adhesion via contact with the surface through large adhesion sites (Figure 5.14 I). Cells cultured on 2Au surfaces attach with ~ 0.5 % of their spread area to

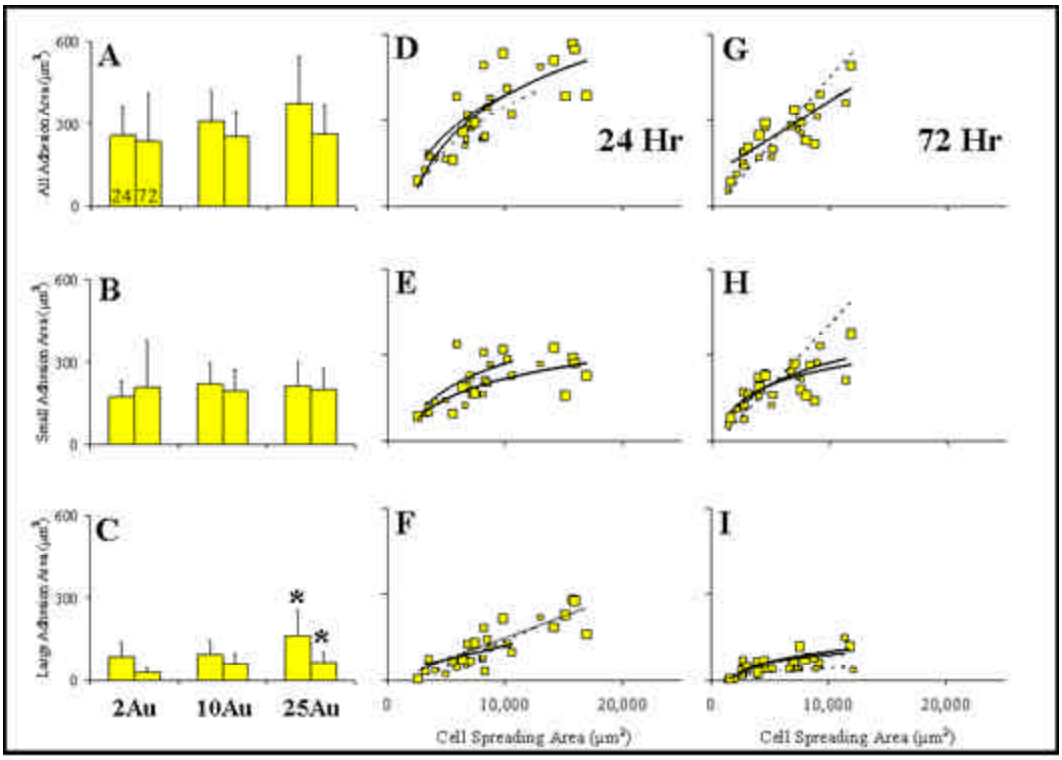

Figure 5.13: Adhesion Area for Cells on 2Au, 10Au, and 25Au Surfaces: After 1 and 3 days in culture, cells on 2Au, 10Au, and 25Au surfaces were fixed, their vinculin-containing adhesions fluorescently labeled, and the adhesion area per cell quantified. The average adhesion area for (A) all of the adhesions, (B) the small adhesions (< 1 μm^2), and (C) the large adhesions (> 1 μm^2)was measured. The relationship between adhesion area and cell spreading is shown in (D,G) for all adhesions, (E, H) for the small adhesions, and (F, I) for the large adhesions for cells on 2Au (smallest squares), 10Au (medium sized squares), and 25Au (largest squares) surfaces. * Indicates more adhesion area than cells on 2Au surfaces ($p < 0.05$).

the underlying surface via large adhesions while cells on 10Au and 25Au surfaces use 1.10 % of their spread area to attach to the surface via large adhesion sites (Figure 5.14 C, I).

The adhesion area and percent adhesion data parallel the observed changes in the number and density of adhesions described in the previous section. As the number of large adhesions decreases in cells cultured on 2Au surfaces so does the adhesion area and percent adhesion of these large adhesions. This data further validates that FN surface density has very little influence on adhesion site formation and that low surface densities of adsorbed FN do not provide enough tightly packed areas of FN and in turn prevent the formation of large adhesions.

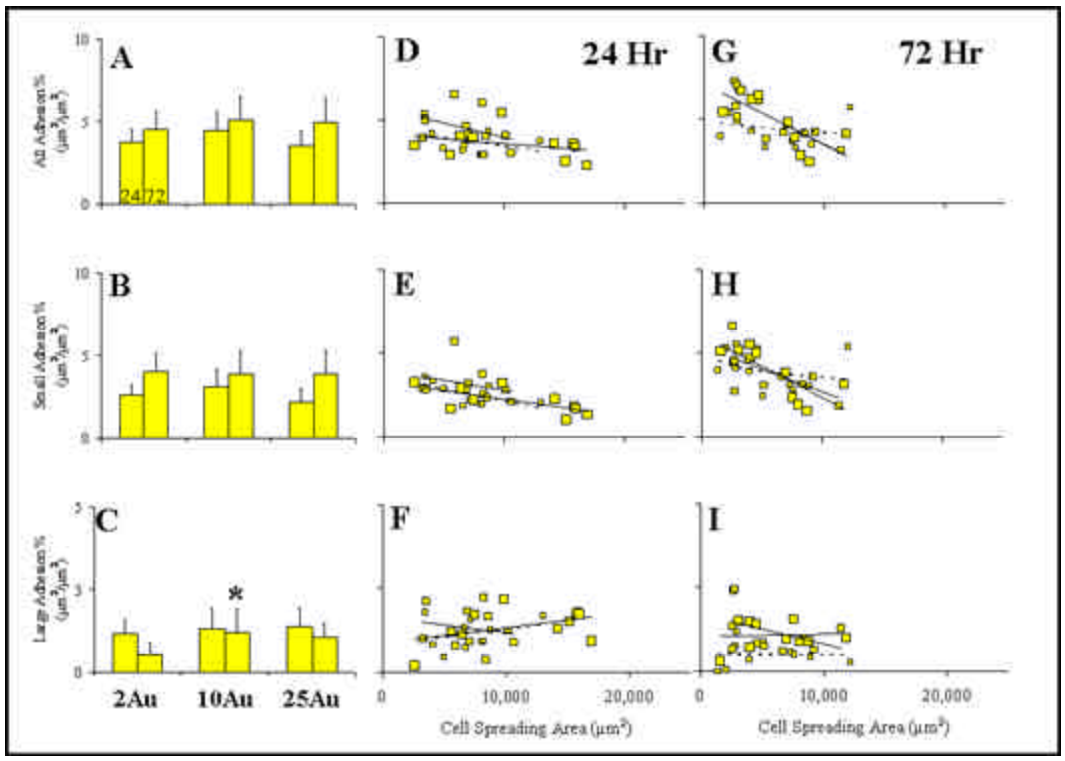

Figure 5.14: Percent Adhesion for Cells on 2Au, 10Au, and 25Au Surfaces: After 1 and 3 days in culture, cells on 2Au, 10Au, and 25Au surfaces were fixed, their vinculin-containing adhesions fluorescently labeled, and the average percent adhesion per cell quantified. The average percent adhesion for (A) all of the adhesions, (B) the small adhesions (< 1 μm^2), and (C) the large adhesions (> 1 μm^2) was measured. The relationship between percent adhesion and cell spreading is shown in (D,G) for all adhesions, (E, H) for the small adhesions, and (F, I) for the large adhesions for cells on 2Au (smallest squares), 10Au (medium sized squares), and 25Au (largest squares) surfaces. * Indicates higher percent adhesions than cells on 2Au surfaces ($p = 0.015$).

Adhesion Site Distributions

While the previous analysis shows that increased FN surface density induces the formation of more large adhesion sites, the distribution plots show the location of the increased numbers of adhesion sites.

After 24 hours in culture the cells on all three gold surfaces show very similar distributions for the small adhesion sites, a linear increase in adhesion sites as you move from the cell center to the cell periphery (Figure 5.15). The only recognizable difference is that cells cultured on 25Au surfaces display a much higher number of large adhesions (Figure 5.15 C). These large adhesions are evenly distributed through out the cell body (Figure 5.15 C). When normalized to cell spreading, the differences are not so drastic (Figure 5.16). This implies that the cells strive to achieve a certain number of large adhesions per area as they spread out. After 72 hours, cells on 10Au and 25Au surfaces maintain the same number and density distributions for both the small and large adhesions (Figure 5.15 E,F and Figure 5.16 E,F) but cells on 2Au surfaces show a slight increase in the density of small adhesions (Figure 5.16 E) and a decrease in the number (Figure 5.15 E,F) and density (Figure 5.16 F) distributions of large adhesions. The analysis indicates that at early time points, surfaces saturated with FN promote increased formation of large adhesions throughout the cell body compared to surfaces presenting less dense FN. Furthermore, surfaces presenting low densities of FN induce a slightly increased number of small adhesions throughout the cell body leading to increased densities of small adhesions that coincide with a simultaneous decrease in the large adhesion site density.

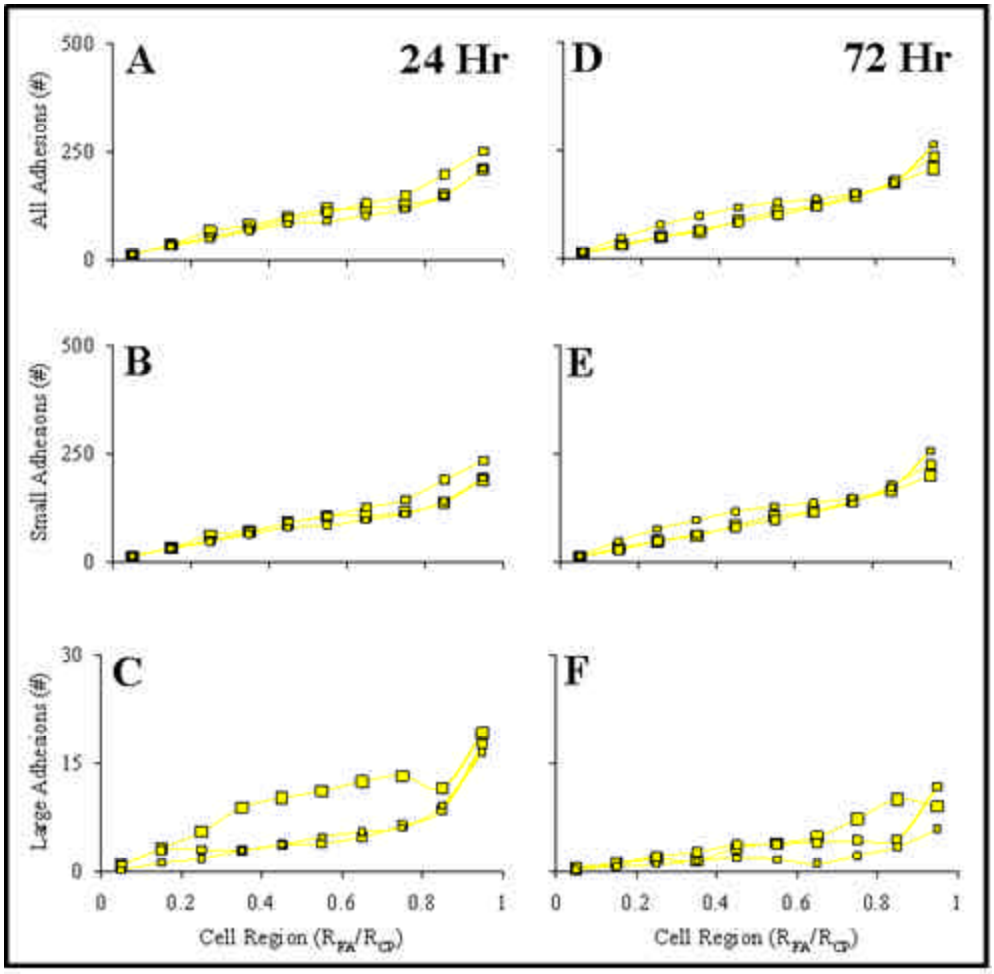

Figure 5.15: Adhesion Number Distributions for Cells on 2Au, 10Au, and 25Au Surfaces: After 1 and 3 days in culture, cells on 2Au (smallest squares), 10Au (medium sized squares), and 25Au (largest squares) surfaces were fixed, their vinculin-containing adhesions fluorescently labeled, and the number of adhesion sites in each cellular region as a function of their normalized distance from the cell center quantified. The adhesion site number distributions for (A, D) all of the adhesions, (B, E) the small adhesions (< 1 μm^2), and (C, F) the large adhesions (> 1 μm^2) are shown.

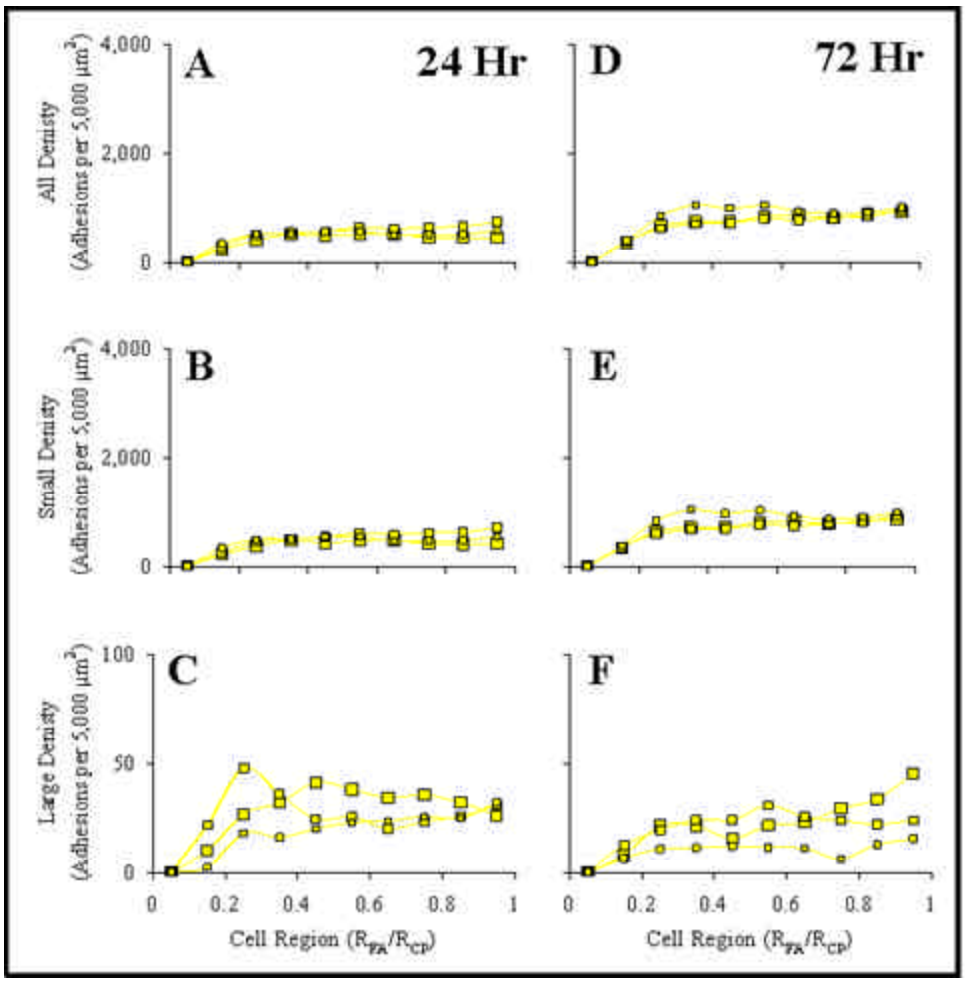

Figure 5.16: Adhesion Density Distributions for Cells on 2Au, 10Au, and 25Au Surfaces: After 1 and 3 days in culture, cells on 2Au (smallest squares), 10Au (medium sized squares), and 25Au (largest squares) surfaces were fixed, their vinculin-containing adhesions fluorescently labeled, and the adhesion site density in each cellular region as a function of their normalized distance from the cell center quantified. The adhesion site density distributions for (A, D) all of the adhesions, (B, E) the small adhesions (< 1 μm^2), and (C, F) the large adhesions (> 1 μm^2) are shown.

Summary

The results indicate the FN surface density has very little influence on cell adhesion. The major finding is that increased FN surface density on thiolated Au surfaces induces the formation of more densely packed large adhesion sites, while low density FN surfaces prevent this occurrence. The finding that cells on all three surfaces maintain similar total adhesion areas regardless of differences in the formation of large adhesions indicates that cells on these surfaces strive to maintain a certain minimum level of contact with the surface through adhesion sites. In situations where the formation of large adhesions is inhibited, such as the cells on the 2Au surfaces, the cells slightly increase their number of small adhesions and reduce their spread area to compensate. Although the molecular composition of these adhesions was not determined and therefore the exact type of adhesion formed can not be concluded, FN fibril formation studies presented in Chapter 7 show that cells on 2Au surfaces form a higher number of FN fibrils and maintain these fibrils for 3 days in culture hinting to the formation of fibrillar adhesions that is not observed in cells on 10Au and 25Au surfaces. In general it can be concluded that FN surface density has little influence on adhesion site formation and that higher density FN surfaces allow for the formation of more large adhesions compared to cells on low density FN surfaces.

5.3.4 Nanopatterned Surface Influence on Adhesion Site Properties

The influences of varying FN surface concentration and underlying surface chemistry on adhesion site formation have been discussed. Now, the question of how limiting adhesion site growth using chemically-defined nanoscale protein islands influences cell adhesive states will be addressed. Determining the correct controls for

comparison to the nanopatterned surfaces is somewhat challenging. Thiolated Au surfaces alone will accurately reproduce the underlying surface chemistry of the adsorbed FN on the nanopatterns but they do not take into account the glass between the patterns, although the glass is functionalized and has been shown to prevent protein adsorption. Furthermore, since the nanopatterned surfaces display very low global densities of FN, cells on these surfaces should be compared to cells cultured on thiolated Au surfaces with similar global densities. Even though the nanopatterned surfaces display low global FN densities, the local FN concentrations on the patterns themselves is very high, ~ 750 FN/μm^2, and the nanopatterns are saturated with tightly packed FN molecules, making the 25Au surface a necessary control since it is also saturated with FN. To keep the comparison relatively simple, cells on the nanopatterned surfaces will be compared to cells cultured on the 10G surfaces to prove that the observed changes in adhesive properties are not due to the glass background and to cells on 25Au surfaces to show that limiting adhesion site growth influences adhesion formation.

Number, Sizes, and Types of Adhesions

The analysis indicates that cells quickly recognize and react to the chemical functionality of the nanopatterned surfaces by forming a significantly higher number of smaller, more densely packed adhesions (Figure 5.17 D-I). The absolute number of adhesions formed by cells on these surfaces is governed by two properties of the nanopatterns, the nanopattern surface coverage and the nanopattern size. The nanopattern surface coverage is the dominate property influencing the number of adhesions formed in cells after 1 day (Figure 5.18 A, B). After 3 days in culture the

nanopattern size becomes more influential (Figure 5.18 A, B). While the absolute number of adhesion sites formed shows temporal dependence on nanopattern properties, the density of adhesions is always highest in cells on the small nanopatterns (Figure 5.19). This observation indicates that cells on these surfaces do not spread as well as cells on controls and larger nanopatterns but strive to maintain a high surface contact area by forming a higher density of small adhesions.

Through visual inspection of the vinculin labeled fluorescent images it is easily seen that cells attach to the nanopatterned surfaces using a significantly increased number of relatively smaller, more evenly distributed, and more tightly packed vinculin-containing adhesions compared to cells on control surfaces (Figure 5.17 D-I). While cells on 2Au, 25Au, and 10G surfaces all form approximately 1,000 vinculin-containing adhesions after 1 day in culture, cells on the nanopatterned surfaces can form up to twice as many adhesions (Figure 5.18 A). The M-type surfaces (0300M, 1500M) both with 7.2 % nanopattern surface coverage induce the formation of more adhesions than cells on control and B-type surfaces (0300B, 1500B) after 1 day in culture indicating that nanopattern surface coverage dictates the number of adhesions formed at early time points (Figure 5.18 A,B). After 72 hours in culture the nanopattern size becomes more influential over the number of adhesions formed and cells on the smallest nanopatterned surfaces, the 0300B and 0300M surfaces, both displaying available adhesion sites less than 10,000 nm^2 in area form significantly more adhesions than cells on both larger nanopatterns and controls (Figure 5.18 A,B). Furthermore, the chemical functionality shows the ability to somewhat suppress the formation of large adhesions to nanopatterned surfaces and cells on all of the nanopatterned surfaces have significantly fewer large adhesion sites than cells on control surfaces after 3 days,

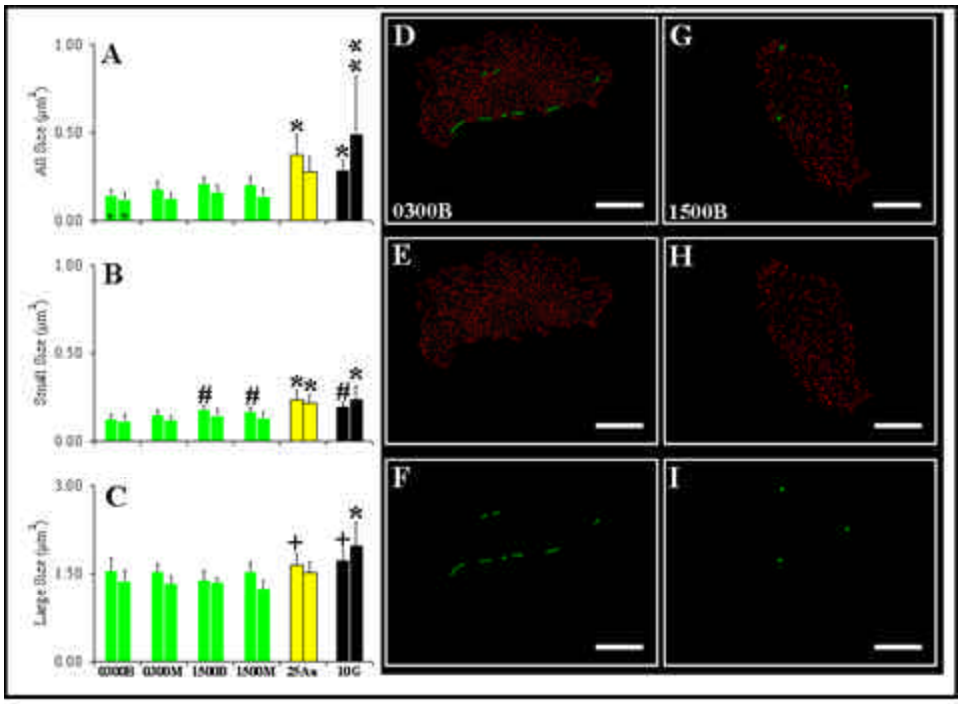

Figure 5.17: Average Adhesion Site Sizes for Cells on Nanopatterned and Control Surfaces: After 1 and 3 days in culture, cells on nanopatterned surfaces and 25Au and 10G control surfaces were fixed, their vinculin-containing adhesions fluorescently labeled, and average size of adhesions measured. The average adhesion site sizes were measured for (A) all of the adhesions (B) the small adhesions (< 1 μm^2), and (C) the large adhesions (> 1 μm^2). FFT/IT processed images of (D-F) a cell on a 0300B surface showing (D) all of the adhesions, (E) the small adhesions (red), and (F) the large adhesions (green). (G-I) Same as (D-F) but for a cell on a 1500B surface. (D-I) Scale bar = 20 µm. * Indicates larger average size than cells on all nanopatterned surfaces ($p < 0.003$). # Indicates larger average size than cells on 0300B surfaces ($p < 0.003$). + Indicates larger average size than cells on 1500B surfaces ($p < 0.04$). ** Indicates larger average size than cells on all nanopatterned surfaces ($p < 0.04$).

although some large adhesions can be made by these cells, particularly by cells on 1500M surfaces (Figure 5.18 C).

The density of adhesions formed is dictated by the nanopattern size at all time points. Cells on the smallest nanopatterned surfaces display a higher density of adhesion sites compared to cells on larger nanopatterns and on controls (Figure 5.19 A). The 0300B and 0300M surfaces induce the formation of 2,705 and 1,934 adhesions/5,000 μm^2 respectively compared to 1,200 adhesions/5,000 μm^2 for cells on larger nanopatterns and 700 adhesions/5,000 μm^2 for cells on control surfaces (Figure 5.19 A). The transition to more dense packing of adhesions with decreased nanopattern size may indicate a size transition point. It may be that limiting adhesion site growth to very small patterns, less than 10,000 nm^2 in size, does not allow for the desired cellular contact area to be formed and cells react by creating extremely high numbers of more densely packed adhesions. This occurrence leads to three regimes of adhesion site formation. Cells on the smallest nanopatterns form significantly more adhesions that are more densely packed than cells on larger nanopatterns and control surfaces. As the available adhesion site size slightly increases to 40,000 nm^2 the cells still form significantly more adhesions than cells on control surfaces but their packing density is similar to that of cells on Au control surfaces. Finally, as the cells have no restrictions imposed on adhesion site growth as with cells on controls surfaces the cells transition to using larger and less densely packed adhesion sites. This occurrence may indicate that a different quality of adhesions is being formed as the restrictions to adhesion site growth are restricted. This indicates that limiting adhesions to the very small patterns may result in the formation of only immature adhesions that are too small to incorporate all of the necessary components to mature. As the size that the

adhesion is allowed to grow slightly increases, a higher level of maturation is reached and as all restrictions on adhesion site growth are lifted the fully matured adhesions can be formed as seen in cells on control surfaces. Studies presented in following chapters support this claim and show impaired cytoskeletal linkage to the small adhesions formed on the smallest nanopatterns as well as a slightly impaired ability for these cells to spread.

Further analysis of the adhesion site properties shows that cells grown on nanopatterned surfaces form smaller focal complexes (Figure 5.17 B) and display the ability to form some focal adhesions (Figure 5.18 C). After 24 hours in culture, the average size of all the adhesions formed by HUVECs on nanopatterned surfaces ranges from 0.14 ± 0.03 μm^2 for cells on the smallest nanopatterns (0300B) to 0.21 ± 0.05 μm^2 for the largest nanopatterns (1500M) compared to 0.29 ± 0.06 to 0.37 ± 0.11 μm^2 for cells on the 10G and 25Au control surfaces (Figure 5.17 A). The lower average adhesion site size of cells cultured on the smaller nanopatterned surfaces compared to cells on larger nanopatterns and control surfaces stems from the formation of extremely small, resolution limited focal complexes. Focal adhesions formed by cells on these surfaces display an average size of 1.5 μm^2, slightly smaller than the size of large adhesions formed by cells on control surfaces, 1.65 μm^2 (Figure 5.17 C), but their ability to form these adhesions is greatly suppressed. Even though cells on nanopatterned surfaces show the ability to form some large adhesions they form significantly fewer large adhesions compared to cells on control surfaces (Figure 5.18 C). The nanopatterns limit the formation of large adhesions from an average of 19 per cell on the smallest patterns to 50 per cell on the largest patterns and show a linear increase in the occurrence of large adhesion formation with increasing pattern size after 24 hours that is diminished

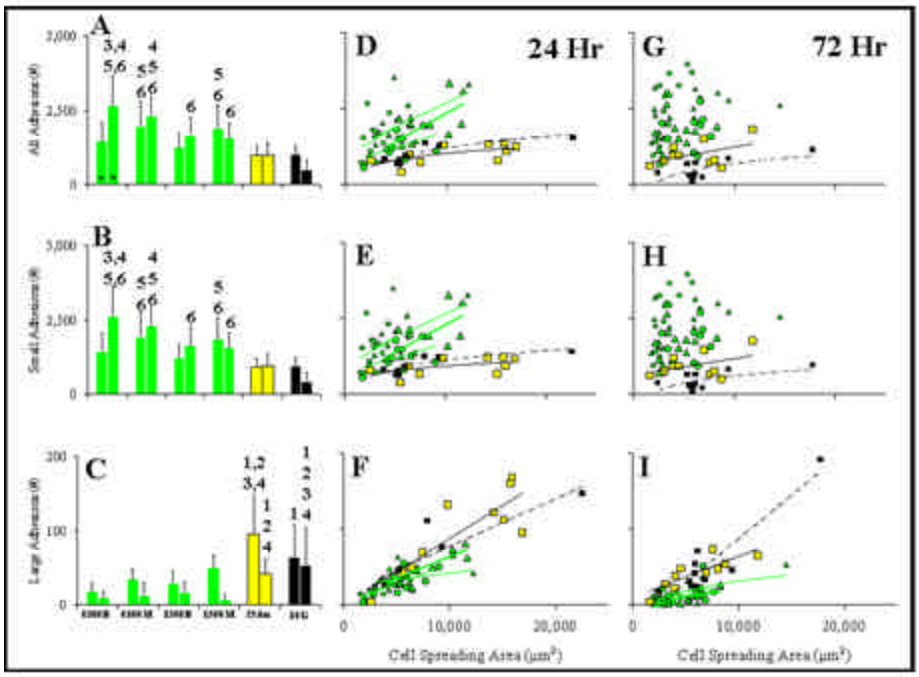

Figure 5.18: Number of Adhesions for Cells on Nanopatterned and Control Surfaces: After 1 and 3 days in culture, cells on nanopatterned surfaces and 25Au and 10G control surfaces were fixed, their vinculin-containing adhesions fluorescently labeled, and the average number of adhesions per cell measured. The average number of adhesions for (A) all of the adhesions, (B) the small adhesions (< 1 μm^2), and (C) the large adhesions (> 1 μm^2) was measured. The relationship between the number of adhesions formed and extent of cell spreading is shown in (D,G) for all adhesions, (E, H) for the small adhesions, and (F, I) for the large adhesions for cells on 0300B (small green triangle), 0300M (small green dot), 1500B (large green dot), 1500M (large green triangle), 25Au (yellow square) and 10G (black square) surfaces. [1-6] Indicates significantly more adhesions than cells on [1] 0300B, [2] 0300M, [3] 1500B, [4] 1500M, [5] 25 Au, and [6] 10G surfaces ($p < 0.05$).

after 3 days in culture (Figure 5.18 C). While cells on these surfaces do show the ability to form some large adhesion sites, the absolute number per cell is much lower than cells on control surfaces and the occurrence of large adhesion formation is greatly suppressed after 3 days in culture, again hinting to a 3 day lag time in full cell response to changes in surface properties as seen in the surface chemistry experiments comparing cells on 10Au to those on 10G surfaces.

Analysis of the number of adhesions formed with increased cell spreading gives further insight into differences in cellular adhesive states induced by limiting adhesion site growth via cell-surface interactions with chemically-defined nanoscale adhesion sites. Cells on both nanopatterned and control surfaces display linear increases in adhesion site formation with increased cell spreading but cells on the nanopatterns show a much higher slope after 24 hours (Figure 5.18 D-F). This occurrence of increased adhesion site formation with increased cell spreading persists for 3 days in culture although the linear trends are not as easily seen at day 3 (Figure 5.18 G-I). Furthermore, cells on control surfaces display a linear increase in large adhesion site formation with increased cell spreading after both 1 and 3 days in culture (Figure 5.18 F, I). Cells on nanopatterned surfaces also show this trend after 1 day although the slope of increase is lower than that of cells on control surfaces, again indicating a suppressed propensity to form large adhesions (Figure 5.18 F). After 3 days the ability of cells to form large adhesions on nanopatterned surfaces is greatly suppressed and many cells do not form any large adhesions at all, particularly cells on the smallest nanopatterns (Figure 5.18 I). This occurrence is similar to what is seen in cells on 2Au surfaces but much more pronounced in cells on nanopatterned surfaces.

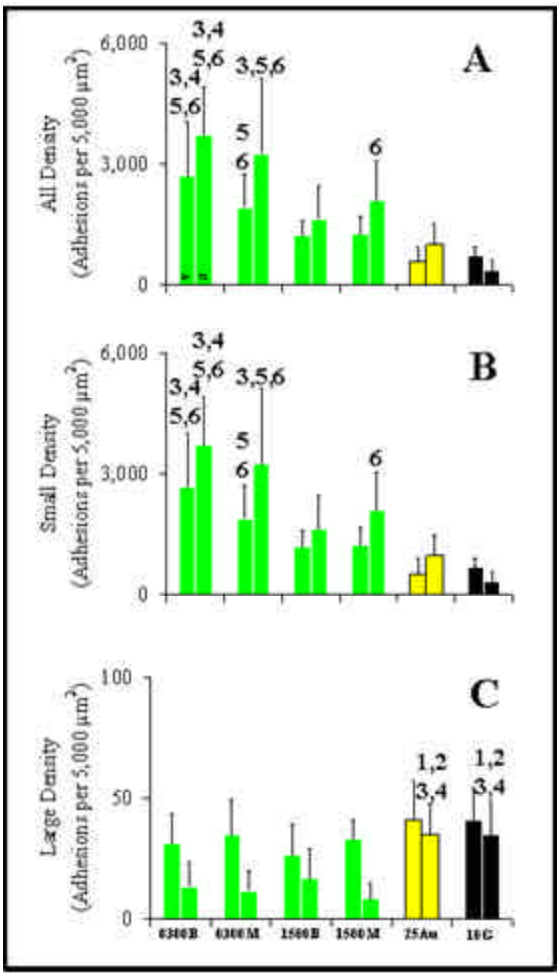

Figure 5.19: Average Adhesion Site Density for Cells on Nanopatterned and Control Surfaces: After 1 and 3days in culture, cells on nanopatterned and 25Au and 10G control surfaces were fixed, their vinculin-containing adhesions fluorescently labeled, and adhesion site densities quantified. The average adhesion site density for (A) all of the adhesions, (B) the small adhesions (< 1 μm^2), and (C) the large adhesions (< 1 μm^2) was measured. [1-6] Indicates significantly more adhesions than cells on [1] 0300B, [2] 0300M, [3] 1500B, [4] 1500M, [5] 25 Au, and [6] 10G surfaces ($p < 0.05$).

Adhesion Area and Percent Adhesion

The adhesion area and percent adhesion analysis were not performed for cells on the nanopatterned surfaces due to the resolution limitations of light microscopy. Although the image processing technique developed here can detect the presence of very small adhesions it grossly overestimates their size and therefore can not be reliably used to analyze adhesive area and percent adhesion for the very small adhesions formed by cells on the nanopatterned surfaces.

Adhesion Site Distributions

Analysis of the location of adhesions formed to nanopatterned surfaces compared to cells on control surfaces validates the observed differences in adhesion site formation and provides further insight into the influence of nanopattern size on adhesion formation. After 24 hours in culture, cells on all surfaces show similar trends with respect to the distribution of small adhesions, increasing numbers of adhesions as you move from the cell center to the cell periphery (Figure 5.20 A). Cells on the M-type nanopatterned surfaces form the highest number of adhesions after 1 day (Figure 5.20 A). After 3 days cells on the smallest nanopatterned surfaces, the 0300B and 0300M surfaces, display the highest number of adhesions, reaffirming the previously discussed nanopattern size influence on increased adhesion site formation (Figure 5.20 D). Furthermore, cells on the 25Au and 10G surfaces show the ability to form large adhesions with a large increase in adhesion site formation at the cell periphery after 1 and 3 days in culture (Figure 5.20 C,F) while cells on all of the nanopatterned surfaces form significantly fewer large adhesions compared to controls that is more evident after 3 days in culture (Figure 5.20 F). Normalizing the number of

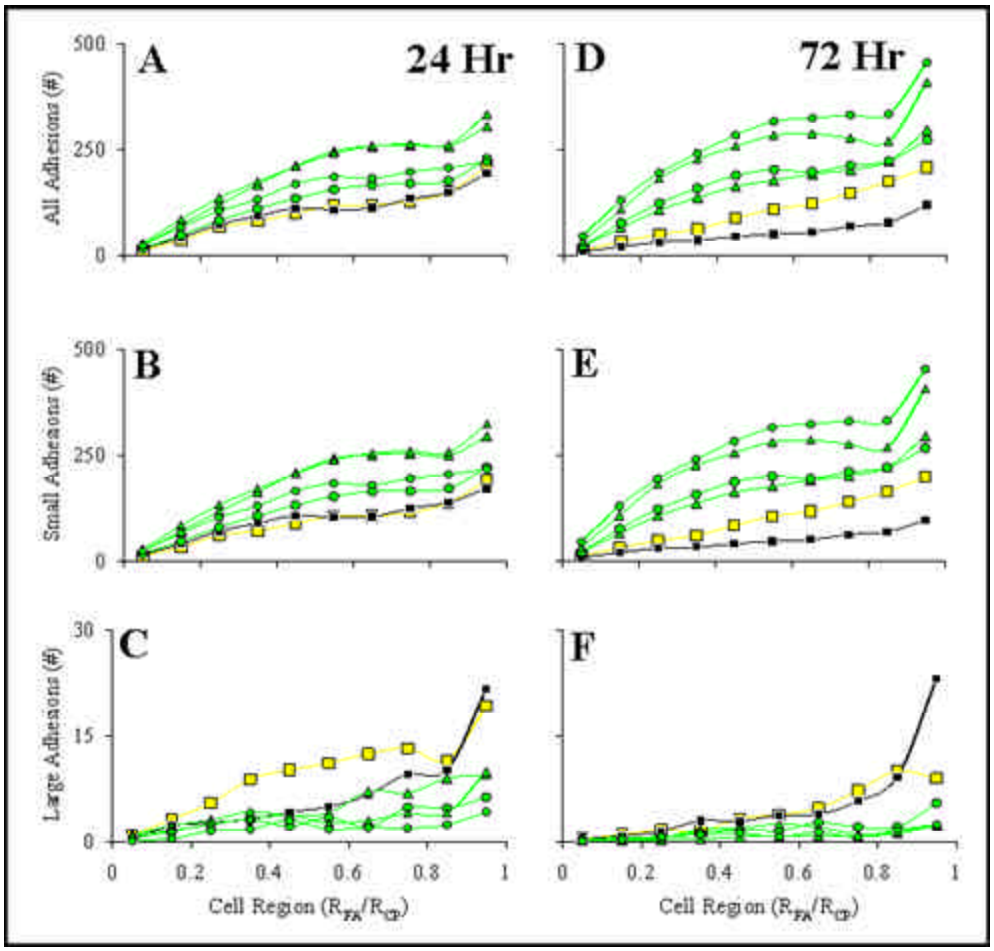

Figure 5.20: Adhesion Number Distributions for Cells on Nanopatterned and Control Surfaces: After 1 and 3 days in culture, cells on 0300B (small green triangle), 0300M (small green dot), 1500B (large green dot), 1500M (large green triangle), 25Au (yellow square) and 10G (black square) surfaces were fixed, their vinculin-containing adhesions fluorescently labeled, and the number of adhesion sites in each cellular region as a function of their normalized distance from the cell center quantified. The adhesion site number distributions for (A, D) all of the adhesions, (B, E) the small adhesions (< 1 μm^2), and (C, F) the large adhesions (> 1 μm^2) are shown.

adhesions per area gives more insight into the adhesive states of cells cultured on the nanopatterned surfaces.

After 24 hours cells on the 0300B surfaces display a significantly higher density of evenly distributed small adhesions throughout the cell body compared to cells on all other surfaces (Figure 5.21 A). The 0300M surfaces display the second highest density of small adhesions followed by cells on both the 1500B and 1500M surfaces which show almost identical adhesion site density distributions (Figure 5.21 A). This indicates that the average adhesion site size is influential over the absolute number of adhesions formed by cells. If the ability to form large adhesions is taken away then cells respond by forming extremely high numbers of smaller, more evenly distributed adhesions. If the adhesion sites are allowed to slightly grow in size as seen in the cells on the 1500B and 1500M surfaces then there is a slight decrease in the number of adhesions formed but still not as low as cells on non-patterned control surfaces that form relatively fewer but larger adhesion sites. Cells grown on non-patterned control surfaces have similar trends in adhesion site density but with much lower overall values (Figure 5.21 A). After 3 days, the nanopattern size has a more significant influence on adhesion site density distribution (Figure 5.21 D). HUVECs cultured on the smallest nanopatterns, 0300B and 0300M with FN nanoislands below 10,000 nm^2 in area, form almost identical density distributions, with a value of 4,000 adhesions/5,000 μm^2 three tenths of the way between the cell center and periphery that steadily drops to a value of 2,000 adhesions/5,000 μm^2 at the cell periphery (Figure 5.21 D). Cells on larger nanopatterned surfaces, 1500B and 1500M surfaces with FN nanoislands larger than 40,000 nm^2 in area follow a similar but not so pronounced increase of adhesion site density near the cell center followed by a decrease in adhesion density at the cell

periphery (Figure 5.21 D). The trends observed in cells on all nanopatterned surfaces are drastically different from the density distributions measured in cells on controls (Figure 5.21 D). Cells on control surfaces quickly reach a density saturation value just outside of the cell center and maintain this constant value all the way to the cell periphery (Figure 5.21 D). Furthermore, the suppression of large adhesion site formation can be observed in the significantly lower large adhesion density values of cells on all nanopatterned surfaces after 3 days in culture (Figure 5.21 F) verifying the effectiveness of the dual surface chemistry.

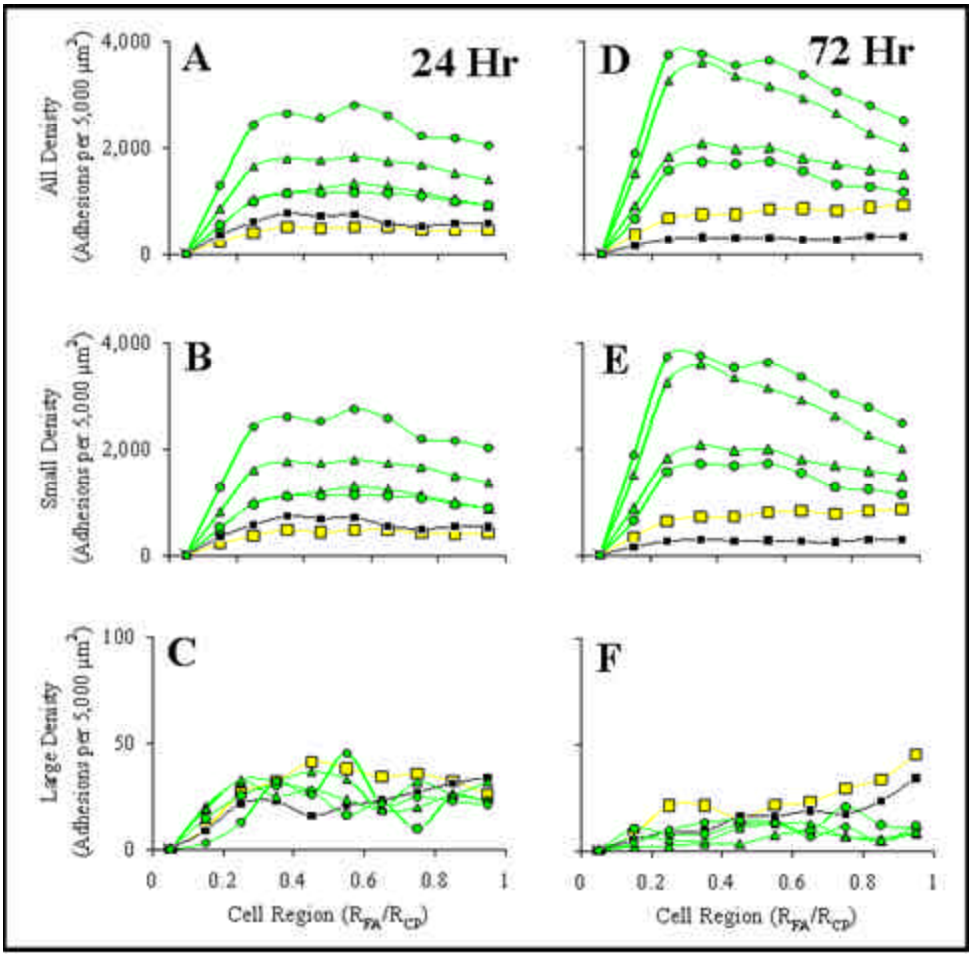

Figure 5.21: Adhesion Site Density Distributions for Cells on Nanopatterned and Control Surfaces: After 1 and 3 days in culture, cells on 0300B (small green triangle), 0300M (small green dot), 1500B (large green dot), 1500M (large green triangle), 25Au (yellow square) and 10G (black square) surfaces were fixed, their vinculin-containing adhesions fluorescently labeled, and the adhesion site density in each cellular region as a function of their normalized distance from the cell center quantified. The adhesion site density distributions for (A, D) all of the adhesions, (B, E) the small adhesions (< 1 μm^2), and (C, F) the large adhesions (> 1 μm^2) are shown.

Summary

The results indicate that restricting adhesion site growth to very small adhesions can have a significant influence on the number, type, density, and distribution of vinculin-containing adhesions. Compared to cells on control surfaces, cells on nanopatterned surfaces adhere with a significantly increased number of more densely packed, smaller adhesions. While the dual surface chemistry shows ability to suppress large adhesion site formation after 1 day in culture this suppression is greatly enhanced after 3 days in culture, again indicating a 3 day response time for cells to fully react to differences in surface properties. Furthermore, cells respond to both the surface density and size of the nanopatterns. After one day in culture, cells on M-type surfaces form more adhesions than cells on B-type surfaces with similar pattern sizes. This occurrence indicates that cells recognize the density of patterns and attach to any available FN after 1 day. After 3 days, imposed restrictions on adhesion site size were shown to have the most influence on the number, density, and distribution of adhesions formed. Cells seeded on nanopatterns with average sizes above 40,000 nm^2 respond by forming higher density, more evenly distributed adhesions than cells on control surfaces. Cells cultured on nanopatterned surfaces presenting FN nanoislands below 10,000 nm^2 form extremely dense adhesions with a higher local of adhesions just outside the cell center. These differences in adhesive states as imposed by limiting adhesion site growth to nanometer size FN islands indicate a different type or quality of adhesion formed by cells on the nanopatterned surfaces. Further studies concerning actin cytoskeletal and FN fibril formation support this proposed change in the quality of adhesions and is discussed in Chapters 6 and 7.

5.4 Discussion

The collective results demonstrate that surface energy, FN surface concentration, and limiting adhesion site growth can all influence cell adhesive properties. Through the comparison of adhesive states between cells cultured on Au and glass surfaces displaying similar surface densities of FN it was shown that differences in surface chemistry can induce some changes in adhesion site behavior. Cells on glass surfaces show the propensity to generate large surface contact areas by enlarging existing focal adhesions while simultaneously dissolving small focal complexes over a 3 day period. Cells on Au surfaces with similar FN densities do not undergo this size enlarging of focal adhesions and maintain their surface contact area by forming a slightly increased number of small adhesions over time. Cells cultured on glass surfaces show the ability to form focal complexes, focal adhesion, and fibrillar adhesions and create dense interconnected FN networks, while cells on similar density Au surfaces do not create FN fibrils and therefore most likely do not create fibrillar adhesions. Further support for this claim comes from the finding that cells on hydrophilic surfaces form adhesion sites rich in $\alpha_5\beta_1$ integrins,[115,117,121] those used for the creation of fibrillar adhesions,[16] while cells on hydrophobic surfaces tend to form adhesion sites rich in $\alpha_v\beta_3$ integrins. This impaired ability of cells on Au surfaces to transition to fibrillar adhesions is the most likely factor in producing the observed differences in adhesive states between cells on Au and glass surfaces.

Further studies using thiolated Au surfaces with varying densities of adsorbed FN indicated that FN concentration can have some influence on adhesion site formation, although not as pronounced as differences in surface chemistry. Surfaces saturated with FN increase the propensity of cells to form more, large focal adhesions. Surfaces

displaying intermediate levels of FN induce cell adhesion formation similar to surfaces with lower levels of FN, although it again should be noted that initial cell attachment and long term proliferation is significantly impaired in cells seeded on 2Au surfaces.[6] Cells on these surfaces display an impaired ability to form large adhesions after 3 days in culture and compensate by forming slightly increased numbers of small adhesions similar to the comparison between cells on 10G and 10Au surfaces. While the influences of surface chemistry and FN surface density take 3 days to induce pronounced differences in cell adhesive states, limiting adhesion site growth through cell interactions with nanopatterned surfaces induces significant differences in adhesive properties after just 1 day in culture and even more significant changes after 3 days.

The results indicate that cells can recognize and react to both nanopattern surface coverage and nanopattern size. The formation of more adhesions by cells to M-type surfaces compared to cells on similar sized B-type surfaces after 1 day indicates that cells adhere to almost all of the available nanopatterns. Even though the absolute number of adhesions on M-type surfaces is higher, the normalized density values show that cells on the smallest nanopatterns, below 10,000 nm^2 in size, form the highest density of adhesions. All cells on all surfaces show a linear increase of large adhesion site formation with increased cell spreading after 24 hours implying that the formation of large adhesions is helpful in producing the traction force for cells to pull themselves to spread across the surface. Since cells on the small nanopatterns show a significant impairment in the formation of large adhesions they do not spread as well and consequently display higher values of adhesion site density. While this explains the changes in adhesion site density after 1 day in culture it does not account for the differences observed after 3 days. Cells on all nanopatterns produce almost no large

adhesions but still remain spread on the surface. This indicates the large adhesions are needed to initiate and to reach desired spreading areas but are not necessary for long term maintenance of spreading. Furthermore, the adhesion site density distributions indicate that nanopattern size has a significant influence on the distribution of adhesion sites. Cells seeded on surfaces displaying the smallest nanopatterns, below 10,000 nm^2 in size, show almost identical trends in adhesion site distribution regardless of the nanopattern surface coverage. This also holds true for cells seeded on nanopatterned surfaces with FN nanoislands greater than 40,000 nm^2. Cells on these surfaces show identical trends in adhesion site distribution even though the nanopattern surface densities are different. This occurrence indicates that nanopattern size becomes the dominating influence over adhesion site formation after 3 days in culture and most likely retains its dominance until the cells form multiple cell-cell contacts with each other and form a confluent sheet.

Limiting adhesion site growth to below 10,000 nm^2 most likely limits the maturation of adhesions and only allows cells to form early complexes and in some cases fibrillar adhesions. Further evidence for this claim is introduced in Chapters 6 and 7 and shows that cells cultured on the smallest nanopatterns are not able to form well-defined actin stress fibers but can still form FN fibrils. This impairment of stress fiber formation indicates that these cells do not form adhesion sites containing high concentrations of cytoskeletal-linking adaptor proteins and most likely are limited in maturation to the formation of early focal complexes. In contrast, cells on the larger nanopatterned surfaces with nanopatterns larger than 40,000 nm^2 are able to form well defined stress fibers although the actin networks are not as dense as those seen in cells on non-patterned control surfaces. This adhesion size dependent transition to

cytoskeletal linkage indicates that cells cultured on larger nanopatterns are able to form more mature focal complexes that contain cytoskeletal-linking adaptor proteins but rarely form large classical focal adhesions as seen in cells on non-patterned control surfaces.

5.5 Conclusions

A semi-automated image processing method was created that allowed for more accurate detection of very small focal complexes than existing available image processing techniques. A semi-automated adhesion analysis algorithm was developed to quantify changes in the number, density, location, size, total adhesion area, and percent adhesion of cells cultured on surfaces. The combined image processing and adhesion site analysis methods provided a powerful tool for analyzing and comparing different states of adhesion as induced by engineered surfaces. Surface chemistry, FN surface density, and imposed limitations on adhesion site growth all have an influence on adhesion site formation. While other studies have shown interesting changes in cell behavior in response to nanostructured surfaces, this is the first study to provide direct evidence over adhesion site size control in the nanometer regime. Furthermore, both focal complexes and focal adhesions were analyzed giving a more complete picture of cell adhesion while most studies only analyze large classical focal adhesions. Most importantly, it was demonstrated that cells react to nanopatterned surfaces by forming an increased number of smaller, more densely packed vinculin-containing adhesions and that the density and distribution of these adhesion sites can be modulated by tuning the size of the underlying FN nanoislands. Further studies concerning cytoskeletal formation and the mechanotransductive abilities of cells including cell spreading, fibrillogenesis,

and cell motility further indicate that limiting adhesion site size can be used to modulate certain aspects of gross cell behavior and are discussed in the following chapters.

Chapter 6

Actin Cytoskeleton Properties

6.1 Introduction

The formation of a well-defined actin cytoskeletal network is essential for cellular force transduction and the creation of traction forces for cell spreading, motility, ECM remodeling, and the intracellular signaling. The actin cytoskeletal network is composed of stress fibers, bundles of small F-actin fibers that are responsible for transmitting force to the underlying surface through direct attachment to adhesion sites via α-actinin, talin, and various other adaptor and scaffold proteins.[13,206,207] To gain an understanding of how restricting adhesion site size can influence actin cytoskeletal formation, a method to quantify the number of actin stress fibers per cell and to account for changes in cell spreading, the actin stress fiber density, was developed. Since actin ties directly into adhesion sites and since recent studies have shown that adhesion site components play an important role in the linking of short F-actin fibers to form longer fibers in freshly seeded cells and in podsome formation it is hypothesized that the nanopatterned surfaces should influence cytoskeletal formation.[68,69,174]

6.2 Materials and Methods

6.2.1 Cells and Reagents

Refer to Section 4.2.5, only non-pooled HUVECs were used for these experiments.

6.2.2 Nanopattern Fabrication and Surface Functionalization

See Sections 3.2.1 and 4.2.2 for nanopattern fabrication and functionalization respectively.

6.2.3 Fluorescent Labeling and Imaging of Actin

See Section 4.2.6.

6.2.4 Image Processing and Actin Analysis

The acquired fluorescently labeled actin images were processed using a technique similar to that described in Section 5.2.4. The images were processed with a FFT filter to reduce noise and remove background signal, but instead of being iteratively thresholded, the FFT filtered images were used directly to measure the number of actin fibers per cell cross section and the actin fiber density (number of fibers per cross section length). The number of stress fibers per cell was determined by drawing a line across the entire cell body perpendicular to the direction of the dense peripheral bands using the line feature in ImageJ (NIH, Bethesda, Maryland). An intensity plot of the line was created and fit with Gaussian peaks using PeakFit software (Systat Software, Point Richmond, CA). The number of Gaussians fit to the drawn line was reflective of the number of actin stress fibers present in the cross section as determined by visual inspection. The fiber density was calculated by measuring the distance across the entire cell from the center point of one peripheral band to the center point of the peripheral band on the other side of the cell and by dividing the number of fibers by this length measurement. The fiber density measurements were scaled to 10 µm giving a measure of actin stress fiber density as the number of stress fibers per 10 µm length across the cell. The dense peripheral bands were not included in the actin stress fiber count or in

the stress fiber density measurements. All cells, even those that did not form many stress fibers were able to create a dense peripheral band and since the cells on some nanopatterned surfaces did not spread well, the inclusion of dense peripheral bands into the stress fiber number and density measurements induced inflated values for these measures.

6.2.5 Statistical Analysis

See Section 5.2.5.

6.3 Results

The results from cells on Au control surfaces with varying FN surface concentrations indicate that FN concentration has some influence on the formation of stress fibers after 1 day in culture but not after 3 days (Figure 6.1 A,B). Nanopatterned surfaces have a significant impact on stress fiber formation and their influence stems from multiple factors including nanopattern size, spacing, and perhaps density. The analysis of cells cultured on thiolated Au control surfaces with varying surface concentrations of FN shows a trend of increased stress fiber formation with increased FN surface concentration, from 10 to 26 fibers per cell for the 2Au and 25Au surfaces respectively (Figure 6.1 A). The stress fiber density measurements verify that FN surface density can influence actin stress fiber formation (Figure 6.1 B). Cells cultured on 2Au surfaces only form 3 stress fibers per 10 µm cross section while cells on 25Au surfaces form twice the density at 6 stress fibers per 10 µm (Figure 6.1 B). The number of stress fibers formed by cells cultured on Au control surfaces displays a linear increase with increased FN surface concentration (Figure 6.1 A) but the actin fiber densities are very similar for cells on all Au controls at 5 stress fibers per 10 µm after 3 days (Figure 6.1 B).

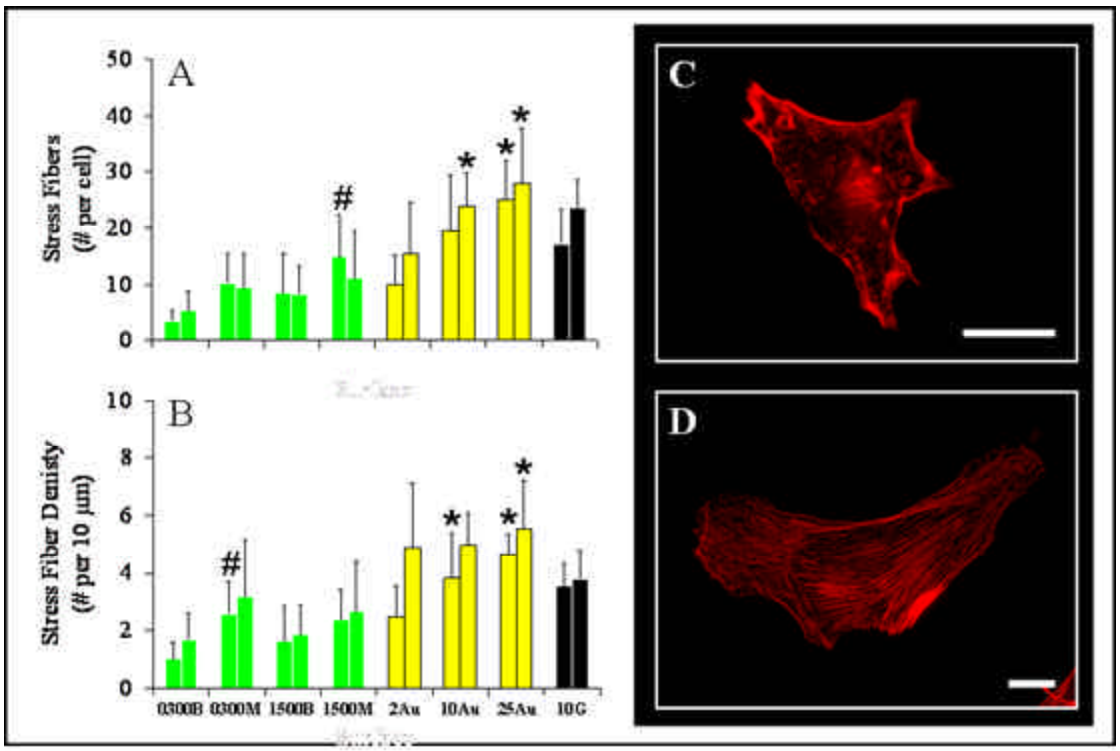

Figure 6.1: Actin Stress Fiber Properties: Cells were seeded on nanopatterned surfaces (green), gold control surfaces with varying FN surface densities (yellow), and glass control surfaces (black). After 1 and 3 days in culture the cells were fixed, stained for stress fibers, imaged, and their actin stress fiber properties measured. (A) The number of stress fibers per cell cross-section was measured and (B) normalized and scaled to determine the stress fiber density. (C) Cells on nanopatterned surfaces (0300B in C) create fewer numbers of stress fibers and less dense stress fiber networks compared to cells on (D) Au control surfaces (25Au in D). * Statistically more actin stress fibers than all nanopatterns ($p < 0.03$). # Statistically more actin stress fibers than cells on 0300B nanopatterned surfaces ($p < 0.03$). Scale bar = 25 μm.

The nanopatterned surfaces somewhat inhibit stress fiber formation and cells cultured on control surfaces form significantly more actin stress fibers with increased densities compared to cells on nanopatterned surfaces (Figure 6.1). Cells on all nanopatterned surfaces create significantly fewer numbers and densities of actin stress fibers over a 3 day period compared to cells seeded on thiolated Au surfaces displaying 2,474 FN/μm^2 (Figure 6.1 A). There were also differences observed between cells seeded on the different nanopatterned surfaces. Cells grown on 0300B surfaces created significantly fewer stress fibers than cells on 1500M surfaces, while cells cultured on 0300M and 1500B surfaces did not show any significant differences in the number of fibers created compared to cells on the other nanopatterned surfaces. Furthermore, the actin fiber density was significantly higher in cells on 0300B surfaces compared to cells on 0300M surfaces (Figure 6.1 A,B).

A closer analysis shows that cytoskeletal formation for cells cultured on nanopatterned surfaces is dependent on both nanopattern size and interpattern spacing. The 0300M and 0300B surfaces present similar attachment areas with different island-to-island spacing but show significant differences in actin fiber densities after 1 day in culture (Figure 6.1 B). While cells on 0300B surfaces created very low density fiber networks, 1 fiber/10 µm, cells on 0300M created significantly more dense networks of 3 fibers/10 µm (Figure 6.1 B). The small nanopattern size on the 0300B surfaces greatly suppresses stress fiber formation as seen in Figure 6.1 A and Figure 6.2 A. Although 0300M surfaces display a similar nanopattern size to 0300B surfaces, the nanoscale adhesive sites are spaced closer together and are only separated by 177 nm compared to 300 nm for the 0300B surfaces. This close proximity of the nanoislands on the 0300M surfaces allowed for thin fibers emanating from small

individual adhesion sites to be joined into larger bundles thereby forming stress fibers (Figure 6.2 B). The white arrows in Figure 6.2 B indicate locations of stress fiber bundling. The white arrow on the left side of Figure 6.2 B shows were four small actin fibers stemming from individual small adhesions are joined together to form a thicker stress fiber bundle. The white arrow on the right points out a similar event where 3 fibers are joined to an existing fiber.

A similar nanopattern spacing dependence on stress fiber bundling was observed between cells on the 1500B and 1500M nanopatterned surfaces (Figure 6.2 C,D). Cells on both of these surfaces are able to form adhesion sites that tie into small stress fibers, yet the adhesions are much smaller than 1 μm^2 implying that the adhesions are not typical of large, classical focal adhesions. While the nanoislands for these surfaces are large enough to allow for the formation of adhesions that tie into well-defined stress fibers, the density of the networks were still significantly lower than those created by cells on homogenously coated controls with high FN surface densities (Figure 6.1 B). The same occurrence of adhesion site spacing influence on stress fiber bundling was also observed in these cells. Cells cultured on 1500M surfaces display the ability to bundle multiple fibers together that each start from an individual adhesion. The larger spacing of 1.5 µm between adhesion sites on 1500B surfaces was too large for cells to bundle fibers together (Figure 6.2 C,D). Figure 6.2 C shows that fibers created on the 1500B surfaces do not get bundled together and continue through the cell body as separate entities from the adhesions they are linked to. Figure 6.2 D shows that the nanopatterns on the 1500M surfaces are spaced close enough so that fibers stemming from individual adhesions can be joined together to form larger stress fibers.

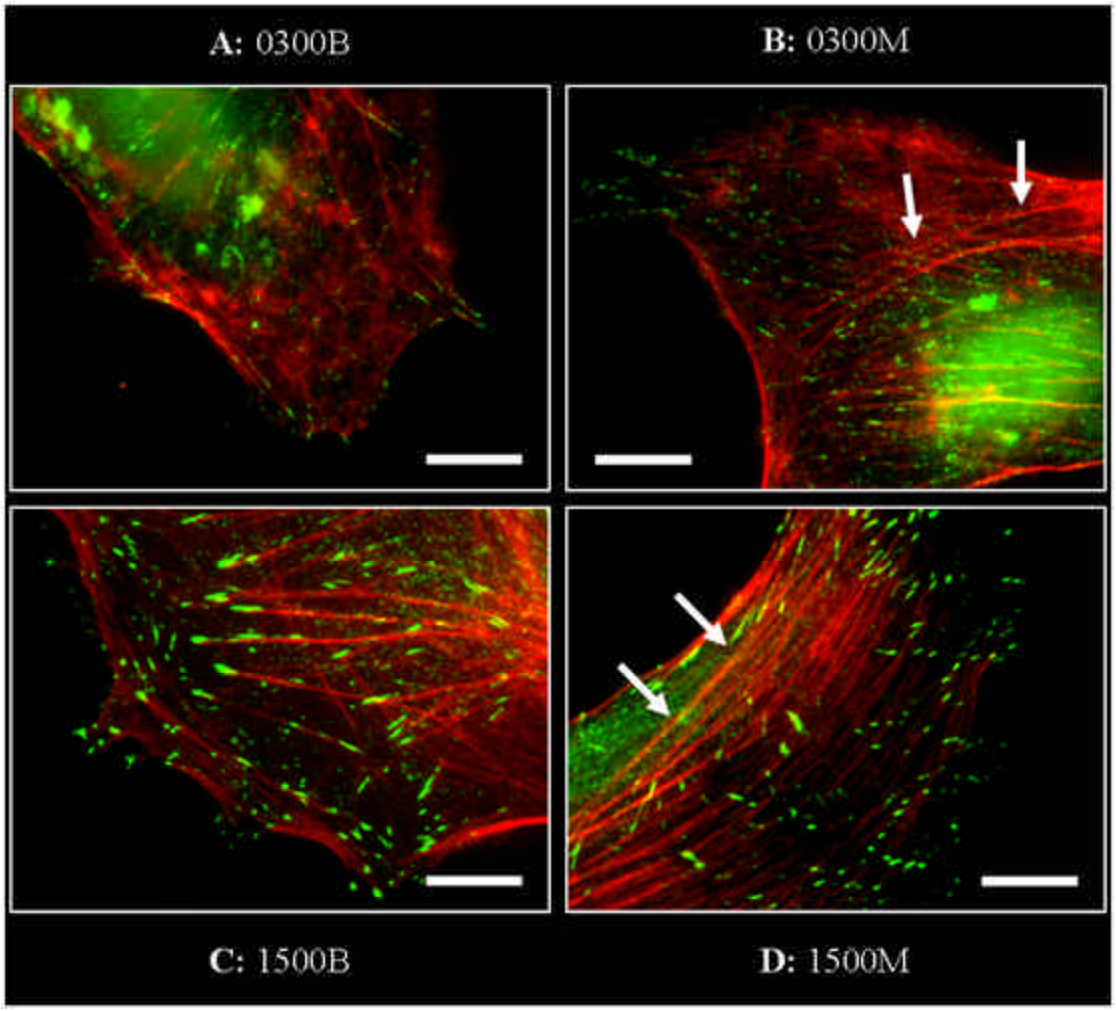
A: 0300B
B: 0300M
C: 1500B
D: 1500M

Figure 6.2: 160X Magnification Images of Actin Stress Fibers and Vinculin-Containing Adhesion Sites of Cells on Nanopatterned Surfaces: Cells were cultured on nanopatterned surfaces for 1 day, fixed, stained for vinculin and actin, and imaged. (A) Cells cultured on 0300B surfaces were not able to form many actin stress fibers. Stress fiber production was increased by (B) culturing cells on nanopatterned surfaces with closer interpattern spacing (0300M) or (C) by culturing cells on larger nanopatterns that allow for the creation of stress fiber linked adhesion sites (1500B). (D) Combining the size and spacing effects induced cells to create more-dense actin fiber networks similar to cells on control surfaces (1500M). The white arrows (B,D) indicate regions were single small fibers were bundled to form larger stress fibers. Scale bar = 10 μm.

The white arrow on the right in Figure 6.2 D highlights a region where approximately 17 individual fibers to the right of the arrow are joined into 7 larger fibers at the arrow that are then bundled again at the white arrow on the left and continue through the cell as 4 large stress fibers. The nanopattern spacing influence on actin fiber bundling is also reflected in the stress fiber density data (Figure 6.1 B). Cells on both B-type surfaces form less dense actin networks compared to cells on M-type surfaces with similar nanopattern sizes, although only the 0300M and 0300B show statistically significant differences from each other (Figure 6.1 B).

6.4 Discussion

The results indicate that FN surface density influences stress fiber formation at early time points and that lower surface concentrations of FN reduce the propensity for cells to create dense stress fiber networks. Limiting adhesion site growth in cells on the nanopatterned surfaces induced three separate regimes of cytoskeletal formation. Cells

on the smallest nanopatterns, 0300B, displayed an impaired ability to form stress fibers due to limitations imposed on adhesion site size. This restriction could be overcome by two means; increasing the nanopattern size as demonstrated with 1500B surfaces or by decreasing the pattern spacing as demonstrated with 0300M surfaces. Both of these changes in nanopattern properties led to more-dense cytoskeletal networks compared to cells on 0300B surfaces but by different means. The 1500B surfaces have much larger nanopatterns, 222 nm, compared to 0300B surfaces with nanopatterns 92 nm in size. Increasing the size of the pattern results in the formation of larger adhesions that support stress fiber linkage to the adhesion plaques thereby increasing the overall actin fiber density in cells on these surfaces, although the density is still significantly lower than cells on control surfaces. Cells cultured on 0300M surfaces also display more-dense stress fiber formation than cells on 0300B surfaces but reach this increased density through a different mechanism than increased adhesion site size. The nanopattern size for both the 0300B and 0300M surfaces is very similar, 92 and 94 nm respectively, yet the spacing between patterns is quite different, 300 and 172 nm respectively. The tighter packing and closer proximity of adhesions formed by cells on the 0300M surfaces allowed small F-actin fibers linked to these sites to be joined into larger bundles thereby creating stress fibers. This demonstrates that more-dense fiber networks can be created by tuning both the nanopattern size and interadhesion site spacing. The fourth regime of cytoskeletal density was created in cells cultured on 1500M surfaces. These surfaces combine the influence of both increased adhesion site size and closer interadhesion site spacing. The combined effects result in cells that produce significantly more actin stress fibers that are much more-dense than those created in cells cultured on 0300B surfaces. While the measures of cytoskeletal networks for cells on 1500M surfaces move toward

that of high FN surface density controls, the number of fibers created and the density of fibers is still significantly lower than cells on 25Au surfaces.

Similar reports of disrupted actin cytoskeletal formation have been reported in cells seeded on soft elastic surfaces.[39,40,208,209] Interestingly, these cells also exhibit similar adhesion site behavior displaying small, more dynamic punctuate adhesions throughout the cell body.[39,126,209] This finding, along with the results presented here, demonstrates that the formation of large adhesions that support force transduction are necessary for the creation of dense actin fiber cytoskeletal networks. Furthermore, it has been shown that cells lacking Shp2 display a higher density of small focal complexes deficient in α-actinin and that force-dependent strengthening of the adhesion sites correlated with α-actinin assembly and decreased adhesion site dynamics.[80] FAK was shown to play an important role in regulating this process.[80] This finding shows that the incorporation of cytoskeletal linking and adaptor proteins into adhesion sites via their indirect association with FAK is important for cytoskeletal formation. Furthermore, elaborate studies examining the interactions of adhesive components with F-actin in freshly seeded cells shows that the formation of vinculin singlets or doublets with F-actin cores is needed to link small F-actin fibers together to form longer F-actin fibers.[174] Similar instances of adhesive components surrounding F-actin cores have been reported in podosome formation, short cellular extensions that release ECM degradation enzymes needed for cell motility in tight matrices.[68,69] These two studies suggest that certain adhesive components can play some role in actin organization for early forms of actin formation. The results demonstrated here further hint to a role of adhesion sites in actin organization.

The finding that cells cultured on 0300B surfaces do not form many adhesion linked stress fibers further validates the claim that the normal maturation process of adhesion sites is retarded in cells on nanopatterned surfaces due to the adhesion site growth restrictions imposed by the orthogonal surface chemistry. Cells on these surfaces display interactions with actin similar to those observed by nascent adhesions in freshly seeded cells before the complexes matured into stress fiber linked focal adhesions. [174] These very small growth limited adhesions may be limited to the formation of early focal complexes that lack much α-actinin and the ability to link to actin stress fibers. The combined effects of limiting adhesion site growth and preventing the application of force to adhesions through actomyosin machinery is shown to have an influence on cell spreading and motility in the following chapters.

6.5 Conclusions

It was demonstrated that cells on all nanopatterned surfaces show a slightly impaired ability to create actin stress fibers that results in less-dense stress fiber cytoskeletal networks compared to cells on control surfaces. It was demonstrated that the ability to form stress fiber linked adhesions is influenced by adhesion site size and that the ability to form stress fibers made of bundled F-actin fibers is dependent on adhesion site spacing. These differences in cytoskeletal properties as regulated by different adhesive states are shown to have an influence on gross cell behavior in the following chapters.

Chapter 7

Fibrillogenesis

7.1 Introduction

Fibronectin is a complex ECM protein composed of three subunits containing both easily accessible and cryptic integrin binding sites, as well as areas for linkage to other ECM proteins and FN itself.[210] It exists as a soluble dimer in solution and upon activation by integrin binding and the application of cellular force undergoes elongation and fibril formation, a process termed fibrillogenesis.[13,43] While still not fully understood, fibrillogenesis is initiated by the binding of $\alpha_v\beta_3$ and $\alpha_5\beta_1$ integrins to the available RGD and synergistic binding sites while FN is in its compact form. FAK is then incorporated into the adhesion, phosphorylated, and begins recruiting Src that provides adhesion site linkage to the cytoskeleton though Shp2 and various other adaptor proteins. More integrins accumulate in the FN associated adhesion site forming a platform for the assembly of a small focal complex that matures into a larger focal adhesion. Through an unknown mechanism a fibrillar adhesion rich in $\alpha_5\beta_1$ integrins and tensin begins breaking away from the focal adhesion. The focal adhesion at the end of the FN acts as an anchoring point as the attached fibrillar adhesion translocates toward the cell center via myosin interactions with actin stress fibers, thereby stretching the FN creating a fibril. Currently, two models of FN fibril formation and fibril elongation exist.[211,212] Both relate the formation of fibrils to applied cellular forces but the exact confirmation of the formed fibrils is still under debate. The first model suggests quaternary transformation in which fibrils under applied stress do not change their tertiary or secondary structures but a transformation from a compact to a more

elongated form is achieved.[43,211,213] The second model suggests that FN extension is achieved by unfolding of the tertiary type III domains which have a free energy of denaturation similar to the force generated by myosin motors.[212] Recent studies have shown that fibril alignment and elongation is dependent on the balance of forces between integrin-FN binding and FN-substrate binding.[214] If the direction of applied force is perpendicular to the elongated fibrils and the FN-surface interactions are not very strong, then the cell can pull the FN underneath itself. If the direction of applied force is parallel to the fibrils and the FN-surface interactions are strong, then the cells will leave the fibrils on the surface resulting in FN trails. Regardless of the exact mechanism, the unfolding or stretching of FN exposes previously hidden ECM and FN binding sites as well as additional cryptic cellular adhesion sites.[43,213] As more force is applied to the protein and fibril formation continues, it begins binding to neighboring stretched FN molecules creating a dense interconnected network underneath the cell that can be interconnected with fibrils under neighboring cells. This dynamic process is crucial to the formation of natural ECM and has been observed in numerous cell types. The importance of mechanotransduction processes in fibrillogenesis is extremely evident and is thought to rely on Rho-dependent actin stress fiber formation as well as the formation of large, mature focal and fibrillar adhesions to act as the necessary machinery to form these fibers.[16,213,215] The ability of cells to perform this task was tested on nanopatterned surfaces. Even though cells on nanopatterned surfaces displayed reduced actin stress fiber cytoskeletal networks some of the nanopatterned surfaces allowed for the creation of FN fibrils. The density of fibrils created by cells on nanopatterned surfaces was less than those created by cells on glass and low FN density

Au controls. Furthermore, the underlying nanogeometry had an influence on the density and length of the formed fibrils.

7.2 Materials and Methods

7.2.1 Cells and Reagents

Refer to Section 4.2.5, only non-pooled HUVECs were used for this experiment.

7.2.2 Nanopattern Fabrication and Surface Functionalization

See Sections 3.2.1 and 4.2.2 for the fabrication and functionalization techniques respectively.

7.2.3 Fluorescent Labeling and Imaging

See Section 4.2.6.

7.2.4 Image Processing of Fluorescently Labeled FN Fibrils

The same image processing technique described in Section 5.2.4 was implemented to process the fluorescently labeled FN images. The FFT filtered and iteratively thresholded images were used to measure the percentage of FN underneath the cells by measuring the total surface area of FN in fibril form and dividing it by the cell spread area. The FN fibril lengths on the nanopatterned surfaces were measured by hand using ImageJ (NIH, Bethesda, Maryland), this measurement was not made for cells on control surfaces. The interconnectedness of the FN networks in cells on control surfaces made it impossible to trace the length of one single fibril. The measurement was applied to fibrils formed on the nanopatterned surfaces due to their lack of branching points and their straight line appearance.

7.2.5 Statistical Analysis

Refer to Section 5.2.5.

7.3 Results

The occurrence and extent of fibrillogenesis was monitored in cells on nanopatterned and control surfaces to gain insight into any possible differences in the mechanotransductive abilities of cells seeded on nanopatterned surfaces. The results indicate that a number of surface properties influence fibrillogenesis. Underlying surface chemistry, FN surface concentration, and nanopattern geometry all have some influence on fibrillogenesis.

Surface Chemistry Influence on Fibrillogenesis

HUVECs were cultured on homogenously FN coated Au and glass surfaces with similar FN densities. The results indicate that fibrillogenesis is induced in cells on glass surfaces but not observed in cells on Au surfaces with similar FN surface densities (Figure 7.1 B versus C). ECs cultured on homogenously coated glass surfaces formed dense, interconnected FN networks covering 11 % of the surface underneath the cell body after 24 hours and these dense networks persisted for 3 days in culture (Figure 7.2 B). In contrast, HUVECs grown on homogenously coated thiolated gold surfaces with FN surface concentrations above 600 FN/μm^2, 10Au and 25Au surfaces, formed almost no fibers at all (Figure 7.1 B and Figure 7.2 B). The reason for limited fibril formation in cells seeded on thiolated Au surfaces compared to cells on glass surfaces is most likely due to differences in the confirmation of the adsorbed FN which can influence integrin type and the molecular composition of the adhesions as discussed in

Section 2.5. It has been demonstrated that cells utilize and express more $\alpha_5\beta_1$ integrins when attaching to FN adsorbed to hydrophilic surfaces (glass) compared to cells attached to FN adsorbed to hydrophobic surfaces (thiolated Au).[117,121] Since $\alpha_5\beta_1$ integrins are known be the dominant integrin type in fibrillar adhesions, one would expect increased fibrillogenesis in cells cultured on glass surfaces compared to those on thiolated Au surfaces.

FN Surface Concentration Influence on Fibrillogenesis

While cells cultured on Au surfaces with FN surface concentrations greater than 600 FN/μm^2 show no signs of fibrillogenesis, cells on low density FN surfaces create a significant number of FN fibrils even though the surfaces were blocked with BSA (Figure 7.1 A versus B). This shows that cells are not only sensitive to the underlying chemistry but also to the initial FN surface concentration at the time that they are seeded. The number of cells that created dense FN fibril networks and the density and interconnectedness increased with decreasing FN surface concentration (Figure 7.1 A versus B, Figure 7.2 B). As the surface concentration of FN was reduced from 2,474 to 537 FN/μm^2 the FN fibril coverage increased from 2 to 15.5 % and the percentage of cells that created these networks increased from 20 to 90 % (Figure 7.2 A,B). Since there is very little FN available for adhesion formation and attachment on the 2Au surfaces, the cells most likely react by producing their own FN.

Close examination of the fluorescent FN images shows that the networks created by cells on Au surfaces have a different appearance then those created by cells on glass surfaces. Cells on glass surfaces create thick, long fibers that are highly interconnected, (compare Figure 7.1 A to C) while cells on Au surfaces create thin relatively shorter FN

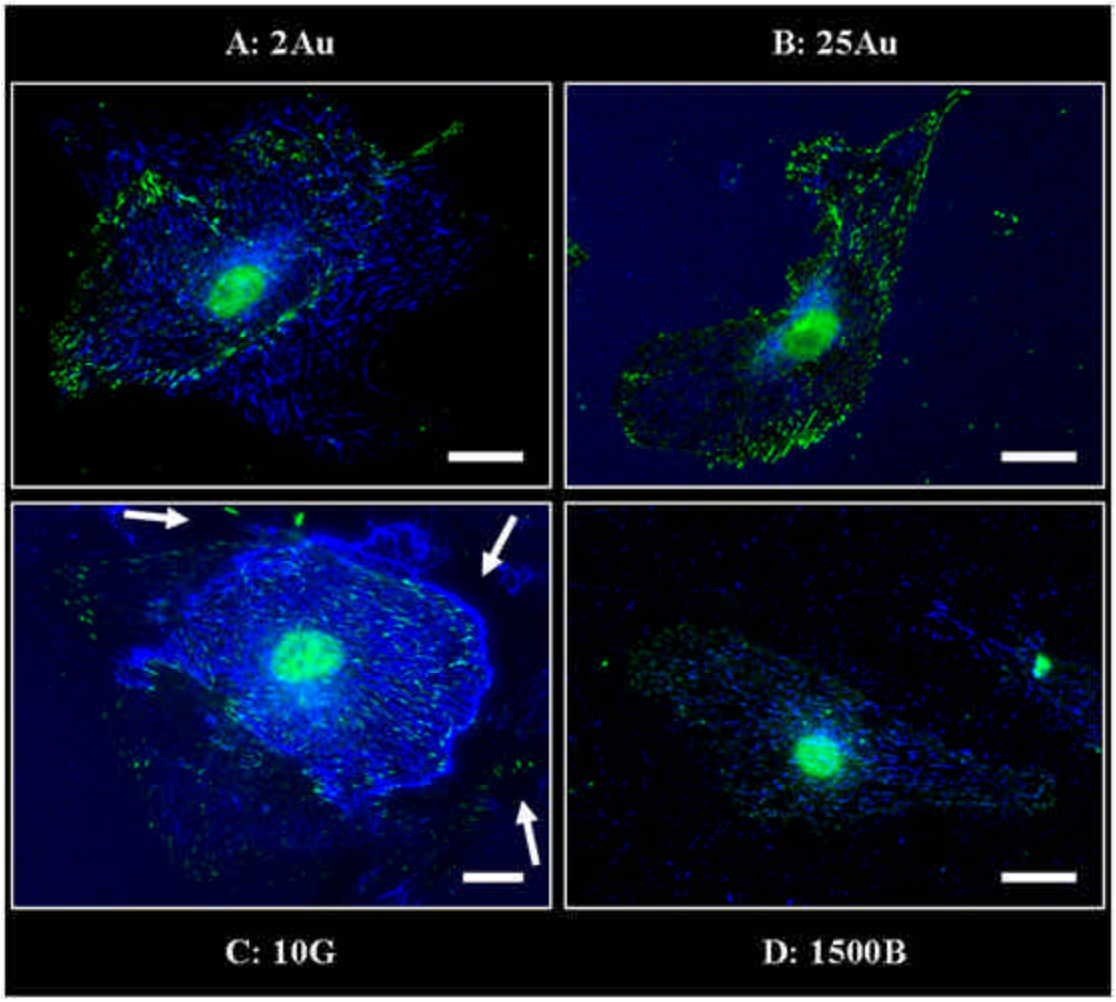
A: 2Au
B: 25Au
C: 10G
D: 1500B

Figure 7.1 FN Fibril Formation: Cells were seeded on control and nanopatterned surfaces, fixed, and stained for FN (blue) and vinculin (green). (A) Cells on low density FN surfaces are able to from thin interconnected FN fibril networks. (B) Cells on high density FN surfaces form almost no FN fibrils. (C) Cells on glass surfaces form thicker more dense and interconnected FN networks. The white arrows in (C) indicate the creation of depletion zones where the cell has scooped the FN from the surrounding surface and bundled it to create the fibril network under the cell. (D) Cells on B-type surfaces form shorter, thinner FN fibrils whose width and length are somewhat determined by the nanopattern size and spacing respectively. Scale bar = 25 μm.

fibrils with many branching points but with relatively less interconnectivity to other fibers. While the exact reason for these differences in FN network appearance is unknown, it may be due to differences in surface properties between Au and glass. The increased hydrophobicity of the thiolated Au surfaces may prevent the bundling of many FN fibrils together since the deposited FN is more tightly bound to the Au surface compared to FN deposited on the glass surface. The arrows in Figure 7.1 C indicate FN depletion zones where the cells on glass surfaces were able to scoop up the surrounding FN and pull it under them to create thicker FN bundles, an occurrence not seen in cells on Au surfaces. This difference in the ability of cells to scoop FN from the surface depending on the surface energy hints to both differences in the direction of applied force from the cell to the FN and possibly to differences in FN-surface binding strength between Au and glass surfaces. [214]

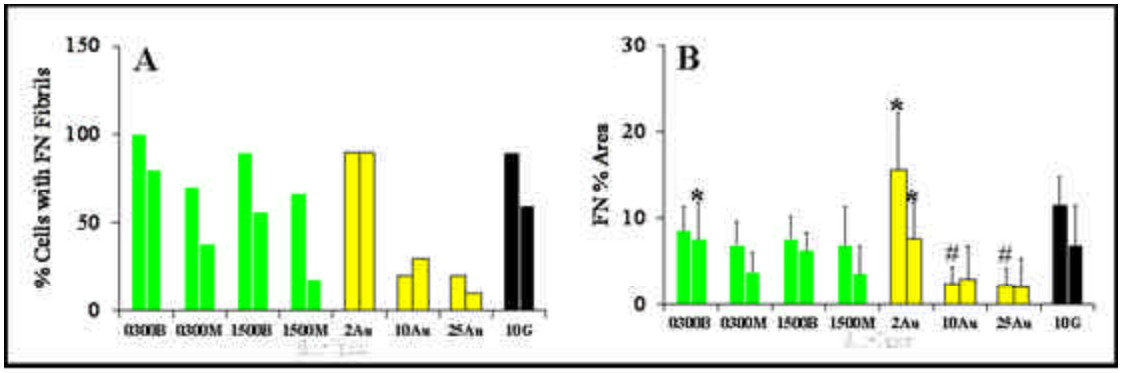

Figure 7.2: FN Fibril Properties Formed by Cells on Control and Nanopatterned Surfaces: (A) Shows that the percentage of cells that undergo fibrillogenesis is dependent on the FN surface density, underlying surface chemistry, and nanopattern geometry. (B) Graph showing the percent surface area covered with FN fibrils underneath the cell with respect to the cell spreading area for cells that create fibrils. Cells on low-density coated Au surfaces and on glass controls create dense interconnected fibril networks, while cells seeded on Au controls with higher FN concentrations do not create many fibrils. Cells on nanopatterned surfaces create similar amounts of fibrils after 24 hours, but the density of the networks is greatly reduced on M-type surfaces after 3 days. * Indicates significantly more FN % area than all surfaces after 24 hours ($p < 0.016$). # Indicates significantly less FN % compared to 2Au, 10G, and all nanopatterned surfaces after 24 hours ($p < 0.05$). * Indicates significantly more FN % compared to 25Au after 72 hours ($p < 0.038$).

Nanopattern Influence on Fibrillogenesis

The extent of fibril formation was also examined in cells cultured on nanopatterned surfaces. The results indicate that nanopattern geometry has some influence on the occurrence and extent of fibrillogenesis. It was hypothesized that fibril formation would be decreased in cells on nanopatterned surfaces; particularly in cells seeded on surfaces with very small nanopatterns due to the lack of dense actin networks in these cells. However, it was discovered that cells seeded on small nanopatterns were indeed able to form thin FN fibrils whose width seemed to be determined by the underlying nanopattern size and whose length was influenced by both the underlying pattern geometry and interisland spacing. The fibrils formed by cells on nanopatterned surfaces were also quite different in their interconnectedness compared to the dense networks created by cells on 10G and 2Au control surfaces (Figure 7.1 D). The fibrils on nanopatterned surfaces were thin, long structures that ran in straight lines and very seldom branched off or made connections with neighboring fibers (Figure 7.1 D). These thinner, long parallel fibrils were similar in appearance to those observed in cells cultured in 3-D FN matrixes. [48]

A slight dependence on the geometrical configuration of the underlying nanopatterns was observed. Cells cultured on B-type surfaces displayed an increased propensity to create fibrils compared to cells on M-type surfaces. 100 % of the cells cultured on 0300B nanopatterned surfaces created fibrils while a slightly lower percentage of cells, 70 %, on 0300M surfaces created fibrils after 24 hours (Figure 7.2 A). This trend was realized between cells on larger nanopatterned surfaces. 90 % of the ECs on 1500B surfaces created fibrils while only 65 % of the cells on 1500M

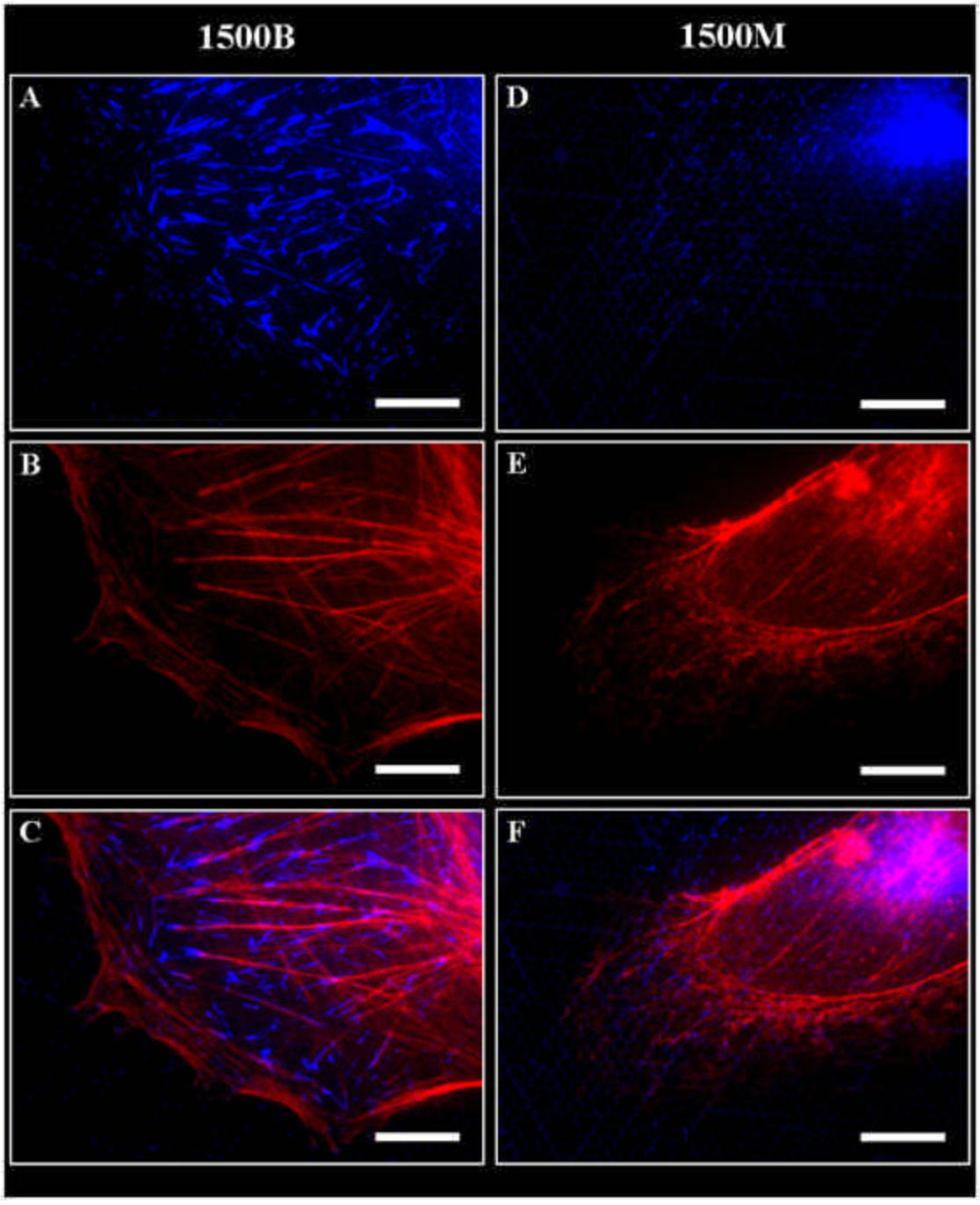
1500B
1500M
A
D
B
E
C
F

Figure 7.3: FN Fibril Formation is Dependent on Nanopattern Properties and Direction of Applied Force: Cells were seeded on 1500B (A-C) and 1500M (D-F) surfaces, fixed, and stained for actin stress fibers (red) and FN (blue). (A) Cells on 1500B surfaces display a higher propensity to create FN fibrils compared to cells on (B)1500M surfaces implying that the underlying geometry influences fibril formation. The direction of fibril formation correlates with the direction of applied force as indicated by colocalization with the actin stress fibers (C). Even though stress fibers are formed by cells on 1500M surfaces, the geometrical configuration of the nanopatterns does not allow for fibers to be bridges across multiple nanopatterns. Scale bar = 10 µm.

surfaces showed signs of fibrillogenesis (Figure 7.2 A). This indicates that the nanogeometry or perhaps spacing of the underlying nanopattern is important in promoting fibrillogenesis. The observed trend of enhanced fibril formation on B-type surfaces was more pronounced after 72 hours although the absolute number of cells undergoing fibrillogenesis was much lower, particularly for cells on M-type surfaces (Figure 7.2 A). Cells seeded on large nanopatterns, 1500M and 1500B, displayed similar adhesion, actin, and cell spreading properties yet the increased occurrence of fibril formation and more extended fibrils were observed in cells on the 1500B surfaces. After 72 hours, 60 % of the cells seeded on the 1500B surface created fibrils with an average length of 3 µm (Figure 7.4), corresponding to the distance between 2 nanopatterns, while only 20 % of the cells seeded on the 1500M created fibrils with slightly shorter average length of 2 µm (Figure 7.4). Fibrils created by cells cultured on 1500B surfaces often spanned multiple patterns, whereas fibrils created on the 1500M surface typically just span between two nanopatterns if they span any at all (Figure 7.3 A,D and Figure 7.4 B). This finding implies that the underlying geometrical or spatial pattern of

FN also has an influence on fibril formation. While the 1500M surface has an interpattern spacing of 883 ± 51 nm, the underlying geometry does not allow for a straight line linking multiple patterns to be formed without an increased probability of changing direction to connect the fibrils to a closer pattern (Compared C versus D in Figure 3.1), in contrast a straight line can be easily drawn on a 1500B nanopatterned surface connecting multiple patterns with low probability of changing the fibril direction even though the interpattern spacing is larger at 1.5 µm (Figure 3.1 D and Figure 7.3 A). Furthermore, cells cultured on 2Au surfaces without any geometrical restrictions on fibril formation tend to form fibrils with a straight line appearance. This implies that FN anchor points with the surface need to be formed and maintained in order to create long extended fibrils and that actin directionality controls fibril formation.

This same occurrence of nanopattern geometrical control of fibril formation was observed between cells on the nanopatterned surfaces with smaller adhesion sites. A much higher percentage of cells created fibrils on the 0300B surfaces, 80 %, compared to 37 % of the cells on the 0300M surfaces after 72 hours in culture (Figure 7.1 A). Cells seeded on these surfaces created fibrils with similar average lengths, 2.15 µm on the 0300M and 2.48 µm on the 0300B (Figure 7.4 A) corresponding to 8 and 15 spanned nanopatterns for the B- and M-type surfaces respectively (Figure 7.4 B). Again, as on the larger nanopatterned surfaces, the extent of fibril formation was similar for both surfaces after 1 day but after 3 days cells on the 0300M surfaces created fewer fibrils while the cells on the 0300B surfaces maintained a high percentage of fibrils underneath the cell (Figure 7.2). These results seem counterintuitive in some ways as the current models of fibrillogenesis includes the formation of large mature focal adhesions at one end of the FN to pin it to the surface while the fibrillar adhesion attaches and through

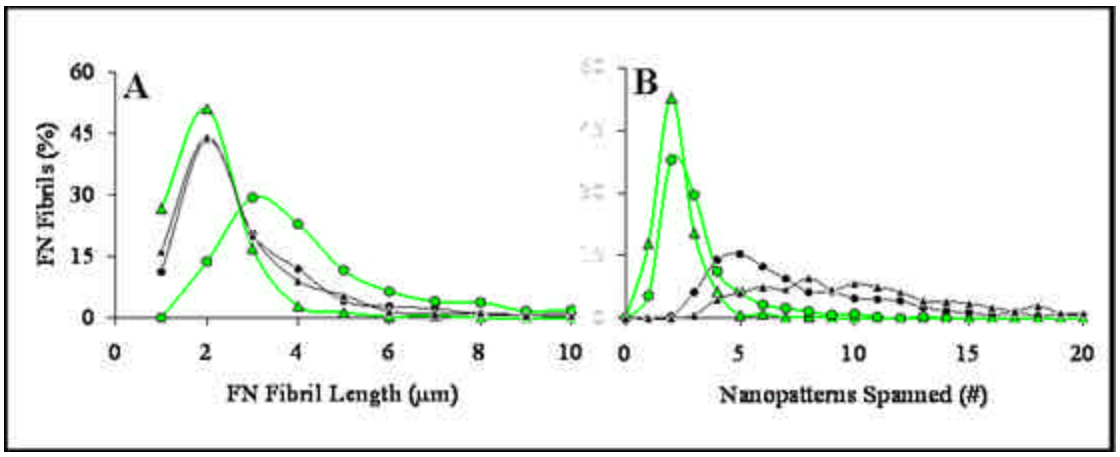

Figure 7.4: FN Fibril Lengths in Cells on Nanopatterned Surfaces: (A) Shows measured FN fibril lengths for cells on nanopatterned surfaces. Cells seeded on the 1500B surface create fibrils that often span 3 or 4 μm in length while cells on the 1500M, 0300M, and 0300B create shorter fibrils. (B) The number of nanopatterns spanned beneath the fibrils for cells on nanopatterned surfaces was also measured. Fibrils created on the 1500M surfaces typically do not span more than 2 nanopatterns while cells on the 1500B surfaces create fibrils that most often span 2 to 3 nanopatterns. Cells on 0300M and 0300B surfaces create fibrils that span 5 or more nanopatterns due to their close proximity to each other.

actomyosin generated forces pulls the FN apart. Cells on the 0300B surfaces neither create large mature adhesions or dense actin networks indicating that other unknown factors may play a role in this process.

While cells on smaller nanopatterns do not form many stress fibers, cells cultured on larger nanopattern surfaces do. A closer analysis of the fibrils shows that the directionality of FN stretching was dictated by the corresponding actin fibers above the fibrils and in cases where the FN could not be extended to the next nanopattern it was

pulled off in the direction of the cell body along the axis of the associated actin fiber, indicating the direction of applied force. Figure 7.3 shows fibril formation in cells cultured on 1500B and 1500M surfaces and the merged pictures indicate that fibril direction is governed by the associated actin fiber.

FN Fibril Location and FN Trails Behind Motile Cells

Trails of FN fibrils were sometimes observed in the wake of motile cells on nanopatterned surfaces and were good markers for indicating the direction of motility and provided historical information concerning the path traveled by the cell. To gain some insight into this phenomenon the location of fibril formation within the cell was analyzed and the fibril persistence was measured. The formation of fibrils is almost always seen between the cell center and trailing edge of motile cells and can be colocalized with dash-like adhesion sites. Figure 7.5 shows a motile cell on a 1500B surface. The leading edge of the cell on the left of the image is full of small dot adhesions. These dot adhesions correspond to the un-stretched form of FN adsorbed to the nanopatterns (Figure 7.5 B,C). The adhesions near the cell center and trailing edge just to the right of the nucleus are more elongated and show a dash like morphology. This conversion in adhesion site shape correlates to the formation of FN fibrils (Figure 7.5 D,E). Close examination of Figure 7.5 E shows trails of fibrils running in straight lines between the nanopatterns are left in the wake of the cells path. These historical fibril trails can often be traced for long distances behind the cell. Figure 7.6 B shows a trail behind the cell that is approximately 90 µm long. Figure 7.6 A shows a zoom in of an area where FN was converted from its globular form on the nanopatterns (arrow on right) to its elongated form after being manipulated by a motile cell (arrow on

left, arrow in middle shows a transition area). Knowing that these cells travel at approximately 0.6 µm/min implies that the FN can last in fibril form for around 2 hours before it snaps back to the nanopattern, it should be noted that the exact speed for the cell in Figure 7.6 is not known.

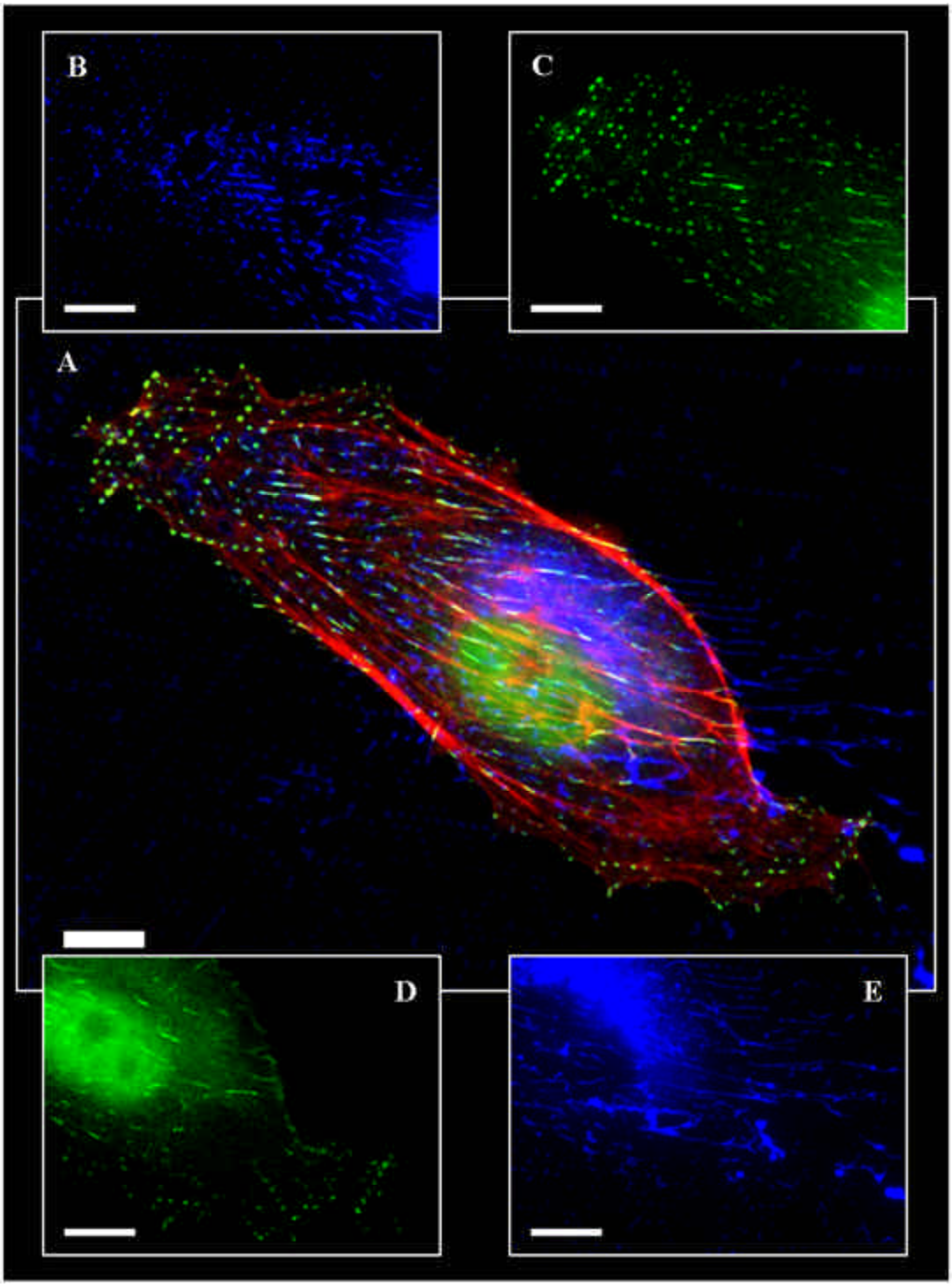
B
C
A
D
E

Figure 7.5: FN Fibril Trail Formation: (A) Cell on a 1500B surface that was fixed and stained for FN (blue), vinculin (green), and actin (red) after 3 days in culture. (B-C) Fibril formation coincides with adhesion site elongation. The stretched FN bridging multiple nanopatterns colocalizes with elongated dash-like vinculin containing adhesions. This typically occurs near the cell center and away from the leading edge. (D-E) The stretched FN is left as trails behind motile cells. The width of the FN fibrils is dictated by the nanopattern size. Scale bar = 10 μm.

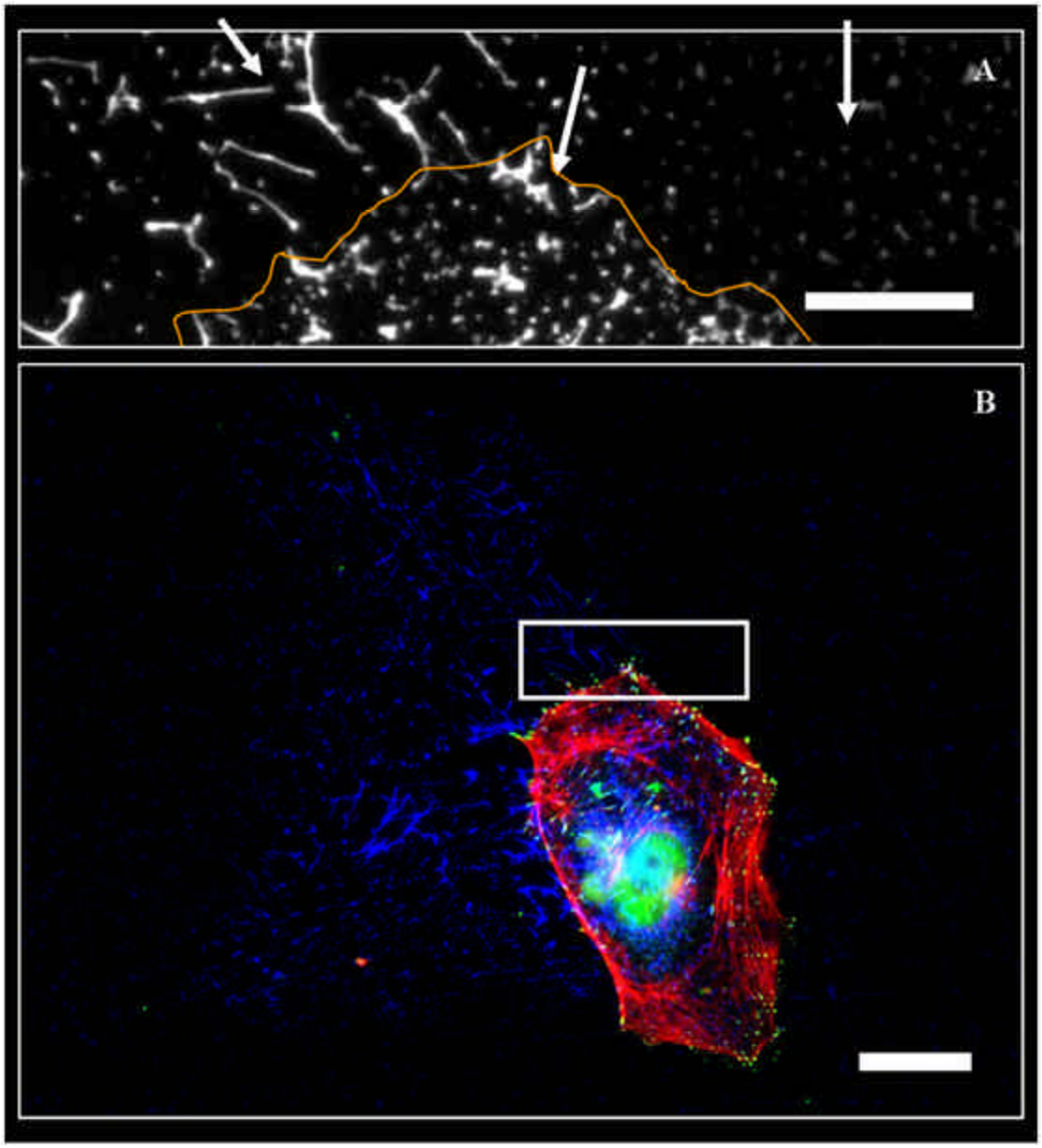
A
B

Figure 7.6: FN Trails Provide Historical Information About Cell Paths for Motile Cells: (B) Shows a motile cell moving from the left to right on a 1500B surface that was fixed and stained for FN (blue), vinculin (green), and actin (red) after 3 days in culture. The cell leaves a trail of relatively short thin FN fibers in its wake. In this case, the fibers are still present up to 90 μm behind the cell. After this the fibrils have snapped back to the nanopatterns and do not stay in an elongated from. (A) White box in (B) showing a zoomed in region of the FN, the cell rim is outlined in orange. The arrow on the right indicates where the cell has not interacted with the FN and it is still isolated on the nanopatterns. The middle arrow shows were the cell began to interact with the FN forming fibrils. The left arrow shows trails of FN that can span 3 to 4 nanopatterns. (A) Scale bar = 10 μm. (B) Scale bar = 25 μm.

7.4 Discussion

The results indicate that fibrillogenesis is dependent on surface chemistry, initial FN surface density, and possibly nanopattern geometry. The differences in fibril formation between cells on Au and glass surfaces can be easily explained. It is known that the confirmation of adsorbed FN is influenced by the surface energy or level of hydrophobicity. [120,121] The more compact confirmation of FN adsorbed to hydrophobic surfaces induces the use of $\alpha_v\beta_3$ integrins while integrin binding to FN adsorbed to hydrophilic surfaces is dominated by $\alpha_5\beta_1$ integrins. [114,115,117,118,121] Since it is known that fibrillar adhesions are rich in $\alpha_5\beta_1$ integrins it makes sense that more fibers are created by cells on glass surfaces compared to cells on Au surfaces. [16] Furthermore, the increased occurrence of fibrillogenesis in cells cultured on low FN surface density Au surface may be explained as a consequence of FN production. Since these surfaces

display low levels of sparsely packed FN the cell is most likely coping with this situation by creating its own FN, although there is no absolute proof for this occurrence.

The reason for the differences in fibrillogenesis between cells on B- and M-type surfaces is not as straight forward. Since dislocation of $\alpha_5\beta_1$ integrins along actin stress fibers supposedly dictates the direction that FN is pulled, then alignment of nanopatterns would allow for FN fibrils to be pulled across multiple patterns, as is the case for B-type surfaces. Since the M-type surfaces display nanopatterns that have an offset geometry, meaning that the nanopatterns can not be aligned or connected by a single straight line without increased probability of running into another pattern with a slight offset direction, may explain why fibrils are not often created by cells on these surfaces. This reasoning applies to differences observed in cells on 1500B surfaces compared to those of 1500M surfaces. Both of these surfaces allow for the formation of adhesion sites that can link to actin stress fibers. While the density of stress fibers is not significantly different between cells on these two surfaces the occurrence of fibrillogenesis is. This geometrical influence indicates that pinning sights or the ability of the cell to apply local forces at regular intervals may also be important in fibrillogenesis.

The occurrence of fibrillogenesis by cells on 0300B surfaces is somewhat surprising. Since the current model of fibrillogenesis includes the creation of a large mature focal adhesion to act as the anchor point holding FN to the surface and since cells on small nanopatterns do not form these adhesions, one would not expect fibril formation on nanopatterned surfaces with small patterns. This implies that other factors including differences in adhesion site composition and phosphorylation levels may play an important role in fibrillogenesis. Applying this reasoning to the cells cultured on 0300M versus 0300B surfaces, one would expect to see similar levels of fibril formation

since the nanopatterns are similar in size, yet a higher occurrence of fibril formation is observed in cells seeded on the 0300B surfaces. This reaffirms that the underlying geometry may play a role in fibril formation as seen on the larger 1500 surfaces. One can not leave out the possibility that the cells are creating their own FN and assembling it; but this does not fully explain the observed differences and it has been demonstrated that fibril formation is not dependent on de novo protein synthesis.[48,216]

7.5 Conclusions

The studies have shown that both surface chemistry and initial FN surface concentration at the time of cell seeding both have an influence on fibrillogenesis. The fibers created on Au surfaces are thinner and show more branching points compared to FN networks created by cells on glass controls. The underlying nanopattern geometry seems to have some influence in fibrillogenesis for cells cultured on nanopatterned surfaces. A regular spacing between patterns and the ability to form straight line fibrils seem to be important factors. Surprisingly, it was also shown that cells on 0300B surfaces were also able to create fibrils even though the lack many actin stress fibers. This hints that a complete understanding of the exact processes in fibrillogenesis has not fully been created and there is debate as to how it occurs.[13,43,211,212] Nonetheless, motile cells seeded on these surfaces tend to leave a wake of fibrils behind them providing historical information about the path they traveled and how long FN can stay stretched after applied cellular force is removed.

Chapter 8

Cell Spreading Studies

8.1 Introduction

Within the first few minutes of cell attachment to surfaces, integrin mediated small focal complexes are formed to the underlying ECM. [16] Shortly after their formation these complexes are linked to actin stress fibers via cytoskeletal adaptor proteins and mature into large focal adhesions through actomyosin mediated force application to the adhesive plaques. [16] The formation of large focal adhesions connected to actin stress fibers provides the necessary machinery for a cell to spread across a surface. Cell spreading is achieved by two separate actin mediated force production zones. Small focal complexes at the extreme periphery push on the cell membrane via interactions with F-actin. As the cell moves forward some of the small focal complexes mature into stress fiber linked focal adhesions that allow for the generation of contractile forces. The combination of these forces allows a cell to push out on the cell membrane thereby slightly increasing its area, create small adhesions that are then coupled to stress fibers, generate force to the adhesions through actomyosin contraction that result in the production of traction forces that then allows the cell to spread across the surface. Cell spreading upon contact with ECM coated surfaces is a universal phenomenon for all adherent-dependent cells. For this reason, cell spreading is often used as a measure of cellular response to differences in surface properties. This study analyzed the extent of cell spreading for cells cultured on nanopatterned surfaces and control surfaces with varying FN surface densities. The results provide insight into the mechanotransductive abilities of cells on nanopatterned surfaces and how imposing limitations on adhesion

site size and the coupling of adhesions to the cytoskeleton can influence cell spreading. The analysis indicates that both the number of large adhesions formed and the ability to create dense actin stress fiber networks are important for providing the necessary machinery for a cell to spread across a surface and that cell spreading can be impaired if large adhesion formation is impeded. Furthermore, the results imply that once a cell has spread, large adhesions are not needed to maintain the spread area.

8.2 Materials and Methods

8.2.1 Cell and Reagents

See Section 4.2.5, only non-pooled HUVECs were used for these experiments.

8.2.2 Nanopattern Fabrication and Functionalization

See Sections 3.2.1 and 4.2.2 for the fabrication and functionalization methods respectively.

8.2.3 Cell Spreading Studies

HUVECs were sparsely seeded at approximately 20 cells/mm^2. Fifteen 40 - 63X magnification fluorescent images of fixed cells were collected every 24 hours for 3 days. See Section 4.2.6 for the imaging system and cell preparation details. The cell spreading areas for a minimum of 15 cells per surface were measured by hand using the outline feature in ImageJ (NIH, Bethesda, MD). To separate surface effects from other stimuli, only cells that had one nucleus and were not in intimate contact with neighboring cells were analyzed for the cell spreading area study.

8.2.4 Statistical Analysis

See Section 5.2.5 for normality tests. The data sets passed the normality tests and were therefore analyzed with ANOVA and post hoc Tukey tests.

8.3 Results

The results indicate that FN surface density and underlying surface chemistry have little influence on cell spreading while limiting adhesion site growth with nanopatterned surfaces can somewhat reduce the ability for a cell to spread across a surface. Extremely small nanopatterns and larger patterns with large interadhesion site spacing both somewhat impair cell spreading compared to cells on high FN surface density control surfaces. The impairment can be lifted by providing nanopatterned surfaces with larger sizes and closer spacing as demonstrated in cells on the 1500M surfaces.

The projected cell spreading area was measured at 24 hour intervals for 3 days for cells cultured on Au control surfaces displaying varying surface concentrations of FN (2Au, 10Au, and 25Au surfaces), for a glass control (10G), and for four nanopatterned surfaces (0300B, 0300M, 1500B, and 1500M), see Table 4 for surface properties. Cell spreading was not to a large extent influenced by either FN surface density or underlying surface chemistry as cells on all four control surfaces displayed similar levels of spreading. Cells cultured on the smallest nanopatterns with an average size of 92 nm and an interpattern spacing of 300 nm spread significantly less than cells on high FN surface density controls, 10Au and 25Au surfaces, and less than cells on nanopatterned surfaces with the largest nanopatterns, 1500M surfaces, that display FN nanoislands with an average size of 405 nm and a corresponding spacing of 885 nm (Figure 8.1). Cells

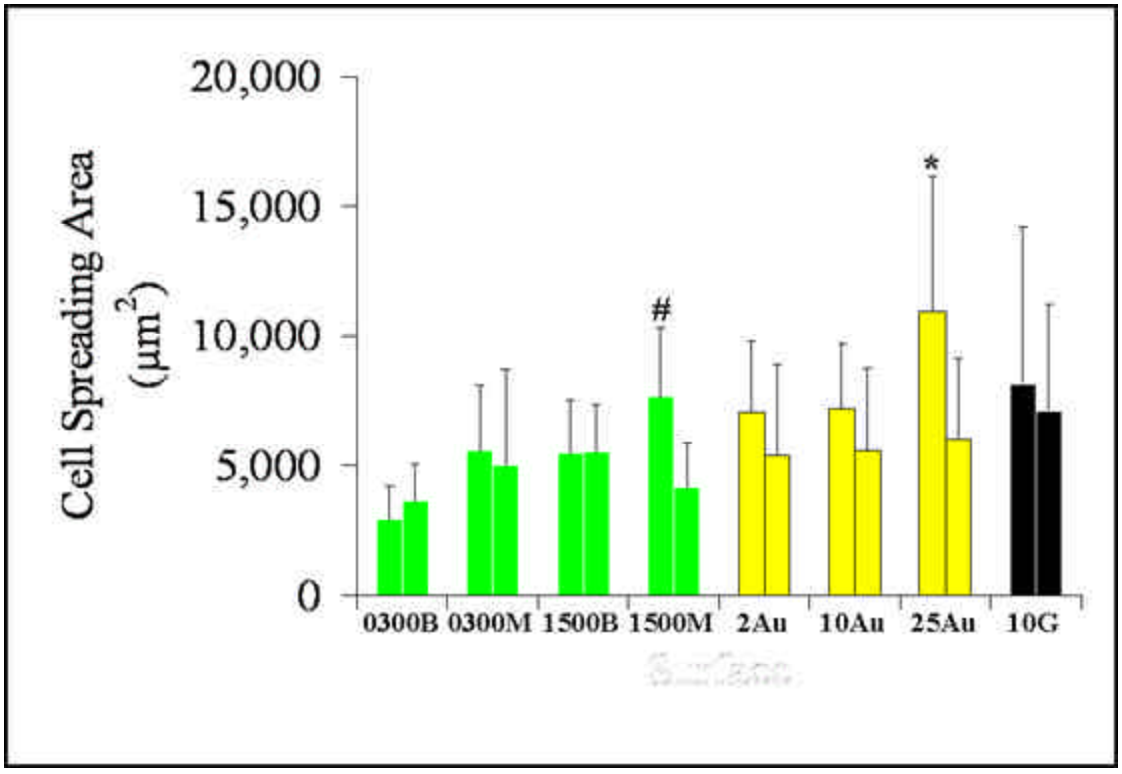

Figure 8.1: Cell Spreading Area: The cell spreading area was measured for cells on four nanopatterned surfaces (green), three gold controls (yellow), and one glass control (black) after 24 and 72 hours in culture. * Indicates significantly more spreading than 0300B, 0300M, 1500B surfaces ($p < 0.012$). # Indicates significantly more spreading than 0300B surfaces ($p = 0.014$).

cultured on nanopatterned surfaces with similar nanoisland sizes to the 0300B surfaces but with a closer nanopattern spacing of 177 nm or cells on nanopatterned surfaces with larger FN nanoislands 222 nm in size separated by 1.5 μm showed intermediate levels of spreading that were between the values measured for cells on 0300B and 1500M surfaces but were not statistically significantly different from the cells on these surfaces (Figure 8.1). Furthermore, cells cultured on nanopatterned surfaces with the

largest FN nanoislands 405 nm in size with an interadhesion site spacing of 885 nm spread as well as cells on high FN surface density control surfaces (Figure 8.1).

These observed differences in cell spreading can be correlated with measured differences in both actin stress fiber formation and in the formation of large adhesion sites. Figure 6.1 shows that stress fiber formation in cells cultured on nanopatterned surfaces follows a similar trend to cell spreading as previously reported by others.[217] As discussed in Chapter 6, cells cultured on 0300B surfaces show an impaired ability to create dense actin stress fiber cytoskeletal networks. This implies that limiting adhesion maturation to very small adhesions impairs adhesive linkage to actin stress fibers. This small adhesion size impairment of stress fiber linkage can be overcome if the nanopatterns are spaced close together or if the adhesion site size is increased. These findings imply that the formation of well-defined actin stress fiber cytoskeletal networks may be helpful but not necessary for cell spreading.

Further insight into why cells on small nanopatterns spread less was obtained by analyzing the relations between cell spreading, average adhesion site size, and the number of large focal adhesions formed. Examination of these trends shows that cells with larger average adhesion sites display an increased propensity to spread more (Figure 8.2 A). Cells cultured on the smallest nanopatterned surfaces displaying FN nanoislands less than 10,000 nm^2 in size displayed reduced spreading compared to cells cultured on both larger patterns and controls that both have larger average adhesion site sizes (Figure 8.2 A). This same trend holds after 72 hours but is less pronounced (Figure 8.2 B). Due to the resolution limitations of light microscopy the exact values of adhesion site size in cells on the small nanopatterned surfaces can not be determined but since the average adhesion site size is reflective of the number of small and large

adhesions formed and since only larger focal adhesions connect to actin stress fibers and allow the production of traction forces needed for cells to spread, cell spreading was plotted as a function of large adhesion formation.

This relationship proved more useful in explaining why cells on small nanopatterns display decreased spreading. After 24 hours cells on the 0300B surfaces create an average of 20 large focal adhesions, while cells on larger nanopatterned surfaces create around 50 large adhesions and cells on control surfaces with the most-dense packing of FN, 25Au surfaces, create about 100 large adhesions per cell (Figure 8.2 C). Observation of the trend shows that the formation of large adhesions is almost directly proportional to cell spreading (Figure 8.2 C). This trend also holds true after 3 days in culture. Comparing the trend after 1 day to that after 3 days shows why cells on all of the controls and 1500M nanopatterned surfaces show a decrease in the extent of spreading (Figure 8.1), they all show a decrease in the total number of large adhesions formed (Figure 8.2 D). Furthermore, cells on 0300B surfaces only make approximately 5 large adhesions per cell and show the least amount of spreading compared to cells on glass surfaces that maintain an average of 53 adhesions per cell with the highest levels of spreading (Figure 8.2 D). The results imply that reductions in cell spreading as induced by culturing cells on very small nanopatterns is a consequence of the underlying surface chemistry and relates impaired abilities in spreading to decreased large adhesion formation that is directly linked to decreased actin stress fiber cytoskeletal formation. However, it is surprising that cells on nanopatterned surfaces maintain their spread area after 3 days in culture when almost no large adhesions are present in cells on these surfaces. This implies that the formation of large adhesions is

necessary to achieve large spread areas but that the small adhesions independent of large adhesions can maintain spreading once it is achieved.

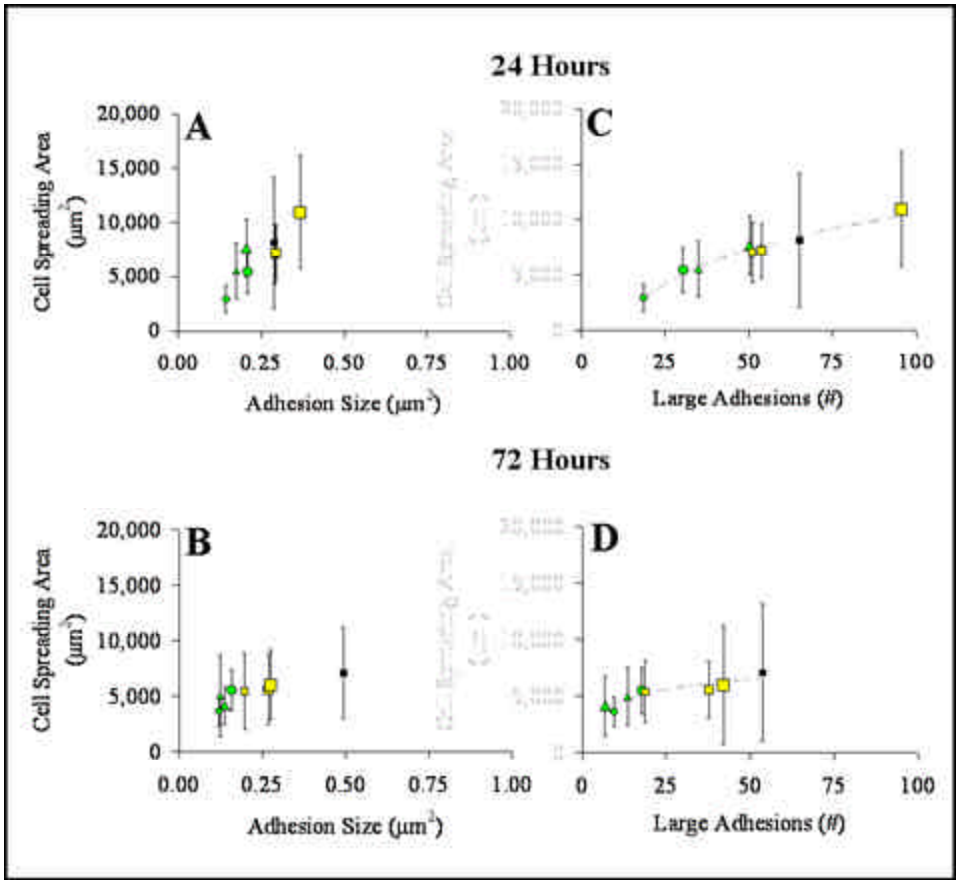

Figure 8.2: Cell Spreading Related to Average Adhesion Site Size and the Number of Large Adhesions Formed: The cell spreading area was measured for cells on 0300B (small green dot), 0300M (small green triangle), 1500B (large green dot), 1500M (large green triangle), 2Au (smallest yellow square), 10Au (medium sized yellow square), 25Au (large yellow square), and 10G (black square) surfaces after 24 and 72 hours in culture. (A) A trend of increased cell spreading with larger average adhesion site size was discovered after 24 hours that does not hold as well after 72 hours (B). A better correlation was seen between cell spreading and the number of large adhesions formed that held true after both 24 hours (C) and 72 hours (D).

8.4 Discussion

The results show that cell spreading is directly related to the formation of large focal adhesions and to the formation of actin stress fiber linked smaller adhesions. The larger adhesion sites have the ability to create traction forces through their association with actin stress fibers. The creation of traction force is necessary for a cell to be able to grab the surface, create force, and then use this force to spread itself. While cells on small nanopatterned surfaces create an increased number of small adhesions they show impaired ability to create many large adhesions compared to cells on higher FN density control surfaces. The creation of increased numbers of small adhesions by cells on nanopatterned surfaces allows for cells on these surfaces to push against the cell membrane via focal complex interactions with F-actin but since the adhesions never fully mature they lack the ability to create the large traction forces needed for cell spreading. As the adhesion site size created by cells on larger nanopatterned, 1500M surfaces, grows in size and allows for connection to actin stress fibers, then the cells behave similar to those on control surfaces. The importance of being able to bundle small F-actin fibers has shown to be important for progression of adhesive states through the maturation process.[174] Furthermore, restrictions on adhesion site size regulation of actin stress fiber formation in cells on 0300B surfaces can be overcome if the interadhesion site spacing is reduced to allow for the actin from individual small adhesions to be linked into larger stress fibers such as what occurs in cells cultured on 0300M surfaces.

Three separate regimes of spreading were discovered. The first regime consists of cells on smaller further spaced nanopatterns that do not form large adhesions. The second regime consists of cells on both small nanopatterns with tight packing or on

larger nanopatterns spaced fairly far apart. Cells cultured on small nanopatterns with tight spacing still show suppressed ability to form large adhesions but can form adhesions in close enough proximity to each other for their actin to be bundled into stress fibers and thereby lead to increased spreading. Cells on larger patterns with the largest spacing between adhesions can form stress fibers that link directly to the adhesion sites, yet never form large classical focal adhesions as seen in cells on control surfaces. The fourth regime is composed of cells on 1500M surfaces. These surfaces display larger FN nanoislands with tighter packing and while cells cultured on these surfaces show suppressed ability to form larger adhesions that are seen in cells on high FN surface density controls, they do show the ability to form actin stress fiber networks with a similar number and density of fibers as cells on controls thereby allowing them to spread as well as cells cultured on high FN surface density control surfaces. The relationships between large adhesion formation, stress fiber creation and linkage, and cell spreading all interplay with each other. [217] However, it is still surprising that cells on 0300B surfaces can spread at all. This implies that the formation of classical focal adhesions and extremely large actin stress fibers as seen in cells on control surfaces may not be that important for cell spreading. Cells still display the ability to spread on a surface even when the adhesion sites are very small and the actin cytoskeleton is not extremely dense.

8.5 Conclusion

These studies have provided insight into the roles of focal adhesion and stress fiber formation in cell spreading. The creation of increased numbers of small adhesions provides the ability for cells to attach to surfaces but the lack of large adhesion sites or

actin stress fibers results in decreased cell spreading. For a cell to properly spread it must be able to use small focal complexes to push against the cell membrane and to create large actin stress fiber classical focal adhesions to create traction force for spreading. Inhibition of either stress fiber formation or large adhesion site formation can result in significantly reduced cell spreading.

Chapter 9

Cell Motility Studies

9.1 Introduction

Cell motility is a complex process involving the synergistic interplay between a number of cellular components including microtubules, F-actin, actin stress fibers, myosin motors, focal complexes, and focal adhesions to name a few. [45,67,168,173,174,218-224] The complex and not fully understood interplay between these components dictates the ability for a cell to move and how fast. The motility process involves the formation of small focal complexes at the cell periphery of advancing lamellapodia. These small adhesions interact with F-actin to act as docking point so that the actin can push against the cell membrane and extend the cell in the direction of movement. [45,219,220] Some of these small complexes link to actin stress fibers via various adaptor proteins and mature into focal adhesions. [16,174] As force is applied to the focal adhesion through actomyosin contraction, a traction force is created at the adhesion-surface interface. [31,40,125,225,226] As the cell continues moving forward these large cytoskeletal associated focal adhesions stay stationary and eventually end up at the rear of the cell where they are disassembled by a not fully understood mechanism, although FAK in known to be important in this process. [32,227,228] This event results in cell polarity with respect to adhesion maturation. Newer focal complexes are continuously being formed at the leading edge while older focal adhesions move to the rear of the cell. [228]

While still not fully understood, a number of models concerning cell motility exist and two of them will be discussed here. One stochastic model implies that younger focal adhesions on the leading edge side of the cell provide traction force for the cell to

move forward while the older focal adhesions at the rear provide a drag force hindering motility. [229] If these forces are balanced, then the cell moves randomly around a central location and exhibits motility similar to Brownian motion known as a random walk. If an imbalance in adhesive forces is created, then the cell can proceed to crawl in a given direction. A second model of motility implies that that the elasticity of F-actin at the leading edge is used to ratchet the cell membrane forward thereby inducing a gliding style of motion. [230,231] The stochastic model applies to a moving body while the second to lamellapodia formation, ruffling, and leading edge advancement. Both models make valid insights into cell motility and the combination the two would more accurately model the actual processes that occur during motility.

Cells respond to a number of factors that can change their state of motility. The binding of soluble factors such as VEGF can induce significant increases in cell motility. [232,233] Surface characteristics such as protein concentration and surface elasticity induce biphasic responses in cells with respect to their speed. [124-126,234,235] Cells adhering to surfaces presenting very low or very high levels of protein are stationary, while cells on surfaces presenting intermediate levels of protein display higher motility than cells in the other two cases. [234] The same holds true for elasticity. If surfaces are too elastic or rigid then cells are relatively stationary whereas if the surfaces have intermediate levels of elasticity then cells are more motile and have higher speeds. [125] The finding of biphasic responses in cells on both elastic and protein adsorbed surfaces implies that the generation of too much or too little force impairs motility while the generation of intermediate levels of force promotes increased motility. Both cases can also be linked to adhesion site formation. Cells on rigid surfaces and on surfaces with high densities of ECM allow for the production of large focal adhesions, while cells on

soft surfaces or surfaces with very low ECM concentrations induce the formation of extremely small adhesions.[40,126,223] Large adhesions, if evenly distributed along the peripheral rim of the cell, induce a more stationary state of motility where the cell is pulled back and forth by opposing actomyosin forces all directed toward the cell center. If cells can only form a few large adhesions or none at all then an imbalance in forces can be created and higher cell motility induced.

While these models can accurately predict cell motility based on surface properties they do not include biochemical differences between different types of adhesions. It has been shown that FAK-null cells form extremely large adhesions and do not move,[227] that FAK is over-expressed in some cancers,[236] and that FAK is important in regulating cytoskeletal linkage to adhesion sites.[80,237] This implies that FAK is an important regulator of cell motility. If it is not present, then cells can not disassemble their adhesions from the surface, if it is over-expressed then the adhesion disassembly rate is very high leading to extremely motile cells such as cancerous cells, and finally, if it is expressed but phosphorylated to a different degree or on different residues, then it can affect cytoskeletal linkage. This implies that manipulating adhesion maturation and not allowing cells to form large stress fiber linked adhesions may influence cell motility. While it is known that actin is important for the cell motility process there is some confusion on which subsets of actin organization are important. The current school of thought is that both F-actin and actin stress fibers are needed for motility. This may not be entirely true. While F-actin is definitely needed for membrane protrusion, the formation of large stress fibers may actually impede or slow down migration in some cases. Evidence for this is supported by findings in cancer cells. Cancer cells over-expressing FAK are highly motile.[236] These overly motile cells can be slowed down by

enhancing cytoskeletal linkage of adhesion sites through activation of tensin genes, an adaptor protein that increases cytoskeletal linkage to adhesions sites.[238] This implies that cytoskeletal linkage can actually induce lower motility in inherently fast cells.

Towards this idea, the motility of cells seeded on nanopatterned surfaces was investigated. The results imply that limiting adhesion site growth to very small adhesions may induce chemically different smaller adhesion sites than large mature adhesions created by cells on high density ECM surfaces. In fact, the most motile cells are those that show very little linkage to the cytoskeleton, implying that the formation of classical focal adhesions that link to stress fibers may not play as large of a role in motility as previously thought.

9.2 Materials and Methods

9.2.1 Cell and Reagents

See Section 4.2.5, only non-pooled HUVECs were used for these experiments.

9.2.2 Nanopattern Fabrication and Functionalization

See Sections 3.2.1 and 4.2.2 for the fabrication and functionalization methods respectively.

9.2.3 Cell Motility Studies

HUVECs were sparsely seeded at approximately 7 – 10 cells/mm^2 to lower the probability of cell-cell contact yet still have enough cells for statistically sound studies. After 24 hours in culture the cells were taken to a Leica DM IRB (Leica Microsystems, Wetzlar Germany) inverted microscope equipped with a home-built incubator. The

incubator maintained the atmosphere at 37 °C and 5 % CO_2 during filming. Time-lapse phase-contrast microscopy was used to capture 15X magnification images of cells at 60 second intervals for 2 hours using a Cooke Sensicam CCD camera (The Cooke Corporation, Romulus, Michigan) operated by Camware software (PCO Imaging, Kelheim, Germany). The time-lapse movies were recorded for 2 hours every 24 hours for 3 days. The cell paths were manually tracked using a particle tracking plug-in in ImageJ (NIH, Bethesda, Maryland) created by Fabrice Cordelieres (Institut Curie, Orsay, France). The measured cell positions, in x, y coordinates, were processed to measure cell speed with an algorithm designed and written by Ted Gaubert. The algorithm corrected for any sample drift during filming and sub-pixel errors during tracking. A minimum of 8 cells per surface were analyzed at each time point.

9.2.4 Statistical Analysis

See Section 5.2.5 for normality tests. The data sets passed the normality tests and were therefore analyzed with ANOVA and post hoc Tukey tests.

9.3 Results

The results of the analysis indicate that limiting adhesion site growth to small submicron adhesions induces increased motility compared to cells on control surfaces. Furthermore, the extent of motility can be significantly reduced by slightly increasing the adhesion site size using larger, but still submicron, nanopatterns. Nanopattern spacing and density seem to have little to no influence on this process.

Figure 9.1 shows cell migration paths over a one hour time period as tracked from the time-lapse movies. For the most part, cells on all of the control surfaces display random movement often hovering around a central location, although occasionally

some cells do show more straight-line motion. FN surface density did not have a significant influence on motility in the studies performed here, although it is known that cells display a biphasic response to ECM surface concentration, exhibiting higher motility at intermediate levels of ECM surface concentration. [234] This biphasic behavior was most likely not induced here due to the FN surface concentrations tested. The 2Au, 10Au, and 25Au surfaces display surface concentrations of 537, 1,882, and 2,474 FN/μm^2 respectively. Examination of the FN surface density calibration curve in Figure 4.2 A shows that the intermediate levels of FN surface concentration were not achieved with the surfaces chosen for these experiments and that exposing surfaces to 5 μg/mL of FN would result in a FN surface concentration of 1,300 FN/μm^2 and most likely induce higher states of motility as previously reported. [234] Regardless, the goal of the study presented here was not to investigate FN surface concentration but to explore how varying adhesion site size can influence cell motility on surfaces presenting FN densities as low as 41 FN/μm^2.

A closer analysis of the cell paths in Figure 9.1 shows that underlying surface chemistry can also influence cell motility. Visual inspection of the tracks in Figure 9.1 shows that cells on homogenously coated glass surfaces tend to move further distances during the same one hour time period than cells on gold control surfaces. This is reflected in the measured cell speed in Figure 9.3. Cells on glass surfaces are significantly faster than cells seeded on Au controls with a speed of approximately 0.64 μm/min, similar to previously published results, [235] while cells on Au surfaces move slower at ~ 0.36 μm/min. This difference in motility is somewhat surprising. Cells are known to attach to FN on glass surfaces primarily using $\alpha_5\beta_1$ integrins while cells on Au surfaces typically use $\alpha_v\beta_3$ integrins. [115,117,118,121] These differences in integrin usage may be

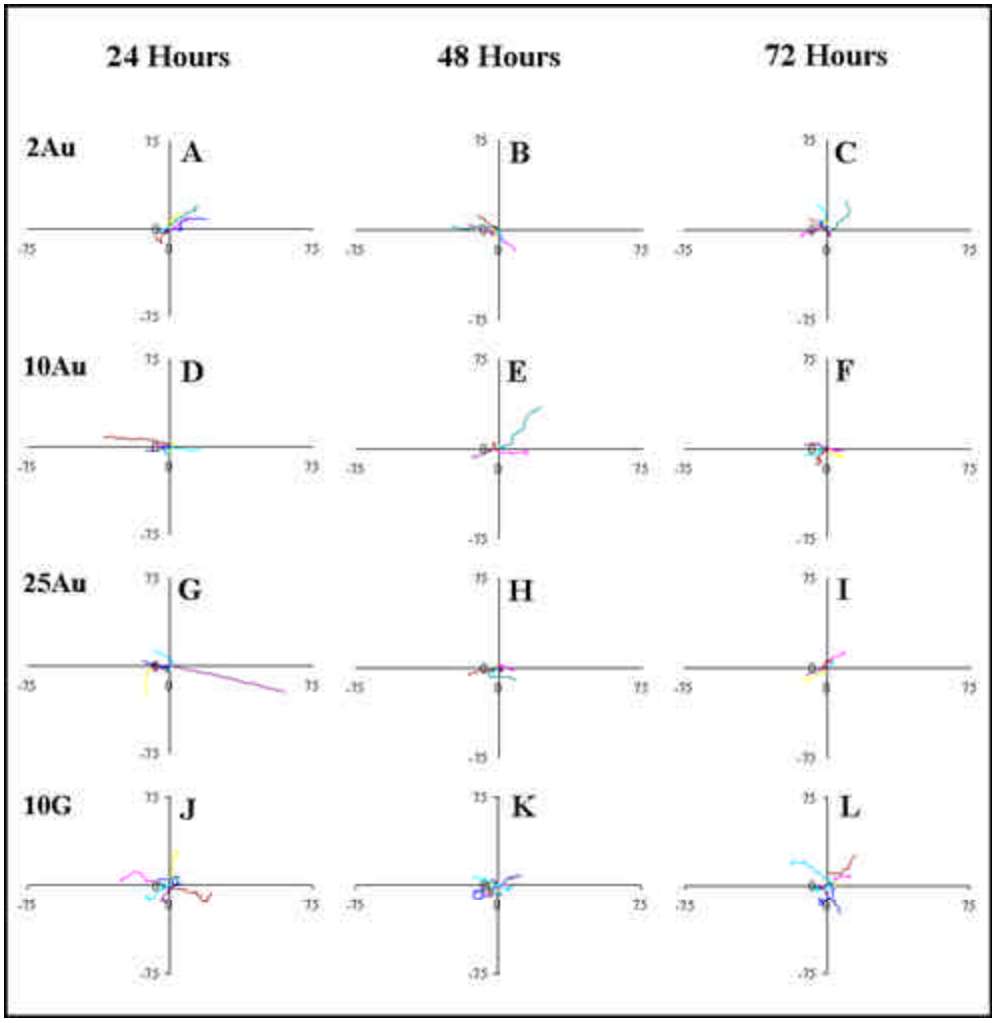

Figure 9.1: Cell Migration Paths of Cells on Au and Glass Control Surfaces: Cell paths over a 1 hour time scale as measured from time-lapse phase-contrast images for cells on (A-C) 2Au, (D-F) 10Au, (G-I) 25Au, and (J-L) 10G surfaces after (left column) 24 hours, (middle column) 48 hours, and (right column) 72 hours in culture. Cells on glass travel slightly faster than cells on all Au control surfaces. The x-axis extends 75 μm from the origin in each direction.

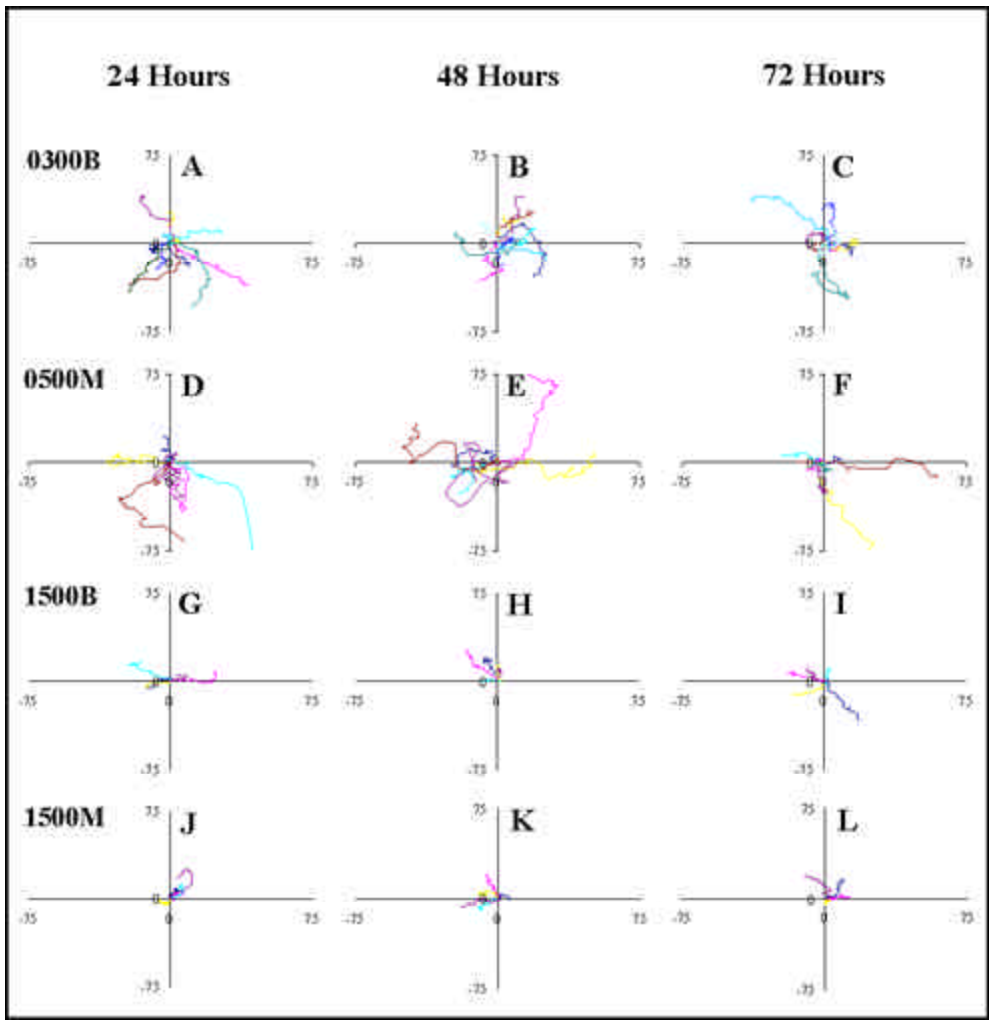

Figure 9.2: Cell Migration Paths of Cells on Nanopatterned Surfaces: Cell paths over a 1 hour time period as measured from time-lapse phase-contrast images for cells on (A-C) 0300B, (D-F) 0500M, (G-I) 1500B, and (J-L) 1500M surfaces after (left column) 24 hours, (middle column) 48 hours, and (right column) 72 hours in culture. Cells on small nanopatterns, 0300B and 0500M surfaces, travel faster and with higher persistence than cells on larger, 1500M and 1500B, nanopatterns. The x-axis extends 75 µm from the origin in each direction.

reflected in the differences in the motility of the cells although no literature currently exists that relates differences in integrin usage to differences in cell motility.

Figure 9.2 shows cell motility tracks for cells cultured on nanopatterned surfaces. Visual inspection of the tracks shows two findings. First, that cells on nanopatterned surfaces move further over a one hour time period compared to the cells on Au control surfaces shown in Figure 9.1 and that cells on smaller nanopatterned surfaces move further than cells on larger nanopatterned surfaces in the same time frame. Cells cultured on 0300B and 0500M surfaces, top two rows in Figure 9.2, have much longer tracks than cells on larger 1500B and 1500M surfaces. These differences in path length are reflected in the cell speed, Figure 9.3. Cells on 0300B and 0500M surfaces, both displaying adhesion sites less than 160 nm in size have an average speed of 1.05 μm/min and maintain this speed for at least 2 days in culture, the cells on 0500M surfaces show a reduction to 0.63 μm/min at 3days while cells on 0300B surfaces maintain high speeds. These values are significantly higher (Figure 9.3) than cells on all controls and than cells on surfaces with larger nanopatterns indicating that adhesion site size is influential in cell motility.

The increased motility of cells on nanopatterned surfaces can be significantly reduced by slightly increasing the pattern size (Figure 9.3). Cells on 1500B and 1500M surfaces show shorter path lengths (Figure 9.2) over the same one hour time period and significantly reduced cell motility, with a value of 0.6 μm/min, (Figure 9.3) compared to cells on smaller nanopatterned surfaces. This indicates that adhesion site size is a major factor in controlling cell speed and is independent of FN surface density or interadhesion site spacing influences. Since both the 0300B and 1500B nanopatterned surfaces have the same FN surface density of 41 FN/μm^2 and the 0500M and 1500M at

217 FN/μm^2 and since cells on both the 0300B and 0500M surfaces display increased motility compared to their larger counterparts, then overall surface density must not play an important role in the observed increased motility. The finding that cells on smaller nanopatterned surfaces have increased values of motility hints that smaller adhesions somehow lead to faster cells. There are two basic ways that this could happen.

First, by limiting adhesion site maturation it could be possible that the molecular composition of the small adhesions is different than the adhesions formed by cells on larger nanopatterns and Au control surfaces. It is known that small focal complexes have fewer and different molecular components than larger focal adhesions. Since FAK is known to play a major role in cell motility, as it is needed for adhesion site disassembly and in cytoskeletal linkage of adhesions to stress fibers, it may be implicated in the observed adhesion size changes in motility. Since cells on smaller nanopatterned surfaces also exhibit differences in cytoskeletal densities compared to cells on larger nanopatterns and control surfaces, this may also indicate that FAK is somehow playing a role in the observed increased motility. So what role would FAK play in inducing increased motility? Since FAK is known to be important for the turnover of adhesions, cells on small nanopatterns may have a higher turn over rate of adhesion sites that most often do not reach higher maturation levels. This decreased propensity to form large mature adhesions may reduce the amount of drag force that these cells experience. The benefits of not forming large actin linked focal adhesions are that they would not have to be disassembled and if not formed, do not result in drag force.

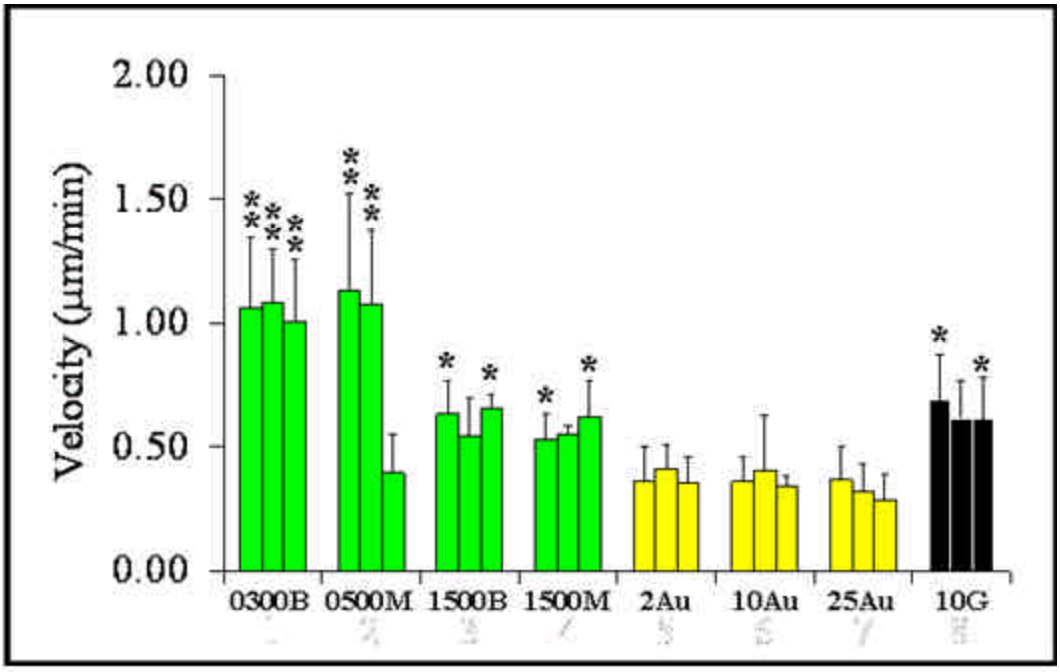

Figure 9.3: Measured Cell Velocities on Nanopatterned and Control Surfaces: Cells were imaged for 2hours with time-lapse photography every 24 hours for 3days. A minimum of 8 cells per surface were tracked and their velocities measured. ** Indicates significantly faster cells than cells on 1500B, 1500M, all Au controls, and 10G surfaces ($p < 0.05$). *Indicates significantly faster cells than cells on all Au controls ($p < 0.05$).

Toward this idea the distributions of both large and small adhesions sites in the leading and trailing edges were measured for very fast cells on 0300B surfaces, somewhat slower cells on 1500M surfaces, and slow cells on 10Au surfaces. The data indicates that cells on 0300B surfaces have an asymmetry in the distribution of large adhesions, while cells on 1500M and 10Au surfaces do not. Figure 9.4 shows the distributions of the number of small and large adhesions as a function of their normalized distance between the cell center and cell periphery. A value of 0 indicates that the adhesions are near the cell centroid, most often indicating the nucleus; a value

of 1 indicates that the adhesions are at the periphery of the leading edge, and a value of -1 indicates that the adhesions are at the cell periphery of the trailing edge. Analysis of the data shows that the small adhesions formed by cells on all surfaces follow similar trends of increased numbers of adhesions as you move from the cell center to the cell periphery but that the absolute number of adhesions formed is different. Cells on the 0300B surfaces have the highest number of small adhesions followed by cells on 1500M surfaces and then cells on 10Au surfaces with the lowest number of small adhesions.

Analysis of the large adhesion distributions gives some possible explanations of why cells on smaller nanopatterned surfaces are faster. Cells on 10Au surfaces form large focal adhesions as demonstrated in Chapter 5. Figure 9.4 shows that these cells display a symmetry in the distribution of these large adhesions with respect to their location toward the leading and trailing edge. Assuming that these large adhesions are actin linked focal adhesions and not fibrillar adhesions, a safe assumption, since cells on these surfaces form almost no fibrillar adhesions as demonstrated in Chapter 8, then the distribution implies that there is a balance in forces. This balance lies in how the large actin linked focal adhesions apply traction force to the surfaces. The focal adhesions will all apply forces with vectors pointing toward the cell center. This balanced force distribution results in a relatively stationary cell that migrates around a central point. In contrast cells on 0300B surfaces do not form large mature focal adhesions but do display the ability to form fibrillar adhesions as discussed in Chapters 5 and 8 respectively. This finding entails two influences on motility. Since no large classical adhesions that tie into actin fibers are formed then there is relatively little drag force imposed on these cells and they do not have to disassemble any large adhesions at the trailing edge. While this holds true for large focal adhesions there is no current

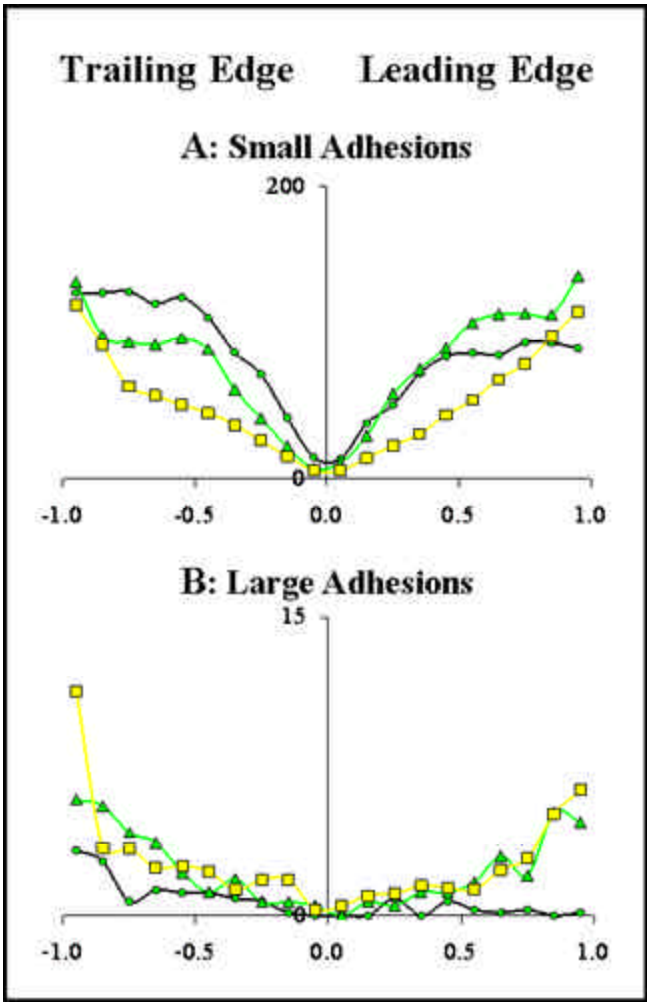

Figure 9.4: Measured Adhesion Site Distributions for Cells on 0300B, 1500M, and 10Au surfaces: The number of small (< 1 μm^2) and large (> 1 μm^2) adhesion sites were measured, their location normalized with respect to their ratiometric distance from the cell center to the cell periphery, and plotted as a function of their normalized location in either the leading (positive x-axis) or trailing edge (negative x-axis) for cells on 0300B (green dots), 1500M (green triangles), and 10Au (yellow boxes) surfaces after 24 hours in culture.

understanding of the forces that fibrillar adhesions exert on surfaces. Whether fibrillar adhesions apply forces that promote or hinder motility is currently unknown. As demonstrated in Chapter 8, it seems that the stretched fibrils must be pinned to the surface or other FN molecules at regular intervals. This pinning process would also involve the disassembly of adhesion sites for the cell to release the FN. Whether this would result in more or less drag compared to focal adhesion is not known. To recapitulate, since there are no large focal adhesions to disassemble then there is relatively little drag force imposed on these cells allowing them to move more quickly.

A similar idea can be applied to the observed differences in speed between cells on the 1500M and 10Au surfaces. In this case rather than it being a function of fibrillar versus focal adhesion formation or differences in large adhesion symmetry, it is a function of differences in drag force due to differences in the contact area of large adhesions between cells on the two surfaces. Since cells on 10Au surfaces form a higher number of larger adhesions at their trailing edge they have more drag force to overcome than cells on 1500M surfaces that form a lower number of large adhesion sites. Since the stress applied at adhesion sites is constant then the total force that cells have to overcome to move is less for cells on 1500M surfaces since they have less total contact area.

9.4 Discussion

The motility studies have shown that limiting the growth of adhesions to small nanometer sized focal complexes in cells can lead to significant increases in cell motility. The observed increase in speed in these cells is dependent on adhesion site size and not nanopattern density or spacing and cells can be induced to slow down by slightly

increasing their adhesion site size. This modulation of cell motility based on adhesion site size is a new discovery and has not been reported in literature, although reports concerning biphasic motility of cells on surfaces with varying elasticity hint to this idea. [40,125] The observed increase in cell motility may be the interplay of a number of factors. One factor is that fast cells on small nanopatterns do not form large actin stress fiber linked focal adhesions and therefore do not experience drag force from these adhesions as they move. Instead, they form many small focal complexes and what appear to be fibrillar adhesions at their trailing edge, although no absolute proof for this exists at this time. The directionality of forces created by fibrillar adhesions is currently unknown. It may be that the forces created by these adhesions do not influence motility. If the FN does not reach a fully stretched confirmation before being connected to other FN fibrils then the force exerted to the fibrillar adhesions would not result in either forward traction or drag force. While this may explain some of the observed differences in this study it is purely hypothetical and no evidence currently exists to support these ideas.

Another explanation of why cells are faster on nanopatterned surfaces may stem from differences in the molecular composition of the small adhesions formed on small nanopatterned surfaces compared to those formed on larger nanopatterns and controls. As discussed in Chapter 6, the actin fiber network properties for cells on these surfaces are different. Cells on the 0300B surfaces do not show the ability to form large actin stress fiber linked adhesions like cells on control surfaces, while cells on larger nanopatterns form a smaller version of large classical adhesions, showing submicron sized adhesions that can still link to smaller stress fibers as demonstrated in Chapter 6. Relating these changes in cytoskeletal properties to observed differences in motility

implies that small adhesions on the 0300B surfaces do not contain all of the necessary machinery to link to large actin stress fibers and hint to either a less complex molecular composition or to differences in FAK expression or phosphorylation. [227,236,239] Furthermore, the current understanding of cell motility usually includes the formation of large stress fiber linked adhesions that apply traction force to the surface so that the cell can move. This may not be entirely true. The work presented here shows that cells with very low density actin stress fibers move faster than cells with well defined stress fiber networks. Support for this finding comes from studies with cancer cells that were able to demonstrate that normal levels of motility could be re-established by inducing the up-regulation of tensin production. [238] Tensin is an adaptor protein that acts to link adhesion sites to cytoskeletal components in the later stages of adhesion maturation. [16] This finding implies that cytoskeletal linkage can indeed inhibit cell motility.

9.5 Conclusions

To summarize, cells on nanopatterned surfaces display more motile states as indicated by higher measured speeds than cells on Au or glass control surfaces. This increased motility can be influenced by changing the nanopattern size, but nanopattern density and spacing show no influence on cell motility for the pattern type used here. The increased motility of cells on very small nanopatterns could be due to differences in molecular composition, cytoskeletal linkage, or to differences in large-adhesion asymmetry that result in lower levels of drag force. Regardless of the exact causes, it is extremely interesting that motility can be modulated by simply tuning the adhesion site size. This finding may be applicable in creating surfaces with desired cellular responses and useful for creating surfaces that induce increased EC infiltration. This ability to make

cells more quickly crawl on a surface may be helpful for linings of stents or vascular grafts and in inducing angiogenesis in artificial tissue constructs.

Chapter 10

Cell Proliferation Studies

10.1 Introduction

Cellular proliferation is a highly regulated process and changes in proliferation rates can be induced by soluble factor finding such as VEGF, [233,240,241] changes in ECM composition such as those that occur at wound sites, [4,242] and through the formation of cell-cell contacts. [87,88] ECs display a dose-dependent response in proliferation as a function of FN surface density showing increased levels of proliferation with increased FN surface concentrations. [102] ECs have also shown impaired ability to adhere to surfaces presenting low levels of FN. [102] While it is known that ECM compositional changes can influence adhesion mediated proliferative signaling responses, the exact underlying mechanisms have yet to be determined. FAK has been proven to be an important regulator of adhesion mediated proliferation and can both activate and suppress growth. [50] Further evidence of FAKs role in governing cellular proliferation comes from the finding that it is often over-expressed in cancer cells. [79,236] To gain a better understanding of which surface parameters influence initial cell attachment and long term proliferation, cells were cultured on homogenously FN coated control surfaces with varying FN surface densities and compared to cells cultured on nanopatterns with varying surface density, size, and spacing. This chapter discusses the results of the proliferation experiments and demonstrates that local ligand density and adhesion site spacing have more influence over cell attachment and proliferation than overall surface density as previously thought.

10.2 Materials and Methods

10.2.1 Cells and Reagents

See Section 4.2.5, only non-pooled HUVECs were used for these experiments.

10.2.2 Nanopattern Fabrication and Functionalization

See Sections 3.2.1 and 4.2.2 for the fabrication and functionalization methods respectively.

10.2.3 Cell Proliferation Studies

HUVECs were sparsely seeded at approximately 20 cells/mm^2. Twenty 15X magnification phase-contrast images were collected 4 hours after initial seeding and at 24 hour time intervals for 3 days for each sample, three independent samples were used for each surface. Cell densities (number of cells per surface area) were measured over a 21 mm^2 area. The measured density values were normalized for all samples by dividing the number of cells at each time point by the average number of cells attached after 4 hours. The normalized data was scaled by a factor of 20, the average number of cells adhered to most surfaces after 4 hours in culture, so that visual comparisons between the raw and normalized data could more easily be made. Cell proliferation assays, such as BrdU DNA synthesis assays or fluorescent-activated cell sorting (FACS), are a more specific proliferation test, but could lead to misleading results due to incomplete nanopattern coverage in some areas of the sample.

10.2.4 Statistical Analysis

The raw measured cell densities were used to evaluate initial cell attachment after 4 hours in culture. The normalized and scaled cell densities were compared at 24 hour time points for 3 days. Since all of the analyzed data contained normal distributions and equal variances as determined by the tests described in Section 5.2.5, ANOVA with a post hoc Tukey test was implemented with a significance level of 0.05 to determine any statistically significant differences in cell behavior.

10.3 Results

10.3.1 Initial Cell Attachment at 4 Hours

ECs display a dose-dependent response to FN surface density and it has been shown that both initial cell attachment and long term proliferation are greatly reduced in ECs cultured on surfaces with FN concentrations below 550 FN/μm. [6,102] This finding was validated and elaborated upon in the studies presented here. Figure 10.1 A displays raw cell density measurements as a function of increased FN surface density for cells on both nanopatterned (green) and thiolated Au control surfaces (yellow). Focusing just on the control surfaces in Figure 10.1 A, it can be seen that statistically fewer cells, 11 cells/20 mm^2, attach to low density FN coated control surfaces with 537 FN/μm^2 compared to an average of 20 cells/20 mm^2 on higher density FN surfaces with concentrations equal to or greater than 1,882 FN/μm^2.

While the previously reported relationships between initial cell attachment, proliferation, and FN surface concentration hold true, new insight into what governs initial cell attachment to surfaces was determined by comparing the density of cells adhered to low FN density control surfaces to the number of cells on nanopatterned

surfaces after 4 hours in culture. The nanopatterned surfaces display much lower FN densities, 41 and 217 FN/μm^2 for B- and M-type surfaces respectively, yet statistically more cells initially adhere to these surfaces compared to control surfaces with higher FN densities of 537 FN/μm^2 (Figure 10.1 A). In fact, the same average density of cells, 20 cells/20 mm^2, that was measured on the higher FN surface density controls was measured on the nanopatterned surfaces. This finding implies that even extremely low levels of FN can support initial cell attachment as long as the cell can cluster integrins to form well-defined adhesion sites. Even though the nanopatterned surfaces display much lower global surface densities of FN, the way that it is presented for cell attachment is quite different compared to homogenously coated control surfaces. Low FN surface density control surfaces, 2Au, are homogenously coated with FN and most likely display irregularly distributed and spaced FN molecules while the nanopatterned surfaces display well-organized nanoscale sites of densely packed FN. The fact that cells initially adhere to and spread on these surfaces shows that local ligand density and ability to quickly cluster integrins to form well-defined adhesions is more important for initial cell attachment than overall ligand density. This idea is supported by existing literature showing that the ability to cluster integrins is more influential than the overall ligand surface density for supporting initial cell attachment, although it has not been demonstrated on the small size scale as presented here. [99]

10.3.2 FN Surface Density Influence on EC Proliferation

As with initial cell attachment, ECs also display dose-dependent increases in proliferation with increasing FN surface concentrations. [102] Focusing only on the control

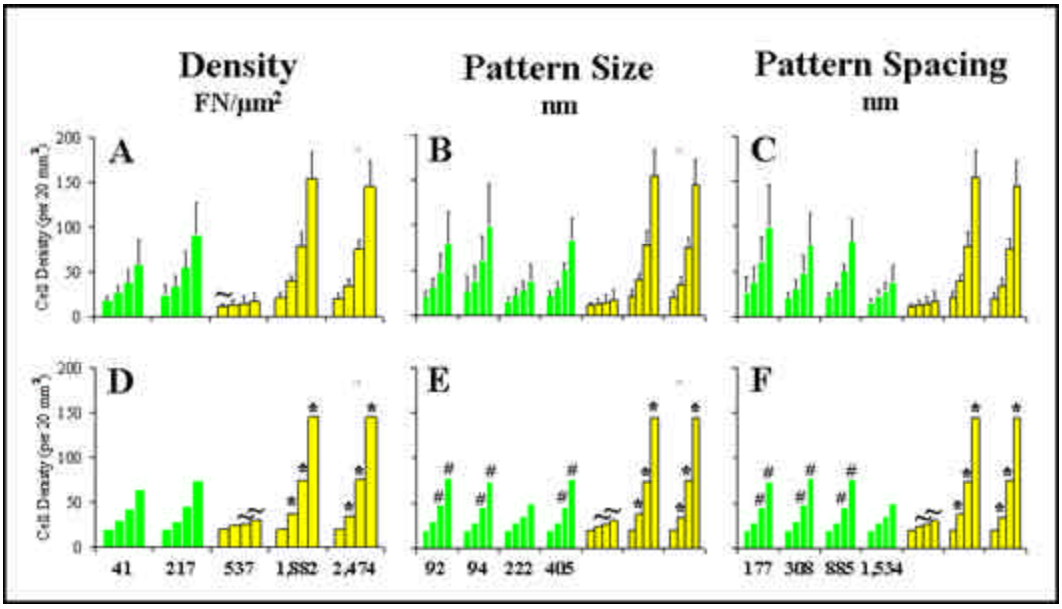

Figure 10.1: Proliferation Graphs for Cells on Nanopatterned and Control Surfaces: (A-C) Raw cell density measurements (cells/20mm^2) for cells on nanopatterned (green) and Au control (yellow) surfaces after 4, 24, 48, and 72 hours in cutlure. (D-F) Same graphs as in (A-C) but after normalization and scaling. The cell densities were plotted as a function of (A,D) increasing FN surface density, (B,E) increasing nanopattern size, and (C,F) increasing nanopattern spacing. The controls were included in (B, C, E, F) for ease of comparison. * Indicates higher cell densities than 2Au and all nanopatterned surfaces ($p < 0.001$). # Indicates higher densities than 2Au and 1500B nanopatterned surfaces ($p < 0.033$). ~ Indicates lower cell densities than all other surfaces ($p < 0.05$).

surfaces in Figure 10.1 D verifies this finding. Cells seeded on low density homogenously coated control surfaces displaying 537 FN/μm^2 show a statistically significant decrease in cellular proliferation over a 3day period compared to cells cultured on control surfaces with 1,882 FN/μm^2. While cells seeded on nanopatterned surfaces show similar initial attachment rates to cells seeded on high density control surfaces, their

proliferation is significantly lower than cells on high density controls but significantly higher than cells cultured on low density FN surfaces (Figure 10.1 D). The fact that proliferation is higher in cells cultured on nanopatterned surfaces compared to low density controls again indicates that the ability to form well-defined adhesion sites is more important in the initiation of signaling cascades responsible for controlling proliferation and overrules global surface density effects. This rule even seems to hold true for extremely low density FN surfaces, the B-type surfaces that display only 41 FN/μm^2. No significant differences in proliferation were observed between cells cultured on the B- and M-type surfaces even though these surfaces have an order of magnitude difference in global FN surface density (Figure 10.1 D). The occurrence of decreased proliferation in cells on nanopatterned surfaces compared to those cultured on high FN surface density controls hints to some importance of global FN density but may be a consequence of the non-discrete FN coating that allows adhesions to grow unhindered or due to differences in adhesive states rather than an influence of FN density.

10.3.3 Nanopattern Size Influence on EC Proliferation

To test whether adhesion site size influences cellular proliferation, cells were cultured on nanopatterned surfaces with FN nanoislands of a characteristic length ranging from 92 to 405 nm corresponding to individual adhesion sites areas of 3,629 to 85,653 nm^2. Previous cell studies in Dr. Frey's lab performed by Ted Gaubert using nanopatterned surfaces created with a different fabrication technique, NOBIL, [164] have demonstrated that cells seeded on small circular nanopatterns with a diameter of 150 nm display increased proliferation compared to cells on larger nanopatterns ranging

from 200 to 300 nm in size. This dependence of cellular proliferation on nanopattern size was not discovered in cells using surfaces created with NSL in this study (Figure 10.1 E). This discrepancy is most likely due to differences in nanopattern size-to-pitch ratios produced by the two different nanofabrication techniques. The results presented here indicate that cellular proliferation is not influenced by nanopattern size, at least for the small size-to-pitch ratios for nanopatterns created using NSL.

10.3.4 Nanopattern Spacing Influence on EC Proliferation

While there were no observed influences of nanopattern density or size on EC proliferation, cells did show a decreased proliferative response to increased adhesion site spacing (Figure 10.1 F). Cells cultured on surfaces presenting large, 222 nm, sized FN nanoislands spaced far apart, 1.534 μm, displayed a statistically significant decrease in proliferation compared to cells on all other nanopatterned surfaces (Figure 10.1 F); these surfaces all presented nanoscale adhesion sites within 900 nm of each other. This occurrence can not be a function of pattern density, as the 0300B nanopatterned surfaces have the same 2.2 % pattern surface coverage as the 1500B surfaces but cells on these surfaces did not show decreased proliferation. Any mechanisms that relate adhesion site spacing to adhesion mediated proliferative changes are currently unknown and no existing literature is available that covers the topic. Speculation as to why adhesion site spacing may have an influence on cellular proliferation will be discussed in the following section.

10.4 Discussion

The work presented here validates that ECs respond to varying surface concentrations of FN by undergoing both increased initial cell attachment and long term

proliferation with increased FN surface density. While this relationship holds true for cells cultured on homogenously coated control surfaces, cells on nanopatterned surfaces behave quite differently. Cells are able to attach to nanopatterned surfaces presenting global FN densities as low as 41 FN/μm^2 as well as they can to homogenously coated control surfaces displaying much higher densities of FN at 1,882 FN/μm^2, and statistically better than cells exposed to homogenously FN coated surfaces with an order of magnitude higher FN concentration at 537 FN/μm^2. This finding suggests that the ability to quickly cluster integrins to form well-defined adhesion sites is more important in promoting initial cell attachment than the overall amount of FN present on the surface as proposed by others.[99] While this holds true for initial cell attachment, long term proliferation may be governed by different aspects of adhesion as cells on nanopatterned surfaces display significantly decreased proliferation compared to cells grown on high density FN control surfaces. Previous work concerning cellular proliferation has demonstrated that cells on soft surfaces display proliferation rates that are similar to cells on more rigid surfaces, although the rates may be slightly lower for cells cultured on extremely soft surfaces.[40] It has also been shown that cells on soft surfaces create less dense actin stress fiber networks and display smaller more diffuse adhesion sites.[39] Since it is known that FAK is a major player in adhesion site regulation over cellular proliferation[50,80] and that FAK also is involved in adhesion site linkage to the cytoskeleton through its interaction with Shp2 and α-actinin,[79] it is tempting to speculate that FAK may be one of the force-sensitive signaling components in adhesion sites, although no available literature has made this connection and FAK has been investigated for many years. Contrary to this idea, the fact that cells cultured on soft surfaces show some deficiencies in the formation of dense actin stress fiber networks

but can still maintain similar proliferation rates to cells on more rigid surfaces implies that FAK and other possible adhesion components that regulate signaling are not force sensitive molecules. Furthermore, the finding that the creation of multiple cell-cell contacts down-regulate proliferation but that polarized cell-cell contact induces proliferation may indicate that ECM has little control over cell proliferation of ECs and that they continue to split until a critical number of surrounding cells are contacted. [88]

More insight into adhesion site regulation of proliferation can be deduced from the discovery of decreased cellular proliferation when cell adhesions are spaced more than 1.5 μm apart. It was demonstrated that both nanopattern surface density and nanopattern size have little influence on proliferation while adhesion site spacing does, at least for very large distances. Cells cultured on nanopatterns presenting 41 FN/μm^2 showed no difference in proliferation compared to cells on nanopatterned surfaces with 217 FN/μm^2. Furthermore, nanopattern size in the range from 92 to 405 nm showed no influence on proliferation, while an interpattern spacing of 1.5 μm induced significantly lower proliferative responses in cells. Previous cell studies in Dr. Frey's lab using nanopatterned surfaces created with NOBIL [164] have shown that pattern size, spacing, and overall density all have some influence on cellular proliferation, but size is the dominating factor for nanopatterned surfaces while density is the dominating influence for homogenously coated surfaces. From these studies it can be concluded that the observed increase in proliferation for cells on some NOBIL surfaces is not seen here due to the tighter packing of the nanopatterns that almost mimics homogenously coated surfaces due to their relative proximity. While NOBIL has many advantages over NSL with respect the pattern-to-pitch ratio control, no surfaces displaying extremely large spacing between the adhesion sites were implemented. The decreased proliferation

observed in cells seeded on the 1500B surfaces that display 222 nm size FN islands separated by 1.5 µm may show another aspect of adhesion site signaling. One may speculate that signaling cascades generated at adhesion sites have a limited spatial distance over which they influence signaling. If a large number of adhesion sites are within a close distance to each other then the signaling cascades initiated at the individual sites may overlap each other producing higher local levels of signaling between adhesions thereby reaching a specific threshold level in which downstream signals can be started, an idea similar to threshold levels met in neurons before they fire. It may be that if adhesion sites are spaced too far apart then there is no spatial overlap of signals and secondary downstream messengers do not get activated. While a speculative model, some studies have shown the possibility of force-sensitive Ca^{2+} channels that are opened by the application of force to the cell membrane presumably by F-actin near focal contacts at the periphery of lamellapodia. [82,83] This would allow very local spatially resolved responses in signaling to be created and if two adhesions are in close enough proximity then their overlap in signaling may reach the necessary threshold to active downstream messengers.

10.5 Conclusions

The analysis has shown that local ligand density and the ability for a cell to cluster integrins on a surface thereby creating well-defined adhesion sites is more important than overall ligand density on initiating cell attachment. While the formation of small adhesions is critical for initial cell attachment, other factors possibly including adhesion size and spacing are more influential over long term proliferation. Furthermore, while FAK plays an important role in governing adhesion mediated

proliferation signaling and in inducing adhesion site linkage to stress fibers it is most likely not a force sensitive adhesion molecule and the formation of cell-cell contacts seems to dominate proliferative responses. The data suggests the possibility of specific threshold signaling levels that have to be spatially resolved in order to promote long term proliferation. Further studies relating these multiple influences will have to be conducted for more detailed conclusions to be made.

Chapter 11

Discussion and Conclusions

11.1 Discussion and Conclusions

Integrin binding to its ECM ligand and integrin clustering are synergistic events needed to induce signaling and full engagement of adhesions with the cytoskeleton. Cluster size is an indicator of the maturation of adhesions, which is driven by the applied force of the actomyosin machinery of the cell. The size of each cluster can range from about 30 nm for a trimer, to submicron-sized for motile cells, to many microns for fully matured adhesions. Due to this wide range of adhesion sizes, restrictions in the growth process induced by cell adhesion to chemically-defined nanopatterns of FN was shown to influence both the adhesion of ECs and the events initiated and controlled by adhesion including cytoskeletal formation, cell spreading, fibrillogenesis, cell motility and proliferation as presented here.

Nanotopographic surfaces created by a variety of techniques have been shown to influence cell adhesion in several ways, including alignment to nano grooves,[130] decreased initial cell attachment and adhesion strength, and impaired spreading on surfaces presenting nanopits,[137-139] as well as increased adhesion, spreading, and cytoskeletal formation on raised nanopatterns.[93,140] The mechanisms of nanotopography influence are not clear, but increased filopodia formation,[141,142] Rac localization to the cell periphery,[93] and an upregulation of genes associated with cell signaling, proliferation, cytoskeletal components, and ECM production[140] have all been documented. While some cells such as ECs and fibroblasts prefer less topography,[93] osteoblasts display increased adhesion, proliferation, and deposition of extracellular

calcium with increased topography.[136,143] Nanotopographic surfaces have been suggested to induce selective adsorption of ECM proteins,[145] and while they demonstrate the importance of nanometer-scale features on cell behavior, they have so far not provided systematic insight into the connections between adhesion site properties and downstream cell behavior.

Chemically defined patterns of cell adhesion ligands, on the other hand, provide direct molecular control over the processes of cell adhesion as well as over the mechanics of force transduction. This control has been implemented to investigate cell adhesion, spreading, and differentiation on the micron scale with tools such as microcontact printing of thiols on gold. Cell adhesion size control down to 0.1 μm^2 using thiol stamping has shown that cells can adhere and spread well using such areas for integrin binding, unless the distance between the adhesion sites exceeds 2μm.[198] Extension of these types of studies into the submicron regime has been much more challenging. Although a multitude of nanopatterning strategies exist most of them are serial in nature and too laborious to fabricate the large surfaces areas needed for systematic cell studies.[146-148,154-162] This time constraint can be circumvented though the use of parallel patterning techniques such as NSL as presented here.[149,163,164,166,167,182]

While many nanofabrication techniques exist, most studies simply demonstrate cell adhesion to these surfaces and no direct proof over submicron adhesion site control has been demonstrated and no detailed cell biology studies as presented here have been performed on this length scale.[199-201] For example, protein and cell adhesion have been observed on PEG pillars, but due to the known repulsive properties of PEG, the number of cells that could adhere was significantly lower than to protein-coated glass.[149] Other techniques such as micelle lithography or star polymers have provided

significant insights into the importance of integrin proximity in the clustering process, but they do not allow for the formation of well-defined larger adhesion clusters except when used in conjunction with a serial technique such as e-beam lithography. Additionally, most techniques rely on RGD sequences for cell adhesion, and investigations of cell interactions with the full FN protein have not yet been possible on nanopatterns. While these tools have been used to gain more significant insight into cell adhesion biology than most reported literature, none of them have shown direct control over adhesion site size on the nanometer scale as presented in this work.

Experimental tools for systematic investigations to control the adhesion size range from about 40 nm to 300 nm, a size range in which a number of critical molecular and mechanical processes in cell adhesion may occur, have been missing so far. Here it was shown that NSL, a highly parallel self-assembly process, can be used to create large, cm^2-sized areas of nanopatterns of exactly this size range, with well defined size, spacing, and topography. These nanopatterned surfaces are a composite of two materials and can therefore be chemically modified with two distinct chemical functionalities. The results presented from detailed XPS, AFM, FN immunolabeling, and cell-seeding experiments consistently show that modification of the glass background with PEG and thiolization of the gold nanostructures directs FN adsorption exclusively to the gold nanostructures. By performing the functionalization for both materials simultaneously, PEG adsorption to the gold areas was minimized and the lack of an XPS sulfur signature on functionalized glass surfaces indicates that no thiol is entrapped in the PEG SAM. The ability to immobilize the full FN protein to the gold nanoislands provides stronger proof that adhesion maturation can be limited to the formation of small focal complexes whereas simply using RGD terminated thiols would not include

adhesive interactions with the synergistic and cryptic binding sites found in the full protein. The terminal functionality used here presents FN in a compact form similar to that found on non-patterned hydrophobic surfaces,[120] but changing the thiol functionality to a hydrophilic end group would induce FN to appear in an extended form.[120] This flexibility in the choice of surface chemistry could allow for more detailed studies of adhesion to be performed including the preferential engagement of different integrins based on the presentation of FN on different thiol terminal functionalities.[117,121] Although non-covalent immobilization of FN to the nanopattern was implemented in these studies, the use of other functional thiols would allow for specific and covalent anchoring of the full FN or sequences of FN domains by bioconjugation procedures. For instance mutated FN molecules lacking certain domains could be covalently linked to further explore the process of fibrillogenesis and to end the debate of whether specific domains unfold or whether the entire protein is stretched during fibril formation. Finally, the presentation of small peptides tethered to thiols could also be easily achieved and libraries of peptide influence on cell adhesion could be created.

The finding that cells even attach to these nanopatterned surfaces gives previously unknown insight into how the presentation of ECM ligands can promote or inhibit adhesion. Studies using homogenous coated protein surfaces have shown a direct correlation between FN surface density and endothelial and epithelial cell proliferation and spreading.[102,243] The selective adhesion of FN to nanopatterned surfaces changes the overall average density of FN and allows comparative studies of cell attachment, spreading, and proliferation between differences in global and local densities of FN. As confirmed by XPS, M-type and B-type nanopatterned surfaces

contain 7 - 8 % and 2 %, respectively, of the saturation amount of FN on a homogenous gold surface, in agreement with the measured average surface coverage of the pattern. It was demonstrated that both initial cell attachment and proliferation are mostly not determined by the average or global FN density as previously thought, as cells on both the 7 % and 2 % coverage surfaces seeded and proliferated far better than cells on non-patterned control surfaces with 537 FN/μm^2. In fact, cell attachment and proliferation were observed in cells at average FN concentrations more than 10 times lower than what was previously thought to be the minimum concentration that would support attachment and induce proliferation. [102]

At later time points, pattern or interadhesion site spacing becomes an important regulator of proliferation. This was indicated by the significantly lower proliferation of cells on 1500B surfaces compared to cells on all other nanopatterned and high FN density control surfaces. 1500B surfaces with a large interadhesion site spacing of 1.5 µm, close to the 2 µm spacing in which cells can not spread well on micropatterned surfaces, have similar adhesion site sizes compared to 1500M surfaces but a much larger interadhesion site spacing. Combining the finding that cells on both small and large nanopatterns proliferate more than cells on 1500B surfaces can provide some insight into how proliferation is governed by adhesion sites. Previous work by Ted Gaubert demonstrated that cellular proliferation rates are sensitive to changes in adhesion site size if the spacing between individual nanopatterns is relatively high (low pattern-to-pitch ratios). The surfaces in his studies did not allow for investigation of large spacing between nanopatterns to be performed as done here with the 1500B surfaces. The results of the two studies indicate a new possible method for adhesion site signaling control over proliferation. If adhesions are spaced very close together, such as

found with the 0300B and 0300M surfaces, then small changes in adhesion site size do not influence proliferation. If the adhesions are not packed very densely, meaning that they are slightly further apart, then adhesion site size has an influence on signaling, and finally, regardless of size, if the adhesions are spaced to far apart then proliferation is suppressed. These trends indicate that proliferative signals emanating from single adhesion sites may work together synergistically. It could be that each individual adhesion site contributes a circular signaling pattern that spreads from the adhesion site and combines with others to produce a "wave front" of signal, similar to Huygen's principle that in turn results in a cellular proliferative response. Hypothetically, it may be that the local signals created at adhesion sites have a particular spatial resolution and that this spatial resolution can be increased by either increasing or decreasing the adhesion site size. While no proof for such a model currently exists, it could explain the findings presented here and in Ted's work. Further studies using intracellular signaling dyes or cells transfected with, for instance GFP mutants of PIP3, could be combined with total internal reflection fluorescent (TIRF) microscopy studies to determine the exact spatial resolution of signaling cascades emanating from adhesion sites.

Furthermore, the time dependence of the proliferation results suggests that initially, the local FN density is important to support fast cluster formation of integrins regardless of adhesion site size. Since homogenous substrates with low levels of FN are randomly covered and the nanopatterns induce the formation of discrete adhesion sites of densely-packed FN, non-patterned surfaces would need a far denser coating to support the same local density of adhesions, as has been suggested recently with experiments on larger cluster sizes.[97,99,198] Also, it is interesting to note that the lowest non-patterned FN surface concentration, which has an average density of 537 FN/μm^2

and very low cell proliferation rates, has an average distance between FN molecules of 43 nm. This value is below the 58 – 70 nm separation between cyclic RGDs found to be the threshold to support fibroblast adhesion using nanopatterned cyclic RGD.[99] This discrepancy could be explained either by the fact that in that study adhesion and spreading but not proliferation were tested, by an inhomogeneous distribution of FN in our non-patterned experiments, or by a significant portion of the adsorbed FN having inaccessible binding sites.

Similar to proliferation, cell spreading area is commonly used to determine cellular reaction to a substrate. Endothelial cell spreading and proliferation have been linked: as the FN concentration on a surface increases, so do both the extent of cell spreading and the proliferation rates.[102] Nanotopographic surfaces have the ability to increase cell spreading in both endothelial cells[143] and fibroblasts,[140] while very high nanocolumns (160 nm) can reverse this effect in fibroblasts.[142] Here it was shown that reduced levels of cell spreading was induced in cells seeded on very small nanopatterns. The fact that HUVECs on the 1500M surfaces with an individual adhesion site area of ~ 0.1 μm^2 and an interadhesion site spacing of 0.9 µm spread more than cells on smaller nanopatterns suggests that there is a different quality to the adhesion for adhesion sizes above ~ 0.04 μm^2.

A threshold of 0.01 – 0.05 μm^2 for a single adhesion area is interesting, as this area is less than half the smallest pattern size of 0.1 μm^2 investigated by Lehnert et al.[198] Their results showed that such a pattern leads to cell behavior indistinguishable from homogeneously coated surfaces as long as the distance between adhesions (pitch) was below 2 µm, although the did not perform any analysis of the adhesions. Such a threshold is far smaller than the 1 μm^2 threshold found in force studies. Cellular traction

and force studies have shown a linear relationship between adhesion site size and the force applied to the surface for adhesion sites larger than 1 μm^2, with larger adhesions applying higher forces per adhesion area.[51-53] Similar studies have also shown an inverse trend, with adhesions smaller than 1 μm^2 at the leading edge of cell movement applying higher forces per attachment area than larger adhesions.[53,60] Additionally, it has been shown that larger well-spread cells exert more force on the surface than smaller rounded cells.[244]

The adhesion site studies performed here show a distinct difference between the size and distribution of adhesions formed by cells on nanopatterned and control surfaces. Au and glass control surfaces induce cells to form larger adhesions mainly along the cell perimeter. Cells on larger nanopatterns (1500B and 1500M) form mostly small adhesions that are more evenly distributed across the cell and only a few large adhesions, and the smallest nanopatterns that are less than 100 nm in size, induce cells to form an extremely high adhesion site density of small adhesions and almost no large adhesions. The analysis of individual adhesions, as characterized by vinculin stains and AFM height scans, has shown that cellular adhesions are located at nanopatterns, although the adhesion complex may bridge between patterns. The complexes can therefore reach lengths in the micron range, but their width is dependent of the pattern size leading to adhesion areas well below 1 μm^2. This study is the first to provide direct proof over adhesion site size control in the nanometer regime. Further analysis into the types of adhesions formed indicates that cells on the smallest nanopatterns, less than 100 nm in size, primarily form focal complexes and occasionally fibrillar adhesions as defined by the colocalization of elongated adhesions with FN fibrils. Cells cultured on larger nanopatterned surfaces, greater than 200 nm in size, were able to form both focal

complexes and smaller versions of large classical focal adhesions. While still well below 1 μm^2 in size, these adhesions showed the ability to interact with stress fibers and if the spacing was close such as with the 1500M surfaces, then the small stress fibers attached to these adhesions could be bundled together to form larger stress fibers.

The dependence of cytoskeletal formation on nanopattern properties gives some insight into the state or maturation levels of adhesions achieved by modulating nanopattern size and spacing. Previous studies have shown that the interplay between small nascent adhesions and F-actin in freshly seeded cells is important for the eventual formation of stress fibers and stress fiber linked focal adhesions.[174] The studies were able to show that in the initial moments of cell adhesion small circular rings of adhesive components are formed around F-actin rich cores. Over time, the highly dynamic F-actin and adhesion components form doublets that could then begin to tie together, similar to the organization seen on the 0300M surfaces. Eventually the F-actin bundles could be pieced together to form stress fiber linked adhesions similar to the observations presented here in cells on 1500B and 1500M surfaces. Finally, these smaller versions of focal adhesions were able to grow into large classical focal adhesions connected to large stress fibers, an occurrence seen in cells on the control surfaces in these studies.[174] This finding further validates the claim that nanopatterned surfaces with varying size and adhesion site spacing can limit maturation of adhesive states. Following this logic would mean that cells on 0300B surfaces have the lowest state of adhesion site maturation followed by cells on 0300M surfaces that begin to show signs of stress fiber formation where the close proximity of the adhesions allows for small bundles of F-actin to be joined together. A similar state of adhesion maturation is achieved by cells on 1500B surfaces that induce the formation of small adhesions that can link to actin fibers

without having to bundle fibers from multiple adhesions. Finally, a more mature state of adhesion is achieved by cells on 1500M that basically form smaller versions of large classical focal adhesions.

Further analysis into nanopattern regulation of mechanotransductive properties shows that nanopattern geometry can have some influence on cellular processes. It was demonstrated that cells on B-type surfaces were able to form thin FN fibrils that could span multiple nanopatterns, while this occurrence was much lower in cells on M-type surfaces. This finding led to the investigation of what is different about these surfaces that could allow fibrils to be formed in one case but not the other. Two possible solutions exist. First, it could simply be a density effect as the B-type surfaces have an order of magnitude lower global density of FN than M-type surfaces but this does not fully make sense in light of cell behavior on Au control surfaces. Cells cultured on high FN density Au control surfaces did not form any fibrils whereas cells on low density FN surfaces did. This shows that cells most likely cope with low levels of FN by producing their own FN. So how does this apply to cells on the nanopatterns? Since the local density of FN is high on the nanopatterned surfaces, and that is what the cells recognize, then the cells should react as if they were on the 25Au control surfaces and not produce fibrils. This implies another mechanism that determines fibril formation. Further analysis of the nanopatterns shows that straight lines connecting multiple patterns can easily be drawn on the B-type surfaces that can not be done on the M-type surfaces due to their offset nanopattern geometry, see Figure 3.1 C versus D. This led to the hypothesis that the local application of force allowed the cells to pull FN from one nanopattern to the next which would implicate the formation of fibrillar adhesions. Currently, fibrillar adhesion formation is thought to be a late maturation state of adhesion formation. [16]

The work presented here that correlates adhesion site properties to varied maturation states, implies that this is not necessarily so. Cells on 0300B surfaces that form very small non-cytoskeletal linked adhesions can still form fibrillar adhesions without the intermediate stage of focal adhesions. Further support for the nanopattern alignment theory of fibrillogenesis is supported by recent findings that show directionality of applied force result in different FN network configurations. [214] The work presented here showing that the fibrillar adhesions align to actin stress fibers further validates that the direction of applied force can influence the density and interconnectedness of FN networks. [214]

Lastly, all of the differences in adhesive states, cytoskeletal formation, and fibrillogenesis were reflected in the different motility studies. The current understanding of motility involves the formation of large stress fiber linked adhesions to apply the traction force necessary for cell motility. Recent evidence has shown that cytoskeletal linkage can act to reduce cell motility as discovered in motile cancer cells that reduced their motility with increased levels of tensin, an adaptor protein that acts to link adhesion and cytoskeletal components together. [238] This apparent slowing of fast cells with increased adhesion-to-cytoskeleton connections implies that these links induce the formation of drag forces before they are disassembled. [238] The work presented here shows that very small nanopatterns induce significantly higher levels of motility compared to cells on larger nanopatterns regardless of pattern spacing and density. These increased levels of motility coincide with cells that have reduced cytoskeletal formation and linkage to adhesions. The results imply that while the formation of stress fiber linked focal adhesions can provide high levels of traction force at the leading edge of cells they can also act as sources or drag force before their disassembly.

This brings FAK into the picture. FAK is an important regulator of many signaling events initiated and governed by adhesion sites and has known important roles in adhesion formation, cytoskeletal linkage, proliferation control, and adhesion site disassembly. [32,37,50,80,117,227,236,237,239,245-247] The more motile states achieved by cells on nanopatterned surfaces may indeed have either more FAK or have more highly phosphorylated FAK, and due to the size restrictions imposed by the nanopatterns are not able to form large actin stress fibers. Further studies using cells transfected with GFP variants of FAK could provide more insight into these questions.

It is interesting to further compare cellular mechanotransduction on homogeneous but elastic substrates with the rigid but nanopatterned substrates used here. ECs on elastic substrates show a strong correlation between elastic modulus and spreading, while proliferation is relatively unaffected. [40] The findings of a relatively small proliferation decrease and decreased cell spreading of ECs on smaller nanopatterns suggests that restricting integrin clustering with nanopatterns and reducing force generation at adhesion sites with elastic surfaces may induce changes in cell behavior through a similar pathway. Considering the importance of cellular mechanotransduction for cell differentiation and phenotype, [122] the nanopatterned surfaces presented here to control integrin clustering could provide a complementary tool to elastic substrates for understanding the molecular mechanisms of integrin-mediated mechanotransduction. Further studies relating the dynamics of focal adhesion properties to cytoskeletal formation and cell motility could elucidate these questions.

It is even more interesting to compare the findings presented here with those of cells in 3-D environments. Currently, an increasing number of scientists are realizing that much of what we have learned about cell adhesion biology may be an artifact of tissue

culture on 2-D rigid surfaces and not representative of *in vivo* conditions, except maybe for osteoblasts. Cell studies using 3-D matrices have shown drastic differences in cell morphology and increased motility and proliferation compared to cells on 2-D surfaces.[43,46-48] These occurrences parallel the findings presented here and those using 2-D elastic surfaces. These observed cellular changes induced by 3-D matrices have been linked to changes in adhesion composition and FAK phosphorylation.[48] Furthermore, 3D matrices are typically more elastic than glass or polystyrene, and therefore the inherent matrix elasticity may also influence adhesion properties of cells cultured in 3-D systems. Cells cultured in cross-linked cell-derived 3-D matrices revert back to using adhesions similar to those seen in 2-D culture systems.[48] Furthermore, recent studies performed on cells in 3-D electrospun nanofibers have reported cell behavioral changes almost identical to those presented here.[248] Cells in these nanostructured 3-D systems displayed decreased cytoskeletal formation, smaller more diffuse adhesion sites, and a slight reduction in cell spreading compared to cells on 2-D culture systems.[248] Based on these results, the formation of large focal adhesions associating with large stress fibers may be a consequence of cell culture on 2-D rigid systems and not indicative of *in vivo* behavior. Even more importantly, the findings presented here imply that limiting adhesion site growth and cytoskeletal formation may produce more *in vivo* like cell responses. Since these experiments were performed on 2-D surfaces that were completely rigid, the comparison with 3-D matrices and planar elastic substrates suggests that it is the local force exerted on each adhesion that determines cell behavior. Despite being rigid and 2-D, these surfaces could be a highly useful alternative to 3-D and planar elastic membrane culture systems for exploring cell adhesion biology

and separate force, 3-D arrangement, and local mechanotransduction influences from each other.

References

1. Kasemo B. Biological surface science. Surface Science 2002;500(1-3):656-677.
2. Lutolf MP, Hubbell JA. Synthetic biomaterials as instructive extracellular microenvironments for morphogenesis in tissue engineering. Nature Biotechnology 2005;23(1):47-55.
3. Kannan RY, Salacinski HJ, Sales K, Butler P, Seifalian AM. The roles of tissue engineering and vascularisation in the development of micro-vascular networks: a review. Biomaterials 2005;26(14):1857-1875.
4. Rosso F, Marino G, Giordano A, Barbarisi M, Parmeggiani D, Barbarisi A. Smart materials as scaffolds for tissue engineering. Journal of Cellular Physiology 2005;203(3):465-470.
5. Langer R, Tirrell DA. Designing materials for biology and medicine. Nature 2004;428(6982):487-492.
6. Slater JH, Frey W. Nanopatterning of fibronectin and the influence of integrin clustering on endothelial cell spreading and proliferation. Journal of Biomedical Materials Research Part A 2008;Published Online: Dec 17 2007 2:52PM(*In Press*: DOI # 10.1002/jbm.a.31725).
7. Topper JN, Gimbrone MA. Blood flow and vascular gene expression: fluid shear stress as a modulator of endothelial phenotype. Molecular Medicine Today 1999;5(1):40-46.
8. Hynes RO. Integrins - Versatility, Modulation, and Signaling in Cell-Adhesion. Cell 1992;69(1):11-25.
9. Short SM, Talbott GA, Juliano RL. Integrin-mediated signaling events in human endothelial cells. Molecular Biology of the Cell 1998;9(8):1969-1980.
10. Miranti CK, Brugge JS. Sensing the environment: a historical perspective on integrin signal transduction. Nature Cell Biology 2002;4(4):E83-E90.
11. Ruegg C, Mariotti A. Vascular integrins: pleiotropic adhesion and signaling molecules in vascular homeostasis and angiogenesis. Cellular and Molecular Life Sciences 2003;60(6):1135-1157.
12. Liddington RC, Ginsberg MH. Integrin activation takes shape. Journal of Cell Biology 2002;158(5):833-839.
13. Geiger B, Bershadsky A, Pankov R, Yamada KM. Transmembrane extracellular matrix-cytoskeleton crosstalk. Nature Reviews Molecular Cell Biology 2001;2(11):793-805.

14. Cohen M, Joester D, Geiger B, Addadi L. Spatial and temporal sequence of events in cell adhesion: From molecular recognition to focal adhesion assembly. Chembiochem 2004;5(10):1393-1399.

15. Geiger B, Bershadsky A. Assembly and mechanosensory function of focal contacts. Current Opinion In Cell Biology 2001;13(5):584-592.

16. Zaidel-Bar R, Cohen M, Addadi L, Geiger B. Hierarchical assembly of cell-matrix adhesion complexes. Biochemical Society Transactions 2004;32:416-420.

17. Knies Y, Bernd A, Kaufmann R, Bereiter-Hahn J, Kippenberger S. Mechanical stretch induces clustering of beta 1-integrins and facilitates adhesion. Experimental Dermatology 2006;15(5):347-355.

18. Hsieh CF, Chang BJ, Pai CH, Chen HY, Tsai JW, Yi YH, Chiang YT, Wang DW, Chi S, Hsu L and others. Stepped changes of monovalent ligand-binding force during ligand-induced clustering of integrin alpha(IIB)beta(3). Journal of Biological Chemistry 2006;281(35):25466-25474.

19. Galbraith CG, Yamada KM, Sheetz MP. The relationship between force and focal complex development. Journal of Cell Biology 2002;159(4):695-705.

20. Cluzel C, Saltel F, Lussi J, Paulhe F, Imhof BA, Wehrle-Haller B. The mechanisms and dynamics of alpha v beta 3 integrin clustering in living cells. Journal of Cell Biology 2005;171(2):383-392.

21. Iber D, Campbell ID. Integrin activation - the importance of a positive feedback. Bulletin of Mathematical Biology 2006;68(4):945-956.

22. Calderwood DA. Talin controls integrin activation. Biochemical Society Transactions 2004;32:434-437.

23. Calderwood DA, Ginsberg MH. Talin forges the links between integrins and actin. Nature Cell Biology 2003;5(8):694-697.

24. Jiang GY, Giannone G, Critchley DR, Fukumoto E, Sheetz MP. Two-piconewton slip bond between fibronectin and the cytoskeleton depends on talin. Nature 2003;424(6946):334-337.

25. Li R, Bennett JS, DeGrado WF. Structural basis for integrin alpha IIb beta 3 clustering. Biochemical Society Transactions 2004;32:412-415.

26. Luo BH, Carman CV, Takagi J, Springer TA. Disrupting integrin transmembrane domain heterodimerization increases ligand binding affinity, not valency or clustering. Proceedings of the National Academy of Sciences of the United States of America 2005;102(10):3679-3684.

27. Sharma DK, Brown JC, Cheng ZJ, Holicky EL, Marks DL, Pagano RE. The glycosphingolipid, lactosylceramide, regulates beta(1)-integrin clustering and endocytosis. Cancer Research 2005;65(18):8233-8241.

28. Yang TY, Zaman MH. Thermodynamics of clustered and unclustered receptor systems in cell adhesion. Chemical Physics Letters 2008;454(4-6):362-366.

29. Brinkerhoff CJ, Linderman JJ. Integrin dimerization and ligand organization: Key components in integrin clustering for cell adhesion. Tissue Engineering 2005;11(5-6):865-876.

30. Mostafavi-Pour Z, Askari JA, Parkinson SJ, Parker PJ, Ng TTC, Humphries MJ. Integrin-specific signaling pathways controlling focal adhesion formation and cell migration. Journal of Cell Biology 2003;161(1):155-167.

31. Lauffenburger DA, Wells A. Getting a grip: new insights for cell adhesion and traction. Nature Cell Biology 2001;3(5):E110-E112.

32. Sieg DJ, Hauck CR, Schlaepfer DD. Required role of focal adhesion kinase (FAK) for integrin-stimulated cell migration. Journal of Cell Science 1999;112(16):2677-2691.

33. Li S, Huang NF, Hsu S. Mechanotransduction in endothelial cell migration. Journal of Cellular Biochemistry 2005;96(6):1110-1126.

34. Sastry SK, Lakonishok M, Wu S, Truong TQ, Huttenlocher A, Turner CE, Horwitz AF. Quantitative changes in integrin and focal adhesion signaling regulate myoblast cell cycle withdrawal. Journal of Cell Biology 1999;144(6):1295-1309.

35. Meredith DO, Owen GR, ap Gwynn I, Richards RG. Variation in cell-substratum adhesion in relation to cell cycle phases. Experimental Cell Research 2004;293(1):58-67.

36. Wary KK, Mainiero F, Isakoff SJ, Marcantonio EE, Giancotti FG. The adaptor protein Shc couples a class of integrins to the control of cell cycle progression. Cell 1996;87(4):733-743.

37. Almeida EAC, Ilic D, Han Q, Hauck CR, Jin F, Kawakatsu H, Schlaepfer DD, Damsky CH. Matrix survival signaling: From fibronectin via focal adhesion kinase to c-Jun NH2-terminal kinase. Journal of Cell Biology 2000;149(3):741-754.

38. Scatena M, Almeida M, Chaisson ML, Fausto N, Nicosia RF, Giachelli CM. NF-kappa B mediates alpha v beta 3 integrin-induced endothelial cell survival. Journal of Cell Biology 1998;141(4):1083-1093.

39. Discher DE, Janmey P, Wang YL. Tissue cells feel and respond to the stiffness of their substrate. Science 2005;310(5751):1139-1143.

40. Yeung T, Georges PC, Flanagan LA, Marg B, Ortiz M, Funaki M, Zahir N, Ming WY, Weaver V, Janmey PA. Effects of substrate stiffness on cell morphology, cytoskeletal structure, and adhesion. Cell Motility and the Cytoskeleton 2005;60(1):24-34.

41. Paszek MJ, Zahir N, Johnson KR, Lakins JN, Rozenberg GI, Gefen A, Reinhart-King CA, Margulies SS, Dembo M, Boettiger D and others. Tensional homeostasis and the malignant phenotype. Cancer Cell 2005;8(3):241-254.

42. Petit V, Thiery JP. Focal adhesions: structure and dynamics. Biology of the Cell 2000;92(7):477-494.

43. Vogel V, Baneyx G. The tissue engineering puzzle: A molecular perspective. Annual Review of Biomedical Engineering 2003;5:441-463.

44. Cohen M, Kam Z, Addadi L, Geiger B. Dynamic study of the transition from hyaluronan- to integrin-mediated adhesion in chondrocytes. Embo Journal 2006;25(2):302-311.

45. Galbraith CG, Yamada KM, Galbraith JA. Polymerizing actin fibers position integrins primed to probe for adhesion sites. Science 2007;315(5814):992-995.

46. Sechler JL, Corbett SA, Wenk MB, Schwarzbauer JE. Modulation of cell-extracellular matrix interactions. Morphogenesis: Cellular Interactions. New York: New York Acad Sciences; 1998. p 143-154.

47. Corbett SA, Wilson CL, Schwarzbauer JE. Changes in cell spreading and cytoskeletal organization are induced by adhesion to a fibronectin-fibrin matrix. Blood 1996;88(1):158-166.

48. Cukierman E, Pankov R, Stevens DR, Yamada KM. Taking cell-matrix adhesions to the third dimension. Science 2001;294(5547):1708-1712.

49. Berrier AL, Yamada KM. Cell-matrix adhesion. Journal of Cellular Physiology 2007;213(3):565-573.

50. Pirone DM, Liu WF, Ruiz SA, Gao L, Raghavan S, Lemmon CA, Romer LH, Chen CS. An inhibitory role for FAK in regulating proliferation: a link between limited adhesion and RhoA-ROCK signaling. Journal of Cell Biology 2006;174(2):277-288.

51. Balaban NQ, Schwarz US, Riveline D, Goichberg P, Tzur G, Sabanay I, Mahalu D, Safran S, Bershadsky A, Addadi L and others. Force and focal adhesion assembly: a close relationship studied using elastic micropatterned substrates. Nature Cell Biology 2001;3(5):466-472.

52. Schwarz US, Balaban NQ, Riveline D, Addadi L, Bershadsky A, Safran SA, Geiger B. Measurement of cellular forces at focal adhesions using elastic micro-patterned

substrates. Materials Science & Engineering C-Biomimetic and Supramolecular Systems 2003;23(3):387-394.

53. Tan JL, Tien J, Pirone DM, Gray DS, Bhadriraju K, Chen CS. Cells lying on a bed of microneedles: An approach to isolate mechanical force. Proceedings of the National Academy of Sciences of the United States of America 2003;100(4):1484-1489.

54. du Roure O, Saez A, Buguin A, Austin RH, Chavrier P, Siberzan P, Ladoux B. Force mapping in epithelial cell migration. Proceedings of the National Academy of Sciences of the United States of America 2005;102(7):2390-2395.

55. DeMali KA, Barlow CA, Burridge K. Recruitment of the Arp2/3 complex to vinculin: coupling membrane protrusion to matrix adhesion. Journal of Cell Biology 2002;159(5):881-891.

56. Martel V, Racaud-Sultan C, Dupe S, Marie C, Paulhe F, Galmiche A, Block MR, Albiges-Rizo C. Conformation, localization, and integrin binding of talin depend on its interaction with phosphoinositides. Journal of Biological Chemistry 2001;276(24):21217-21227.

57. Gilmore AP, Burridge K. Regulation of vinculin binding to talin and actin by phosphatidyl-inositol-4-5-bisphosphate. Nature 1996;381(6582):531-535.

58. Bjorge JD, Jakymiw A, Fujita DJ. Selected glimpses into the activation and function of Src kinase. Oncogene 2000;19(49):5620-5635.

59. Lele TP, Pendse J, Kumar S, Salanga M, Karavitis J, Ingber DE. Mechanical forces alter zyxin unbinding kinetics within focal adhesions of living cells. Journal of Cellular Physiology 2006;207(1):187-194.

60. Beningo KA, Dembo M, Kaverina I, Small JV, Wang YL. Nascent focal adhesions are responsible for the generation of strong propulsive forces in migrating fibroblasts. Journal of Cell Biology 2001;153(4):881-887.

61. Riveline D, Zamir E, Balaban NQ, Schwarz US, Ishizaki T, Narumiya S, Kam Z, Geiger B, Bershadsky AD. Focal contacts as mechanosensors: Externally applied local mechanical force induces growth of focal contacts by an mDia1-dependent and ROCK-independent mechanism. Journal of Cell Biology 2001;153(6):1175-1185.

62. Bershadsky AD, Balaban NQ, Geiger B. Adhesion-dependent cell mechanosensitivity. Annual Review of Cell and Developmental Biology 2003;19:677-695.

63. Hu K, Ji L, Applegate KT, Danuser G, Waterman-Stirer CM. Differential transmission of actin motion within focal adhesions. Science 2007;315(5808):111-115.

64. Jay DG. The clutch hypothesis revisited: Ascribing the roles of actin-associated proteins in filopodial protrusion in the nerve growth cone. Journal of Neurobiology 2000;44(2):114-125.

65. Schaus TE, Taylor EW, Borisy GG. Self-organization of actin filament orientation in the dendritic-nucleation/array-treadmilling model. Proceedings of the National Academy of Sciences of the United States of America 2007;104(17):7086-7091.

66. Mejillano MR, Kojima S, Applewhite DA, Gertler FB, Svitkina TM, Borisy GG. Lamellipodial versus filopodial mode of the actin nanomachinery: Pivotal role of the filament barbed end. Cell 2004;118(3):363-373.

67. Pollard TD, Borisy GG. Cellular motility driven by assembly and disassembly of actin filaments. Cell 2003;112(4):453-465.

68. Destaing O, Saltel F, Geminard JC, Jurdic P, Bard F. Podosomes display actin turnover and dynamic self-organization in osteoclasts expressing actin-green fluorescent protein. Molecular Biology of the Cell 2003;14(2):407-416.

69. Chabadel A, Banon-Rodriguez I, Cluet D, Rudkin BB, Wehrle-Haller B, Genot E, Jurdic P, Anton IM, Saltel F. CD44 and beta 3 integrin organize two functionally distinct actin-based domains in osteoclasts. Molecular Biology of the Cell 2007;18(12):4899-4910.

70. Miyamoto S, Teramoto H, Coso OA, Gutkind JS, Burbelo PD, Akiyama SK, Yamada KM. Integrin Function - Molecular Hierarchies Of Cytoskeletal And Signaling Molecules. Journal of Cell Biology 1995;131(3):791-805.

71. Dembo M, Wang YL. Stresses at the cell-to-substrate interface during locomotion of fibroblasts. Biophysical Journal 1999;76(4):2307-2316.

72. Galbraith CG, Sheetz MP. A micromachined device provides a new bend on fibroblast traction forces. Proceedings of the National Academy of Sciences of the United States of America 1997;94(17):9114-9118.

73. Burridge K, ChrzanowskaWodnicka M. Focal adhesions, contractility, and signaling. Annual Review of Cell and Developmental Biology 1996;12:463-518.

74. Felsenfeld DP, Schwartzberg PL, Venegas A, Tse R, Sheetz MP. Selective regulation of integrin-cytoskeleton interactions by the tyrosine kinase Src. Nature Cell Biology 1999;1(4):200-206.

75. Howe A, Aplin AE, Alahari SK, Juliano RL. Integrin signaling and cell growth control. Current Opinion in Cell Biology 1998;10(2):220-231.

76. Chicurel ME, Chen CS, Ingber DE. Cellular control lies in the balance of forces. Current Opinion in Cell Biology 1998;10(2):232-239.

77. Zhong CL, Chrzanowska-Wodnicka M, Brown J, Shaub A, Belkin AM, Burridge K. Rho-mediated contractility exposes a cryptic site in fibronectin and induces fibronectin matrix assembly. Journal of Cell Biology 1998;141(2):539-551.

78. Shaub A. Unravelling the extracellular matrix. Nature Cell Biology 1999;1(7):E173-E175.

79. Alberts B, Johnson A, Lewis J, Raff M, Roberts K, Walter P. Molecular Biology of the Cell. New York: Garland Science; 2002. 1423 p.

80. von Wichert G, Haimovich B, Feng GS, Sheetz MP. Force-dependent integrin-cytoskeleton linkage formation requires downregulation of focal complex dynamics by Shp2. Embo Journal 2003;22(19):5023-5035.

81. Cattaruzza M, Lattrich C, Hecker M. Focal adhesion protein zyxin is a mechanosensitive modulator of gene expression in vascular smooth muscle cells. Hypertension 2004;43(4):726-730.

82. Matthews BD, Overby DR, Mannix R, Ingber DE. Cellular adaptation to mechanical stress: role of integrins, Rho, cytoskeletal tension and mechanosensitive ion channels. Journal of Cell Science 2006;119(3):508-518.

83. Pommerenke H, Schreiber E, Durr F, Nebe B, Hahnel C, Moller W, Rychly J. Stimulation of integrin receptors using a magnetic drag force device induces an intracellular free calcium response. European Journal of Cell Biology 1996;70(2):157-164.

84. Chen BM, Grinnell AD. Integrins and Modulation of Transmitter Release from Motor-Nerve Terminals by Stretch. Science 1995;269(5230):1578-1580.

85. Dike LE, Chen CS, Mrksich M, Tien J, Whitesides GM, Ingber DE. Geometric control of switching between growth, apoptosis, and differentiation during angiogenesis using micropatterned substrates. In Vitro Cellular & Developmental Biology-Animal 1999;35(8):441-448.

86. Huang S, Chen CS, Ingber DE. Control of cyclin D1, p27(Kip1), and cell cycle progression in human capillary endothelial cells by cell shape and cytoskeletal tension. Molecular Biology of the Cell 1998;9(11):3179-3193.

87. Nelson CM, Chen CS. Cell-cell signaling by direct contact increases cell proliferation via a PI3K-dependent signal. Febs Letters 2002;514(2-3):238-242.

88. Nelson CM, Chen CS. VE-cadherin simultaneously stimulates and inhibits cell proliferation by altering cytoskeletal structure and tension. Journal of Cell Science 2003;116(17):3571-3581.

89. Ingber DE. Mechanical signalling and the cellular response to extracellular matrix in angiogenesis and cardiovascular physiology. Circulation Research 2002;91(10):877-887.

90. Brock A, Chang E, Ho CC, LeDuc P, Jiang XY, Whitesides GM, Ingber DE. Geometric determinants of directional cell motility revealed using microcontact printing. Langmuir 2003;19(5):1611-1617.

91. Chen CS, Tan J, Tien J. Mechanotransduction at cell-matrix and cell-cell contacts. Annual Review of Biomedical Engineering 2004;6:275-302.

92. McBeath R, Pirone DM, Nelson CM, Bhadriraju K, Chen CS. Cell shape, cytoskeletal tension, and RhoA regulate stem cell lineage commitment. Developmental Cell 2004;6(4):483-495.

93. Dalby MJ, Giannaras D, Riehle MO, Gadegaard N, Affrossman S, Curtis ASG. Rapid fibroblast adhesion to 27 nm high polymer demixed nano-topography. Biomaterials 2004;25(1):77-83.

94. Dalby MJ, Riehle MO, Sutherland DS, Agheli H, Curtis ASG. Fibroblast response to a controlled nanoenvironment produced by colloidal lithography. Journal of Biomedical Materials Research Part A 2004;69A(2):314-322.

95. Irvine DJ, Hue KA, Mayes AM, Griffith LG. Simulations of cell-surface integrin binding to nanoscale-clustered adhesion ligands. Biophysical Journal 2002;82(1):120-132.

96. Dalby MJ, Riehle MO, Johnstone HJH, Affrossman S, Curtis ASG. Nonadhesive nanotopography: Fibroblast response to poly(n-butyl methacrylate)-poly(styrene) demixed surface features. Journal of Biomedical Materials Research Part A 2003;67A(3):1025-1032.

97. Koo LY, Irvine DJ, Mayes AM, Lauffenburger DA, Griffith LG. Co-regulation of cell adhesion by nanoscale RGD organization and mechanical stimulus. Journal of Cell Science 2002;115(7):1423-1433.

98. Massia SP, Hubbell JA. An RGD Spacing of 440nm Is Sufficient for Integrin Alpha-V-Beta-3-Mediated Fibroblast Spreading and 140nm for Focal Contact and Stress Fiber Formation. Journal of Cell Biology 1991;114(5):1089-1100.

99. Arnold M, Cavalcanti-Adam EA, Glass R, Blummel J, Eck W, Kantlehner M, Kessler H, Spatz JP. Activation of integrin function by nanopatterned adhesive interfaces. Chemphyschem 2004;5(3):383-388.

100. Liu YQ, Senger DR. Matrix-specific activation of Src and Rho initiates capillary morphogenesis of endothelial cells. Faseb Journal 2004;18(3):457-468.

101. Rhodes JM, Simons M. The extracellular matrix and blood vessel formation: not just a scaffold. Journal of Cellular and Molecular Medicine 2007;11(2):176-205.

102. Ingber DE. Fibronectin Controls Capillary Endothelial-Cell Growth by Modulating Cell-Shape. Proceedings of the National Academy of Sciences of the United States of America 1990;87(9):3579-3583.

103. Mrksich M, Dike LE, Tien J, Ingber DE, Whitesides GM. Using microcontact printing to pattern the attachment of mammalian cells to self-assembled monolayers of alkanethiolates on transparent films of gold and silver. Experimental Cell Research 1997;235(2):305-313.

104. Folch A, Toner M. Microengineering of cellular interactions. Annual Review of Biomedical Engineering 2000;2:227-+.

105. Chen CS, Jiang XY, Whitesides GM. Microengineering the environment of mammalian cells in culture. Mrs Bulletin 2005;30(3):194-201.

106. Xia YN, Whitesides GM. Soft lithography. Annual Review of Materials Science 1998;28:153-184.

107. Folkers JP, Gorman CB, Laibinis PE, Buchholz S, Whitesides GM, Nuzzo RG. Self-Assembled Monolayers of Long-Chain Hydroxamic Acids on the Native Oxides of Metals. Langmuir 1995;11(3):813-824.

108. Mrksich M, Whitesides GM. Patterning Self-Assembled Monolayers Using Microcontact Printing - a New Technology for Biosensors. Trends in Biotechnology 1995;13(6):228-235.

109. Ostuni E, Yan L, Whitesides GM. The interaction of proteins and cells with self-assembled monolayers of alkanethiolates on gold and silver. Colloids and Surfaces B-Biointerfaces 1999;15(1):3-30.

110. Bernard A, Delamarche E, Schmid H, Michel B, Bosshard HR, Biebuyck H. Printing patterns of proteins. Langmuir 1998;14(9):2225-2229.

111. James CD, Davis RC, Kam L, Craighead HG, Isaacson M, Turner JN, Shain W. Patterned protein layers on solid substrates by thin stamp microcontact printing. Langmuir 1998;14(4):741-744.

112. Ostuni E, Kane R, Chen CS, Ingber DE, Whitesides GM. Patterning mammalian cells using elastomeric membranes. Langmuir 2000;16(20):7811-7819.

113. Singhvi R, Kumar A, Lopez GP, Stephanopoulos GN, Wang DIC, Whitesides GM, Ingber DE. Engineering Cell-Shape and Function. Science 1994;264(5159):696-698.

114. Lan MA, Gersbach CA, Michael KE, Keselowsky BG, Garcia AJ. Myoblast proliferation and differentiation on fibronectin-coated self assembled monolayers presenting different surface chemistries. Biomaterials 2005;26(22):4523-4531.

115. Keselowsky BG, Collard DM, Garcia AJ. Integrin binding specificity regulates biomaterial surface chemistry effects on cell differentiation. Proceedings of the National Academy of Sciences of the United States of America 2005;102(17):5953-5957.

116. Curran JM, Chen R, Hunt JA. Controlling the phenotype and function of mesenchymal stem cells in vitro by adhesion to silane-modified clean glass surfaces. Biomaterials 2005;26(34):7057-7067.

117. Keselowsky BG, Collard DM, Garcia AJ. Surface chemistry modulates focal adhesion composition and signaling through changes in integrin binding. Biomaterials 2004;25(28):5947-5954.

118. Garcia AJ, Vega MD, Boettiger D. Modulation of cell proliferation and differentiation through substrate-dependent changes in fibronectin conformation. Molecular Biology of the Cell 1999;10(3):785-798.

119. Chen CS, Mrksich M, Huang S, Whitesides GM, Ingber DE. Geometric control of cell life and death. Science 1997;276(5317):1425-1428.

120. Bergkvist M, Carlsson J, Oscarsson S. Surface-dependent conformations of human plasma fibronectin adsorbed to silica, mica, and hydrophobic surfaces, studied with use of Atomic Force Microscopy. Journal of Biomedical Materials Research Part A 2003;64A(2):349-356.

121. Keselowsky BG, Collard DM, Garcia AJ. Surface chemistry modulates fibronectin conformation and directs integrin binding and specificity to control cell adhesion. Journal of Biomedical Materials Research Part A 2003;66A(2):247-259.

122. Engler AJ, Sen S, Sweeney HL, Discher DE. Matrix elasticity directs stem cell lineage specification. Cell 2006;126(4):677-689.

123. Gupton SL, Waterman-Storer CM. Spatiotemporal feedback between actomyosin and focal-adhesion systems optimizes rapid cell migration. Cell 2006;125(7):1361-1374.

124. Lo CM, Wang HB, Dembo M, Wang YL. Cell movement is guided by the rigidity of the substrate. Biophysical Journal 2000;79(1):144-152.

125. Peyton SR, Putnam AJ. Extracellular matrix rigidity governs smooth muscle cell motility in a biphasic fashion. Journal of Cellular Physiology 2005;204(1):198-209.

126. Pelham RJ, Wang YL. Cell locomotion and focal adhesions are regulated by substrate flexibility. Proceedings of the National Academy of Sciences of the United States of America 1997;94(25):13661-13665.

127. Engler AJ, Griffin MA, Sen S, Bonnetnann CG, Sweeney HL, Discher DE. Myotubes differentiate optimally on substrates with tissue-like stiffness: pathological implications for soft or stiff microenvironments. Journal of Cell Biology 2004;166(6):877-887.

128. Griffin MA, Sen S, Sweeney HL, Discher DE. Adhesion-contractile balance in myocyte differentiation. Journal of Cell Science 2004;117(24):5855-5863.

129. Barbucci R, Pasqui D, Wirsen A, Affrossman S, Curtis A, Tetta C. Micro and nano-structured surfaces. Journal of Materials Science-Materials in Medicine 2003;14(8):721-725.

130. Teixeira AI, Abrams GA, Bertics PJ, Murphy CJ, Nealey PF. Epithelial contact guidance on well-defined micro- and nanostructured substrates. Journal of Cell Science 2003;116(10):1881-1892.

131. Turner S, Kam L, Isaacson M, Craighead HG, Shain W, Turner J. Cell attachment on silicon nanostructures. Journal of Vacuum Science & Technology B 1997;15(6):2848-2854.

132. Agheli H, Malmstrom J, Hanarp P, Sutherland DS. Narlostructured biointerfaces. Materials Science & Engineering C-Biomimetic and Supramolecular Systems 2006;26(5-7):911-917.

133. Dalby MJ, Berry CC, Riehle MO, Sutherland DS, Agheli H, Curtis ASG. Attempted endocytosis of nano-environment produced by colloidal lithography by human fibroblasts. Experimental Cell Research 2004;295(2):387-394.

134. Chen X, Chen ZM, Fu N, Lu G, Yang B. Versatile nanopatterned surfaces generated via three-dimensional colloidal crystals. Advanced Materials 2003;15(17):1413-1417.

135. Palin E, Liu HN, Webster TJ. Mimicking the nanofeatures of bone increases bone-forming cell adhesion and proliferation. Nanotechnology 2005;16(9):1828-1835.

136. Zinger O, Anselme K, Denzer A, Habersetzer P, Wieland M, Jeanfils J, Hardouin P, Landolt D. Time-dependent morphology and adhesion of osteoblastic cells on titanium model surfaces featuring scale-resolved topography. Biomaterials 2004;25(14):2695-2711.

137. Curtis ASG, Gadegaard N, Dalby MJ, Riehle MO, Wilkinson CDW, Aitchison G. Cells react to nanoscale order and symmetry in their surroundings. Ieee Transactions on Nanobioscience 2004;3(1):61-65.

138. Martines E, McGhee K, Wilkinson C, Curtis A. A parallel-plate flow chamber to study initial cell adhesion on a nanofeatured surface. Ieee Transactions on Nanobioscience 2004;3(2):90-95.

139. Dalby MJ, Gadegaard N, Riehle MO, Wilkinson CDW, Curtis ASG. Investigating filopodia sensing using arrays of defined nano-pits down to 35 nm diameter in size. International Journal of Biochemistry & Cell Biology 2004;36(10):2005-2015.

140. Dalby MJ, Yarwood SJ, Riehle MO, Johnstone HJH, Affrossman S, Curtsi ASG. Increasing fibroblast response to materials using nanotopography: morphological and genetic measurements of cell response to 13-nm-high polymer demixed islands. Experimental Cell Research 2002;276(1):1-9.

141. Dalby MJ, Riehle MO, Johnstone H, Affrossman S, Curtis ASG. Investigating the limits of filopodial sensing: a brief report using SEM to image the interaction between 10 nm high nano-topography and fibroblast filopodia. Cell Biology International 2004;28(3):229-236.

142. Dalby MJ, Riehle MO, Sutherland DS, Agheli H, Curtis ASG. Changes in fibroblast morphology in response to nano-columns produced by colloidal lithography. Biomaterials 2004;25(23):5415-5422.

143. Dalby MJ, Riehle MO, Johnstone H, Affrossman S, Curtis ASG. In vitro reaction of endothelial cells to polymer demixed nanotopography. Biomaterials 2002;23(14):2945-2954.

144. Webster TJ, Siegel RW, Bizios R. Nanoceramic surface roughness enhances osteoblast and osteoclast functions for improved orthopaedic/dental implant efficacy. Scripta Materialia 2001;44(8-9):1639-1642.

145. Webster TJ, Ergun C, Doremus RH, Siegel RW, Bizios R. Specific proteins mediate enhanced osteoblast adhesion on nanophase ceramics. Journal of Biomedical Materials Research 2000;51(3):475-483.

146. Rundqvist J, Hoh JH, Haviland DB. Directed immobilization of protein-coated nanospheres to nanometer-scale patterns fabricated by electron beam lithography of poly(ethylene glycol) self-assembled monolayers. Langmuir 2006;22(11):5100-5107.

147. Kunzi PA, Lussi J, Aeschimann L, Danuser G, Textor M, de Rooij NF, Staufer U. Nanofabrication of protein-patterned substrates for future cell adhesion experiments. Microelectronic Engineering 2005;78-79:582-586.

148. Zhang GJ, Tanii T, Zako T, Hosaka T, Miyake T, Kanari Y, Funatsu TW, Ohdomari I. Nanoscale patterning of protein using electron beam lithography of organosilane self-assembled monolayers. Small 2005;1(8-9):833-837.

149. Kim P, Kim DH, Kim B, Choi SK, Lee SH, Khademhosseini A, Langer R, Suh KY. Fabrication of nanostructures of polyethylene glycol for applications to protein adsorption and cell adhesion. Nanotechnology 2005;16(10):2420-2426.

150. Falconnet D, Pasqui D, Park S, Eckert R, Schift H, Gobrecht J, Barbucci R, Textor M. A novel approach to produce protein nanopatterns by combining nanoimprint lithography and molecular self-assembly. Nano Letters 2004;4(10):1909-1914.

151. Falconnet D, Koenig A, Assi T, Textor M. A combined photolithographic and molecular-assembly approach to produce functional micropatterns for applications in the biosciences. Advanced Functional Materials 2004;14(8):749-756.

152. Bae C, Shin HJ, Moon J, Sung MM. Contact area lithography (CAL): A new approach to direct formation of nanometric chemical patterns. Chemistry of Materials 2006;18(5):1085-1088.

153. Valsesia A, Colpo P, Meziani T, Bretagnol F, Lejeune M, Rossi F, Bouma A, Garcia-Parajo M. Selective immobilization of protein clusters on polymeric nanocraters. Advanced Functional Materials 2006;16(9):1242-1246.

154. Piner RD, Zhu J, Xu F, Hong SH, Mirkin CA. "Dip-pen" nanolithography. Science 1999;283(5402):661-663.

155. Wilson DL, Martin R, Hong S, Cronin-Golomb M, Mirkin CA, Kaplan DL. Surface organization and nanopatterning of collagen by dip-pen nanolithography. Proceedings of the National Academy of Sciences of the United States of America 2001;98(24):13660-13664.

156. Lee KB, Park SJ, Mirkin CA, Smith JC, Mrksich M. Protein nanoarrays generated by dip-pen nanolithography. Science 2002;295(5560):1702-1705.

157. Ginger DS, Zhang H, Mirkin CA. The evolution of dip-pen nanolithography. Angewandte Chemie-International Edition 2004;43(1):30-45.

158. Lee SW, Oh BK, Sanedrin RG, Salaita K, Fujigaya T, Mirkin CA. Biologically active protein nanoarrays generated using parallel dip-pen nanolithography. Advanced Materials 2006;18(9):1133-+.

159. Liu GY, Xu S, Qian YL. Nanofabrication of self-assembled monolayers using scanning probe lithography. Accounts of Chemical Research 2000;33(7):457-466.

160. Wadu-Mesthrige K, Amro NA, Garno JC, Xu S, Liu GY. Fabrication of nanometer-sized protein patterns using atomic force microscopy and selective immobilization. Biophysical Journal 2001;80(4):1891-1899.

161. Xu S, Miller S, Laibinis PE, Liu GY. Fabrication of nanometer scale patterns within self-assembled monolayers by nanografting. Langmuir 1999;15(21):7244-7251.

162. Wadu-Mesthrige K, Xu S, Amro NA, Liu GY. Fabrication and imaging of nanometer-sized protein patterns. Langmuir 1999;15(25):8580-8583.

163. Hoff JD, Cheng LJ, Meyhofer E, Guo LJ, Hunt AJ. Nanoscale protein patterning by imprint lithography. Nano Letters 2004;4(5):853-857.

164. Gaubert HE, Frey W. Highly parallel fabrication of nanopatterned surfaces with nanoscale orthogonal biofunctionalization imprint lithography. Nanotechnology 2007;in press.

165. Glass R, Moller M, Spatz JP. Block copolymer micelle nanolithography. Nanotechnology 2003;14(10):1153-1160.

166. Glass R, Arnold M, Cavalcanti-Adam EA, Blummel J, Haferkemper C, Dodd C, Spatz JP. Block copolymer micelle nanolithography on non-conductive substrates. New Journal of Physics 2004;6.

167. Garno JC, Amro NA, Wadu-Mesthrige K, Liu GY. Production of periodic arrays of protein nanostructures using particle lithography. Langmuir 2002;18(21):8186-8192.

168. Cavalcanti-Adam EA, Volberg T, Micoulet A, Kessler H, Geiger B, Spatz JP. Cell spreading and focal adhesion dynamics are regulated by spacing of integrin ligands. Biophysical Journal 2007;92(8):2964-2974.

169. Maheshwari G, Brown G, Lauffenburger DA, Wells A, Griffith LG. Cell adhesion and motility depend on nanoscale RGD clustering. Journal of Cell Science 2000;113(10):1677-1686.

170. Comisar WA, Hsiong SX, Kong HJ, Mooney DJ, Linderman JJ. Multi-scale modeling to predict ligand presentation within RGD nanopatterned hydrogels. Biomaterials 2006;27(10):2322-2329.

171. Coussen F, Choquet D, Sheetz MP, Erickson HP. Trimers of the fibronectin cell adhesion domain localize to actin filament bundles and undergo rearward translocation. Journal of Cell Science 2002;115(12):2581-2590.

172. Garcia AJ, Takagi J, Boettiger D. Two-stage activation for alpha(5)beta(1) integrin binding to surface-adsorbed fibronectin. Journal of Biological Chemistry 1998;273(52):34710-34715.

173. Zaidel-Bar R, Ballestrem C, Kam Z, Geiger B. Early molecular events in the assembly of matrix adhesions at the leading edge of migrating cells. Journal of Cell Science 2003;116(22):4605-4613.

174. Zimerman B, Volberg T, Geiger B. Early molecular events in the assembly of the focal adhesion-stress fiber complex during fibroblast spreading. Cell Motility and the Cytoskeleton 2004;58(3):143-159.

175. Deckman HW, Dunsmuir JH. Natural Lithography. Applied Physics Letters 1982;41(4):377-379.

176. Haynes CL, Van Duyne RP. Nanosphere lithography: A versatile nanofabrication tool for studies of size-dependent nanoparticle optics. Journal of Physical Chemistry B 2001;105(24):5599-5611.

177. Hulteen JC, Vanduyne RP. Nanosphere Lithography - a Materials General Fabrication Process for Periodic Particle Array Surfaces. Journal of Vacuum Science & Technology a-Vacuum Surfaces and Films 1995;13(3):1553-1558.

178. Matsushita SI, Yagi Y, Miwa T, Tryk DA, Koda T, Fujishima A. Light propagation in composite two-dimensional arrays of polystyrene spherical particles. Langmuir 2000;16(2):636-642.

179. Matsushita SI, Miwa T, Fujishima A. Stable two-dimensional fine-particle arrays in solution. Langmuir 2001;17(4):988-992.

180. Park KH, Lee S, Koh KH, Lacerda R, Teo KBK, Milne WI. Advanced nanosphere lithography for the areal-density variation of periodic arrays of vertically aligned carbon nanofibers. Journal of Applied Physics 2005;97(2).

181. Frey W, Woods CK, Chilkoti A. Ultraflat nanosphere lithography: A new method to fabricate flat nanostructures. Advanced Materials 2000;12(20):1515-1519.

182. Haupt M, Ladenburger A, Sauer R, Thonke K, Glass R, Roos W, Spatz JP, Rauscher H, Riethmuller S, Moller M. Ultraviolet-emitting ZnO nanowhiskers prepared by a

vapor transport process on prestructured surfaces with self-assembled polymers. Journal of Applied Physics 2003;93(10):6252-6257.

183. Papra A, Gadegaard N, Larsen NB. Characterization of ultrathin poly(ethylene glycol) monolayers on silicon substrates. Langmuir 2001;17(5):1457-1460.

184. McFarland CD, Thomas CH, DeFilippis C, Steele JG, Healy KE. Protein adsorption and cell attachment to patterned surfaces. Journal of Biomedical Materials Research 2000;49(2):200-210.

185. Lee MH, Ducheyne P, Lynch L, Boettiger D, Composto RJ. Effect of biomaterial surface properties on fibronectin-alpha(5)beta(1) integrin interaction and cellular attachment. Biomaterials 2006;27(9):1907-1916.

186. Burr JG, Dreyfuss G, Penman S, Buchanan JM. Association of the Src Gene-Product of Rous-Sarcoma Virus with Cytoskeletal Structures of Chicken-Embryo Fibroblasts. Proceedings of the National Academy of Sciences of the United States of America-Biological Sciences 1980;77(6):3484-3488.

187. Plopper G, Ingber DE. Rapid Induction and Isolation of Focal Adhesion Complexes. Biochemical and Biophysical Research Communications 1993;193(2):571-578.

188. Chen CS, Alonso JL, Ostuni E, Whitesides GM, Ingber DE. Cell shape provides global control of focal adhesion assembly. Biochemical and Biophysical Research Communications 2003;307(2):355-361.

189. Sharma S, Johnson RW, Desai TA. XPS and AFM analysis of antifouling PEG interfaces for microfabricated silicon biosensors. Biosensors & Bioelectronics 2004;20(2):227-239.

190. Lhoest JB, Detrait E, van den Bosch de Aguilar P, Bertrand P. Fibronectin adsorption, conformation, and orientation on polystyrene substrates studied by radiolabeling, XPS, and ToF SIMS. Journal of Biomedical Materials Research 1998;41(1):95-103.

191. Zhu YB, Chian KS, Chan-Park MB, Mhaisalkar PS, Ratner BD. Protein bonding on biodegradable poly(L-lactide-co-caprolactone) membrane for esophageal tissue engineering. Biomaterials 2006;27(1):68-78.

192. Surface Analysis: The Principal Techniques. West Sussex: John Wiley & Sons, Inc.; 1997.

193. Tidwell CD, Castner DG, Golledge SL, Ratner BD, Meyer K, Hagenhoff B, Benninghoven A. Static time-of-flight secondary ion mass spectrometry and x-ray

photoelectron spectroscopy characterization of adsorbed albumin and fibronectin films. Surface and Interface Analysis 2001;31(8):724-733.

194. Galtayries A, Warocquier-Clerout R, Nage MD, Marcus P. Fibronectin adsorption on Fe-Cr alloy studied by XPS. Surface and Interface Analysis 2006;38(4):186-190.

195. Price TM, Rudee ML, Pierschbacher M, Ruoslahti E. Structure of Fibronectin and Its Fragments in Electron-Microscopy. European Journal of Biochemistry 1982;129(2):359-363.

196. Erickson HP, Carrell NA. Fibronectin in Extended and Compact Conformations - Electron-Microscopy and Sedimentation Analysis. Journal of Biological Chemistry 1983;258(23):4539-4544.

197. Rocco M, Carson M, Hantgan R, McDonagh J, Hermans J. DEPENDENCE OF THE SHAPE OF THE PLASMA FIBRONECTIN MOLECULE ON SOLVENT COMPOSITION - IONIC-STRENGTH AND GLYCEROL CONTENT. Journal of Biological Chemistry 1983;258(23):4545-4549.

198. Lehnert D, Wehrle-Haller B, David C, Weiland U, Ballestrem C, Imhof BA, Bastmeyer M. Cell behaviour on micropatterned substrata: limits of extracellular matrix geometry for spreading and adhesion. Journal of Cell Science 2004;117(1):41-52.

199. Sniadecki N, Desai RA, Ruiz SA, Chen CS. Nanotechnology for cell-substrate interactions. Annals of Biomedical Engineering 2006;34(1):59-74.

200. Blattler T, Huwiler C, Ochsner M, Stadler B, Solak H, Voros J, Grandin HM. Nanopatterns with biological functions. Journal of Nanoscience and Nanotechnology 2006;6(8):2237-2264.

201. Christman KL, Enriquez-Rios VD, Maynard HD. Nanopatterning proteins and peptides. Soft Matter 2006;2(11):928-939.

202. Franz CM, Muller DJ. Analyzing focal adhesion structure by atomic force microscopy. Journal of Cell Science 2005;118(22):5315-5323.

203. Chinga G, Johnsen PO, Dougherty R, Berli EL, Walter J. Quantification of the 3D microstructure of SC surfaces. Journal of Microscopy-Oxford 2007;227(3):254-265.

204. Nelson CM, Pirone DM, Tan JL, Chen CS. Vascular endothelial-cadherin regulates cytoskeletal tension, cell spreading, and focal adhesions stimulating RhoA. Molecular Biology of the Cell 2004;15(6):2943-2953.

205. Zamir E, Katz BZ, Aota S, Yamada KM, Geiger B, Kam Z. Molecular diversity of cell-matrix adhesions. Journal of Cell Science 1999;112(11):1655-1669.

206. Brakebusch C, Fassler R. The integrin-actin connection, an eternal love affair. Embo Journal 2003;22(10):2324-2333.

207. Pavalko FM, Otey CA, Simon KO, Burridge K. Alpha-Actinin - a Direct Link between Actin and Integrins. Biochemical Society Transactions 1991;19(4):1065-1069.

208. Schwarz US, Bischofs IB. Physical determinants of cell organization in soft media. Medical Engineering & Physics 2005;27(9):763-772.

209. Deroanne CF, Lapiere CM, Nusgens BV. In vitro tubulogenesis of endothelial cells by relaxation of the coupling extracellular matrix-cytoskeleton. Cardiovascular Research 2001;49(3):647-658.

210. Wierzbicka-Patynowski I, Schwarzbauer JE. The ins and outs of fibronectin matrix assembly. Journal of Cell Science 2003;116(16):3269-3276.

211. Smith ML, Gourdon D, Little WC, Kubow KE, Eguiluz RA, Luna-Morris S, Vogel V. Force-induced unfolding of fibronectin in the extracellular matrix of living cells. Plos Biology 2007;5:2243-2254.

212. Abu-Lail NI, Ohashi T, Clark RL, Erickson HP, Zauscher S. Understanding the elasticity of fibronectin fibrils: Unfolding strengths of FN-III and GFP domains measured by single molecule force spectroscopy. Matrix Biology 2006;25(3):175-184.

213. Baneyx G, Baugh L, Vogel V. Fibronectin extension and unfolding within cell matrix fibrils controlled by cytoskeletal tension. Proceedings of the National Academy of Sciences of the United States of America 2002;99(8):5139-5143.

214. De Jong KL, MacLeod HC, Norton PR, Petersen NO. Fibronectin organization under and near cells. European Biophysics Journal with Biophysics Letters 2006;35(8):695-708.

215. Zhang QH, Magnusson MK, Mosher DF. Lysophosphatidic acid and microtubule-destabilizing agents stimulate fibronectin matrix assembly through Rho-dependent actin stress fiber formation and cell contraction. Molecular Biology of the Cell 1997;8(8):1415-1425.

216. Pankov R, Cukierman E, Katz BZ, Matsumoto K, Lin DC, Lin S, Hahn C, Yamada KM. Integrin dynamics and matrix assembly: Tensin-dependent translocation of alpha(5)beta(1) integrins promotes early fibronectin fibrillogenesis. Journal of Cell Biology 2000;148(5):1075-1090.

217. Engler A, Bacakova L, Newman C, Hategan A, Griffin M, Dischery D. Substrate compliance versus ligand density in cell on gel responses. Biophysical Journal 2004;86(1):617-628.

218. Huang S, Brangwynne CP, Parker KK, Ingber DE. Symmetry-breaking in mammalian cell cohort migration during tissue pattern formation: Role of random-walk persistence. Cell Motility and the Cytoskeleton 2005;61(4):201-213.

219. Wheeler AP, Ridley AJ. Why three Rho proteins? RhoA, RhoB, RhoC, and cell motility. Experimental Cell Research 2004;301(1):43-49.

220. Ponti A, Machacek M, Gupton SL, Waterman-Storer CM, Danuser G. Two distinct actin networks drive the protrusion of migrating cells. Science 2004;305(5691):1782-1786.

221. Verkhovsky AB, Chaga OY, Schaub S, Svitkina TM, Meister JJ, Borisy GG. Orientational order of the lamellipodial actin network as demonstrated in living motile cells. Molecular Biology of the Cell 2003;14(11):4667-4675.

222. Albuquerque MLC, Flozak AS. Lamellipodial motility in wounded endothelial cells exposed to physiologic flow is associated with different patterns of beta(1)-integrin and vinculin localization. Journal of Cellular Physiology 2003;195(1):50-60.

223. Kaverina I, Krylyshkina O, Small JV. Regulation of substrate adhesion dynamics during cell motility. The International Journal of Biochemistry & Cell Biology 2002;34(7):746-761.

224. Small JV, Geiger B, Kaverina I, Bershadsky A. How do microtubules guide migrating cells? Nature Reviews Molecular Cell Biology 2002;3(12):957-964.

225. Galbraith CG, Sheetz MP. Keratocytes pull with similar forces on their dorsal and ventral surfaces. Journal of Cell Biology 1999;147(6):1313-1323.

226. Burton K, Park JH, Taylor DL. Keratocytes generate traction forces in two phases. Molecular Biology of the Cell 1999;10(11):3745-3769.

227. Illc D, Furuta Y, Kanazawa S, Takeda N, Sobue K, Nakatsuji N, Nomura S, Fujimoto J, Okada M, Yamamoto T and others. Reduced Sell Motility and Enhanced Focal Adhesion Contact Formation in Cells from Fak-Deficient Mice. Nature 1995;377(6549):539-544.

228. Ballestrem C, Hinz B, Imhof BA, Wehrle-Haller B. Marching at the front and dragging behind: differential alpha-V beta 3-integrin turnover regulates focal adhesion behavior. Journal of Cell Biology 2001;155(7):1319-1332.

229. Dickinson RB, Tranquillo RT. A Stochastic-Model for Adhesion-Mediated Cell Random Motility and Haptotaxis. Journal of Mathematical Biology 1993;31(6):563-600.

230. Paku S, Tovari J, Lorincz Z, Timar F, Dome B, Kopper L, Raz A, Timar J. Adhesion dynamics and cytoskeletal structure of gliding human fibrosarcoma cells: a hypothetical model of cell migration. Experimental Cell Research 2003;290(2):246-253.

231. Mogilner A, Oster G. Cell motility driven by actin polymerization. Biophysical Journal 1996;71(6):3030-3045.

232. Soga N, Namba N, McAllister S, Cornelius L, Teitelbaum SL, Dowdy SF, Kawamura J, Hruska KA. Rho family GTPases regulate VEGF-stimulated endothelial cell motility. Experimental Cell Research 2001;269(1):73-87.

233. Rousseau S, Houle F, Huot J. Integrating the VEGF signals leading to actin-based motility in vascular endothelial cells. Trends in Cardiovascular Medicine 2000;10(8):321-327.

234. Gaudet C, Marganski WA, Kim S, Brown CT, Gunderia V, Dembo M, Wong JY. Influence of type I collagen surface density on fibroblast spreading, motility, and contractility. Biophysical Journal 2003;85(5):3329-3335.

235. Kouvroukoglou S, Dee KC, Bizios R, McIntire LV, Zygourakis K. Endothelial cell migration on surfaces modified with immobilized adhesive peptides. Biomaterials 2000;21(17):1725-1733.

236. Jones RJ, Brunton VG, Frame MC. Adhesion-linked kinases in cancer; emphasis on Src, focal adhesion kinase and PI 3-kinase. European Journal of Cancer 2000;36(13):1595-1606.

237. Eliceiri BP, Puente XS, Hood JD, Stupack DG, Schlaepfer DD, Huang XZZ, Sheppard D, Cheresh DA. Src-mediated coupling of focal adhesion kinase to integrin alpha v beta 5 in vascular endothelial growth factor signaling. Journal of Cell Biology 2002;157(1):149-159.

238. Rodrigue CM, Porteu F, Navarro N, Bruyneel E, Bracke M, Romeo PH, Gespach C, Garel MC. The cancer chemopreventive agent resveratrol induces tensin, a cell-matrix adhesion protein with signaling and antitumor activities. Oncogene 2005;24(20):3274-3284.

239. Li S, Butler P, Wang YX, Hu YL, Han DC, Usami S, Guan JL, Chien S. The role of the dynamics of focal adhesion kinase in the mechanotaxis of endothelial cells. Proceedings of the National Academy of Sciences of the United States of America 2002;99(6):3546-3551.

240. Fernandez-Sauze S, Delfino C, Mabrouk K, Dussert C, Chinot O, Martin PM, Grisoli F, Ouafik L, Boudouresque F. Effects of adrenomedullin on endothelial cells in the multistep process of angiogenesis: Involvement of CRLR/RAMP2 and CRLR/RAMP3 receptors. International Journal of Cancer 2004;108(6):797-804.

241. Salani D, Taraboletti G, Rosano L, Di Castro V, Borsotti P, Giavazzi R, Bagnato A. Endothelin-1 induces an angiogenic phenotype in cultured endothelial cells and stimulates neovascularization in vivo. American Journal of Pathology 2000;157(5):1703-1711.

242. Weber KSC, Nelson PJ, Grone HJ, Weber C. Expression of CCR2 by endothelial cells - Implications for MCP-1 mediated wound injury repair and in vivo inflammatory activation of endothelium. Arteriosclerosis Thrombosis and Vascular Biology 1999;19(9):2085-2093.

243. Warchol ME. Cell density and N-cadherin interactions regulate cell proliferation in the sensory epithelia of the inner ear. Journal of Neuroscience 2002;22(7):2607-2616.

244. Tolic-Norrelykke IM, Wang N. Traction in smooth muscle cells varies with cell spreading. Journal of Biomechanics 2005;38(7):1405-1412.

245. Caron-Lormier G, Berry H. Amplification and oscillations in the FAK/Src kinase system during integrin signaling. Journal of Theoretical Biology 2005;232(2):235-248.

246. Avraham HK, Lee TH, Koh YH, Kim TA, Jiang SX, Sussman M, Samarel AM, Avraham S. Vascular endothelial growth factor regulates focal adhesion assembly in human brain microvascular endothelial cells through activation of the focal adhesion kinase and related adhesion focal tyrosine kinase. Journal of Biological Chemistry 2003;278(38):36661-36668.

247. Abedi H, Zachary I. Vascular endothelial growth factor stimulates tyrosine phosphorylation and recruitment to new focal adhesions of focal adhesion kinase and paxillin in endothelial cells. Journal of Biological Chemistry 1997;272(24):15442-15451.

248. Ahmed I, Ponery AS, Nur-E-Kamal A, Kamal J, Meshel AS, Sheetz MP, Schindler M, Meiners S. Morphology, cytoskeletal organization, and myosin dynamics of mouse embryonic fibroblasts cultured on nanofibrillar surfaces. Molecular and Cellular Biochemistry 2007;301(1-2):241-249.

Vita

John Hundley Slater was born in Pascagoula, Mississippi on March 22, 1978. He completed his Bachelor of Science in Mechanical Engineering from the University of North Carolina at Charlotte in December of 2001. As an undergraduate researcher he designed and implemented a microfluidic shear chamber to investigate the influence of shear stress on liver sinusoidal endothelial cells at hypothermic temperatures for machine perfusion preservation of livers. His abilities as an undergraduate researcher resulted in two Old Guard Best Paper Awards from the American Society of Mechanical Engineers. To pursue his research interests, he enrolled in graduate school in the Department of Biomedical Engineering at the University of Texas at Austin in 2002. As a National Science Foundation Graduate Research Fellow he investigated the design of advanced, nanostructured biomaterials for cell engineering purposes. He completed his Ph.D. in Biomedical Engineering along with a Doctoral Portfolio Degree in Nanotechnology in May 2008. After completing his Ph.D., he joined Dr. Jennifer West's lab at Rice University as a postdoctoral researcher.

Permanent address: 11 Marietta Road, Glen Cove, NY 11542

Note: This dissertation was typed by John H. Slater.